



Svensk Djupstabilisering
Swedish Deep Stabilization Research Centre

Rapport 7

Deformation Behaviour of Lime/Cement Column Stabilized Clay

Sadek Baker



CHALMERS

Svensk Djupstabilisering

Svensk Djupstabilisering (SD) är ett centrum för forskning och utveckling inom djupstabilisering med kalk-cementpelare. Verksamheten syftar till att initiera och bedriva en branschsamordnad forsknings- och utvecklingsverksamhet, som ger säkerhetsmässiga, funktionsmässiga och ekonomiska vinster som tillgodoser svenska intressen hos samhället och industrin. Verksamheten baseras på en FoU-plan för åren 1996 – 2000. Medlemmar är myndigheter, kalk- och cementleverantörer, entreprenörer, konsulter, forskningsinstitut och högskolor.

Verksamheten finansieras av medlemmarna samt genom anslag från Byggforskningsrådet, Svenska byggbranschens utvecklingsfond och Kommunikationsforskningsberedningen.

Svensk Djupstabilisering har sitt säte vid Statens geotekniska institut (SGI) och leds av en styrgrupp med representanter för medlemmarna.

Ytterligare upplysningar om verksamheten lämnas av SD:s projektledare Göran Holm, tel: 013-20 18 61, 070-521 09 39, fax: 013-20 19 14, e-post: goran.holm@swedgeo.se

Swedish Deep Stabilization Research Centre

The Swedish Deep Stabilization Research Centre coordinates research and development activities in deep stabilization of soft soils with lime-cement columns. A joint research programme based on the needs stated by the authorities and the industry is being conducted during the period 1996 – 2000. Members of the Centre include authorities, lime and cement manufactures, contractors, consultants, research institutes and universities.

The work of the Swedish Deep Stabilization Research Centre is financed by its members and by research grants.

The Swedish Deep Stabilization Research Centre is located at the Swedish Geotechnical Institute and has a Steering Committee with representatives chosen from among its members.

Further information on the Swedish Deep Stabilization Research Centre can be obtained from the Project Manager, Mr G Holm, tel: +46 13 20 18 61, fax: +46 13 20 19 14 or e-mail: goran.holm@swedgeo.se



Svensk Djupstabilisering
Swedish Deep Stabilization Research Centre

Rapport 7

Deformation Behaviour of Lime/Cement Column Stabilized Clay

Sadek Baker



CHALMERS

Denna rapport är även publicerad som Doktorsavhandling
vid Chalmers tekniska högskola
Geoteknik med grundläggning

ISBN 91-7197-950-6
ISSN 0346-718x

Linköping 2000

Förord

Svensk Djupstabiliserings (SD) verksamhet som baseras på en FoU-plan med fem delområden genomförs bl a som doktors- eller licentiatprojekt.

Föreliggande rapport redovisar ett projekt inom delområdet ”Förstärkningars funktionssätt”. Projektet är också ett led i SD:s strävan för kompetensutveckling inom djupstabilisering.

Linköping i november 2000

Göran Holm

Projektledare för SD

Rapport	Svensk Djupstabilisering c/o Statens geotekniska institut 581 93 Linköping
Beställning	Tel: 013-20 18 42 Fax: 013-20 19 14 E-post: birgitta.sahlin@swedgeo.se
ISSN	1402-2036
ISRN	SD-R--00/7--SE
Upplaga	200
Tryckeri	Roland Offset AB, Linköping, nov 2000

PREFACE

The present thesis deals with the deformation behavior of the lime/cement column stabilized clay. The study includes the development of analytical and numerical models together with field and laboratory tests

The work was carried out at the Department of Geotechnical Engineering, Chalmers University of Technology, under the supervision of Professor Göran Sällfors. The project was financially supported by the Swedish Transport and Communication Research Board, the Swedish Council for Building Research, the Swedish Deep Stabilization Research Center and Chalmers University of Technology.

The field tests could not have been accomplished without the assistance and supply of material from the Swedish National Rail Administration, LC Markteknik, Hercules Grundläggning and PEAB Entreprenad.

I am very grateful to Professor Göran Sällfors. His guidance, encouragement and fruitful discussions throughout the work have been invaluable for this project.

I would like to thank Professor emeritus Sven Hansbo and Per-Evert Bengtsson, SGI, for their critical examination of the manuscript, as well as fruitful discussions. I also would like also to thank Dr. Torebjörn Edstam, J&W, for his critical examination of parts of the manuscript.

I would like to express my special thanks to:

- *the research engineers at the department, Jacques Connant, Kjell Nätterdahl, Aaro Pirohnen and Ingemar Forsgren for helping me with the field tests, laboratory tests and laboratory equipment.*
- *my colleague Malin Gustafsson for her help with part of the laboratory hydraulic conductivity tests.*
- *my colleagues at the department for their friendship and support.*

Part of the experimental work was carried out under my supervision by Helena Kernell, Birgitta Petersson, Ulf Dahlén and Håkan Mohlin, whose contributions are greatly appreciated

Finally, I want to express my thanks to my family, my wife Nadeyeh and my son Forat, for their patience, encouragement and endless support throughout the years.




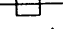
Göteborg, October 2000

Sadek Baker

Deformation Behavior of Lime/Cement Column Stabilized Clay

Sadek Baker
Department of Geotechnical Engineering
Chalmers University of Technology
S-412 96 Göteborg, Sweden

Errata

Page	Location	Printed text	Corrected text (or add after)
x	d 4	see .figure S. 1	see figure S. 1
xiii	d 6	origional	original
xv	u 2	increased very slightly with the increase of confining pressure.	decreases slightly with the increase of the confining pressure due to destructurization.
27	Figure 2.11	 Modified Barron (Mcol/Msoil = 40)  PLAXIS (Mcol/Msoil = 40)	 PLAXIS (Mcol/Msoil = 40)  Modified Barron (Mcol/Msoil = 40)
53	Figure 3.7	equation (3.8)	equation (3.9)
68	d 2	triaxial tests were	were
91	d 18	total creep deformation	creep deformation increment
91	Figure 5.14	creep deformation [mm]	creep deformation increment [mm]
93	d 3	very stiff	stiff
108	d 10	middle	remaining
108	Figure 5.26	4.7	4.7 m
124	d 11	3.6 m	3.7 m
141	u 6	the related degree of	the degree of
155	u 18	two laboratory	two large laboratory
156	u 19	F3	F3-b
157	u 5	in the case of lime/cement column	in this case
168	u 16	no significant increase	a slight decrease due to destructurization
171	d 3	ground: I	ground-I:
172	u 10	8th	8 th

Note: d = rows downward; u = rows upward

Preface	iii
Summary.....	ix
List of symbols and abbreviations	xvii
1. Introduction	1
1.1 Background.....	1
1.2 Objective and scope of the study	1
2. Survey of literature.....	3
2.1 Introduction	3
2.2 Settlement analytical methods.....	4
2.3 Stiffness and shear strength of lime, lime/cement and cement columns	30
2.4 Hydraulic conductivity	40
3. Analytical and numerical models.....	43
3.1 General.....	43
3.2 Analytical elastic model for vertically loaded lime/cement stabilized soil	44
3.3 Numerical analysis of load distribution between lime/cement columns and surrounding soil using the finite element method	47
3.3.1 Introduction	47
3.3.2 Finite element analysis, linear elastic model	48
3.4 One-dimensional consolidation settlement of stabilized soil using lime/cement column	55
3.4.1 Introduction	55
3.4.2 Assumptions	55
3.4.3 Analysis	56
3.4.4 Solution	63
3.4.5 Typical results and comparison.....	63
4. Test sites.....	67
4.1 General.....	67
4.2 The Varberg site	68

4.2.1 Introduction	68
4.2.2 Geotechnical properties.....	68
4.2.3 Installation of lime/cement columns	69
4.3 The Fjärås test site.....	70
4.3.1 Introduction	70
4.3.2 Geotechnical properties.....	70
4.3.3 Installation of lime/cement columns	71
4.4 The Löftaån test site	72
4.4.1 Introduction	72
4.4.2 Geotechnical properties.....	72
4.4.3 Installation of lime/cement columns	74
5. Field tests	77
5.1 Load test	77
5.1.1 General	77
5.1.2 Installation.....	77
5.1.3 Instrumentation and test procedure.....	79
5.1.4 Finite element model.....	81
5.1.5 The compression modulus and the creep load of the lime/cement column	84
5.1.6 The Varberg test site	86
5.1.6.1 Test results	86
5.1.6.2 Finite element simulations	92
5.1.7 The Löftaån test site	100
5.1.7.1 Test results	100
5.1.7.2 The finite element simulations	106
5.2 Hydraulic conductivity tests.....	111
5.2.1 Test instrumentation.....	111
5.2.2 Installation and test procedure	113
5.2.3 Traditional methods	114
5.2.4 Finite element model.....	115
5.2.5 The Fjärås test site.....	122
5.2.5.1 Test results	122

5.2.6 The Löftaån test site	126
5.2.6.1 Test results	126
6. Laboratory tests.....	135
6.1 Laboratory tests on standard size samples	135
6.1.1 Introduction	135
6.1.2 The Varberg test site results.....	137
6.1.2.1 Classification parameters	137
6.1.2.2 Unconfined compression tests and evaluation of column stiffness.	137
6.1.3 The Fjärås test site results	139
6.1.3.1 Hydraulic conductivity tests	139
6.1.4 The Löftaån test site results	141
6.1.4.1 Classification parameters	141
6.1.4.2 Unconfined compression tests and evaluation of column stiffness.	142
6.1.4.3 Hydraulic conductivity test	144
6.2 Laboratory tests on large-scale samples.....	147
6.2.1 Triaxial tests	147
6.2.1.1 Introduction.....	147
6.2.1.2 Test instrumentation	147
6.2.1.3 Calibrations and corrections.....	149
6.2.1.4 Installation and test procedure	150
6.2.1.5 Evaluation of test results and compression modulus	151
6.2.2 Hydraulic conductivity.....	162
7. Conclusions.....	165
7.1 Settlement, load distribution and rate of consolidation.	165
7.2 Mechanical properties of the lime/cement columns	167
7.3 Hydraulic conductivity of the lime/cement columns	169
7.4 Future research	170
References.....	171
Appendix A.....	177
Appendix B.....	183
Appendix C.....	197

SUMMARY

INTRODUCTION

Deep soil stabilization with lime/cement columns has lately become one of the most frequently used methods for soil improvement. An injection of a dry mixture of lime and cement into the clay will form vertical columns. The method has been used mainly to reduce settlement of highway and railway embankments as well as to increase the safety against failure. Moreover, this method can be used to reduce settlement of buildings up to two stories high. The theories used for design were originally developed for lime columns. Today the major part of all columns are manufactured by using a mixture of lime and cement, which results in somewhat different stress strain, strength and hydraulic properties.

The objective of the present study is to modify the design theories and broaden the knowledge about the material properties in order to better predict the deformation of the lime/cement stabilized soil under working load.

ANALYTICAL AND NUMERICAL MODELS

Three mathematical models are presented in this study, two of which are numerical and one is an analytical elastic model based on a unit cell concept.

The analytical elastic model is used to increase the understanding of long-term total settlement as well as the stress distribution within the stabilized soil caused by an applied load. The equations derived for calculation of the axial vertical strain can be written as

$$\varepsilon_z = \frac{\sigma_v}{a_s \cdot (M_{col} + 2 \cdot \lambda_{col} \cdot F_{z0}) + (1 - a_s) \cdot (M_{soil} - 2 \cdot \frac{a_s}{1 - a_s} \cdot \lambda_{soil} \cdot F_{z0})} \quad (S.1)$$

If the factor F_{z0} is set to zero then equation (S.1) becomes similar to the equation traditionally used to calculate the total long-term settlement of a single or a group of lime/cement columns (when both the treated and the untreated materials are assumed to act as linear elastic) and can be written as

$$\varepsilon_z = \frac{\sigma_v}{a_s \cdot M_{col} + (1 - a_s) \cdot M_{soil}} \quad (S.2)$$

The axial strain calculated by equation (S.1) is greater than the axial strain calculated by the traditional method using equation (S.2). The ratio increases with an increase in both the area ratio, a_s , and the modulus ratio, see Figure S. 1. Using E_{col} instead of M_{col} in equation (S.2), the results become closer to that obtained by the analytical solution.

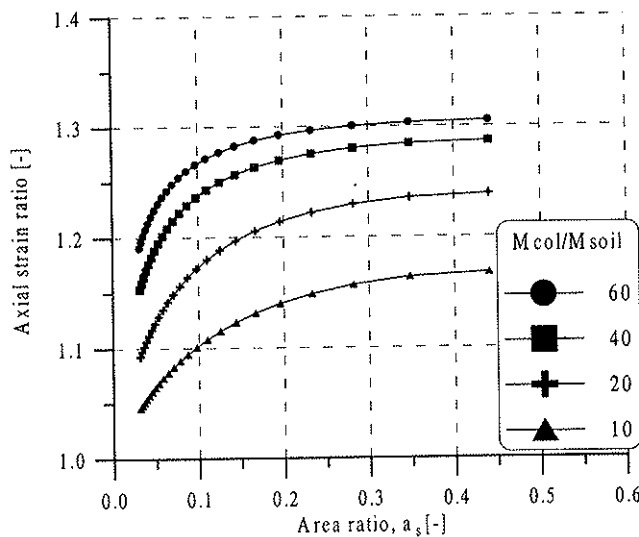


Figure S. 1 The ratio of the strains calculated by equations (S.1) and (S.2) versus area ratio a_s for different modulus ratios.

In the first numerical model, the finite element method has been applied using a three-dimensional linear elastic model to study the stress distribution behavior.

For simplicity, the circular columns were modeled as square columns with corresponding cross sectional area. The dimensions of the square columns used in the analysis are 1.8, 1.16, 0.9 and 0.7 m, which in terms of the relative column area, a_s , together with the 3 m spacing, can be written as 0.36, 0.15, 0.09 and 0.05 respectively. Four column lengths were considered; 6, 12, 18 m and 50 m. In the last case, the columns are extended all the way to firm bottom. Three stiffness ratios (M_{col}/M_{soil}), 10, 30, and 70 were used, and a total of 40 models were analyzed. Poisson's ratio used for the two materials was 0.3. The numerical results showed that the vertical stress in the columns increased to a maximum value few meters

below the top of the columns where the vertical load was applied, and then started to decrease again.

Traditionally, the stress increase in the column is calculated using the following equation

$$\sigma_{col} = \frac{n \cdot \sigma_v}{1 + a_s \cdot (n - 1)} \quad (S.3)$$

On the other hand, the analytical model presented in this study suggest that the stress increase in the column can be written as

$$\sigma_{col} = (M_{col} + 2 \cdot \lambda_{col} \cdot F_{z0}) \cdot \varepsilon_z \quad (S.4)$$

The maximum vertical stress increase in the column evaluated from equations (S.3) and (S.4) is together with the 3-D numerical simulation presented in Table S. 1. The vertical stresses in the column were normalized by dividing its values with the value of the applied stress $\left(\frac{\sigma_{col}}{\sigma_v}\right)$.

Table S. 1 The normalized maximum vertical stresses in columns calculated by equations (S.3) and (S.4) together with results from the finite element analysis for different areas and modulus ratios.

a_s [-]	n [-]	Normalized vertical stress in the column					
		Eq. (S.3)	Eq. (S.4)	L= 6 m	L= 12 m	L= 18 m	L= 50 m
0.05	10	6.7	5.6	4.9	5.3	5.4	5.4
0.05	30	11.6	10.3	7.7	9.1		
0.05	70	14.7	13.8	9.3	11.5	12	13.1
0.09	10	5.5	4.8	4.1	4.4	4.5	4.6
0.09	30	8.3	7.6	5.8	6.7		
0.09	70	9.7	9.3	6.6	7.8	8.1	8.9
0.15	10	4.3	3.8	3.3	3.5	3.6	3.7
0.15	30	5.6	5.3	4.2	4.6		
0.15	70	6.2	6.0	4.6	5.1	5.3	5.9
0.36	10	2.4	2.2	2.0	2.1	2.6	2.8
0.36	30	2.6	2.6	2.2	2.3		
0.36	70	2.7	2.7	2.3	2.3	3.1	3.7

Numerical results obtained from simulation of columns extended to firm bottom and located at the embankment center are more similar to those

obtained by using equation (S.4) than those evaluated by the traditional method based on equation (S.3).

At the bottom of the reinforced block, there are stress concentrations directly under the tip of the column, and the stresses there were higher than in the rest of the untreated soil at the same level. This may be due to numerical problem that can appear at the boundary between two materials with a high stiffness difference. It is interesting to notice that the vertical stresses below the bottom of the reinforced block are equal to the vertical stresses calculated by Boussinesq's equation with the load acting on the ground surface, see Figure S.2.

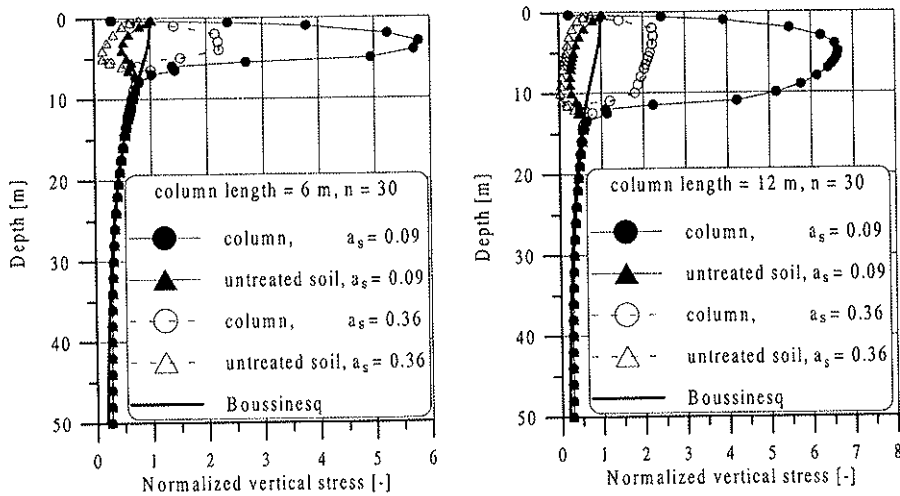


Figure S. 2 Vertical stress distribution under the reinforced block compared with Boussinesq's solution.

The second numerical model is a finite difference model used to calculate the consolidation settlement of a lime/cement column stabilized soil.

Using lime/cement mixture instead of lime will increase the stiffness of the treated soil and cause stress concentration in the columns, while at the same time the hydraulic conductivity is decreased. In this model it is assumed that both soft soil and lime/cement columns possess material linearity.

The numerical model is based on Yoshikuni's consolidation theory. The finite difference method was used to solve the following equation

$$\frac{\partial u}{\partial t} = c_{vsol} \cdot \frac{\partial^2 u}{\partial z^2} + \chi_l \cdot \frac{\partial \bar{u}}{\partial t} \quad (S.5)$$

The consolidation of the stabilized soil due to vertical drainage is examined. Evaluations are made for different column to soil ratios of compression modulus. It is shown that the rate of consolidation increases as the ratio of the compression modulus of the lime/cement column to that of the untreated soil increases, in spite of equal or less hydraulic conductivity of the lime/cement columns compared to that of the original soil. The results obtained from this model are compared with those predicted using the finite element program, PLAXIS, see Figure S. 3.

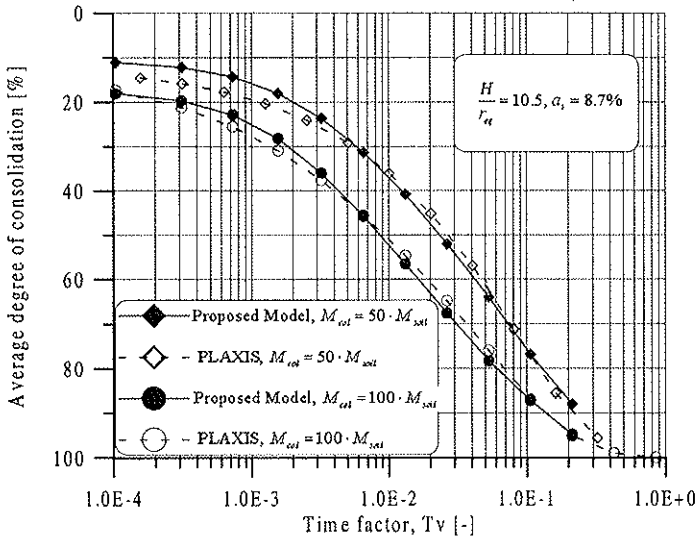


Figure S. 3 Proposed model versus PLAXIS, for two different compression modulus ratios.

FIELD TESTS

In-situ measurements were made to measure the stiffness and the hydraulic conductivity of the lime/cement column stabilized clay.

The load tests used to obtain the column stiffness were carried out at two sites, the Varberg and Löftaån test sites, while the hydraulic conductivity tests were conducted at the Fjärås and Löftaån test sites.

A special method was used to carry out the in-situ load tests. Four holes were made in the column at different levels to measure the deformations there caused by loads applied stepwise at both ends of the column.

Young's modulus for lime/cement column was evaluated using the finite element method by finding the best fitting curve for the load-displacement relationship obtained from the field measurements. Short-time creep deformation was measured during each load step.

The column stiffness obtained from field tests was higher than that evaluated from unconfined compression tests, carried out in laboratory. The load-deformation curve consists of an almost straight part, linear with low deformation, followed by a non-linear part with large deformations. The creep deformations in the columns increase rapidly directly at the beginning of the non-linear portion of the load-deformation curve, and a creep load capacity can be evaluated, see Figure S. 4.

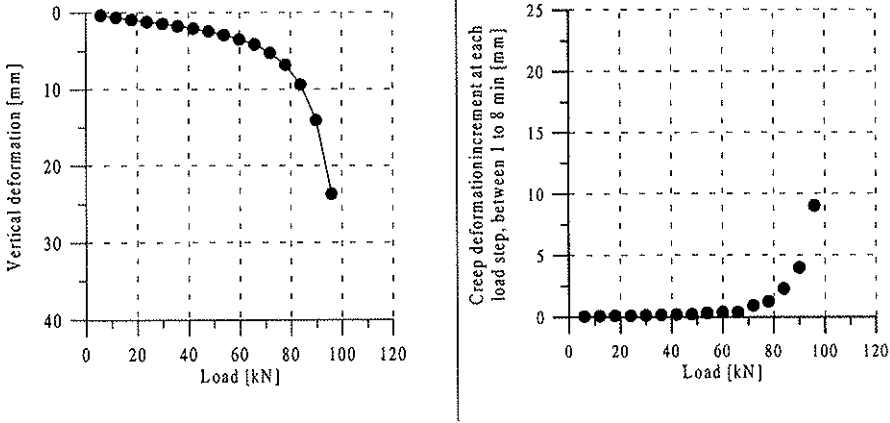


Figure S. 4 Total and creep deformation at the top of column 7 as a function of load.

No standard method exists so far for testing and evaluating the hydraulic conductivity of lime/cement column in field. The method used in this study is called the packer test and is similar to the method used for measurement of hydraulic conductivity in a rock mass.

Two equations are mainly used to calculate the hydraulic conductivity of the clay based on the in-situ packer test.

In the case of constant head measurement, the hydraulic conductivity is determined by the following equation:

$$K_{col} = \frac{1}{F} \cdot \frac{Q}{\Delta H} \quad (S.6)$$

In the falling head case, the equation is given as:

$$K_{col} = \frac{1}{F} \cdot \frac{A_{c2}}{(t_2 - t_1)} \cdot \ln \left(\frac{H_1}{H_2} \right) \quad (S.7)$$

The shape factor F , shown in equations (S.6) and (S.7) was evaluated using the finite element program PLAXIS.

The obtained hydraulic conductivity of the lime/cement columns varies between about 10 and 100 times that of the original soil with an average value of about 40.

LABORATORY TESTS

Laboratory tests were carried out on both standard size and large size lime/cement samples to study the mechanical and hydraulic properties of the material.

Unconfined compression and hydraulic conductivity tests were conducted on laboratory prepared and field mixed samples.

Results from unconfined compression test showed that the behavior of the lime/cement columns is less ductile compared with the lime columns. Moreover, it was observed that the failure strain decreased with increasing curing time.

Like previous studies, the stiffness of the lime/cement column increased proportionally to the compressive strength. In connection with the Löftaån test site, the secant modulus, E_{50} , was about 100 times the unconfined compressive strength.

The values of hydraulic conductivity obtained from laboratory tests carried out on field-mixed and laboratory prepared lime/cement samples are similar and vary between 3 and 25 times that of the clay.

Large samples were only extracted from the Löftaån test site and subjected to triaxial compression and hydraulic conductivity tests. The lime/cement columns were trimmed down to a diameter of 0.5 m and 0.5 m height.

There are many reasons why a soil sample may not be fully saturated during laboratory tests. In the case of the lime/cement columns, the manufacturing of the column is performed using a dry stabilizing agent together with very high air pressure, may be up to 500 kPa. Evidence from field and laboratory tests shows that lime/cement columns are not fully saturated. In the case of a stiff material, like the lime/cement column, the presence of a small amount of air will have a large impact on the pore pressure developing during a triaxial test.

The results of the triaxial compression tests confirmed that the lime/cement column behavior is similar to that of stiff overconsolidated clay. Negative pore pressure due to dilation was observed directly before failure.

It was observed that the secant Young modulus, E_{50} , evaluated from the undrained compression triaxial tests increased very slightly with the increase of the confining pressure.

Short-term creep strain measured in all the columns during the undrained triaxial compression tests became significant at about 90 % of the failure load.

The value of the measured hydraulic conductivity when no deviator stress was applied on the sample was about the same as that of standard size samples. An increase in the hydraulic conductivity was observed with the increase of the deviator stress applied on the large sample.

LIST OF SYMBOLS AND ABBREVIATIONS

Roman letters

a_s	ratio of area of the treated soil to the area of the unit cell
A	pore pressure parameter
A_{c2}	area of cylinder 2
A_{col}	cross sectional area of the columns
A_{corr}	corrected area
A_o	initial area of the consolidated specimen
A_p	area of the standpipe
B	pore pressure parameter
c'	effective cohesion
c_u	undrained shear strength of the soil
C_{vsoil}	consolidation coefficient of the untreated soil
C_d	compressibility of soil skeleton
C_w	compressibility of the pore water
d	diameter of the piezometers
D_i	diameter of the sample
e	void ratio of the medium at any time t
E_{50}	secant modulus evaluated at stress levels related to 50 % of the failure load
$E_{50,col}$	column secant modulus evaluated at stress levels related to 50 % of the failure load
E_{col}	Young's modulus of the column
E_{50}''	undrained secant modulus at 50 % of the failure load
E_{qu}	secant modulus related to stress failure
E_{ref}	reference Young's modulus
F	shape factor
g	acceleration due to gravity
G	shear modulus
G_s	column specific gravity
G_{col}	shear modulus of the columns
G_{soil}	shear modulus of untreated soil
h	hydraulic head
h_z	elevation head
H	depth of the column-soil system
H_1, H_2	the heads between which the hydraulic conductivity is determined
H_h	hydraulic head

H_i	Height of the sample
h_p	pressure head
i	hydraulic gradient
k	intrinsic hydraulic conductivity
K	bulk modulus
K_{col}	hydraulic conductivity of the column
K_{soil}	hydraulic conductivity of the soil
L_{col}	length of the column
L	length of the column
l	length of the piezometers
M	oedometer compression modulus
M_{col}	oedometer compression modulus of the columns
M_{soil}	oedometer compression modulus of the untreated soil
n	stiffness ratio between the treated and untreated soils, (M_{col}/M_{soil}).
n_i	initial porosity
\bar{p}	mean effective stress, $(\sigma'_1 + \sigma'_2 + \sigma'_3/3)$
P	absolute pressure in the pore air after application of stress increment.
P_i	initial absolute pressure in the pore air corresponding to $S_{r,i}$
q	deviator stress, $\sigma_1 - \sigma_3$
q	specific discharge
Q	flow rate
r_{col}	radius of the column
r_{eff}	effective radius which is related to the column spacing
r_{eq}	radius of the unit cell
S	spacing of the columns
S_r	degree of saturation
$S_{r,i}$	initial degree of saturation
$t1$	the time when the water level in the standpipe is $H1$
$t2$	the time when the water level in the standpipe is $H2$
Tr	time factor for radial drainage
T_v	time factor for vertical drainage
u	excess pore water pressure
\bar{u}	average value of excess pore water pressure
u_{soil}	excess pore water pressure in the untreated soil
v	discharge velocity
$V_{col,o}$	volume after consolidation
w	water content
w_n	natural water content
w_r	radial deformation

$w_r(r_{col}, t)$	radial deformation at the boundary between the column and the surrounding soil at time t
$w_r(r_{eq}, t)$	radial deformation at the outer vertical boundary of the unit cell at time t
X	integration constant
Y	integration constant
Z	integration constant

Greek letters

β	compressibility of the fluid
χ_1	constant depending on the geometry of the unit cell and the stiffnesses of the lime/cement column and the surrounding soil
δ_{col}	vertical displacement of the column
ΔH	constant difference in head
Δr	Distance increment in the r-direction
Δu	change in pore pressure under undrained condition.
ΔV_{col}	volume change
Δz	Distance increment in the z-direction
$\Delta \sigma_3$	change in the isotropic cell pressure.
ϵ_a	axial strain
ϵ_{bou}	radial deformation at the boundary between the two materials (at $r = r_{col}$)
ϵ_i	strain in the i -direction
ϵ_j	strain in the j -direction
ϵ_k	strain in the k -direction
ϵ_r	radial strain
ϵ_{vol}	volumetric strain
ϵ_z	vertical elastic strain in the column-soil system
$\epsilon_z(t)$	vertical elastic strain in the column-soil system at time t
ϵ_θ	tangential strain
ϕ	angle of internal friction
ϕ'	effective angle of internal friction
Φ	Yoshikuni's potential function
$\overline{\Phi}$	average value of the potential function
$\Phi(t)$	potential function at time t
γ	unit weight
γ_{col}	column unit weight

γ_w	unit weight of the water
λ	Lamés constant
λ_{col}	elastic coefficient (Lamés constant) of the columns
λ_{soil}	elastic coefficient (Lamés constant) of the surrounding soil
μ	absolute viscosity of the fluid
ν	Poisson's ratio
ν_{col}	Poisson's ratio of the column
ν_{soil}	Poisson's ratio of the untreated soil
ρ_f	mass density of the fluid
σ_1	axial stress
σ_3	radial stress
σ_i	stress in the i -direction
σ_j	stress in the j -direction
σ_k	stress in the k -direction
σ'_r	effective radial stress
σ_{rb}	radial stress at the boundary between the column and the untreated soil
$\sigma_r(r_{col}, t)$	radial stress at the boundary between the column and the surrounding soil at time t
σ_{top}	vertical stress at the top of the column
σ_v	vertical applied stress
σ_{vcol}	vertical stress in the lime/cement column
$\sigma_{vcol}(t)$	vertical stress in the lime/cement column at time t
σ_{zcol}	column stress in the z -direction
$\overline{\sigma_{vsoil}}(t)$	average vertical stress in the untreated soil at time t
σ_{vsoil}	vertical stress in the untreated soil
$\sigma_{vsoil}(t)$	vertical stress in the untreated soil at time t
$\sigma'_{vsoil}(t)$	effective vertical stress in the untreated soil at time t
σ_y	vertical stress in the column at depth y
τ_y	shear stress on the column periphery at depth y
ω	rotation of displacement
ψ	dilation angle
ζ_1	constant depending on the geometry of the unit cell and the stiffnesses of the lime/cement column and the surrounding soil
∇	gradient

Abbreviations

ASTM American Society for Testing and Materials
VFH Variation Falling Head

1. INTRODUCTION

1.1 BACKGROUND

Deep stabilization using lime columns to improve soft soil is a technology, which was developed in Sweden in the middle of the seventies.

The method was mainly used for stabilizing soil under highway and railway embankments, but also for stabilizing cuts and excavations. At the end of the 1980's, the lime/cement column was first introduced and became one of the most frequently used methods for soil improvement. The method is cost effective, as it results in an increased factor of safety against failure as well as drastic reduction of settlement. The number of installed lime/cement columns in Sweden has increased dramatically from about 0.2 million meters of columns per year at the end of the 1980's to about 3.4 million in 1994.

The theories used for design were originally developed for lime columns, Broms (1984). Today, the major parts of all columns are manufactured by using a mixture of lime and cement, which results in somewhat different mechanical and hydraulic properties. Hence, the need for modified design theories and more information about the material properties has been actualized. The uncertainty in the calculation of settlements and how they develop with time has been fairly large. In combination with a simplified method of analysis, this has in many cases probably led to a somewhat conservative design. A study of a number of case records has also shown this to be the case, Edstam (1996).

1.2 OBJECTIVE AND SCOPE OF THE STUDY

The objective of this study is to investigate the mechanical and hydraulic properties of lime/cement stabilized clay to improve the prediction of these properties. Furthermore, this study is aimed at developing a settlement design method that takes account the effect of stiffness difference between the column and the surrounding soil on the rate of consolidation.

The literature survey in this study is focused on different analytical and numerical methods used to calculate the settlement and the rate of consolidation of soft soil stabilized by stone, lime, cement and lime cement columns. Furthermore, the properties of lime and lime/cement treated soil are presented based on laboratory and field tests.

Three mathematical models are presented in this study, two of which are numerical and one is an analytical elastic model.

The analytical model is used to increase the understanding of long-term total settlement as well as the stresses caused by an applied load.

In the first numerical model, the finite element method has been applied using a three-dimensional model to study the stress distribution behavior.

The second numerical model is a finite difference model used to calculate the consolidation settlement of lime/cement column stabilized soil.

In-situ field tests were carried out to determine the stiffness and the hydraulic conductivity of the treated soil at three sites. Special test methods were used for this purpose.

To study the mechanical and hydraulic properties of lime/cement stabilized clay, laboratory tests were conducted on both laboratory mixed and field prepared standard size samples. Furthermore, hydraulic conductivity and triaxial compression tests were carried out on large lime/cement samples, of 0.5 m height and 0.5 m diameter, extracted from the Löftaån test site.

2. SURVEY OF LITERATURE

2.1 INTRODUCTION

Settlements are usually calculated under the assumption that the strains in the column and the surrounding soils are equal and that no distribution of the load occurs within the stabilized area. Normally, the settlements are monitored during construction, to ensure that the stabilized soil functions as expected. Edstam (1996) reported that, on average, the observed settlements were only 40 % of those calculated when lime and lime/cement columns were used to reduce the settlement.

The settlement of deep stabilized soil and its development with time is dependent on the modulus of compressibility and the hydraulic conductivity of the treated as well as the untreated soil. A fair knowledge of these two parameters is needed to decide the method of analysis to be used for estimating the settlement and the rate of consolidation for the modified soil. Many techniques are used for improvement of soft soils. Among these methods are: stabilization by stone columns, cement columns, lime columns and lime/cement columns.

The common factor for these methods is that a stiffer material replaces part of the soft soil. On the other hand, the hydraulic properties of this material are different, which in turn means that different boundary conditions must be used to evaluate the settlement as a function of time. Several methods were developed to estimate the settlement of stabilized soil, using both analytical and numerical solutions by applying linear or nonlinear material properties. Some of these methods are discussed in the next section.

Field and laboratory tests used to predict the lime/cement column modulus and hydraulic properties are presented in another section.

2.2 SETTLEMENT ANALYTICAL METHODS

Several theoretical approaches have been presented to predict the deformation behavior of soft soil improved by using columnar inclusions such as stone, cement, lime and lime/cement columns. The concept of a unit cell is the base of most of the analytical methods developed to predict the settlement of the modified soil. The unit cell is part of a treated soil where the loaded area is of long extent compared with the depth, and hence the stress concentration ratio is constant with depth. The unit cell consists of the column inclusion surrounded by the soft soil media. The stress concentration ratio is the distribution of the vertical stress within the unit cell and expressed as

$$m = \frac{\sigma_{col}}{\sigma_{soil}}$$

Where

σ_{col} stress in the column
 σ_{soil} stress in the surrounding soil

The unit cell is assumed to rest on rigid frictionless strata and the outer vertical boundaries surrounding the soil are confined by stiff frictionless wall.

The radius of the unit cell r_{eq} , is related to the column spacing so that

$$r_{eq} = c_g \cdot S$$

Where

c_g factor depending on geometry
 S column inclusion spacing

The factor c_g is equal to 1.13 and 1.05 respectively for a square and a triangular column pattern.

The column inclusion is considered as a solid cylinder with a radius of r_{col} . The applied vertical stresses at the top of the cell unit are sheared by both the column inclusion and the surrounding soil according to their stiffness and geometry. This means that they undergo the same total vertical strain and, hence, no slips take place at the column soil interface.

Goughnour (1983) presented a unit cell model for evaluating the settlement of a vertically loaded stone column in soft soil. Depending on the magnitude of the applied load and the confining lateral pressure, two analyses, plastic and elastic, were proposed. If the stone column is

assumed to be incompressible and the surrounding soft soil to act ideally as saturated clay soil, then the applied load is sheared almost equally between the two materials, and no immediate settlement will take place. However, the stone column is a permeable material, which provides a short drainage path for the surrounding soil. The soft soil will immediately start to consolidate, which results in load transfer from the soft soil to the stone column. If the total applied load is less than a certain value, then only elastic deformation will occur. On the other hand, if the applied load is higher than the limited value, then the column strength will be exceeded and part of the column will reach a state of plastic behavior.

In the elastic analysis, both the stone column and the surrounding soil were assumed to behave as linear elastic materials. The behavior of the stone column was described by the modulus of elasticity E_s and Poisson's ratio ν_s , while special attention was paid to the selection of the surrounding soft soil. The modulus of elasticity of the clay soil was determined as

$$E_c = \frac{(1 + \nu_c) \cdot (1 - 2 \cdot \nu_c) \cdot (1 + e_o) \cdot (P_{AVG})_{vc}}{0.435 \cdot (1 - \nu_c) \cdot c_c}$$

Where

ν_c	clay soil Poisson ratio
e_o	initial void ratio of the clay soil
c_c	compression index of the clay soil
$(P_{AVG})_{vc}$	average vertical effective stress on the clay for the loading increment

In case of normally consolidated soil, the clay Poisson's ratio was calculated based on the initial coefficient of earth pressure K_o as

$$\nu_c = \frac{K_o}{1 + K_o}$$

The vertical strain was calculated as

$$\varepsilon_v = F_2 \cdot \overline{m_v} \cdot (\Delta p)_v^* \quad (2.1)$$

Where

ε_v	Vertical strain (equal for stone column and surrounding soil)
$F_2, \overline{m_v}$	factors depending on the replacement area a_s , which is the ratio of the cross-sectional area of stone column to the cross-sectional area of the

	unit cell, and the elastic properties of the stone and surrounding soil material
$(\Delta p)_v^*$	effective vertical stress increase averaged over horizontal projected area of the unit cell

In the plastic analysis, yielding in the stone column was assumed to obey the Mohr-Coulomb criterion, which can be defined by the angle of internal friction $\bar{\phi}_s$. Terzaghi's consolidation theory, modified to accommodate both radial and vertical strains, was used to define the behavior of the in situ soil. The calculation of the initial stresses is an important phase in the plastic analysis, and the disturbance caused by the installation processes of the column inclusions, be it stone, cement, lime or lime/cement column is always a very complicated problem to deal with. In the case of stabilization of normally consolidated clay using stone column, it was assumed that the coefficient of earth pressure during the short time of construction would revert very close to the initial value K_o .

When the clay soil starts to consolidate, the coefficient of earth pressure will, due to the radial strains induced by the column bulging, start to increase to approach a value between K_o and $1/K_o$ depending on the geometry of the problem. For example, if the spacing between the columns is large, then the radial strains in the surrounding soil will be small, and very limited increases in the coefficient earth pressure take place.

The vertical strain of the plastic phase was calculated as

$$\varepsilon_v = (1 - a_s) \cdot \frac{c_c}{1 + e_o} \log_{10} \left[\frac{(P_o)_{vc} + \Delta P}{(P_o)_{vc}} \right] \quad (2.2)$$

$$\Delta P = \frac{(\Delta P)_{vc}^*}{1 + 2 \cdot K_o} \cdot \left[1 + K + K_o \begin{pmatrix} K & \text{if } K > 1 \\ 1 & \text{if } K < 1 \end{pmatrix} \right]$$

Where

$(P_o)_{vc}$	initial effective vertical stress in the clay
$(\Delta P)_{vc}^*$	effective vertical stress increase in clay averaged over the horizontal projected area of the clay
K	earth pressure coefficient applying to the load increment

In equation (2.2), besides the unknown vertical strain ε_v , the effective vertical stress in the clay $(\Delta P)_{vc}^*$ is unknown as well.

The vertical strain in the cell without the column inclusion can simply be written as

$$\varepsilon_v^{unstab} = \frac{c_c}{1 + e_o} \log_{10} \left[\frac{(P_o)_{vc} + (\Delta P)_v^*}{(P_o)_{vc}} \right]$$

Considering the above equation, a reduction factor, R_p , can be defined as the ratio of the computed strain in the unit cell element, when the stone column was considered to be in the plastic state, to the vertical strain calculated from the above equation. The author presented a series of curves to show the relation between the plastic reduction factor R_p and the ratio of the effective vertical stress increase, $(\Delta p)_v^*$, to the effective vertical stress increase in the clay, $(\Delta P)_{vc}^*$ for different values of replacement ratio, a_s , and different angles of internal friction $\bar{\phi}_s$.

Another elastoplastic model was presented by Wallays et al. (1983). The load transfer mechanism and the settlement caused by the applied load in the soil, stabilized by using stone or sand inclusion, were analyzed for both a rigid and a flexible raft foundation supported by the modified soil.

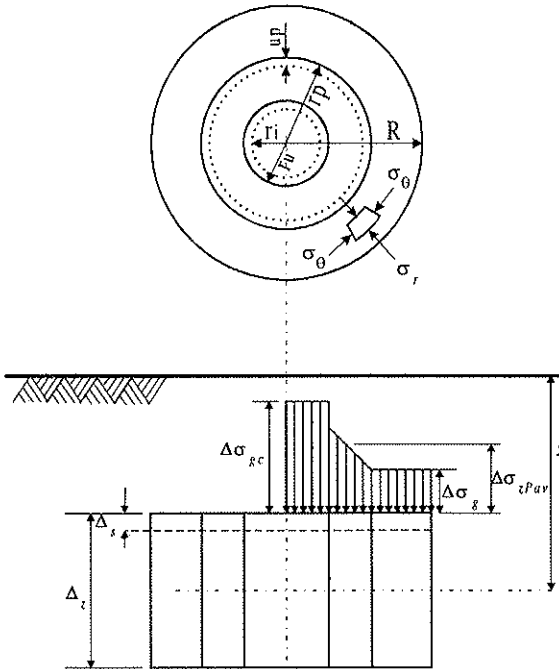


Figure 2.1 Definition of the soil layer with Δz thickness, after Wallays et al. (1983).

In the case of a rigid raft, the deformation in the column and the surrounding soil at a certain level was assumed to be equal, while in the case of a flexible raft the settlements of the surrounding soil were only slightly larger than those of the column inclusions.

When the vertical load was applied by the rigid raft to the modified soil, the loads were transferred to the columns because of the bulging, and the initial radius of the column, r_i , increased to become equal to r_u , see Figure 2.1.

Since the radial deformation at the unit cell boundaries located at $r = R$ from the cell center was prevented, the bulge of the column could cause yield in the surrounding soil. Thus, the surrounding soil was divided into two parts; an inner soil ring, with thickness of $(r_p - r_u)$, which was in the plastic state and the rest of the soil bounded by the cell radius, R , and the plastic radius, r_p , was in the elastic state.

The plastic radius was evaluated to be a function of the unit cell radius, the modulus and Poisson's ratio of the surrounding soil, the vertical stress increase in the elastic soil ring, the radial stress at the unit cell boundaries and the angle of internal friction of the soil. The effective soil cohesion was neglected in this analysis.

The vertical stress acting on the plastic ring varied between a maximum value at the column boundary and a minimum value at the boundary between the elastic and plastic rings and, for simplicity, an average stress was assumed in the analysis. The average vertical strain in the plastic ring was assumed to be equal to the vertical strain in the elastic soil ring.

As for the deformation and the vertical stress in the column inclusion, a condition was first defined to show whether the column is in the elastic or plastic state. This condition is dependent on many factors, such as the column elastic properties, the shear parameters, the initial stresses, the column geometry and the radial contact pressure. Equations were then derived to evaluate the stresses and the axial strains in the column for the elastic and plastic states.

In most of the analytical models published, the load assumed to be shared between the column inclusion and the surrounding soil is based on the assumption that the two materials undergo the same vertical deformation, that is horizontal sections in the ground remain horizontal. This can be the case for rigid loading, but for flexible loading the deformation of the two materials is obviously different.

Alamgir et al. (1996) presented a simple theoretical approach taking the difference in deformation between the column inclusion and the surrounding soil into account. For the sake of simplicity, only elastic analysis was considered. The analysis was made so that the column-soil system was divided into a number of uniformly loaded elements.

Since only elastic analysis was considered, the column-soil interface remained elastic as well and, thus, no slip took place between the two materials. As a result the displacements of the column and the surrounding soil at the interface were the same. The analysis neglected the effect of the radial deformation and hence only the vertical deformations of the system were considered.

The most important step in the analysis was to define a deformation shape of the column inclusion and the soil. The deformation of the column was assumed to be the same across the column area, while the deformations in the surrounding soil had the same value as the column deformation at the column-soil interface and then decreased to a minimum value at the unit cell outside boundary.

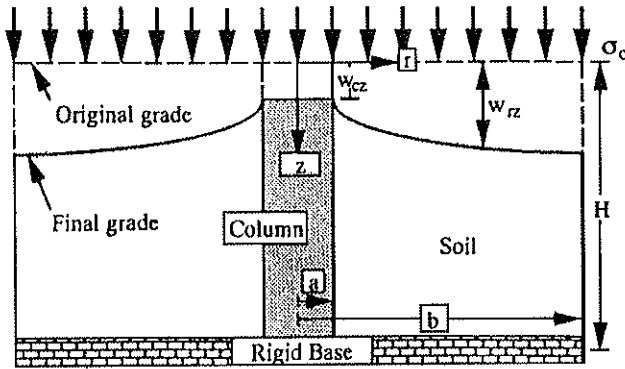


Figure 2.2 Assumed mode of deformation, after Alamgir et al. (1996).

Alamgir et al. supported this assumption by experimental evidence and experiences gained from the field of reinforced earth. The equation used to define the deformation in the surrounding soil was written as

$$w_{rz} = w_{cz} + \alpha_{cz} \cdot \left[\frac{r}{a} - e^{\beta_c \left(\frac{r}{a} - 1 \right)} \right] \quad \text{for } a \leq r \leq b$$

Where

- a radius of the column
- b radius of the unit cell
- r radial distance measured from the center of column
- w_{rz} displacement of the surrounding soil at depth z and radius r
- w_{cz} displacement of the column at depth z
- α_{cz}, β_c displacement parameters

The above equation shows that the deformation in the soft soil varies both with depth and radius distance, and consequently the mobilized shear stresses and the shear strains will vary in the two directions.

The shear strain, γ_{rz} , and shear stress, τ_{rz} , in the soft soil can be expressed as

$$\gamma_{rz} = \frac{\alpha_{cz}}{a} \cdot \left[1 - \beta_c \cdot e^{\beta_c \left(\frac{r}{a} - 1 \right)} \right]$$

$$\tau_{rz} = \frac{E_s \cdot \alpha_{cz}}{2 \cdot a \cdot (1 + \nu_s)} \cdot \left[1 - \beta_c \cdot e^{\beta_c \left(\frac{r}{a} - 1 \right)} \right]$$

Due to symmetry, the shear stresses at the outer boundary are equal to zero, which will cause that

$$\beta_c \cdot e^{\beta_c \left(\frac{b}{a} - 1 \right)} - 1 = 0$$

The value of β_c is only a function of the spacing ratio b/a , and this can be expressed graphically in Figure 2.3.

The two remaining factors needed to evaluate the deformation in the system are the vertical deformation of the column, w_{cz} and the α_{cz} factor.

The vertical deformation of the column can be obtained by considering the vertical equilibrium of an element of the column, where the normal stress in the column can be derived first and then the vertical deformation in the column be obtained, which is directly related to the normal stress by the column modulus of elasticity.

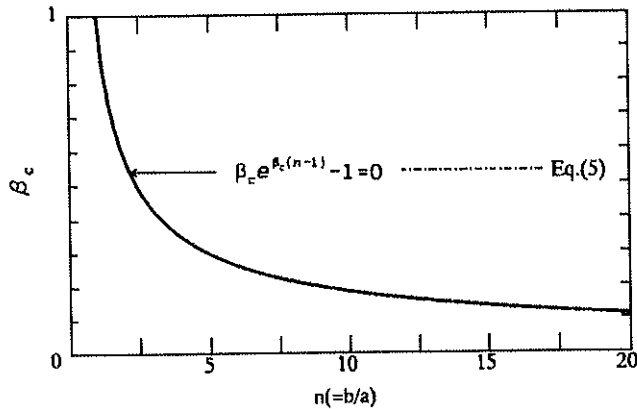


Figure 2.3 Variation of β_c with the spacing of the columns, after Alamgir et al. (1996).

The factor α_{cz} was obtained by first considering the vertical equilibrium of a soft soil element located along the outer boundaries of the unit cell and then combined with the displacement compatibility between the column and the surrounding soil. The results for a typical problem solved by using this approach were compared with results calculated by the finite element program CRISP, and fair agreement was achieved.

Poorooshasb and Meyerhof (1997) introduced two very interesting mathematical models for analyzing the behavior of stone columns and lime columns. In these two analyses, only end bearing columns were treated.

In the first model, the lime-soil system materials were assumed to behave as a linearly deformable homogeneous material defined by the modulus of elasticity, E , and constant Poisson's ratio, ν . Both vertical and radial deformations were considered and the column-soil system was assumed to deform equally.

The equations derived to evaluate the deformation of the column-soil system are

$$\begin{aligned}\frac{UDL}{(\delta/L_c)} &= A \cdot \{1 + B \cdot \nu_c\} \cdot \frac{b^2 - a^2}{b^2} + \\ &\{E_c + 2 \cdot \nu_c \cdot [A \cdot C \cdot (1 + B \cdot \nu_c) + D \cdot \nu_c]\} \cdot \frac{a^2}{b^2} \\ A &= \frac{(1 - \nu)}{(1 - \nu - 2 \cdot \nu^2)} \cdot E_s \\ B &= \frac{2 \cdot \nu}{1 - \nu} \cdot \frac{a^2}{b^2 - a^2} \\ C &= \frac{\nu}{1 - \nu} \\ D &= \frac{(1 + \nu) \cdot a^2 + (1 - \nu) \cdot b^2}{(1 - \nu^2) \cdot (b^2 - a^2)} \cdot E_s\end{aligned}$$

Where

a	radius of the column
b	radius of the unit cell
E_c	Young's modulus of the column
E_s	Young's modulus of the soil
ν_c	Poisson's ratio of the column

ν	Poisson's ratio of the surrounding soil
UDL	intensity of the uniformly distributed load carried by the rigid mat plus the self-weight of the mat.
δ	settlement of the system
L_c	column height

In the case of the second model, where the behavior of stone columns was analyzed, the surrounding soil in the unit cell was assumed to possess material linearity, while elastoplastic behavior was assumed for the column material.

Two curves, η/ε_1 and V/ε_1 , are usually used to define the deformation of the granular material, where η is the ratio of the major stress, σ_1 , to the minor stress, $\underline{\sigma}_3$, ε_1 is the axial strain of the column and V is the volume strain of the column with a negative value for a dilatatory material. Two equations were then derived to represent the deformation behavior in the stone column. These equations are:

$$\eta = \frac{\sigma_1}{\underline{\sigma}_3} = \eta(\varepsilon_1) \quad (2.3)$$

$$V = \varepsilon_1 + 2 \cdot \varepsilon_3 = V(\varepsilon_1) \quad (2.4)$$

It is important to mention that the elastic component of the principal strain increment, $d\varepsilon_1$, was neglected in the derivation and that only the plastic component was considered. The minor principal stress, $\underline{\sigma}_3$, was assumed to be equal to the summation of the side pressure caused by the column tendency to expand laterally plus the residual stress due to the self weight of the soil and the stresses caused during the installation phase.

$$\underline{\sigma}_3 = \sigma_3 + \sigma_{res} \quad (2.5)$$

The load carried by the surrounding soil and the radial stress caused by the lateral column expansion are derived as

$$p = \frac{(1-\nu) \cdot E_s}{1-\nu-2 \cdot \nu^2} \cdot \left[\varepsilon_1 - \frac{2 \cdot \nu}{1-\nu} \cdot \frac{a^2}{b^2-a^2} \cdot \varepsilon_3 \right] \quad (2.6)$$

$$\sigma_3 = \frac{\nu}{1-\nu} \cdot p - E_s \cdot \varepsilon_3 \cdot \frac{(1+\nu) \cdot a^2 + (1-\nu)b^2}{(1-\nu^2) \cdot (b^2-a^2)} \quad (2.7)$$

The final equation was derived by considering the vertical equilibrium in the column-soil system and was written as

$$UDL = \frac{a^2 \cdot \sigma_1 + (b^2 - a^2) \cdot p}{b^2} \quad (2.8)$$

The above set of equations can now be solved for the six unknown terms. In Sweden, the existing design method used to evaluate the final settlement of soft soil modified by lime and lime/cement column inclusions is based on the assumption that the horizontal sections in the ground remain horizontal in the course of the settlement. In fact this design method is originally based on a model developed by Broms (1984) for soil stabilized by lime columns.

The soft soil in the column-soil system was assumed to behave as linearly elastic material while the column inclusion was assumed to behave as an elastoplastic material. The load-deformation relationship of the column material is shown in Figure 2.4.

The failure strength of the lime/cement column is estimated empirically according to the following equation

$$\sigma_{failure}^{col} = 2 \cdot c_{uk} + 3 \cdot \sigma_h \quad (2.9)$$

Where

- c_{uk} characteristic undrained shear strength of the column
 σ_h total horizontal stress at the column-soil boundary

The column material is elastic when the stress in the column caused by the applied load is smaller than the column creep load, σ_{creep}^{col} .

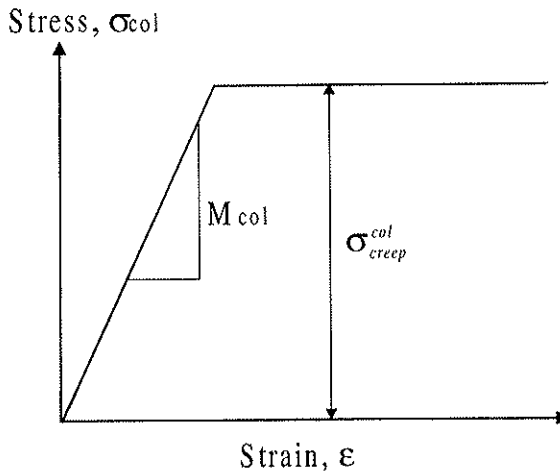


Figure 2.4 Stress- strain relationship of the stabilized soil.

The creep load in the lime and lime/cement column is assumed to be about 65 % of the column failure strength, $\sigma_{failure}^{col}$, calculated by the empirical equation (2.9).

The slope of the line in the stress-strain relationship shown in the above figure is equal to the compression modulus of the column M_{col} .

The load distribution in the column-soil system is assumed to depend on the ratio of the column compression modulus, M_{col} , to the compression modulus of the surrounding soil, M_{soil} as long as the column creep load, σ_{creep}^{col} , is not exceeded and the stress in the column-soil system can be written as

$$\sigma_{soil} = \frac{q}{1 + (m - 1) \cdot a_s} \quad (2.10)$$

$$\sigma_{col} = \frac{m \cdot q}{1 + (m - 1) \cdot a_s} \quad (2.11)$$

Where

σ_{col}	vertical stress in the column
σ_{soil}	vertical stress in the surrounding soil
q	total applied stress
m	compression modulus ratio, (M_{col}/M_{soil})
a_s	area replacement ratio, ($[d/D]^2$)
d	column diameter
D	diameter of the cylindrical cell

In the light of the above discussion, the calculation of the settlement of the reinforced block can be treated in two cases. In the first case when the column vertical stress is smaller than the creep stress, the settlement of the reinforced block can simply be calculated as

$$\Delta h_1 = \frac{\sigma_{col}}{M_{col}} \cdot L_{col} = \frac{\sigma_{soil}}{M_{soil}} \cdot L_{col} \quad (2.12)$$

Where

L_{col}	length of the column
-----------	----------------------

In the second case, when the stresses in the column exceed the creep stress, then the vertical stress in the column must be set to be equal to the creep stress. As a consequence, the stresses will redistribute and the stress in the surrounding soil increase. In this case, the settlement of the reinforced

block will be dominated by the surrounding soil and the vertical settlement become equal to

$$\Delta h_1 = \frac{q - \sigma_{creep}^{col} \cdot a_s}{M_{soil}} \cdot \frac{L_{col}}{(1 - a_s)} \quad (2.13)$$

It is important to point out that, in the above design method, only the deformation in the reinforced block was discussed. The calculation of the settlement of the untreated soil under the reinforced soil block will be discussed in another section in this chapter.

As mentioned before, some of the physical properties of the different types of column inclusion, such as the hydraulic conductivity, are different from each other. This results in different behavior of the columns during and after installation. From the consolidation analysis standpoint, the stone column which acts as a drain with zero pore water pressure at the common boundaries with the surrounding soil will not behave as the lime/cement or cement columns where the hydraulic conductivity in these two materials is much smaller than stone column.

Another important factor is the deformation condition of the surrounding soil and its effect on the consolidation process.

Terzaghi's consolidation theory is identical with the one-dimensional heat flow. From the thermodynamic point of view, it is possible to extend Terzaghi's one-dimensional consolidation theory to two or three-dimensional cases.

Barron (1948) presented a solution for a radial consolidation by considering Terzaghi's equation for three-dimensional consolidation in polar coordinates. The basic partial differential equation for three-dimensional consolidation can be written as

$$\frac{\partial u}{\partial t} \cdot \left(\frac{a_v}{1+e} \right) = \frac{k_v}{\gamma_w} \cdot \left(\frac{\partial^2 u}{\partial z^2} \right) + \frac{k_h}{\gamma_w} \cdot \left(\frac{1}{r} \cdot \frac{\partial u}{\partial r} + \frac{\partial^2 u}{\partial r^2} \right) \quad (2.14)$$

Where

u	excess pore water pressure
t	time
a_v	coefficient of compressibility of the soil
e	void ratio of the soil
K_v	vertical coefficient of hydraulic conductivity of the soil
K_h	horizontal coefficient of hydraulic conductivity of the soil
γ_w	unit weight of water

From the viewpoint of the soil deformation, Barron presented two different cases for the solution of equation (2.14). These are the equal and free vertical strain cases. During radial consolidation with free strain permitted, the soil around the drain well consolidates and compresses faster than the soil located away from the drain center. This will cause differences in settlement in the soil surrounding the drain well. In the case of free strain, it was assumed that these differential settlements did not affect the redistribution of the load to the soil or the rate of consolidation.

The arching developed in the material above the compressible soil, such as road embankments, will redistribute the load, to some extent depending on the amount of the arching. It can happen that in a severe condition, the arching will develop to such an extent that the load will redistribute, whereby all vertical strains in the consolidated soil become equal.

This condition can be obtained in the laboratory when using a rigid loading platform. In the field, this may be obtained if the ratio of the vertical drainage path, H , to the diameter of soil cylinder dewatered by the drain, d_e , is large.

The solution of equation (2.14) for the case of equal vertical strain is

$$U = 1 - \exp \left[\frac{-8 \cdot T}{F(n)} \right] \quad (2.15)$$

in which

$$F(n) = \frac{n^2}{n^2 - 1} \cdot \ln(n) - \frac{3 \cdot n^2 - 1}{4 \cdot n^2} \quad (2.16)$$

$$T = \frac{C_v \cdot t}{d_e^2}$$

$$n = \frac{d_e}{d_w}$$

Where

C_v	coefficient of consolidation
d_w	diameter of the vertical drain

Barron showed that the difference in numerical values of the average degree of consolidation obtained from equal and free vertical strain cases is small. At 50 % consolidation and above, the values of the two solutions are almost identical. See Figure 2.5.

In the consolidation problem, the deformation conditions are a very important factor, because the rate of the K_0 -condition of a cylindrical sample is different from that of the isotropic condition. The consolidation in the isotropic case is caused by an increment in all-round pressure, which is kept constant during the course of the consolidation process.

The consolidation in the second case is caused by a deviator stress developed as the lateral confining pressure decreases when, at the same time, no lateral displacement is allowed at the outside boundaries.

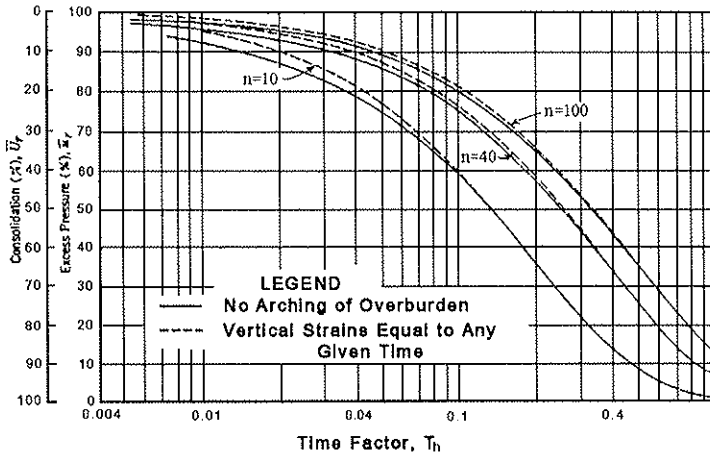


Figure 2.5 Comparison of average consolidation rate in clay cylinders by radial drainage only for various values of n under conditions of equal vertical strain at any given time and no arching of overburden, after Barron (1948).

The dissipation of the pore water pressure occurs not only because of the squeezing, like the case in the isotropic consolidation, but also due to the stress relaxation in the horizontal direction.

The mechanism of the K_0 -consolidation clearly has been explained by Nakano and Ito (1983), and is presented briefly below.

The dissipation of pore water pressure, Δu , in the K_0 -consolidation is expressed as

$$\Delta u = \Delta u' + \Delta u'' \quad (2.17)$$

where

$\Delta u'$ change in pore water pressure due to consolidation drainage (isotropic)

$\Delta u''$ change in pore water pressure due to change in the lateral confining pressure

Since $\Delta u''$ is proportional to the change in the lateral confining pressure $\Delta\sigma_3$, then

$$\Delta u'' = \alpha \cdot \Delta\sigma_3 \quad (2.18)$$

where

α coefficient of pore water pressure

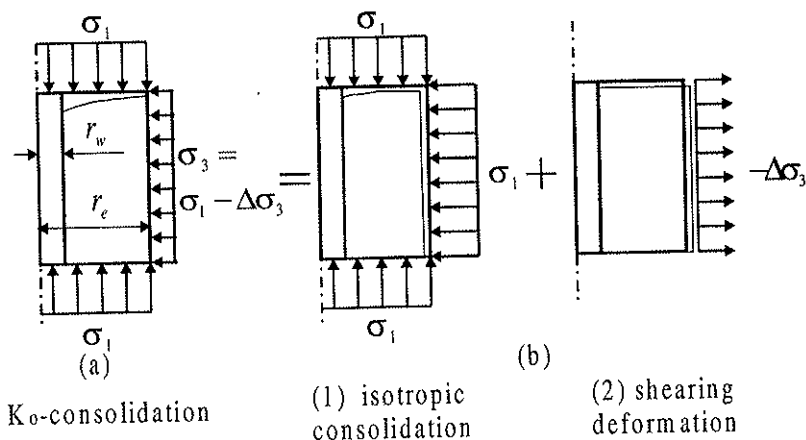


Figure 2.6 Deformation characteristics of K_0 -consolidation, after Nakano and Ito (1983).

The radial displacement at the outside boundary of the clay cylinder caused by the isotropic stress can be written as

$$u'_r(r_e, t) = \frac{1 - 2\bar{\nu}}{\bar{E}} \cdot \int_{r_w}^{r_e} \Delta u'(r, t) \cdot dr \quad (2.19)$$

where

$\bar{\nu}$ Poisson's ratio in drained condition
 \bar{E} drained Young's modulus

while in case (2) shown in Figure 2.6 the radial deformation at the same boundary is

$$u''(r_e, t) = -\frac{1}{2 \cdot E} \cdot \Delta\sigma_3 \cdot (r_e - r_w) \quad (2.20)$$

where

E Young's modulus in the undrained condition

Since the radial deformation at the outer boundary of the clay cylinder is equal to zero, the summation of equations (2.19) and (2.20) is equal to zero. From the last relationship, the two equations can be solved for the lateral confining pressure, $\Delta\sigma_3$, as

$$\Delta\sigma_3(t) = 2 \cdot E \cdot \frac{1}{r_e - r_w} \cdot \int_{r_w}^{r_e} \Delta u'(r, t) \cdot dr \quad (2.21)$$

The volumetric strain due to consolidating drainage is proportional to the change in isotropic stress. Since the volumetric strain in case (2) is equal to zero, the volumetric strain in the K_0 -consolidation is expressed as

$$\varepsilon_v = \frac{3 \cdot (1 - 2 \cdot \bar{\nu})}{\bar{E}} \cdot (\Delta u(r, t) - \alpha \cdot \Delta\sigma_3) \quad (2.22)$$

Equation (2.22) can now be substituted into the equation of continuity of the radial consolidation under the axisymmetric condition to obtain the following equation

$$\frac{\partial u}{\partial t} = c_{v3} \cdot \left(\frac{\partial^2 u}{\partial r^2} + \frac{1}{r} \cdot \frac{\partial u}{\partial r} \right) + f(t) \quad (2.23)$$

In which

$$f(t) = \frac{\partial}{\partial t} (\alpha \cdot \Delta\sigma_3) = \frac{\partial}{\partial t} \left(\frac{2 \cdot E \cdot \alpha}{r_e - r_w} \cdot \int_{r_w}^{r_e} \Delta u'(r, t) \cdot dr \right) \quad (2.24)$$

It can be noticed that, besides the term usually used in the radial consolidation equation, another time dependent term appears in equation (2.23). In fact, this term is a function of the lateral radial stress at the outside boundary of the clay cylinder, $\Delta\sigma_3$, as is shown in equation (2.24).

Yoshikuni and Nakanodo (1975) studied the consolidation process of a clay cylinder with external radial drainage. They believed that the rate of consolidation depended upon the deformation condition.

The triaxial consolidation of a cylindrical sample with external radial flow is usually analyzed by the solution given by Da Silveira as an extension of Terzaghi's theory on radial consolidation problem. This theory ignores the deformation condition during the consolidation process.

Yoshikuni and Nakanodo studied four cases with different deformation conditions. In case (1), a K_0 -consolidation with constant average vertical load, \bar{P}_z , with decreasing radial load, p_r at the boundary was considered.

Case (2) also used K_0 -consolidation, but in this case the radial load, p_r , was kept constant with increasing vertical load, \bar{p}_z . In the third case the clay cylinder was subjected to constant isotropic load. In the last case, the vertical strain was prevented while the radial load was kept constant. All these cases are shown in Figure 2.7.

A new concept called consolidation potential was applied in the analysis of the four cases. Irrotational flow was assumed in the analysis and the consolidation equation derived for the radial condition was written as

$$\frac{\partial u}{\partial t} = C_h \cdot \left(\frac{\partial^2 u}{\partial r^2} + \frac{1}{r} \cdot \frac{\partial u}{\partial r} \right) + \frac{d\Phi}{dt} \quad (2.25)$$

where

C_h coefficient of consolidation in the radial direction
 Φ potential function

For irrotational flow the potential function, Φ , and any point become equal to the average value, $\bar{\Phi}$, and can be expressed as

$$\Phi = \bar{\Phi} = (\lambda + 2 \cdot \mu) \cdot \varepsilon_v + \bar{u} \quad (2.26)$$

where

λ, μ Lamé's constants related to the bulk modulus K ,
 and the shear modulus, G .

$$\lambda = K - \frac{2}{3} \cdot G, \quad \mu = G$$

\bar{u} average excess pore water pressure

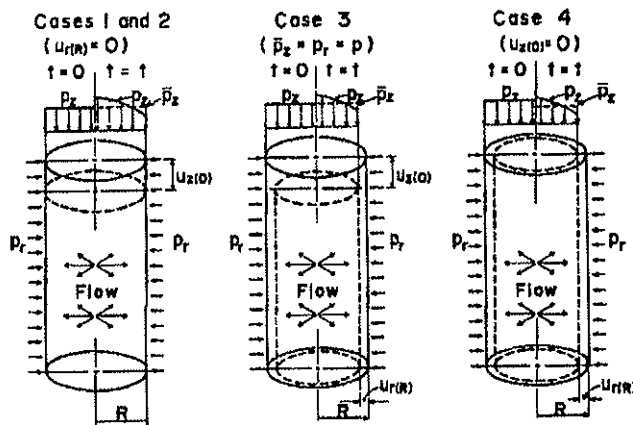


Figure 2.7 The deformation of the clay cylinder in consolidation, after Yoshikuni and Nakanodo (1975).

Yoshikuni and Nakanodo concluded that the rate of consolidation of the clay cylinder by external flow depended on the deformation conditions and Poisson's ratio ν . If Poisson's ratio came close to 0.5, then Terzaghi's equation came close to the actual state of consolidation. The radial consolidation equation developed by Da Silva is applicable in K_0 -consolidation if the average vertical load is kept constant.

Mckinley (1998) derived a coupled formulation for the plane strain axisymmetric consolidation problem. The change of the pore water pressure with time was derived as

$$\frac{\partial u}{\partial t} = c_h \cdot \left(\frac{\partial^2 u}{\partial r^2} + \frac{1}{r} \cdot \frac{\partial u}{\partial r} \right) + (1 + \nu') \cdot \frac{\partial F}{\partial t}$$

in which

$$F(t) = \frac{u}{1 - \nu'} + \delta\sigma'_r + \delta\sigma'_\theta$$

In the same derivation, the summation of the increment of radial and tangential effective stresses, $\delta\sigma'_r$ and $\delta\sigma'_\theta$ is related to the strain deformations in the z , r and θ directions by the following relationship

$$\delta\sigma'_r + \delta\sigma'_\theta = \frac{E'}{(1 + \nu') \cdot (1 - 2 \cdot \nu')} \cdot (\delta\varepsilon_z + \delta\varepsilon_r + \delta\varepsilon_\theta)$$

The time dependent factor, $F(t)$, together with the constant, $(1 - \nu')$, can be written as

$$F(t) \cdot (1 - \nu') = \frac{(1 - \nu') \cdot E'}{(1 + \nu') \cdot (1 - 2 \cdot \nu')} \cdot (\delta\varepsilon_z + \delta\varepsilon_r + \delta\varepsilon_\theta) + u \quad (2.27)$$

Since the oedometer compression modulus can be written as

$$M = \frac{(1 - \nu') \cdot E'}{(1 + \nu') \cdot (1 - 2 \cdot \nu')}$$

and since $M = (\lambda + 2 \cdot \mu)$ and $\delta\varepsilon_v = (\delta\varepsilon_z + \delta\varepsilon_r + \delta\varepsilon_\theta)$, equation (2.27) can be written as

$$F(t) \cdot (1 - \nu') = (\lambda + 2 \cdot \mu) \cdot \delta\varepsilon_v + u \quad (2.28)$$

It is interesting to find that equation (2.28) is very similar to Yoshikuni's potential function, Φ , defined in equation (2.26).

Terashi and Tanaka (1983) applied Yoshikuni's equation to solve the one-dimensional vertical consolidation problem for soft soil stabilized by lime and lime/cement column inclusions. They verified calculated results with results from laboratory experiments, and good agreement was obtained. Furthermore, they showed that the rate of consolidation of composite ground was accelerated with increasing ratio of the coefficient of volume compressibility of the untreated soil, m_{vu} , to the coefficient of volume compressibility of the treated, m_{vt} , see Figure 2.8.

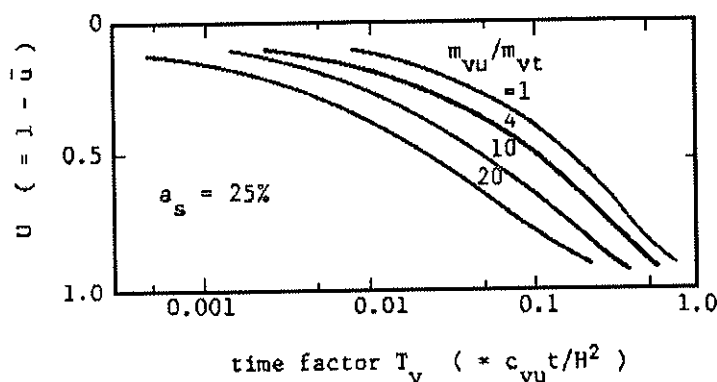


Figure 2.8 Influence of m_{vu}/m_{vt} on the rate of consolidation, after Terashi and Tanaka (1983).

When the ratio becomes equal to 1, then there will be neither stress concentration nor lateral deformation. Yoshikuni and Terzaghi's one-dimensional consolidation theory has then become identical.

Previously in this chapter, an approach developed by Poorooshasb and Meyerhof (1997) was presented. The approach was used to analyze the settlement of soft soil stabilized by stone columns. Non-linear behavior was assumed for the stone column material, while the soft soil surrounding the columns was assumed to possess material linearity. The same authors extended this approach, Poorooshasb and Meyerhof (1996), to study the consolidation settlement of a rigid raft supported by stone columns. The study showed that the rate of consolidation was influenced by many factors, among them the mechanical properties of both the stone columns and the surrounding soil. The consolidation of the soft soil was assumed to occur due to radial drainage toward the column. The pore water pressure at the boundary between the column and the surrounding soil was assumed to

be equal to zero. For the sake of simplicity, Poisson's ratio of the soft soil was assumed to be zero. As in the case of other unit cell models, the radial deformation at the outer boundary of the unit cell was assumed to be zero. However, the lateral stress at the same boundary varies with time and is derived as

$$\sigma_r(b) = \sigma_r + \sigma_\theta - u$$

where

$\sigma_r(b)$	lateral stress at the outer boundary of the unit cell
b	radius of the unit cell
σ_r	radial stress in the soft soil
σ_θ	tangential stress in the soft soil
u	excess pore water pressure

In its initial form, the differential equation derived for radial flow was expressed as

$$\frac{\partial u}{\partial t} = c_h \cdot \nabla^2 u + \frac{\partial \sigma_z}{\partial t} + \frac{\partial \sigma_r(b)}{\partial t} \quad (2.29)$$

where

c_v	coefficient of consolidation in the radial direction
∇^2	Laplace operator
σ_z	vertical stress in the soft soil

Despite the fact that the time dependent factor, $\sigma_r(b)$, derived above is not the same as $\Delta\sigma_3$, derived by Nakano and Ito (1983), which is expressed in equation (2.21), the principal is still the same when comparing equation (2.23) and equation (2.29).

The final form of the consolidation equation was written as

$$\frac{\partial}{\partial t} \left[\left(u - \frac{2}{b^2 - a^2} \right) \cdot \int_a^b r \cdot u \cdot \partial r \right] = c_h \cdot \nabla^2 u - E \cdot \left[\frac{\partial \varepsilon_1}{\partial t} - \frac{2 \cdot a^2}{b^2 - a^2} \cdot \frac{\partial \varepsilon_3}{\partial t} \right] \quad (2.30)$$

where

ε_1	vertical strain
ε_3	lateral strain

A unique relationship was assumed to exist between the vertical and the lateral strains for the case of granular material so that

$$\varepsilon_1 = f(\varepsilon_3)$$

The last term in equation (2.30) was written as

$$E \cdot \left(1 - \frac{2 \cdot a^2}{b^2 - a^2} \cdot \frac{\partial f}{\partial t} \right) \cdot \frac{\partial \varepsilon_1}{\partial t}$$

The problem is of a nonlinear nature due to the vertical strain parameter, ε_1 .

Some of the results obtained by this analysis are shown in Figure 2.9.

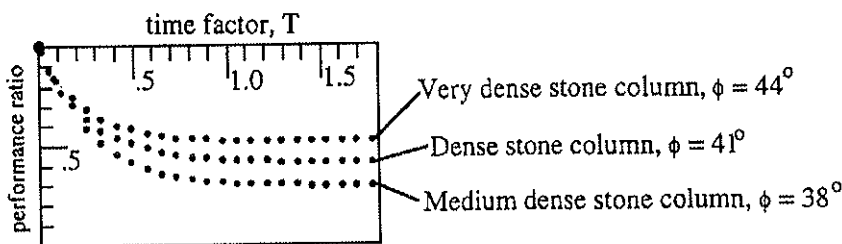


Figure 2.9 Effect of compaction of stone on the settlement of the system. Spacing = 2.5 diameters, after Poorooshasb and Meyerhof (1996).

In the above figure, the performance ratio is defined as the ratio of the settlement of the treated soil to that of the untreated soil. It is clear that the stiffness of the column influences the settlement of the column-soil system. As the Baron equation neglects the stress concentration in the column as well as the deformation behavior of the unit cell during consolidation, Poorooshasb and Meyerhof suggested a method for modifying this equation to take into account the stress concentration in the columns by using the following expression

$$\frac{PR}{PR_{\infty}} = 1 - \exp \left[-\frac{2 \cdot T}{f(\rho)} \right] \quad (2.31)$$

where

- PR the ratio of the settlement of the treated soil compared to the maximum settlement of the untreated soil.
- PR_{∞} the ratio of the maximum settlement of the treated soil to the maximum settlement of the untreated soil.

$$T = \frac{c_h \cdot t}{b^2}$$

$$\rho = \frac{a}{b}$$

$f(\rho)$ a function defined in equation (2.16).

A special case was selected where the column spacing was 2.5 times the diameter of the column and with an internal friction angle, ϕ , of the column equal to 41° . Figure 2.10 shows a comparison between results from the Barron modified equation and that calculated by the proposed numerical solution. Barron's modified equation shows a slightly higher rate of consolidation at the initial stages of the loading (the loads are applied as a step function at time $T=0+$).

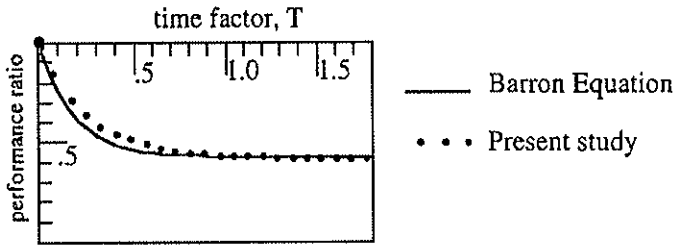


Figure 2.10 Comparison of the modified Barron equation with the present analysis, after Poorooshasb and Meyerhof (1996).

In fact the method used by Poorooshasb and Meyerhof to modify Barron's equation was already used in Sweden when the consolidation of lime columns had been developed. Hansbo (1981) modified the Barron equation so that it could be applied to vertical drain with finite hydraulic conductivity. Furthermore, the drainage condition at the end of the vertical drain was considered as well, and thus the length of the column was considered in the same equation. The new consolidation equation is the same as equation (2.15) presented previously in this section, but the term, $F(n)$, was changed to take into account the two factors explained above and expressed as

$$F(n) = \frac{n^2}{n^2 - 1} \cdot \left[\ln(n) - 0.75 + \frac{1}{n^2} - \frac{1}{4 \cdot n^4} \right] + \left[\frac{n^2 - 1}{n^2} \cdot \frac{1}{r^2} \cdot \frac{K_{soil}}{K_{col}} \cdot L_D^2 \right] \quad (2.32)$$

where

n	the ratio of the radius of the unit cell to the column radius
r	radius of the column
K_{soil}	hydraulic conductivity of the soil
K_{col}	hydraulic conductivity of the drain
L_D	drain length for single drainage path or half drain length for double drainage path

The final settlement of the column-soil system calculated by equation (2.12) or (2.13) was then used to calculate the settlement at any time during the consolidation process. The degree of consolidation was calculated according to Hansbo's equation and set to be equal to the ratio of the settlement of the system at any time, t , to the final settlement.

A major drawback of this method is that the consolidation process is affected by the stress concentration during the whole consolidation period. In Barron's equation the consolidation was assumed to occur with constant applied load during the course of the consolidation while, due to the stiffness difference between the drain and the surrounding soil, load transfer will take place from the surrounding soil to the drain material. This means that consolidation in the surrounding soil will occur with decreasing vertical load. In Figure 2.8, which represents the time factor versus the degree of consolidation, different curves were obtained for different stiffness ratio of the two materials.

To confirm the above point of view, a study was made using the finite element program PLAXIS. Three different columns with soil stiffness ratios, 1, 10 and 40, were selected, and the results from the finite element and the Swedish method based on the Baron modified equation are shown in Figure 2.11. It is important to know that the finite element results are calculated based on the axisymmetric model, where the consolidation is allowed in the radial direction as well as in the vertical direction.

Furthermore, to have the same performance ratio at each of the three cases presented in the figure, the final settlements obtained from the finite element calculations were used with the modified Barron equation instead of using equation (2.12). The hydraulic conductivity of the vertical drain was assumed to be 100 times that of the surrounding soil.

In the case when the stiffness ratio was 1, the change of the performance ratio with time is almost identical. When the stiffness ratio was increased to 10 and 40, the change in the performance ratio between the two methods increased in proportion to the stiffness ratio.

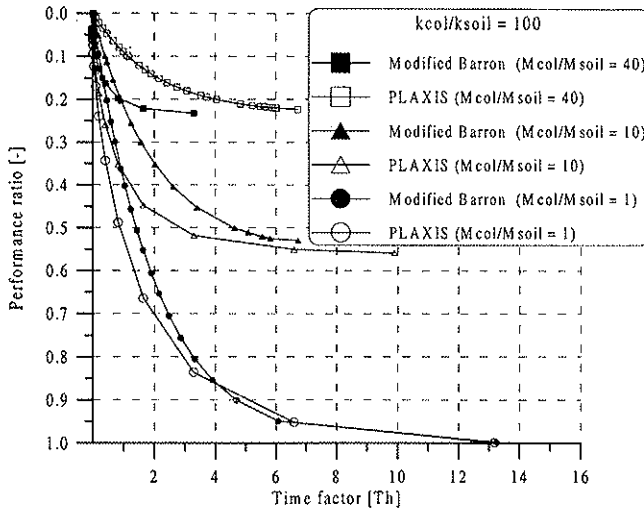


Figure 2.11 Comparison of the finite element results with the Swedish design method based on the modified Barron equation.

Bengtsson and Holm (1984) conducted finite element analyses to study the consolidation settlement of lime columns installed under a road embankment.

Many factors were studied including the function of the lime column acting as a vertical drain and the effect of the overconsolidation on the settlement.

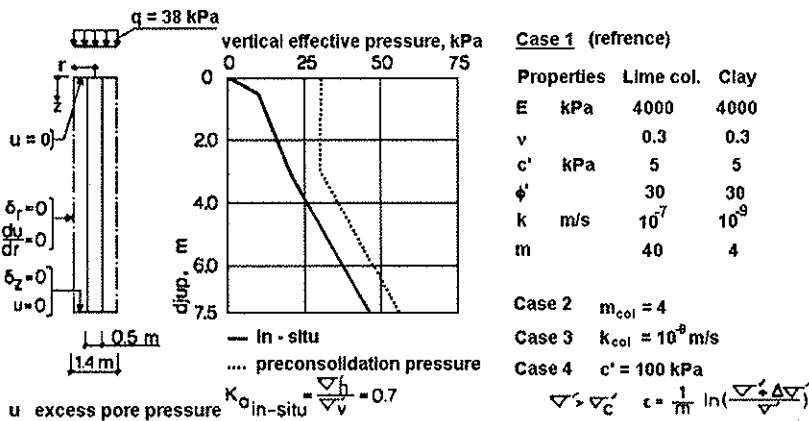


Figure 2.12 The assumptions and the data used in the analysis, after Bengtsson and Holm (1984).

Figure 2.12 presents the geometry, the boundary conditions as well as the conditions for preconsolidation and material properties of the lime column and the clay. Four cases were analyzed. The first case was considered as a reference where Young's modulus, Poisson's ratio and the strength parameters of the two materials were assumed to be equal. Furthermore, the hydraulic conductivity of the lime column was assumed to be 100 times that of the clay. In the second case, the compression index, m , of the lime column was reduced and set to be equal to that of the clay. In the third case the hydraulic conductivity of the column was assumed to be equal to that of the clay. In the last case, the strength of the column was essentially increased.

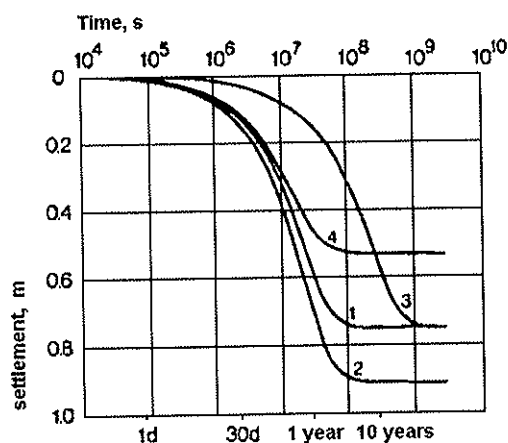


Figure 2.13 Settlement as a function of time for the four cases, after Bengtsson and Holm (1984).

Figure 2.13 shows results from the finite element analysis for the four cases mentioned above. The settlement at the early stage of consolidation for case 1, 2 and 4 was almost identical. An obvious reduction in the rate of consolidation of the system was observed when the hydraulic conductivity of the lime column, in case 3, was reduced. 80 % of the consolidation was obtained within one year when $K_{col}/K_{clay} = 100$, while it took about 10 years to reach the same degree of consolidation when the hydraulic conductivity ratio was reduced from 100 to 1.

Very limited studies have been done on the load distribution and settlement of untreated soil below the stabilized floating block.

Lahtinen and Vepsäläinen (1983) and Liedberg et al. (1996) used the two-dimensional, plane-strain finite element model for the analysis of this

problem. The columns were modeled as rectangular strips with axial stiffness equal to that of the circular column.

Carlsten and Ekström (1995) suggested that the entire applied load at the top of the reinforced block can be transferred to the bottom of the block and then distributed in the untreated soil using an approximate method called the 2:1 method. Liedberg et al. (1996) believed that the settlements in the untreated soil calculated by this method are overestimated by about 25 %. It must be pointed out that the model used to estimate the settlement was, as mentioned above, the plane-strain model and that the thickness of the untreated soil below the 10 m deep reinforced block was only 5 m deep. This no doubt will produce stress concentration due to the boundary effect and, for this particular reason, the settlements of the soil below the reinforced block are in fact overestimated by more than 25 %.

2.3 STIFFNESS AND SHEAR STRENGTH OF LIME, LIME/CEMENT AND CEMENT COLUMNS

The shear strength and the deformation characteristics of a soft soil will change drastically when treated with lime, lime/cement or cement stabilizing agent.

The shear strength of the treated soil increases and it becomes stiffer compared to the untreated soil.

The behavior of the treated soil becomes similar to the behavior of stiff overconsolidated clay. Many laboratory test, and, to some extent, field tests to study the mechanical properties of treated soil are reported in the literature.

The unconfined compression test is the most common laboratory test used for evaluating the shear strength of the treated soil since it is both quick and an inexpensive method. Results from these tests are sometimes used to evaluate the modulus of elasticity of treated soil. However, the determined elasticity modulus must be treated with caution.

Using triaxial and oedometer tests, the modulus of elasticity of treated soil and its change as a function of the stress level can be evaluated. It is interesting to note that the stiffness of the treated soil is proportional to the shear strength.

The treated soil is less ductile compared to the untreated soil, depending on many factors, including, the amount and the type of the added stabilizing agent, curing time and the type of the original soil.

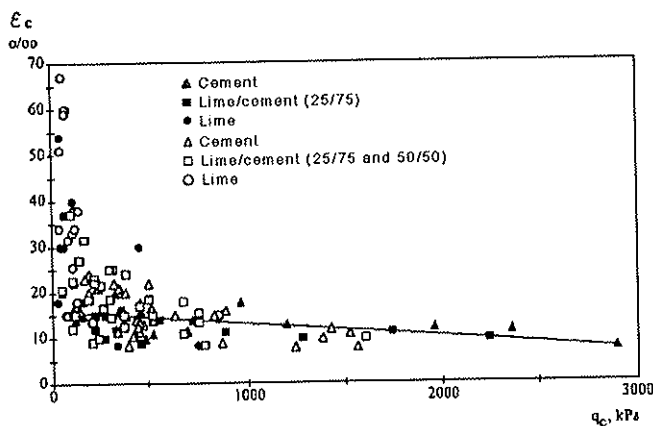


Figure 2.14 Relation between compressive strength and failure deformation, after Åhnberg et al. (1995).

Figure 2.14 shows results from unconfined compression tests carried out on stabilized soil prepared by adding lime, lime/cement and cement stabilizing agent to different types of untreated soil. The figure shows the vertical axial strain at failure, ϵ_c , versus the unconfined compression strength, q_c .

In the case of lime treated soil, the axial strain at failure varied between 1.5 % and 10 % for an interval of unconfined compression strength between 20 kPa and 100 kPa. For lime/cement and cement treated soil, less ductile behavior was observed and the vertical axial strain at failure varied between 0.8 % and 3 % within an unconfined compression strength interval of between 100 kPa and 500 kPa.

Balasubramaniam and Buensuceso (1989) studied the overconsolidation behavior of lime treated soft Bangkok clays.

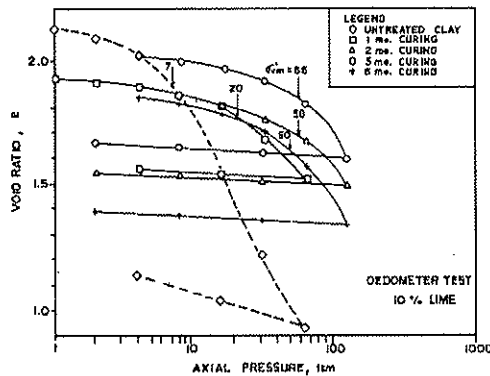


Figure 2.15 Void ratio-axial stress relationships, after Balasubramaniam and Buensuceso (1989).

The water content of the untreated soil was between 76% and 88 %, and the liquid limit was about 104 %. The sensitivity of the clay was about 7. The ratio of the weight of lime to dry weight of the soil used in the study was between 2.5 % and 15 %. However, most of the results presented in the study were mainly based on 10 % lime content since it was believed to be the optimum ratio.

Results from oedometer tests show that the behavior of the treated soil was similar to that of a stiff overconsolidated clay with a low volume change at stresses lower than that equivalent to the preconsolidation pressure, see Figure 2.15. Furthermore, data in the figure clearly shows that there is an increase in the stiffness of the treated soil compared to the untreated soil.

The fact that the treated soil behaved as a stiff overconsolidated clay was observed also from the consolidated undrained triaxial test results presented in Figure 2.16.

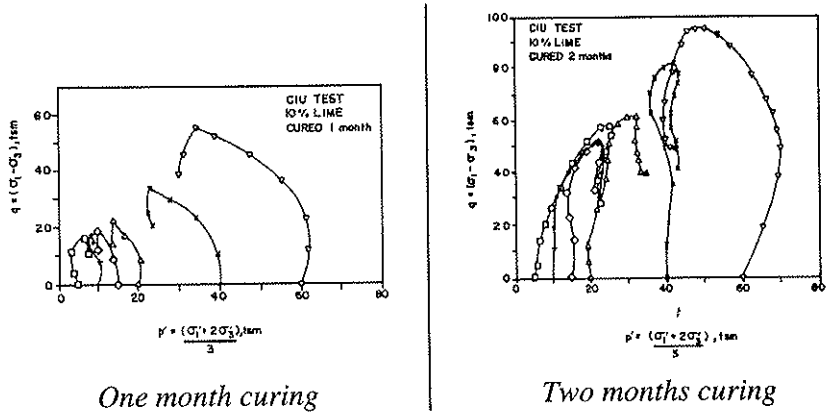


Figure 2.16 Undrained stress paths, after Balasubramaniam and Buensuceso (1989).

Low pore pressure was developed during the test, which resulted in less rounded stress paths. This behavior was clearly noticed for tests with two months curing.

The deviator stress-strain relationship shows that the axial strain increases as the deviator stress increases up to a peak value.

As the peak value is reached, the stress start to decrease with continuos strain increase. Again, this was observed clearly for samples tested after two months curing age. The axial strain at failure for two months curing age was between 3 % and 4 %, see Figure 2.17.

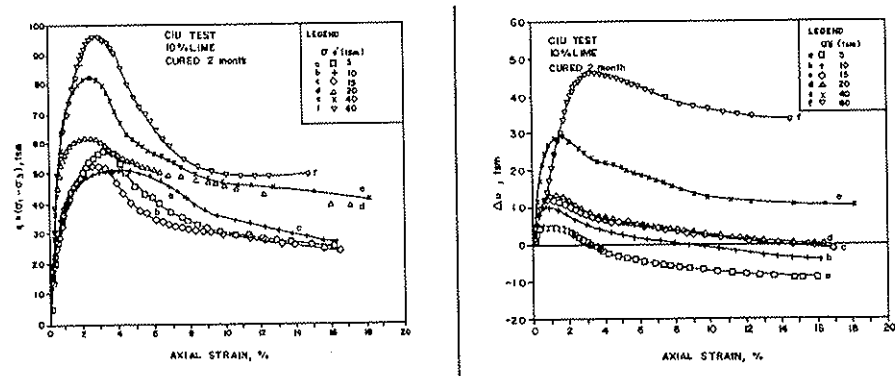


Figure 2.17 Deviator stress-axial strain and pore pressure-axial strain plots for consolidated undrained triaxial tests carried out after two months curing time, after Balasubramaniam and Buensuceso (1989).

For one month curing time the axial strain was higher than 6 %. Furthermore, Figure 2.17 shows that, for a confining pressure of between about 50 kPa and 150 kPa, the pore water pressure developed during the test decreased and negative pore pressures were measured. This is to be expected from overconsolidated clay.

The same behavior was observed in test results presented by Åhnberg et al. (1995). These tests were carried out on samples prepared by mixing lime, lime/cement and cement as stabilizing agents with soils of different categories. Curing time for these samples was about 115 days. Negative pore water pressure was developed in all cases when a low consolidation pressure of 20 kPa was used. The only exception was lime treated clay samples.

Figure 2.18 shows result from unconfined compression tests carried out on lime, lime/cement and cement treated clay samples.

Failure strain varied between 2 % and 4 %. It is important to point out that a relative high back pressure between 300 kPa and 400 kPa, was applied to the sample in an attempt to saturate it.

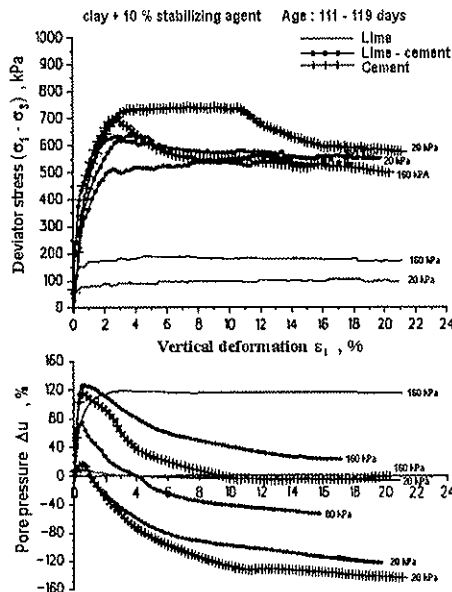


Figure 2.18 Results of triaxial undrained compression tests. Measured deviator stress and pore pressure change at $\sigma'_{3c}=20$ kPa, 80 kPa and 160 kPa respectively, after Åhnberg et al. (1995).

The same authors carried out a series of drained compression triaxial tests on a similar type of samples. The failure strains of these tests varied

between 1 % and 7 %, for lime/cement and cement treated clay samples and up to 19 % in the case of lime treated clay samples. Dilation was observed at tests with low consolidation pressures. Lime treated clay samples at high consolidation showed no sign of dilation and behaved as normally consolidated clay.

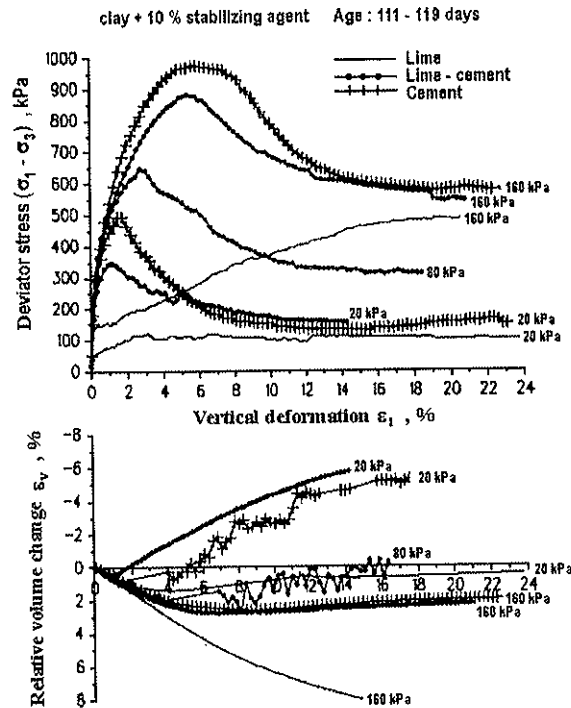


Figure 2.19 Results of drained triaxial compression tests. Measured deviator stress and pore pressure change at $\sigma'_{3c}=20$ kPa, 80 kPa and 160 kPa respectively, after Åhnberg et al. (1995).

Using these test results and results from unconfined compression tests, the relationship between the shear strength and the modulus of elasticity of treated soils was investigated. It was shown that the drained initial elastic modulus, E_o , and the secant modulus, E_{50} , at a point on the stress-strain curve corresponding to half the failure strength, of the treated soil increased with the increase of the curing time and the confining pressure. The results in Figure 2.20 show a relative linear relationship between the drained secant modulus of elasticity, E_{50} , and the undrained shear strength, τ_{uc} , which was expressed as

$$E_{50} \approx 200 \cdot \tau_{uc}$$

The ratio E_{50}/τ_{uc} at low consolidation pressures of about 20 kPa varied between 200 and 400 while this ratio varied between 100 and 300 at consolidation pressures of 160 kPa.

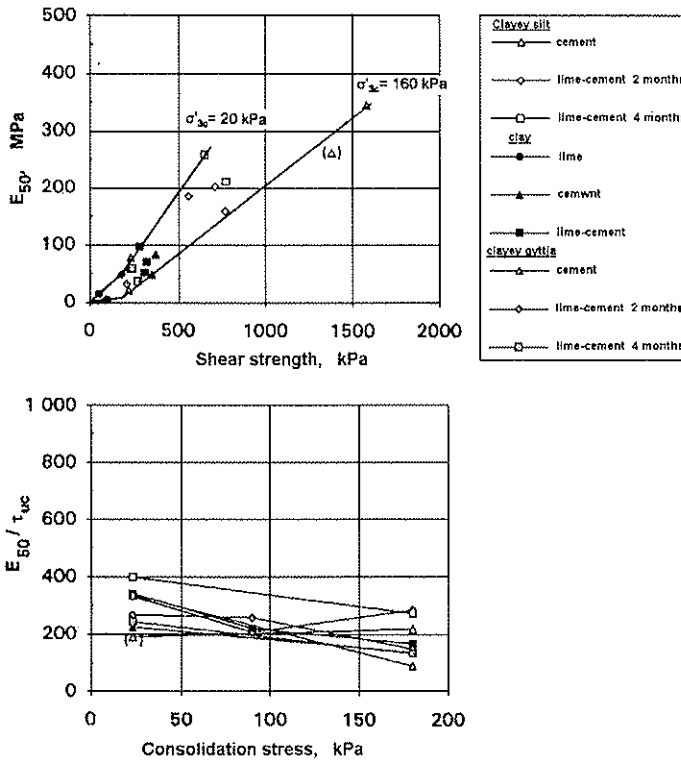


Figure 2.20 Relation between secant modulus E_{50} according to drained triaxial compression tests and measured undrained shear strength in the stabilized soils at different consolidation stresses, after Åhnberg et al. (1995).

In the case of lime/cement columns, the E_{50}/τ_{uc} ratio varied about between 350 at low consolidation pressure and about 150 at higher consolidation pressure.

The relation between the drained and undrained secant modulus, E_{50} , for different consolidation stresses is presented in Figure 2.21.

The undrained secant modulus for lime/cement treated clay is about 0.5 to 1 times the drained secant modulus at a consolidation pressure of between about 25 kPa and 75 kPa. At a consolidation pressure higher than 100 kPa, the undrained secant modulus is higher than the drained secant modulus.

This can be explained by the dilatation behavior of the treated soil, where less dilatation was observed at high consolidation pressure.

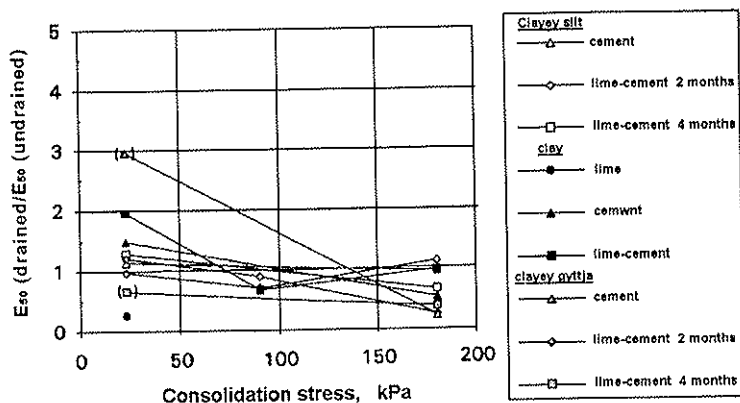


Figure 2.21 Relation between evaluated modulus E_{50} according to drained and undrained triaxial compression tests with different consolidation stresses, after Åhnberg et al. (1995).

The authors also carried out oedometer tests and observed that the compression modulus of treated soil varied considerably with the increase in stress level. Furthermore, for lime/cement treated clay, the initial modulus was about 200 and 600 times the shear strength at 14 and 91 days curing time, respectively.

The elastic modulus was evaluated from the unconfined compression tests. Åhnberg et al. (1995) suggested that, for samples prepared by mixing lime, lime/cement and cement stabilizing agents with clay, the secant modulus at shear strength, q_c , and at 33 % of the failure load, depending on the shear strength, can be expressed as

For $q_c < 120$ kPa, then

$$E_{q_c} = 30 \cdot q_c$$

$$E_{q_c/3} = 50 \cdot q_c$$

For $120 \text{ kPa} < q_c < 300 \text{ kPa}$, then

$$E_{q_c} = 50 \cdot q_c$$

$$E_{q_c/3} = 90 \cdot q_c$$

For $q_c > 300$ kPa, then

$$E_{qc} = 120 \cdot (q_c - 175)$$

$$E_{qc/3} = 270 \cdot (q_c - 200)$$

Ekström (1994) carried out unconfined compression tests on both samples taken from mixed-in place columns and samples prepared in the laboratory, see Figure 2.22.

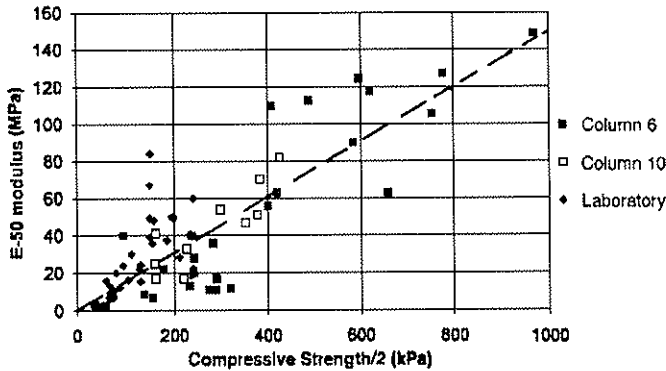


Figure 2.22 Relation between unconfined compressive strength $q_{u,col}$ of lime/cement columns and modulus of elasticity E_{50} , after Ekström (1994).

A large scatter was observed of the undrained secant modulus, E_{50} , at different values of shear strength. The figure shows that the undrained secant modulus, E_{50} , can be evaluated to be about 50 and 150 times the shear strength.

The in-situ load tests carried out by Kivelö (1994) showed that the undrained modulus, E_{50} , is about between 1.2 and 1.6 larger than that evaluated from unconfined compression tests carried out in the laboratory. Kivelö found the E_{50} modulus to be about 250 and 350 times the unconfined shear strength.

All the laboratory tests mentioned above were carried out on standard size samples of 50 mm diameter and 100 mm height.

Lime/cement column is not a perfect homogeneous material, and more reliable results can be obtained when tests are carried out on large-scale samples.

Steensen-Bach et al. (1996) conducted triaxial compression tests on three lime/cement samples 500 mm in diameter. The samples were taken from lime/cement columns installed to reduce settlements for the Svealand rail link in Sweden.

The soil profile consisted of 1 m to 7 m gyttja clay having a 90 % to 135 % liquid limit and 6 kPa to 15 kPa undrained shear strength, which overlies a clay layer up to 17 m having a liquid limit of between 55 % and 95 % and in the undrained shear strength varying from 14 kPa to 20 kPa.

The mixture used in the stabilizing of the soil was 50/50 per cent lime/cement and the amount of the mixture was 23 kg per meter column length. Eight-meter columns had been taken up, and three large samples were sent to the laboratory, which were trimmed down to specimens of 500 mm diameter and 500 mm height.

Triaxial compression tests were carried out on these samples. The specimens were first consolidated with a confining pressure of between 20 and 30 kPa. Then drained triaxial tests to a stress level below the failure load were carried out. At the drained triaxial tests, the sample was unloaded and reloaded again, and during each load step the creep deformation of the sample was observed. After unloading the sample in the drained test, undrained test was carried out to failure. As a last step in the test program the sample was consolidated again at a pressure of about 100 kPa. An undrained compression test was then carried out to study the effect of the confining pressure and the destructurelization on the mechanical properties of the treated soil.

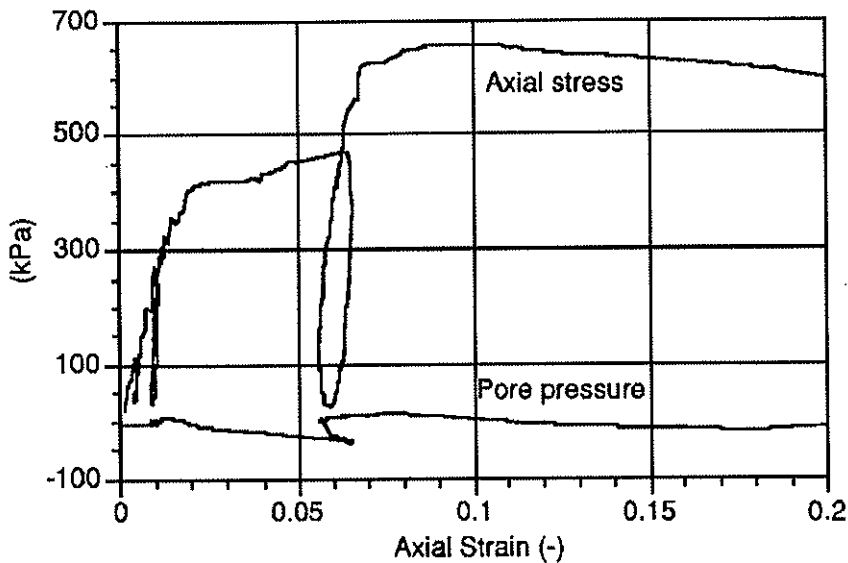


Figure 2.23 Axial stress and pore pressures versus axial compression (specimen 2), after Steensen-Bach et al. (1996).

Figure 2.23 shows the axial stress and the pore water pressure versus axial compression strain for specimen 2. The figure shows very low pore water pressure development during the undrained test. A negative pore pressure was observed directly before failure at the undrained test with low confining pressure.

The drained Young modulus for the assumed stress path in-situ was between 30 and 50 MPa, while the values of the undrained Young modulus determined at stress level, related to 50 % of the failure load, E_{50} , were between 45 MPa and 105 MPa. The undrained secant modulus was in the order of about 200 to 500 times the undrained shear failure.

A very small creep component of the axial strain was observed for effective vertical axial stress below 150 kPa. The undrained shear strength for samples 1 and 2 was between 185 kPa and 280 kPa, while that of sample 3 was between 127 kPa and 179 kPa.

Carlsten and Ekström (1995) suggested that the characteristic value of the compression modulus, M_k , for lime treated soils is between 50 and 100 times the characteristic value of undrained shear strength, c_{uk} . The undrained shear strength is calculated from unconfined compression tests or based on results from in-situ tests. However, the maximum value is limited to 150 kPa regardless of what the result from laboratory or field tests show.

In the case of lime/cement columns, the characteristic value of the compression modulus, M_k , is suggested to be between 50 and 150 times the characteristic value of undrained shear strength.

2.4 HYDRAULIC CONDUCTIVITY

The addition of lime usually increases the hydraulic conductivity of soft clay. However, the hydraulic conductivity will not increase as much or even decrease when using lime/cement or cement mixture. The results of oedometer tests carried out by Terashi and Tanaka (1983), show that the hydraulic conductivity of lime and cement treated soils was of the same order or smaller than that of the untreated soils.

The hydraulic conductivity of cement treated Kawasaki clay was tested by triaxial tests. The untreated soil was typical Japanese marine clay with a natural water content of 95 % and liquid limit of 90 %.

Figure 2.24 shows results from hydraulic conductivity tests for treated soil with varying cement content, a_w , and varying water content, w_a . The hydraulic conductivity of the cement treated soil, K_{cement} , decreased with increasing cement content and decreasing water content. Terashi and Tanaka observed the same tendency for lime treated marine clays.

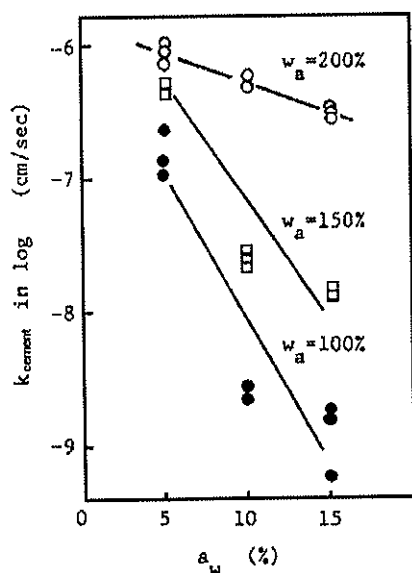


Figure 2.24 Change of hydraulic conductivity with cement content and water content, after Terashi and Tanaka (1983).

Åhnberg et al. (1995) observed that the measured hydraulic conductivity of laboratory prepared lime treated soils was two or three times higher than the hydraulic conductivity of the untreated soil. Moreover, the authors indicated that the hydraulic conductivity of lime/cement treated soils was

somewhat higher than that of untreated soil, while in the case of cement treated soil the hydraulic conductivity was of the same order or lower than that of the untreated soil. These authors also indicated that the in-situ measured hydraulic conductivity of treated soil was somewhat higher than that of laboratory prepared samples, but lower than the values usually assumed and used for the settlement calculations. The difference in hydraulic conductivity was related to the possibility of having more homogeneous treated samples in the laboratory compared with the in-situ mixed columns. Hence, no drainage layers or cracks occurred.

Bengtsson and Holm (1984) reported that lime treated soil functions as a drain and that the hydraulic conductivity of treated soil was about 100 times the hydraulic conductivity of the untreated soil.

Pramborg and Albertsson (1992) carried out in-situ hydraulic conductivity tests on lime/cement columns and determined that the measured hydraulic conductivity, two months after the installation, ranged between $5 \cdot 10^{-8}$ m/s and $3.5 \cdot 10^{-7}$ m/s, with an average value of $1.4 \cdot 10^{-7}$ m/s. The hydraulic conductivity of the original soil was about $7 \cdot 10^{-10}$ m/s.

Carlsten and Ekström (1995) suggested that, for calculation of consolidation settlements using the method described previously in this chapter, the hydraulic conductivity of the lime and lime/cement columns should be 1000 and between 400 and 800 times the hydraulic conductivity of treated soil, respectively.

3. ANALYTICAL AND NUMERICAL MODELS

3.1 GENERAL

Three mathematical models are presented in this chapter, two of which are numerical and one is an analytical elastic model based on a unit cell concept. The analytical model is used to increase the understanding of long-term total settlement as well as the stresses caused by an applied load. This model was compared with the current design method followed in Sweden, where the column is assumed to behave as a linear elastic material.

For a correct estimate of the settlement due to the static load transmitted from the structure to the underlying soil, it is necessary to know the stress concentration ratio and its change with depth. In homogenous soils, the stress distribution is calculated assuming that the soil is a linear elastic material. The estimate of the stress distribution will become more complicated in the case of soil improved by lime/cement columns. In the first numerical model, the finite element method has been applied using a three-dimensional model to study the stress distribution behavior.

The second numerical model is a finite difference model used to calculate the consolidation settlement of a lime/cement column stabilized soil.

The hydraulic conductivity and compression modulus of the lime/cement columns have a large impact on the rate of consolidation of stabilized soil. Using lime/cement mixture instead of lime will increase the stiffness of the treated soil and cause stress concentration in the columns, while at the same time the hydraulic conductivity is decreased. Results and evidence from field and laboratory tests presented in this study shows that no or very low pore pressure was developed during the tests. Moreover, the hydraulic conductivity of the treated soil was not much larger than that of the original soil. In this model it is assumed that both soft soil and lime/cement columns possess material linearity. The consolidation of the stabilized soil due to vertical drainage is examined using the finite difference technique. It is shown that the rate of consolidation increases as the ratio of the compression modulus of the lime/cement column to that the untreated soil increases, in spite of equal hydraulic conductivity of both the lime/cement columns and the original soil. The results obtained from this model are compared with those predicted using the finite element program, PLAXIS. The comparison shows good agreement with predicted results.

3.2 ANALYTICAL ELASTIC MODEL FOR VERTICALLY LOADED LIME/CEMENT STABILIZED SOIL

In the analysis of soil stabilized by lime-cement column, a unit cell system is considered. This system refers to a case where the loaded area is large compared with the depth so that the vertical stress increase in the column and in the surrounding soil is constant with depth.

The equations derived for calculation of the axial vertical strain, the vertical stresses acting on the treated and the untreated soil, the radial strain and the stress acting at the column boundary are given below. A detailed derivation of the equations can be found in appendix A.

$$\varepsilon_z = \frac{\sigma_v}{a_s \cdot (M_{col} + 2 \cdot \lambda_{col} \cdot F_{z0}) + (1 - a_s) \cdot (M_{soil} - 2 \cdot \frac{a_s}{1 - a_s} \cdot \lambda_{soil} \cdot F_{z0})} \quad (3.1)$$

$$\sigma_{zcol} = (M_{col} + 2 \cdot \lambda_{col} \cdot F_{z0}) \cdot \varepsilon_z \quad (3.2)$$

$$\sigma_{zsoil} = \left(M_{soil} - 2 \cdot \frac{a_s}{1 - a_s} \cdot \lambda_{soil} \cdot F_{z0} \right) \cdot \varepsilon_z \quad (3.3)$$

$$\varepsilon_{bou} = F_{z0} \cdot \varepsilon_z \quad (3.4)$$

$$\sigma_{rb} = \lambda_{soil} \cdot \varepsilon_{zsoil} - \frac{2}{1 - a_s} \cdot G_{soil} \cdot \varepsilon_{bou} - \frac{a_s}{1 - a_s} \cdot \frac{\lambda_{soil}}{v_{soil}} \cdot \varepsilon_{bou} \quad (3.5)$$

$$F_{z0} = - \frac{\lambda_{col} - \lambda_{soil}}{2 \cdot (\lambda_{col} + G_{col}) + \frac{1}{1 - a_s} \cdot \left(2 \cdot G_{soil} + \frac{a_s \cdot \lambda_{soil}}{v_{soil}} \right)} \quad (3.6)$$

Where

ε_z	vertical elastic strain in the column-soil system
σ_v	vertical applied stress
a_s	ratio of area of the treated soil to the area of the unit cell
M_{col}	oedometer compression modulus of the columns
M_{soil}	oedometer compression modulus of the untreated soil

$\lambda_{col}, \lambda_{soil}$	elastic coefficient (Lamé's constant) of the columns and the untreated soil respectively
G_{col}	shear modulus of the columns
G_{soil}	shear modulus of untreated soil
σ_{zcol}	column stress in the z-direction
σ_{zsoil}	soil stress in the z-direction
σ_{rb}	radial stress at the boundary between the column and the untreated soil
ϵ_{bou}	radial deformation at the boundary between the two materials (at $r = r_{col}$)
ν_{soil}	Poisson's ratio of the untreated soil

The traditional method used to calculate the total long-term settlement of a single or a group of lime/cement columns (when both the treated and the untreated materials are assumed to act as linear elastic) is based upon the following equation:

$$\epsilon_z = \frac{\sigma_v}{a_s \cdot M_{col} + (1 - a_s) \cdot M_{soil}} \quad (3.7)$$

Equation (3.1) account for the radial stress effect on the vertical axial strain, while equation (3.7) is more simplified. Figure 3.1 shows that the ratio between the vertical and radial stresses, $\sigma_{zcol}/\sigma_{rb}$, acting on the column at low modulus ratios is not specifically sensitive to the area ratio a_s . The stress ratio will start to increase as the modulus ratio increases and, for a specific modulus ratio, the stress ratio will decrease as the area ratio increases. In case of extremely high modulus ratios, the radial stress acting on the column becomes insignificant and, thus, the stress ratio is expected to be extremely high. In such a case, the column Young modulus, E_{col} , and not the oedometer compression modulus, M_{col} , must be used in equation (3.7) to obtain results close to that calculated by the analytical model.

The variation of the ratio between the axial strain calculated by equation (3.1) and equation (3.7) with the area ratio a_s for different modulus ratios is presented in Figure 3.2. The axial strain calculated by equation (3.1), which is based on a unit cell system, is greater than the axial strain calculated by using equation (3.7). The ratio increases with an increase in both the area ratio, a_s , and the modulus ratio.

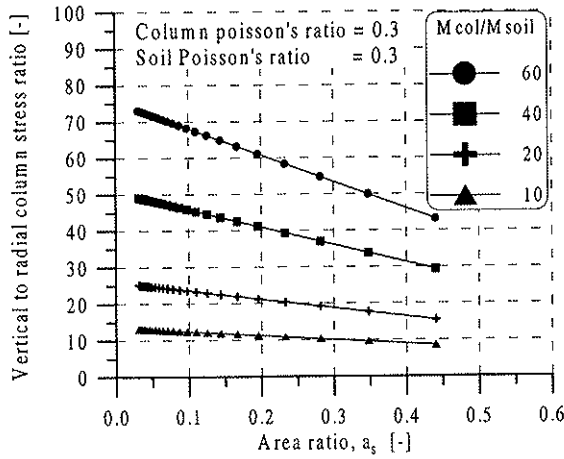


Figure 3.1 Ratio of vertical to radial stresses acting on the column for different area and modulus ratios.

The results presented in Figure 3.2 are based on a Poisson ratio value of 0.3 for both column and untreated soil materials. It is important to emphasize that the axial strain calculated by equation (3.1) is not very sensitive to the change in Poisson's ratio of the untreated soil. On the other hand, if Poisson's ratio of the column material increases slightly, then the ratio of the vertical stress in the column to the vertical stress in the surrounding soil will decrease and, as a consequence, the vertical axial strain will increase.

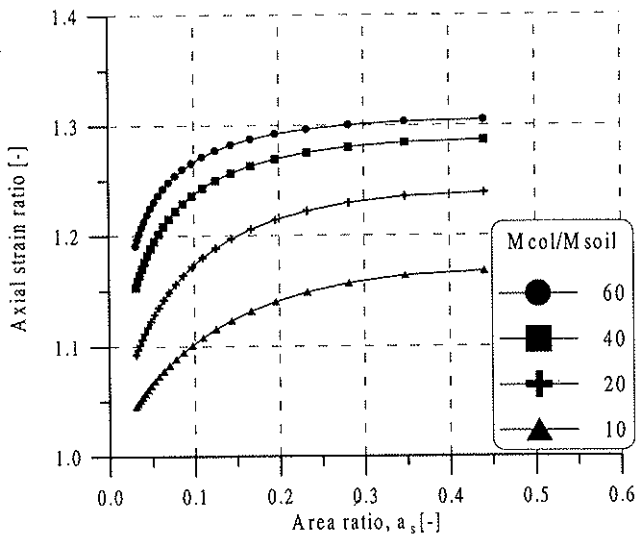


Figure 3.2 The ratio of the strains calculated by equations (3.1) and (3.7) versus area ratio a_s for different modulus ratios.

3.3 NUMERICAL ANALYSIS OF LOAD DISTRIBUTION BETWEEN LIME/CEMENT COLUMNS AND SURROUNDING SOIL USING THE FINITE ELEMENT METHOD

3.3.1 Introduction

The load distribution within and under a lime/cement column reinforced block depends on many factors. Among these factors we find geometry, magnitude of applied load and stiffness ratio between lime/cement columns and the untreated soil. The geometry refers to spacing, diameter and length of the columns.

The magnitude of the applied load will determine whether the analysis is to be linear or non-linear.

No general solution to the load distribution appears to have been published; yet there are many simplified approaches that can be used to tackle this problem. By using plane-strain models, analyses with the finite element program were presented by Lahtinen and Vepsäläinen (1983) and Liedberg et al. (1996). In both of these studies, it was assumed that the axial stiffnesses of the stabilized columns in the three-dimensional and the plane-strain models were equal. This assumption may be acceptable for the columns located at the center of the loaded area but not for those columns located away from the center, where they will be subjected to large horizontal forces.

In a method proposed by Broms and Boman (1979), which has been widely used in Sweden, two cases were considered, case (A) and case (B). Case (A) is applicable when the load carried by the column exceeds its yield strength, i.e. within the reinforced block, the stresses in the stabilized column are equal to the yield strength, and the rest of the applied load will be transferred to the untreated soil. The stresses under the reinforced block are assumed to be the sum of the load carried by the columns, transferred totally to the bottom of the reinforced block, and the load in the untreated soil distributed from the level of the applied load to the bottom of the block. Case (A) can be considered as a elastoplastic solution to the problem.

Case (B) can be regarded as a linear solution. The applied load will be shared between the treated and the untreated soils in proportion to the stiffness ratio of the two materials. Further, it is assumed that the relative deformation of the treated soil with respect to the untreated soil, within the block, is the same. The stresses in the untreated soil below the reinforced block are calculated by assuming that the applied load will be distributed from the bottom of the block.

This section presents a study of the load distribution within and under the reinforced block by using results from a three-dimensional finite element model. Since deep stabilization of soil using lime/cement columns has been used to a great extent in Sweden to improve the soil under road and railroad embankments, a road embankment model was chosen in the numerical analysis presented.

3.3.2 Finite element analysis, linear elastic model

Below, the results from the finite element analysis using a three-dimensional model are presented and discussed.

The treated and untreated soils are assumed to behave as linear elastic materials.

The diameter of the lime/cement columns is often chosen as 0.6 m, while the column spacing varies. In order to keep the loaded area constant in the model, the spacing of the columns, S , was kept constant while different column diameters were used in the analysis. In this way the results can easily be compared. The spacing, S , was selected as 3 m, and 5 columns were used in each row beneath the embankment.

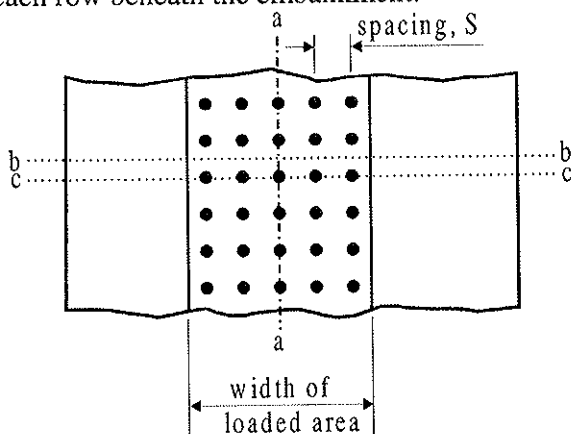


Figure 3.3 Plan of the load area

The symmetrical planes, a-a, b-b and c-c, shown in Figure 3.3, were used to simplify the model geometry. The idealized model shown in Figure 3.4 has a depth of 50 m and a width of 30 m and half the spacing is 1.5 m. The length and depth of the model were selected to be long enough to minimize the boundary effects. For simplicity, the circular columns were modeled as square columns with corresponding cross sectional area.

The dimensions of the square columns used in the linear analysis are 1.8, 1.16, 0.9 and 0.7 m, which in terms of the relative column area, a_s , together with the 3 m spacing, can be written as 0.36, 0.15, 0.09 and 0.05 respectively.

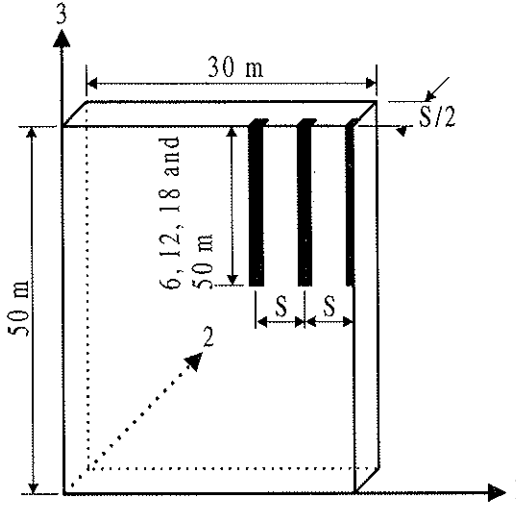


Figure 3.4 The idealized model.

The relative column area, a_s , is already defined in the previous section as the ratio of the column area, A_{col} , to the effective area. In case of a square column arrangement, the effective area is equal to $S \cdot S$, see Table 1.

Four column lengths were considered; 6, 12, 18 m and 50 m column, the later extending all the way to firm bottom. Three stiffness ratios (M_{col}/M_{soil}), 10, 30, and 70 were used, and a total of 40 models were analyzed. Poisson's ratio used for the two materials was 0.3.

Table 3.1 Column dimension and spacing.

Column dimension	A_{col}	Spacing, S	a_s
[m]	[m ²]	[m]	[-]
0.7	0.49	3	0.05
0.9	0.81	3	0.09
1.16	1.35	3	0.15
1.80	3.24	3	0.36

The general finite element code ABAQUS was used in the analysis and the model consisted of 3432 elements. The elements were of 20-node quadratic brick, reduced integration type.

As mentioned previously, it was assumed in the simplified linear analysis that the stress distribution within the reinforced block depends on the stiffness ratio and the geometry of the lime/cement columns. Furthermore, it was assumed that the relative deformation of the treated soil with respect

to the untreated soil within the block was the same (equal strain condition). With these two assumptions in mind it is easy to predict the stress distribution in the lime/cement column and the untreated soil by using the simplified approach compared with the analytical solution mentioned in the previous section. The two equations are expressed as

$$\sigma_{vsoil} = \frac{\sigma_v}{1 + a_s \cdot (n-1)} \quad (3.8)$$

$$\sigma_{vcol} = \frac{n \cdot \sigma_v}{1 + a_s \cdot (n-1)} \quad (3.9)$$

n stiffness ratio between the treated and untreated soils, (M_{col}/M_{soil}).

σ_v applied vertical stress

σ_{vsoil} vertical stress in the untreated soil

σ_{vcol} vertical stress in the lime/cement column

The stresses calculated by equations (3.8) and (3.9) were used in order to make comparisons between with the results predicted using finite element analysis.

The results shown in Figure 3.5 refer to the normalized vertical stresses in columns located at the center of the embankment.

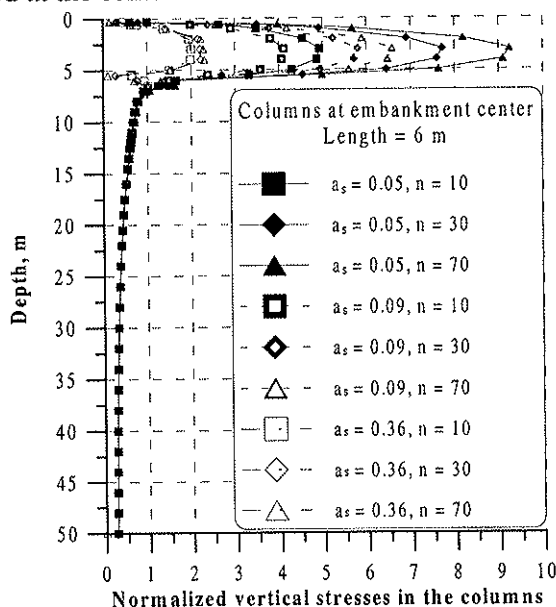


Figure 3.5 Normalized vertical stress in columns located at the embankment center for different areas and modulus ratios. Column length = 6 m.

The vertical stresses in the columns were normalized by dividing its values with the value of the applied stress $\left(\frac{\sigma_{vcol}}{\sigma_v}\right)$. It can be noticed that, with low values of area ratio, a_s , the stresses in the columns increased with depth, reaching a maximum value at few meters below ground level and thereafter decreased directly. At higher values of area ratio, a_s , the maximum stresses will be generated at smaller depth.

In Figure 3.5, results from the finite element analyses are given for a column of 6 m length.

The stiffness ratio, n , does not significantly affect the stresses developed in the columns when higher area ratio, a_s , values are chosen, while this factor has a large impact on the maximum stresses in the columns when low a_s values are used.

Columns will develop higher stresses when large stiffness ratio, n , values are used together with low area ratio, a_s , values. The conclusions drawn from the analysis of the 6 m long column are applicable also for the 12 m and 18 m column lengths.

As expected, the stresses in the columns at the edge of the embankment are lower than the stresses within the columns located at the embankment center. Figure 3.6 shows a comparison between typical results of these two columns.

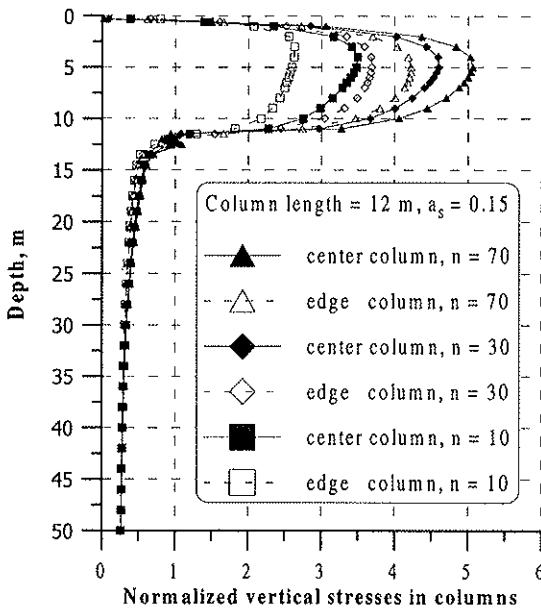


Figure 3.6 Comparison between normalized vertical stresses at the edge and the center columns for different stiffness ratios.

In Table 3.2, the vertical stresses in the columns based on results calculated by equation (3.9) are presented and compared with the maximum normalized vertical stresses in columns located at the center of the loaded area resulting from the finite element calculations.

The maximum vertical stresses in the columns calculated by equation (3.9) are 15 to 35 % higher than the vertical stresses in the 6 m columns calculated by the finite element method, depending on the a_s and n values. Furthermore, these stresses are approximately 20 % higher than the vertical stresses in columns of 12 m length calculated by the finite element method. As the column length increases, the stresses in the column calculated by the finite element method will become close to the stresses calculated analytically and, with an area ratio of 0.36, the column vertical stresses calculated by the finite element method become higher than those calculated by equation (3.9). Equation (3.2), which is based on the analytical solution, shows almost similar results as that obtained from the 3-D numerical solution for columns extended to the firm bottom.

Table 3.2 The normalized maximum vertical stresses in columns calculated by equations (3.9) and (3.2) together with results from the finite element analysis for different areas and modulus ratios.

a_s [-]	n [-]	Normalized vertical stress in the column					
		Eq. (3.9)	Eq. (3.2)	L= 6 m	L= 12 m	L= 18 m	L= 50 m
0.05	10	6.7	5.6	4.9	5.3	5.4	5.4
0.05	30	11.6	10.3	7.7	9.1		
0.05	70	14.7	13.8	9.3	11.5	12	13.1
0.09	10	5.5	4.8	4.1	4.4	4.5	4.6
0.09	30	8.3	7.6	5.8	6.7		
0.09	70	9.7	9.3	6.6	7.8	8.1	8.9
0.15	10	4.3	3.8	3.3	3.5	3.6	3.7
0.15	30	5.6	5.3	4.2	4.6		
0.15	70	6.2	6.0	4.6	5.1	5.3	5.9
0.36	10	2.4	2.2	2.0	2.1	2.6	2.8
0.36	30	2.6	2.6	2.2	2.3		
0.36	70	2.7	2.7	2.3	2.3	3.1	3.7

One special case in Table 3.2 with an area ratio a_s equal to 0.15 and a modulus ratio value n of 70 is presented in Figure 3.7 to illustrate the vertical stress change with depth for different column lengths and to compare these numerical results with the results calculated by equations (3.9).

At the bottom of the reinforced block, there are stress concentrations directly under the tip of the column, and the stresses there were higher than in the rest of the untreated soil at the same level. This may be due to numerical problem that can appear at the boundaries between two materials with high stiffness difference. This difference in vertical stresses disappears at about 1 to 2 m depth below the bottom of the reinforced block.

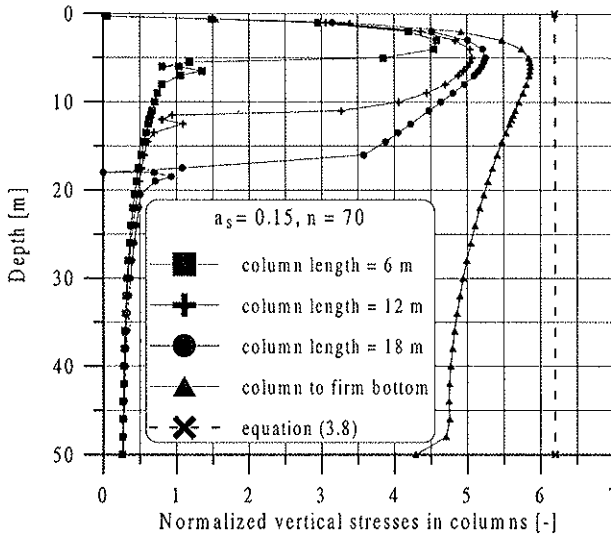


Figure 3.7 The change with depth of the normalized vertical stress in columns for different column lengths.

It is interesting to notice that the vertical stresses below the bottom of the reinforced block are almost identical to the vertical stresses calculated by Boussinesq's equation with the load acting on the ground surface.

Figure 3.8 shows a comparison between the vertical stress distributions calculated by Boussinesq's equation on the one hand and by using the 3-D finite element model on the other. As can be noticed, the vertical stress distribution below the reinforced block obtained by the two methods is almost identical for all cases, except for a limited region directly under the bottom of the columns. The very small difference, which may be noticed at larger depths, is related to the boundary effects, even though the depth of the model was selected to be 50 m. This was confirmed by comparing Boussinesq's solution with finite element results where the stiffness ratio n was assumed to be equal to one. In Figure 3.8 some selected results are presented, but it is important to point out that all other cases were tested and that the results indicated the same pattern.

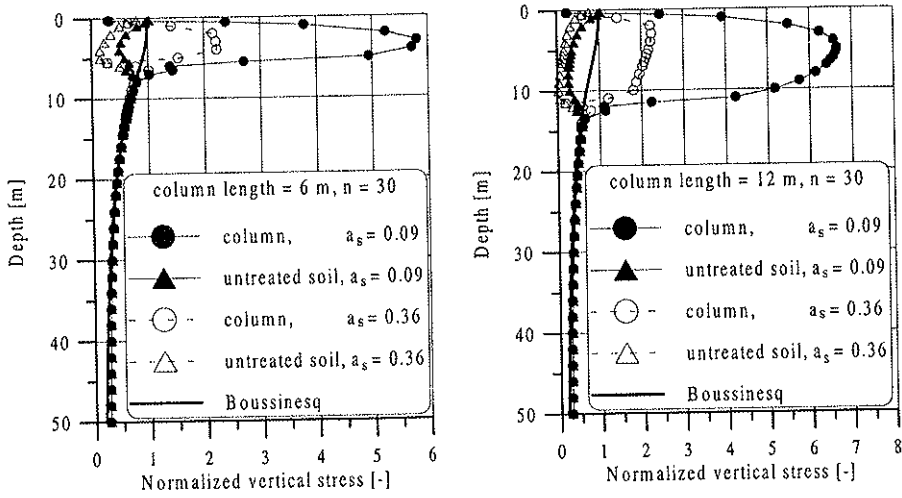


Figure 3.8 Vertical stress distribution under the reinforced block compared with Boussinesq's solution.

3.4 ONE-DIMENSIONAL CONSOLIDATION SETTLEMENT OF STABILIZED SOIL USING LIME/CEMENT COLUMN

3.4.1 Introduction

Most of the models dealing with consolidation of soil stabilized with lime/cement columns are based on an analytical or a numerical solution for vertical drains, where the influence of the stiffness of the treated soil is neglected. Yoshikuni and Nakanodo (1974) developed equations, which accounted for the effect on the consolidation process on the stress concentration in drain wells when compacted sand piles of large diameter were used. Terashi and Tanaka (1983) studied the effect of the difference in stiffness between the treated and untreated soil on the consolidation process of the untreated soil using both numerical analysis and a series of model tests in an oedometer.

Results and evidence from field and laboratory tests presented in this study shows that no or very low pore pressure developed during the load tests. Moreover, the hydraulic conductivity of the treated soil was only somewhat larger than that of the original soil. A numerical one-dimensional solution of the consolidation process in treated soil is presented in this section. The model is similar to that presented by Terashi and Tanaka (1983). All the steps of the derivation are listed. The differential equation is solved using the finite difference technique. Some results from this model were compared with results evaluated by using the PLAXIS finite element program.

3.4.2 Assumptions

- The columns are extended to bedrock or a hard layer.
- The stress increase caused by the load is constant with depth.
- The total applied vertical load on the surface of the cylindrical body is kept constant.
- Both columns and untreated soil act as linear elastic materials.
- The boundary surface of a cylindrical body is smooth, which means that the displacements are parallel with their original surface. The rotation of displacement, ω , is zero at any point of a clay cylinder during consolidation.
- Original soil is homogeneous, isotropic and fully saturated.
- Darcy's law is valid.
- Hydraulic conductivity in the original soil and column is equal.
- Pore pressure in the treated soil is neglected.

3.4.3 Analysis

Yoshikuni's consolidation theory takes into account the deformation condition in a clay cylinder with vertical drain. The fundamental equation is written as

$$\frac{\partial u}{\partial t} = c_{vsoil} \cdot \frac{\partial^2 u}{\partial z^2} + \frac{\partial \Phi}{\partial t} \quad (3.10)$$

u	excess pore water pressure
c_{vsoil}	consolidation coefficient of the untreated soil
Φ	potential function

The index soil is an indication for the untreated soil, while the index col, which will appear later, is an indication for the lime/cement column. The potential function in equation (3.10) is defined as

$$\Phi = (\lambda + 2 \cdot G) \cdot \varepsilon_{vol} + u \quad (3.11)$$

Where

$$\lambda = K - \frac{2}{3} \cdot G$$

ε_{vol}	volumetric strain
G	shear modulus
K	bulk modulus

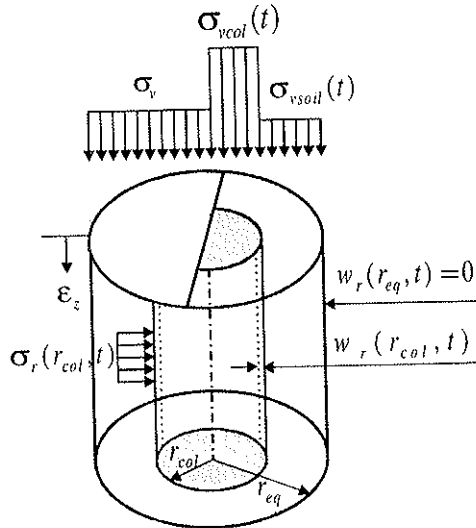


Figure 3.9 The geometry of the model.

Since equal strain conditions are assumed and since the surfaces of the clay are smooth, the value of Φ at any point is equal to the average value of Φ at any stage of consolidation, and equation (3.11) can be written as

$$\Phi = \bar{\Phi} = (\lambda + 2 \cdot G) \cdot \bar{\varepsilon}_{vol} + \bar{u} \quad (3.12)$$

To consider the effect on the consolidation process of the stress concentration in the treated soil, Yoshikuni (1974) derived the following equation

$$\frac{\partial u}{\partial t} = c_{vsoil} \cdot \frac{\partial^2 u}{\partial z^2} + \chi_1 \cdot \frac{\partial \bar{u}}{\partial t} + \zeta_1 \cdot \frac{\partial \sigma_v}{\partial t} \quad (3.13)$$

χ_1, ζ_1 constants to be specified later by derivation

\bar{u} average value of excess pore water pressure

σ_v average stress caused by the applied load

If the external load is applied rapidly then $\frac{\partial \sigma_v}{\partial t} = 0$ and equation (3.13) will be

$$\frac{\partial u}{\partial t} = c_{vsoil} \cdot \frac{\partial^2 u}{\partial z^2} + \chi_1 \cdot \frac{\partial \bar{u}}{\partial t} \quad (3.14)$$

The stress-strain relationship can in general be written as

$$\sigma'_i = 2 \cdot G \cdot \varepsilon_i + \lambda \cdot (\varepsilon_i + \varepsilon_j + \varepsilon_k)$$

Since the oedometer modulus M is equal to $\lambda + 2 \cdot G$, the above equation can be written as

$$\sigma'_i = M \cdot \varepsilon_i + \lambda \cdot (\varepsilon_j + \varepsilon_k)$$

By using the above relationships, the potential function Φ can be defined in three different ways as

$$\Phi = \sigma_i + 2 \cdot G \cdot (\varepsilon_j + \varepsilon_k) \quad (3.15)$$

$$\Phi = M \cdot (\varepsilon_i + \varepsilon_j + \varepsilon_k) + u \quad (3.16)$$

$$\Phi = \sigma_j + 2 \cdot G \cdot (\varepsilon_i + \varepsilon_k) \quad (3.17)$$

From the vertical load equilibrium condition, which is shown in Figure 3.9, the following equation can be established

$$\sigma_v = \sigma_{vcol}(t) \cdot a_s + \overline{\sigma_{vsoil}(t)} \cdot (1 - a_s) \quad (3.18)$$

The stresses acting on the treated soil must be defined first. The treated soil will be considered as a solid cylinder.

The general solution for the axisymmetric system with z and r axis is

$$w_r = X \cdot r \quad (3.19)$$

$$\varepsilon_r = -\frac{dw_r}{dr} = -X \quad (3.20)$$

$$\varepsilon_\theta = -\frac{w_r}{r} = -X \quad (3.21)$$

w_r	radial deformation
ε_r	radial strain
ε_θ	tangential strain
X	integration constant

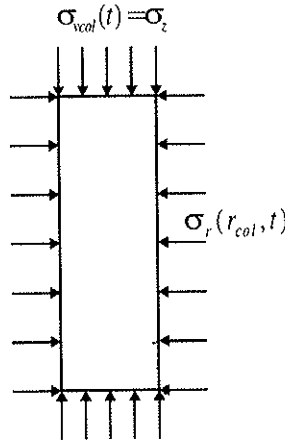


Figure 3.10 Stresses acting on the treated soil.

Equations (3.20) and (3.21) give that $\varepsilon_r = \varepsilon_\theta$, which in turn means that $\sigma_r = \sigma_\theta$. By applying the previously defined general stress-strain equation, the stresses acting on the column can be written as

$$\sigma_z = \sigma_{vcol}(t) = \lambda_{col} \cdot (\varepsilon_z + 2 \cdot \varepsilon_r) + 2 \cdot G_{col} \cdot \varepsilon_z \quad (3.22)$$

$$\sigma_r = \sigma_{rcol} = \lambda_{col} \cdot (\varepsilon_z + 2 \cdot \varepsilon_r) + 2 \cdot G_{col} \cdot \varepsilon_r \quad (3.23)$$

The radial deformation at the treated soil boundaries is equal to $w_r(r_{col}, t)$. By applying this boundary condition in equation (3.19), the constant factor X can be evaluated as

$$X = \frac{w_r(r_{col}, t)}{r_{col}}$$

The radial strain at the boundaries is

$$\varepsilon_r = \varepsilon_\theta = -\frac{w_r(r_{col}, t)}{r_{col}} \quad (3.24)$$

Substituting equation (3.24) into equations (3.22) and (3.23) the following is obtained:

$$\sigma_{vcol}(t) = (\lambda_{col} + 2 \cdot G_{col}) \cdot \varepsilon_z(t) - 2 \cdot \lambda_{col} \cdot \frac{w_r(r_{col}, t)}{r_{col}} \quad (3.25)$$

$$\sigma_r = \sigma_r(r_{col}, t) = \lambda_{col} \cdot \varepsilon_z(t) - 2 \cdot (\lambda_{col} + G_{col}) \cdot \frac{w_r(r_{col}, t)}{r_{col}} \quad (3.26)$$

The untreated soil will act as a thick cylinder. The treated soil will exert stresses on the interior wall of the cylinder and cause the hole to expand, and the radial deformation at the exterior wall will be equal to zero as a result of the symmetry.

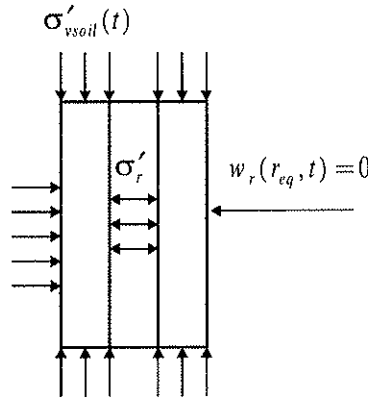


Figure 3.11 Stresses acting on the untreated soil.

The general solution of the radial deformation for the thick cylinder is:

$$w_r = Y \cdot r + \frac{Z}{r} \quad (3.27)$$

Y, Z integration constants

$$\varepsilon_r = -\frac{dw_r}{dr} = -Y + \frac{Z}{r^2}$$

$$\varepsilon_\theta = -\frac{w_r}{r} = -Y - \frac{Z}{r^2}$$

By adding the axial and the tangential strains, we get

$$\varepsilon_r + \varepsilon_\theta = -2 \cdot Y$$

The boundary conditions to be applied to the untreated soil are

$$\text{at } r = r_{eq}, \quad w_r(r_{eq}, t) = 0$$

By substituting these into equation (3.27), the following relation is obtained

$$Z = -Y \cdot r_{eq}^2$$

at $r = r_{col}$, $w_r = w_r(r_{col}, t)$ and by substituting the second boundary condition in equation (3.27) and using the result from the first boundary condition, the integration constant Y can be written as

$$Y = w_r(r_{col}, t) \cdot \frac{r_{col}}{(r_{col}^2 - r_{eq}^2)}$$

Since $\varepsilon_r + \varepsilon_\theta = -2 \cdot Y$, the result of the summation of the strain components is

$$\varepsilon_r + \varepsilon_\theta = 2 \cdot w_r(r_{col}, t) \cdot \frac{r_{col}}{(r_{eq}^2 - r_{col}^2)} \quad (3.28)$$

By introducing equation (3.28) into equations (3.15), (3.16) and (3.17), the potential function Φ will be written as

$$\Phi(t) = M_{soil} \cdot \left[\left(\varepsilon_z(t) + 2 \cdot w_r(r_{col}, t) \cdot \frac{r_{col}}{(r_{eq}^2 - r_{col}^2)} \right) + \overline{u(t)} \right] \quad (3.29)$$

$$\Phi(t) = \overline{\sigma_{vsol}(t)} + 4 \cdot G_{soil} \cdot w_r(r_{col}, t) \cdot \frac{r_{col}}{(r_{eq}^2 - r_{col}^2)} \quad (3.30)$$

$$\Phi(t) = \sigma_r(r_{col}, t) + 2 \cdot G_{soil} \cdot \left[\varepsilon_z(t) - \frac{w_r(r_{col}, t)}{r_{col}} \right] \quad (3.31)$$

Solving equation (3.29) with equation (3.30) and then with equation (3.31) will result in the following two equations

$$\overline{\sigma_{vsoil}(t)} + (4 \cdot G_{soil} - 2 \cdot M_{soil}) \cdot \frac{a_s}{1 - a_s} \cdot \frac{w_r(r_{col}, t)}{r_{col}} - M_{col} \cdot \varepsilon_z(t) = \overline{u(t)} \quad (3.32)$$

$$\overline{\sigma_{vsoil}(t)} + \frac{a_s}{(1 - a_s)} \cdot (4 \cdot G_{soil} - 2 \cdot M_{soil}) \cdot \frac{w_r(r_{col}, t)}{r_{col}} - M_{soil} \cdot \varepsilon_z(t) = \overline{u(t)} \quad (3.33)$$

Equations (3.18), (3.25), (3.26) and (3.29) can be rewritten as

$$\sigma_{vcol}(t) \cdot a_s + \overline{\sigma_{vsoil}(t)} \cdot (1 - a_s) = \sigma_v \quad (3.34)$$

$$\sigma_{vcol}(t) - (\lambda_{col} + 2 \cdot G_{col}) \cdot \varepsilon_z(t) - 2 \cdot \lambda_{col} \cdot \frac{w_r(r_{col}, t)}{r_{col}} = 0 \quad (3.35)$$

$$\sigma_r(r_{col}, t) - \lambda_{col} \cdot \varepsilon_z(t) + 2 \cdot (\lambda_{col} + G_{col}) \cdot \frac{w_r(r_{col}, t)}{r_{col}} = 0 \quad (3.36)$$

$$\Phi(t) - M_{soil} \cdot \left[(\varepsilon_z(t) + 2 \cdot w_r(r_{col}, t)) \cdot \frac{r_{col}}{(r_{eq}^2 - r_{col}^2)} \right] = \overline{u(t)} \quad (3.37)$$

The time dependent variables located at the left side of equations (3.32) to equation (3.37) i.e. $\Phi(t)$, $\varepsilon_z(t)$, $\sigma_{vcol}(t)$, $\overline{\sigma_{vsoil}(t)}$, $\sigma_r(r_{col}, t)$ and $w_r(r_{col}, t)$, are functions of the average excess pore water pressure and the total applied load.

By considering equations (3.32) and (3.33) the potential function $\Phi(t)$ in equation (3.37) can be written in general form as

$$\Phi(t) = \chi_1 \cdot \overline{u(t)} + \zeta_1 \cdot \sigma_v$$

By solving the system of the linear equations, (3.32) to (3.37), the factor χ_1 was calculated as

$$\chi_1 = \frac{n_1 - n_2}{2 \cdot (d_1 + d_2 + d_3)} \quad (3.38)$$

where

$$n_1 = 6 \cdot a_s \cdot \lambda_{col} \cdot (G_{soil} - G_{col})$$

$$n_2 = 4 \cdot G_{col} \cdot a_s \cdot (G_{col} + G_{soil}) + 8 \cdot a_s \cdot G_{soil}^2$$

$$d_1 = 3 \cdot a_s \cdot M_{soil} \cdot (G_{col} - G_{soil})$$

$$d_2 = M_{soil} \cdot \left[G_{col} - G_{soil} + \frac{1}{a_s - 1} \cdot (\lambda_{col} + 2 \cdot G_{col}) \right]$$

$$d_3 = a_s \cdot (4 \cdot G_{soil}^2 + 3 \cdot G_{soil} \cdot \lambda_{col} - 3 \cdot G_{col} \cdot \lambda_{col} - 2 \cdot G_{col}^2 - 2 \cdot G_{soil} \cdot G_{col})$$

Equation (3.14) can now be written in terms of a cylindrical coordinate as

$$\frac{\partial u}{\partial t} = c_{vsoil} \cdot \frac{\partial^2 u}{\partial z^2} + \chi_1 \cdot \frac{\partial \bar{u}}{\partial t} \quad (3.39)$$

Equation (3.39) will be solved numerically by the finite difference method. As a last step in this process, the initial and the boundary conditions must be defined. At time $t = 0$, the excess pore water is constant and equal to the applied load.

Furthermore, there are two types of boundary conditions, see Figure 3.12. First, the drainage boundary at $z = 0$, where

$$\text{at } t > 0 \quad u = 0$$

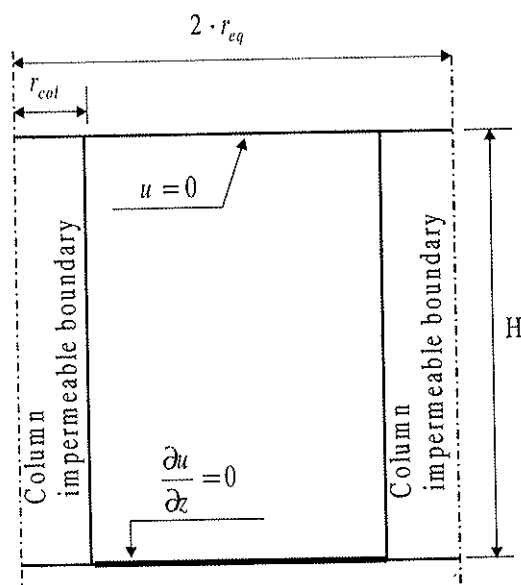


Figure 3.12 The geometry and the boundary conditions.

The second type is the impermeable boundary at the bottom.

$$\text{at } z = H \text{ and for } t > 0 \quad \frac{\partial u}{\partial z} = 0$$

3.4.4 Solution

Equation (3.39), together with the initial and boundary conditions, was solved using a finite difference technique.

Special attention should be paid to the last term in equation (3.39). At each time step, the average excess pore water pressure in the treated soil has to be calculated by iteration, see Figure 3.13.

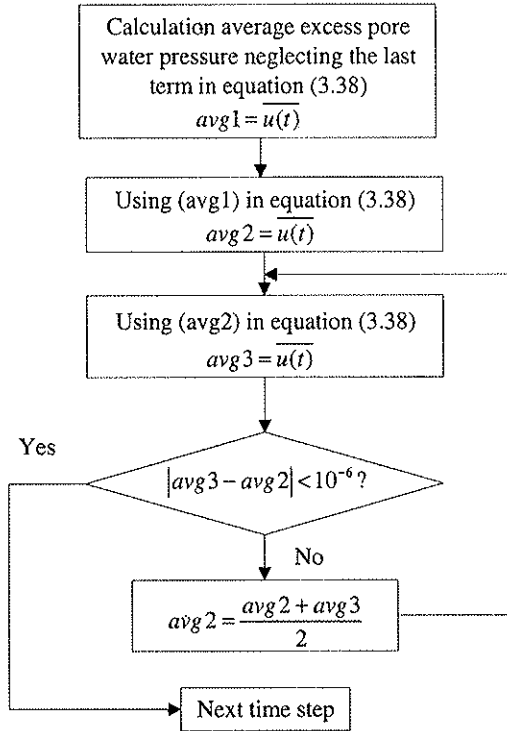


Figure 3.13 Average excess pore water pressure flow chart.

3.4.5 Typical results and comparison

Many studies have shown that the cement in the lime/cement mixture will increase both the shear strength and the compression modulus of the stabilized soil. It will also result in a decrease of the hydraulic conductivity

of the treated soil. When Terashi and Tanaka (1983) tested a typical Japanese marine clay, they found that the hydraulic conductivity of standard size samples of lime and cement treated soil was of the same order or smaller than that of the untreated soil.

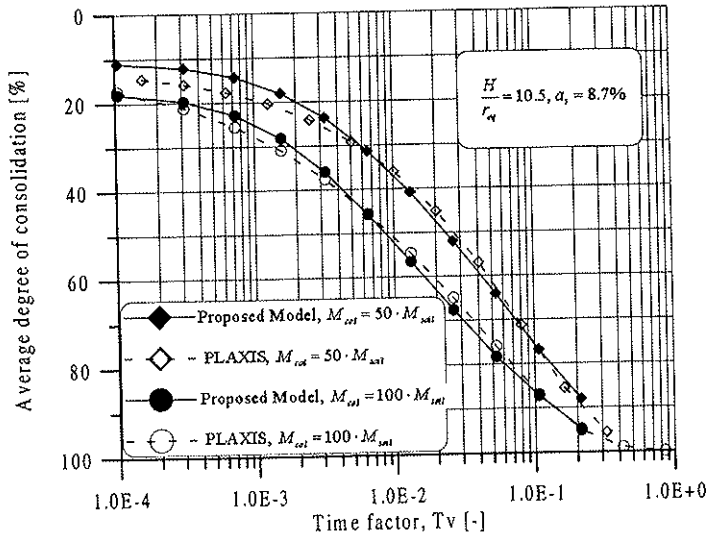


Figure 3.14 Comparison between the proposed model and the PLAXIS program for $\alpha_s = 8.7\%$.

The results presented in Figure 3.14 show the comparison between the degree of consolidation and the time factor, T_v , between the proposed model and the finite element program PLAXIS. It was assumed that the treated and untreated soils had the same hydraulic conductivity. The compression modulus ratio was equal to 50, the ratio between the soil depth H to the effective radius r_{eq} was equal to 10.5, and the area ratio, α_s , was equal to 8.7 %. Fair agreement is observed between the proposed model and the finite element analysis.

Figure 3.14 also shows that there is an increase in the rate of consolidation when the compression modulus ratio is increased. Since there is no radial flow from the untreated soil to the treated soil, the vertical time factor was selected which is defined as

$$T_v = \frac{c_v \cdot t}{H^2}$$

where

$$c_v = \frac{K_{soil} \cdot M_{soil}}{\gamma_w}$$

Similar behavior was obtained by increasing the area ratio, a_s , as shown in Figure 3.15.

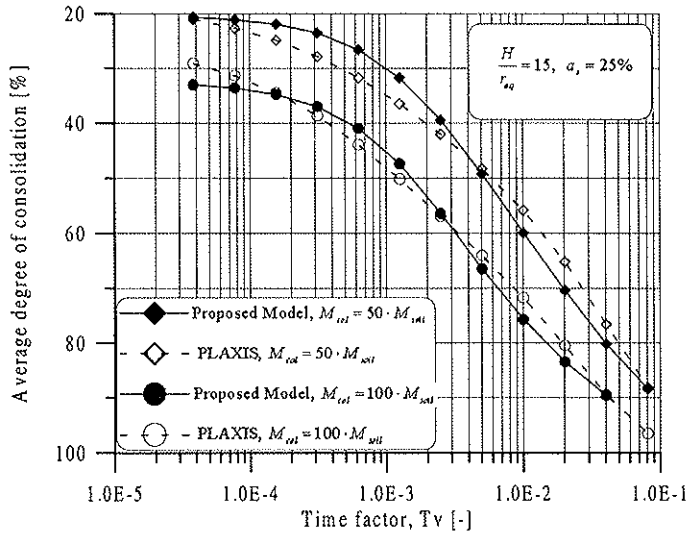


Figure 3.15 Comparison between the proposed model and the PLAXIS program for $a_s = 25\%$.

4 TEST SITES

4.1 GENERAL

This chapter describes the location, soil properties, and the installation of the lime/cement columns at three test sites. These test sites were selected in connection with the West Coast Railroad project, a project aiming at constructing a new double-track railway line along the Swedish west coast between Göteborg and Malmö, making it possible for trains to travel at a speed of up to 250 km/h. All the three test sites are located in Halland, a province south of Göteborg. Deep stabilization using lime/cement columns has been applied in some sections under the railway embankments. The location of the sites is shown in Figure 4.1.

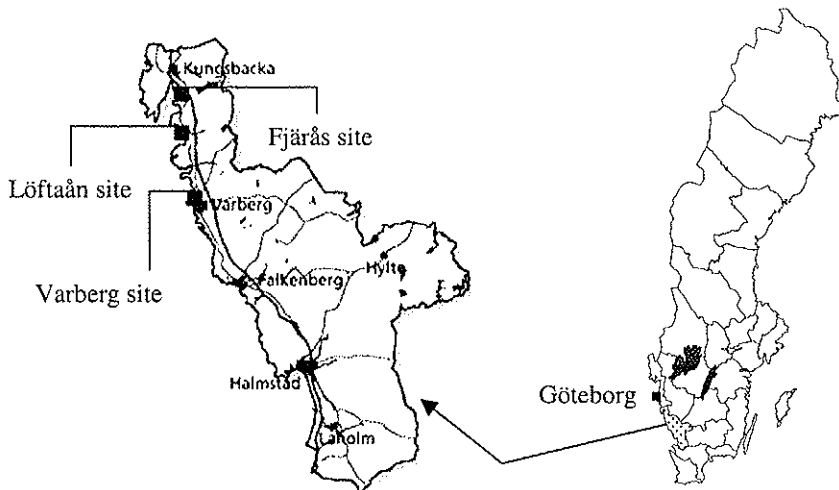


Figure 4.1 Location of the test sites.

At the Varberg test site, large-scale compression tests were performed to determine the modulus of elasticity of the lime/cement columns. To prepare columns for the tests, a steel plate connected to a wire running throughout the length of the column was installed at the bottom of the column simultaneously with the mixing of the soil. At the Fjärås test site, large-scale permeability tests at different levels were performed to measure the permeability of the columns in-situ. At the Löftaån test site both in-situ load tests and permeability tests were performed, and large samples of the columns were taken and transported to the laboratory, where large-scale triaxial tests and permeability tests were carried out. For all these test sites,

a large number of unconfined compression tests, permeability tests and triaxial tests were carried out on standard size samples of stabilized soil. The laboratory tests were performed at the laboratory of the department of Geotechnical Engineering at Chalmers University of Technology.

4.2 THE VARBERG SITE

4.2.1 Introduction

The main objective of this test site was to perform field load tests on lime/cement columns to evaluate the deformation characteristics of the columns and to compare the results with laboratory tests on standard size samples. This test site was located a few kilometers north of Varberg, see Figure 4.1.

4.2.2 Geotechnical properties

The geotechnical properties are presented in Figure 4.2. The length of the stabilized columns was chosen equal to about 5 to 6 m, and the maximum depth for the undisturbed sampling was chosen to be 8 m.

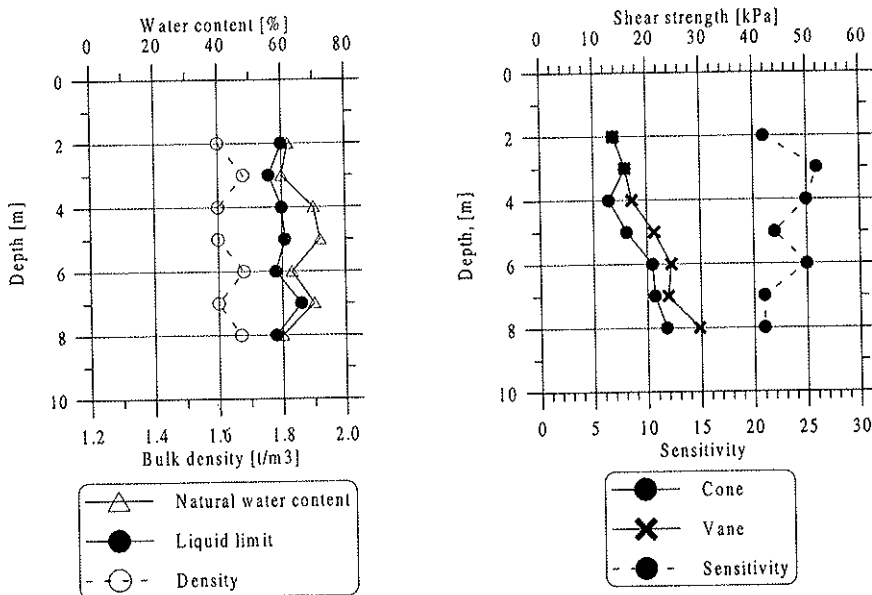


Figure 4.2 Geotechnical properties at the Varberg test site.

The soil profile consists of about 1.0 m topsoil, overlying soft, medium sensitive clay, between 20 and 25 m thick.

The undrained shear strength determined by the field vane test is about 14 kPa at 2 m depth and increases to about 30 kPa at 8 m depth. The bulk density is between 1.6 t/m^3 to 1.68 t/m^3 .

The natural water content varies between 62 and 72 %, which is higher than the liquid limit. The ground water table is situated about 1.2 m below the ground surface.

Table 4.1 shows a summary of the results from the CRS-oedometer tests. The soil is lightly overconsolidated and the oedometer modulus is between 500 and 550 kPa in the normally consolidated region.

Table 4.1 Oedometer test results at the Varberg test site.

Depth [m]	Oedometer modulus	
	Initial modulus, M_o [kPa]	Modulus in linear range, M_l [kPa]
2	9500	500
4	10000	540
6	14000	550

4.2.3 Installation of lime/cement columns

The installed lime/cement columns, about 5 to 6 m in length, were constructed by using 26 kg /m and the proportion by weight was 50 % cement to 50 % lime.

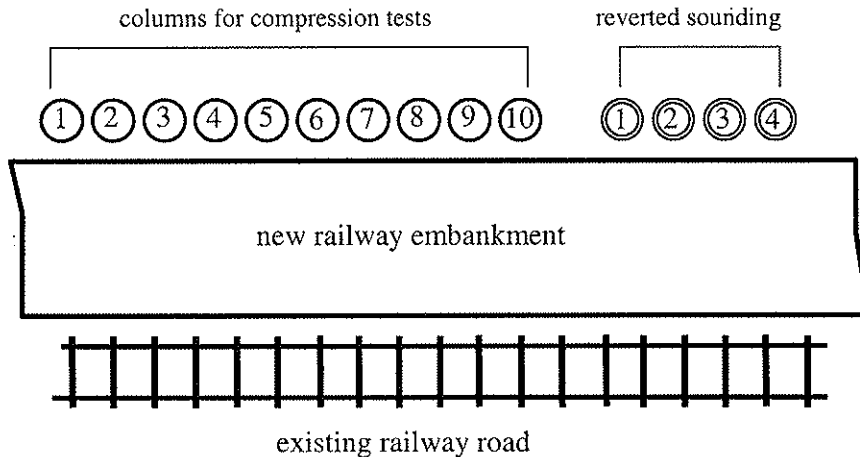


Figure 4.3 Plane of installation of lime/cement columns at the Varberg site.

The diameter of the columns was 0.6 m, which means that the stabilizing agent used was about 92 kg/m^3 of the clay. In total, 14 lime/cement columns were installed, of which 4 columns were used to determine the

shear strength of the columns. This was done by using a pre-installed probe with specially formed wings connected to a wire running through the centre of the column from the bottom to the top. The wire was installed during the installation of the columns. The remaining 10 columns were to be used for large-scale in situ compression tests. See Figure 4.3. For column 1 it was not possible to place the steel plate at the bottom of the column, while for columns 3 and 10 mixing problems resulted in a very poor column quality. No compression tests could be made on these three columns.

4.3 THE FJÄRÅS TEST SITE

4.3.1 Introduction

This site was selected in order to be able to perform field permeability tests on lime/cement columns and to compare the results with laboratory tests carried out on standard size samples taken from the field. The test site is located at Fjärås, 35 km south of Göteborg, see Figure 4.1.

4.3.2 Geotechnical properties

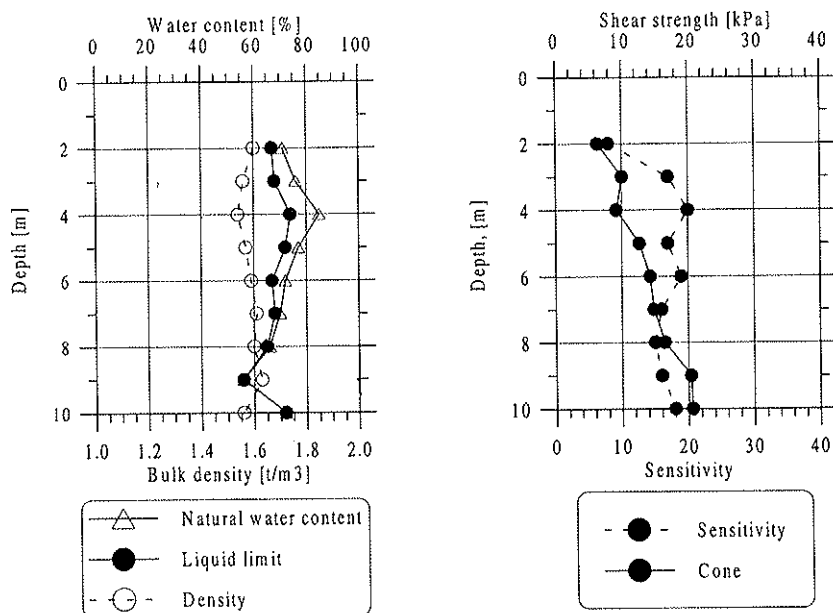


Figure 4.4 Geotechnical properties at the Fjärås test site.

The soil profile consists of a topsoil of a few centimeters followed by about one meter of dry crust. Underlying these layers there is about 25 m post-glacial clay, and the geotechnical properties of this layer are shown in Figure 4.4. The ground water table is located about 1.0 m below the ground surface, and the undrained shear strength of the clay under the hard crust was determined by fall-cone tests. The minimum undrained shear strength was 8 kPa at 2 m depth, then increasing to about 20 kPa at 10 m depth below the ground surface. The sensitivity was found to vary from 8 to 20 (medium sensitive according to the Swedish standard). The bulk density varies between 1.55 and 1.65 t/m³. The natural water content is about 70 % at 2 m depth. It increases to 85 % at 4 m depth, and then decreases to 55% at 9 m depth. At depths between 2 and 7 m, the liquid limit is less than the natural water content.

The pore pressure can be assumed to be hydrostatic. The preconsolidation pressure and the permeability of the clay were determined by CRS-tests. A summary of the results of these tests is presented in Table 4.2.

Table 4.2. CRS-oedometer test results at the Fjärås test site.

Depth [m]	Preconsolidation pressure, σ'_c [kPa]	Permeability at preconsolidation pressure, k [m/sec]	Oedometer modulus	
			Initial modulus, M_o [kPa]	Modulus in linear range, M_l [kPa]
3.2	42	$3 \cdot 10^{-09}$	8600	560
4.2	47	$8 \cdot 10^{-10}$	9000	400
6.2	69	$3 \cdot 10^{-09}$	14000	445
8.2	86	$1 \cdot 10^{-09}$	15000	665

The clay under the hard crust is slightly overconsolidated, with an overconsolidation ratio of about 1.25 at the top and 1.4 at 8 m depth.

4.3.3 Installation of lime/cement columns

The installation of the columns was done in the beginning of 1995. The columns had a diameter of 0.6 m and the length was about 15 m. The mixing was done by using 50% lime and 50% cement, and the amount of the lime/cement mixture was about 30 kg/m, representing 106 kg/m³ for columns with a diameter of 0.6 m.

The columns selected for testing were located between the side of the newly constructed railway embankment and a road passing under the

embankment, see Figure 4.5. At the test site, 1.5 m excavation work was done to expose the top of the columns. The permeability tests were performed in two stages. In the first stage, both full-scale field tests on three columns at different levels and permeability tests on standard size samples from column in situ at the laboratory were carried out. Two of these columns were single columns, while the third one was selected from columns installed in a row, see Figure 4.5. Tests at stage one were carried out during the summer of 1996. In stage two, two other columns; CTH1 and CTH2, were selected at the same site. Only field permeability tests at different levels were performed during 1997.

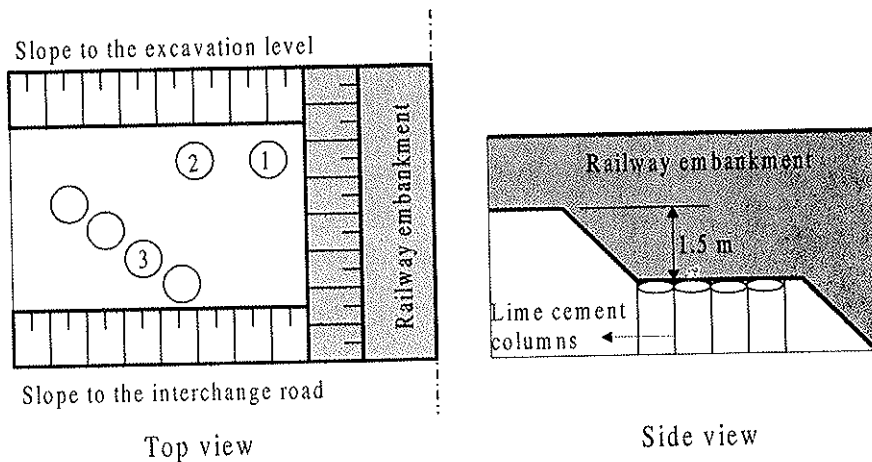


Figure 4.5. Location of lime/cement column at Fjärås test site.

4.4 THE LÖFTAÅN TEST SITE

4.4.1 Introduction

This test site was selected in order to be able to perform all laboratory and field tests on samples chosen from a limited area and to make it possible to compare the test results. This test site was located at Löftaån region about 50 km south of Göteborg. See Figure 4.1.

4.4.2 Geotechnical properties

The results of the site investigations show that the upper 0.6-0.8 m consists of silty sandy soil.

Underlying the silty sand layer is a clay layer, which extends to about 35 m depth. Both disturbed and undisturbed samples were taken to determine the

soil properties. The samples were taken from a depth of between 2 and 7 m, where 7 m is the maximum length of the lime/cement column to be installed.

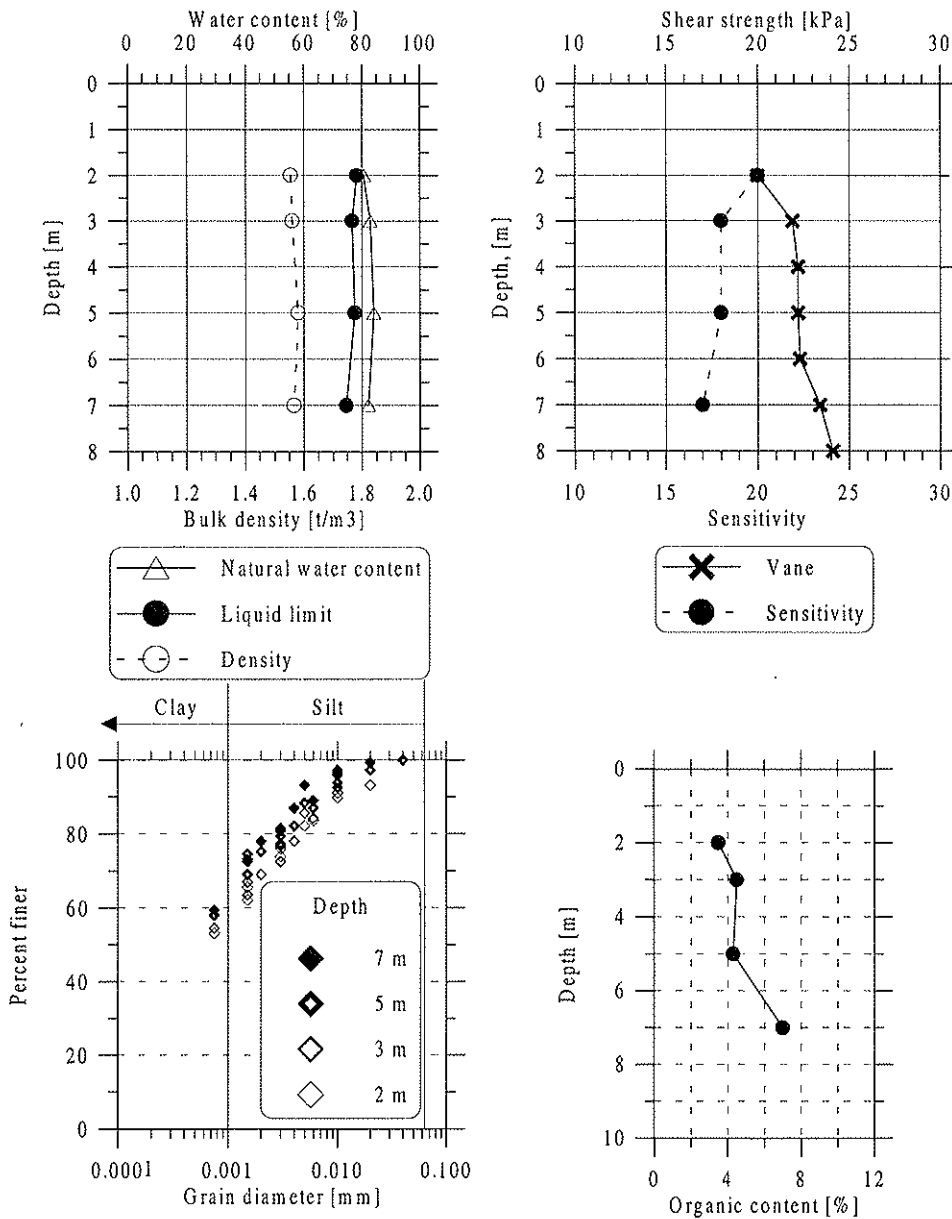


Figure 4.6 Geotechnical properties at the Löftaån test site.

The geotechnical properties are given in Figure 4.6. The tests indicate that the soil is clay, with an organic content of between 3.5 and 7%. The natural water content varies between 81% and 86% while the liquid limit varies between 74 % and 79 %, and the plasticity index is around 70 %. The shear strength from the field vane test is 20 kPa at 2 m depth and increases to 24 kPa at 7 m depth. The sensitivity is about 18, classified as medium sensitive clay (according to the Swedish standard). The pore water pressure situation after the lime/cement column installation was studied using two piezometers placed at 2.1 m and 6.1 m below ground level. The pore water pressure measured was 13.8 kPa and 57.8 kPa at 2.1 m and 6.1 m below ground level, respectively. The pore pressure observed at 2.1 m depth indicated that the ground water level was located about 0.7 m below ground level, which corresponds to the lower level of the silty sandy soil. The piezometer reading at 6.1 m depth indicates that the ground water level was only about 0.22 m below the ground surface. This most likely depends on the excess pore water pressure developed at that level due to the lime/cement column installation. CRS oedometer tests were carried out on samples taken at different depths. The test results indicate that the clay is overconsolidated. The over consolidation ratio is 4 at 2 m depth and decreases to 2 at 7 m depth. The ground level at a distance of 150 m north of the test site is about 2.8 m higher than the ground level at the test site, while at a distance of 100 m south of the site the ground level was about 1.2 m higher. Considering the topography of the region, the overconsolidation is very likely due to local soil erosion. The oedometer compression modulus values are summarized in Table 4.3.

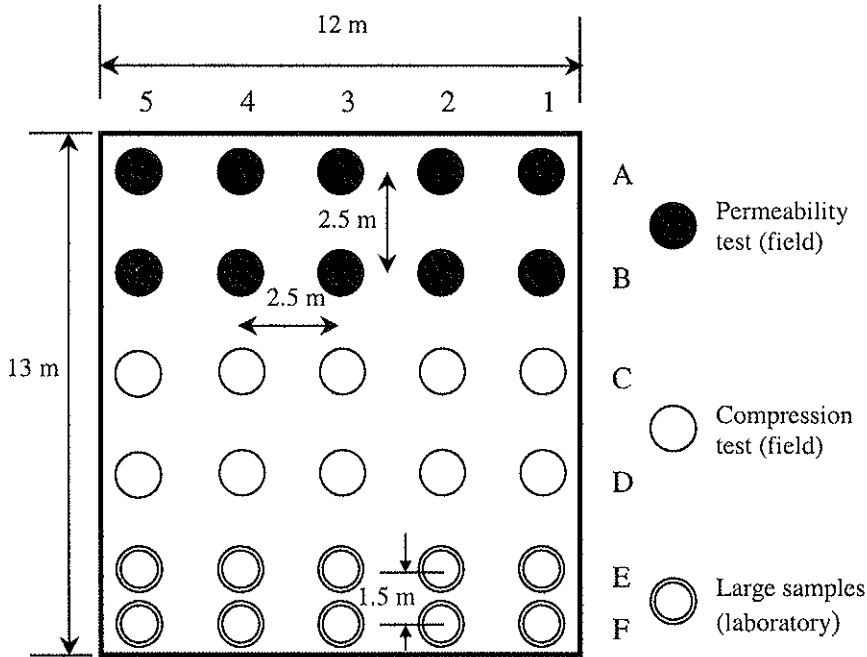
Table 4.3 Oedometer test results at the Löftaån test site.

Depth [m]	Oedometer modulus	
	Initial modulus, M_o [kPa]	Modulus in linear range, M_l [kPa]
2	6000	450
3	6000	540
5	7000	390
8	8000	440

4.4.3 Installation of lime/cement columns

Totally 30 lime/cement columns were installed to a depth of 7 m, see Figure 4.7. The columns were installed in early March 1999.

Twenty of the columns were intended for field permeability tests and to take large samples to be tested in the laboratory. The remaining 10 columns were used for performing field compression tests. The columns installed had a lime/cement mixture of 50/50 per cent by weight with 38



kg/m column length. Since the column diameter was 0.6 m, this corresponds to about 135 kg/m³.

Figure 4.7 Plan of columns installation at the Löftaån test site.

5 FIELD TESTS

5.1 LOAD TEST

5.1.1 General

Different methods can be used to determine the compression modulus of a lime/cement column. In the laboratory, the compression modulus can be determined by performing triaxial tests on both large and standard size samples, oedometer tests and unconfined compression tests. In the field, the modulus of a lime/cement column can be determined by full-scale embankment load test. Another alternative is to perform field load tests on a single column with fairly short length. Kivelö (1994) performed field load tests on short columns supported at firm bottom. Wires anchored at the firm bottom were used to counteract the load applied at the top of the column. In case of deep clay deposits, it is impossible to use this method. A new method, developed by LC-Markteknik, was used to perform load tests at the Varberg and Löftaån test sites. This method is described in detail in the following section.

5.1.2 Installation

When the column is being installed, a cross-shaped plate connected to a wire is placed at the bottom of the column. The sides of the plate are shaped as a propeller. This makes it easy to press down the plate by the aid of rotation to the desired depth, see Figure 5.1.

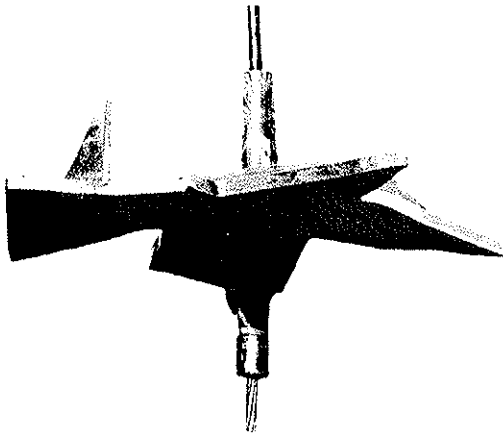
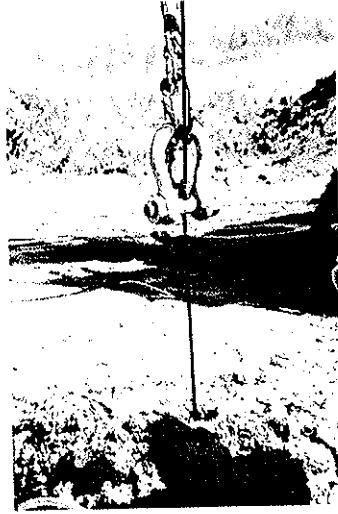


Figure 5.1 The cross-shaped plate connected to the wire.

The wire runs through the center of the column to the ground surface, and the area of the plate is about 70% of the column area. The wire used in the installation is coated with smooth plastic material to minimize the friction against the column material surrounding the wire at the time of the test. At the upper side of the plate, two small plates are welded, which will be in contact with the mixing tool arms to rotate the plate during the penetration, see Figure 5.2.



The mixing tools and the bottom plate



The upward pulling of the bottom plate

Figure 5.2 The starting and the finishing of the column installation.

The binder outlet hole in the mixing tool is located about 0.5 m above the bottom of the plate, and it is expected that the soil between the plate and the bottom of the column will be almost unmixed.

To ensure that the plate will be in direct contact with the column bottom and to avoid problems during the load test, the wire connected to the plate must be pulled in the upward direction at least 0.5 m, directly after the installation of the column, see Figure 5.2.

To be able to measure the deformation in the column at different levels during load test, holes must be made in the column directly after the column installation or drilled a few days before the load test. At the Varberg test site, four holes in each column were made at levels of about 15%, 35%, 60% and 95% of the column length. The holes were made directly after the installation of the columns by pushing down a corrugated plastic tube to the desired level. The end of the plastic tube which penetrated the column was connected to a conical steel tip in order to

facilitate the penetration of the tube and to have better support for the tell tales during the load test.

At the Löftaån test site, the holes were drilled using the water washing drill method. The drilling was made shortly before the load test. One of the advantages of this method is that the drilling log gives information about the drill resistance at very close intervals and thereby also information about the quality of the column along its length. However, there is a disadvantage of using this method in that the drilling equipment may damage the top surface of the column and that the damaged part must be removed before the instrumentation phase. Columns at this site were between 5.8 m and 6.2 m long and the holes were drilled to depths of 20%, 40%, 80% and 100% of the total column length.

5.1.3 Instrumentation and test procedure

The upper part of the lime/cement column is usually weaker than the rest of the column. This is due to the mixing procedure, as the high air pressure used to distribute the binder will cause the soil surface to deflect upwards. The other reason is the type of soil, which in the case of Varberg is dry crust soil and, in the case of the Löftaån site, silty sandy soil. Thus the first step to prepare the column for load tests is to expose the top of the column and to identify better column quality.

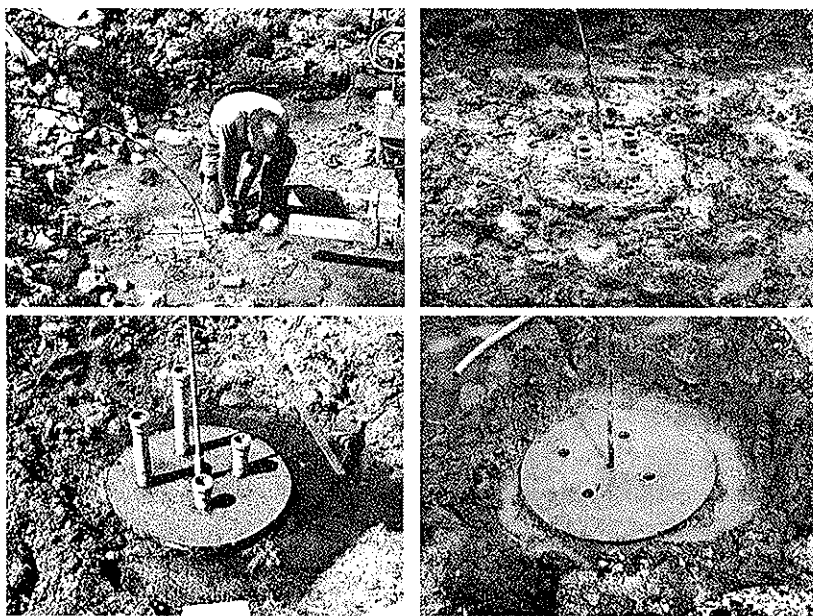


Figure 5.3 Preparation of the top of the column at the Löftaån test site.

A steel casing, 0.2 m in length with an inner diameter equal to the column diameter, was used for each column to support the upper part of the column and to act as a form for the leveling cement. It is very important to make sure that the upper steel plate will be in proper contact with the top of the column, Figure 5.3.

A steel plate was then placed at the top of the column and four tell tales were installed. A hydraulic jack with a hole in the center was placed on the top plate, followed by a load cell. Finally, a lock ring was used to lock the wire to the jack and the load cell, see Figure 5.4.

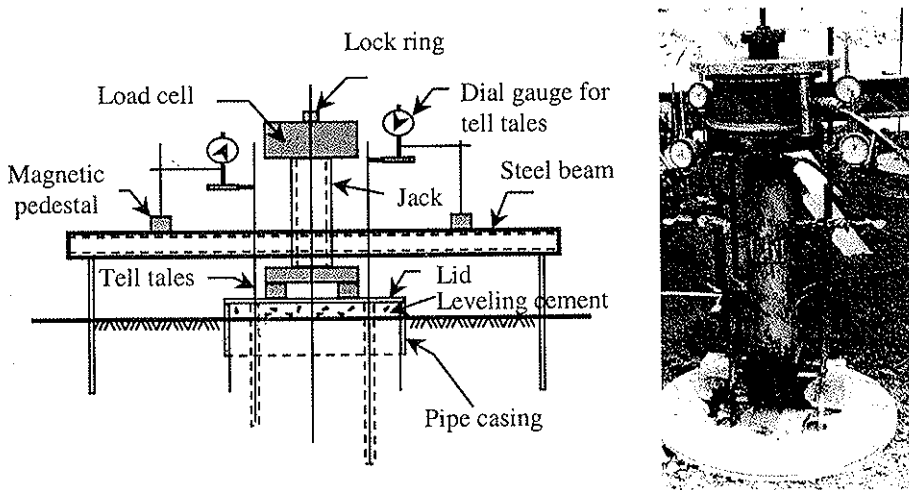


Figure 5.4 Instrumentation used for load test.

To measure the displacement at the top of the column and at the four levels inside the column, five dial gauges with 1/100 mm reading accuracy were used. The gauges were held by magnetic pedestals, which in turn were placed on steel beam. Two augers driven to a certain depth were used to support the beam. Leveling was done at the top of the augers before and during the load test to measure a possible downward movement of the beam and to be able to correct the dial gauge measurement as a result of this movement. Applying a tension force to the wire using the hydraulic jack thus compressed the column and the load test was then carried out.

From the result of laboratory tests on standard size samples, and in the case of the Varberg test site results from reverse column penetration tests, the failure load was estimated. The tests were carried out as maintained load tests with constant load increment. At the Varberg test site, the load increment was 6 kN and a new increment was applied every 8 minute.

At each load step dial gauge readings were carried out at 1, 2, 4 and 8 minute time intervals. At the LÖftaån test site, the load step selected was 10 kN with a new increment every 16 minutes. In case of a very good column quality or when no local failure was possible to occur, the wire capacity, which was about 180 kN, was the factor that decided the end of the load test. The instruments used in the tests were always protected from direct sunlight during the load tests to avoid errors resulting from temperature changes.

5.1.4 Finite element model

The objective of the finite element analysis is to estimate the compression modulus of the lime/cement column based on the load test results. An iterative procedure is needed to ensure that the deformations from a load test at a certain applied load and on different depth levels of the column are about the same as the results calculated from numerical analysis based on assumed values of column compression moduli. Although the lime/cement column is considered to be a somewhat heterogeneous material, the column in this model was treated as a homogenous material for the sake of simplicity.

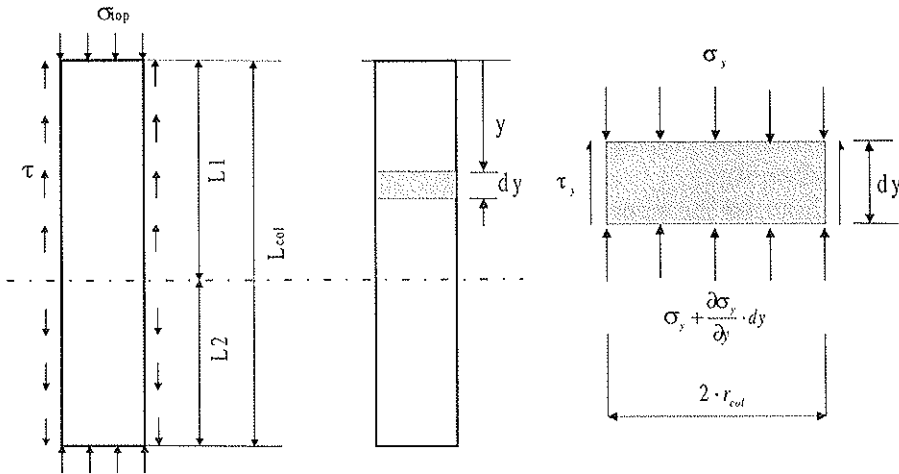


Figure 5.5 Vertical stresses acting on the column.

A simple analytical model will first be discussed briefly. In this model the lime/cement column and the clay are assumed to behave as linearly deformable homogeneous materials. Part of the applied load at the top and the bottom of the column is transformed to the surrounding clay by the development of shear stresses along the boundaries between the two

materials. From the vertical load equilibrium of a small element of the column shown in Figure 5.5, the following relationship can be established:

$$\frac{\partial \sigma_y}{\partial y} = -\frac{2 \cdot \tau_y}{r_{col}} \quad (5.1)$$

σ_y vertical stress in the column at depth y
 τ_y shear stress on the column periphery at depth y
 r_{col} radius of the column

The vertical axial strain in the same element is expressed as

$$\frac{\partial \delta_{col}}{\partial y} = -\frac{\sigma_y}{E_{col}} \quad (5.2)$$

δ_{col} vertical displacement of the column
 E_{col} Young's modulus of the column

By differentiate equation (5.2) with respect to (y) and solving the new equation with equation (5.1), the shear stress can be written as

$$\tau_y = \frac{E_{col} \cdot r_{col}}{2} \cdot \frac{\partial^2 \delta_{col}}{\partial y^2} \quad (5.3)$$

The shear stresses along the boundary of the column depend on many factors, such as the dimension of the column, the stress level in the column and the material properties of the column as well as the properties of the surrounding soil.

In the light of the above-mentioned simple elastic model, it is expected that, in the case of the elastic-perfect plastic model, the possible failure mechanisms during load tests are bulging failure of the lime/cement column or shear failure the boundaries between the column and the clay when the shear stresses there exceed the shear strength of the clay.

To have a wider view of the above discussion, a numerical model was created and a number of numerical simulations were carried out. The geometry of the numerical model used in these simulations is shown in Figure 5.6. Since the problem is symmetric, only one half of the problem requires modeling. The lime/cement column and the clay are modeled using 15-noded triangular elements with 12 integration points at which the stresses are calculated. The steel plates at the top and bottom of the column are modeled using a 5-noded beam element. The input parameters for the beam element are the flexural rigidity EI , Poisson's ratio ν , and the normal stiffness EA . The weight of the plates was neglected. The applied load

resulting from the tension in the steel wire was modeled as a distributed load at the ends of the column and was given as load per unit area. In the preliminary calculations, the applied load was modeled as a pretension load in an anchor element connected to the two plates at the top and bottom of the column.

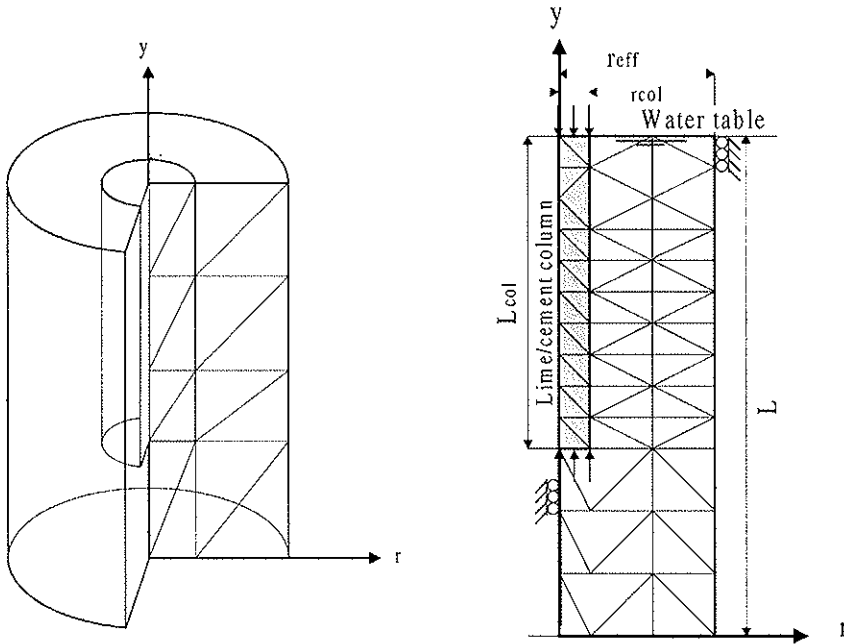


Figure 5.6 The axial symmetrical model.

The two ways of defining the applied load give the same results, and simulation using the first model was selected from a practical point of view.

The left vertical boundary was by definition an axis of symmetry. The vertical sides in this model were assumed to have roller conditions, which means that vertical displacements were free to develop and that no horizontal displacements were allowed. As for the base of the model, full fixity was assumed.

The model used in these simulations was linear elastic, and both the column and the surrounding soil were assumed to be isotropic. A drained material type with a Poisson's ratio of 0.3 was assumed for the column materials and the surrounding soil was assumed to behave as an undrained material. The results from these simulations are presented in Figure 5.7. In these figures the ratio between Young's modulus of the column and the

surrounding soil was varied from 5 to 100. The normalized shear stress change along the column length is presented together with the normalized vertical stress. As the stiffness ratio increases for the same load applied at the top and the bottom of the column, the shear stress decreases. By considering equation (5.1), the shear stress at any depth is related to the derivative of the normal vertical stress at that depth and, as the shear stress decreases, the slope of the vertical stress-depth curve will decrease. As the stiffness ratio increases to infinity, no shear stresses will develop along the boundaries, the slope at any depth becomes equal to zero and the normal vertical stress becomes constant along the depth and equal to the applied load.

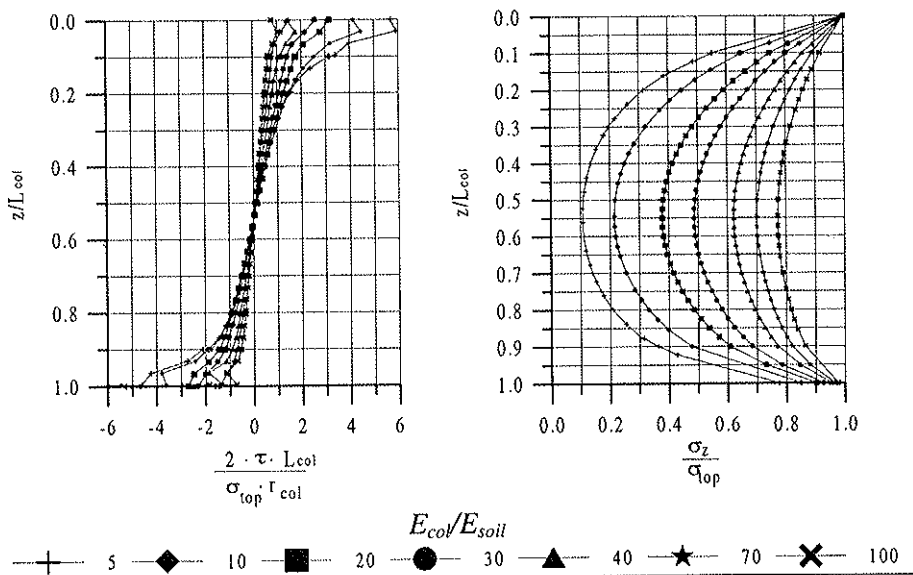


Figure 5.7 Distribution of the shear stress and the normal vertical stress along the column for different modulus ratios.

5.1.5 The compression modulus and the creep load of the lime/cement column

In the next sections finite element simulations are carried out to back-calculate Young's modulus of the lime/cement columns based on the results from the load test. The question is for which load a representative Young's modulus is to be calculated and what the suggestions are for how to determine that representative load.

In soil mechanics, it has often been the practice to select the secant modulus, E_{50} , at a point on the stress-strain curve corresponding to half the failure strength and to use this for predictions of deformations, see Figure

5.8. Furthermore, the evaluation of the column modulus from the laboratory tests carried out on standard size and large samples was based on the secant modulus E_{50} and, thus, the evaluation of the column Young's modulus for the field tests will be based on the same principle.

To study the column modulus change with the variation of the stress level, the column secant modulus was in some cases evaluated at other stress levels than those related to 50 % of the failure load.

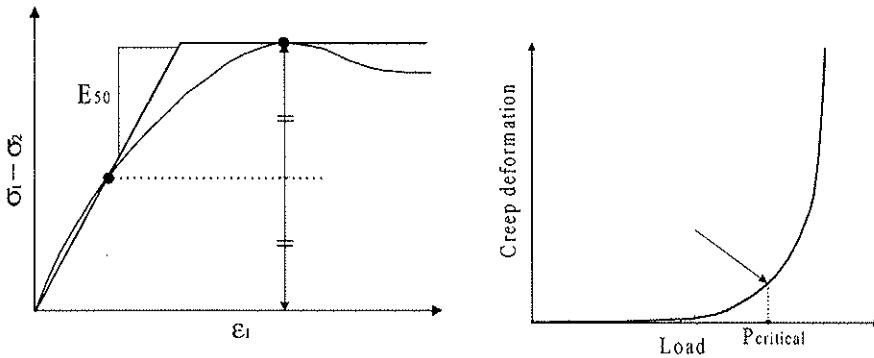


Figure 5.8 The definition of the E_{50} modulus and the critical load.

The critical load evaluated from the load-displacement curve of a pile load test is defined as the break point in the creep curve, and the creep load of the lime/cement columns was evaluated using the same procedure.

5.1.6 The Varberg test site

As mentioned in chapter 4, a total of 10 lime/cement columns were installed assigned for load tests. Due to installation problems, no compression tests could be performed on columns 1, 3 and 10. During the instrumentation and test process, problems appeared, and test results from another two columns, 2 and 6, were disregarded. Load tests were carried out on the remaining five columns and, for column number 5, a special test was made trying to measure creep deformation in the lime/cement column. The instrumentation was the same with the only exception that a spring with known stiffness was placed between the top plate and the hydraulic jack, with a lock ring located between the spring and the jack. The lock ring can be used at any load step to isolate the hydraulic jack so that the loading on the column can be applied by the spring, which is in compression. For column 5, the estimated load at which large vertical deformations start to develop was about 60 kN. At load steps of 30 kN and 60 kN applied load, the lock ring was used, and the column was subjected to the load induced in the spring during 24 hours. In this case another two dial gauges were used on a steel plate above the spring to measure the relaxation of the spring. Column 9 was tested with the same procedure as column 5 with the exception that the column was unloaded before reaching failure. The column was then reloaded using the normal step load procedure. Only results from the reload test are presented.

5.1.6.1 Test results

Before the load tests were started, three reverse column penetration tests were conducted. Results from these tests are presented in Figure 5.9.

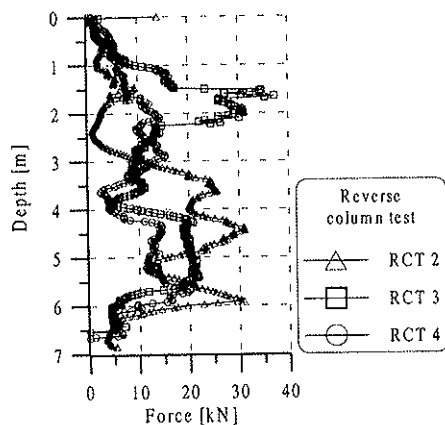


Figure 5.9 Results from reverse column penetration tests at the Varberg test site.

The results showed very low resistance at the upper 0.5 m of the lime/cement column, and this was the reason behind the excavation of the column top by about 0.5 m. Load test results are given as axial vertical deformations versus depth below the top of the column for different load steps.

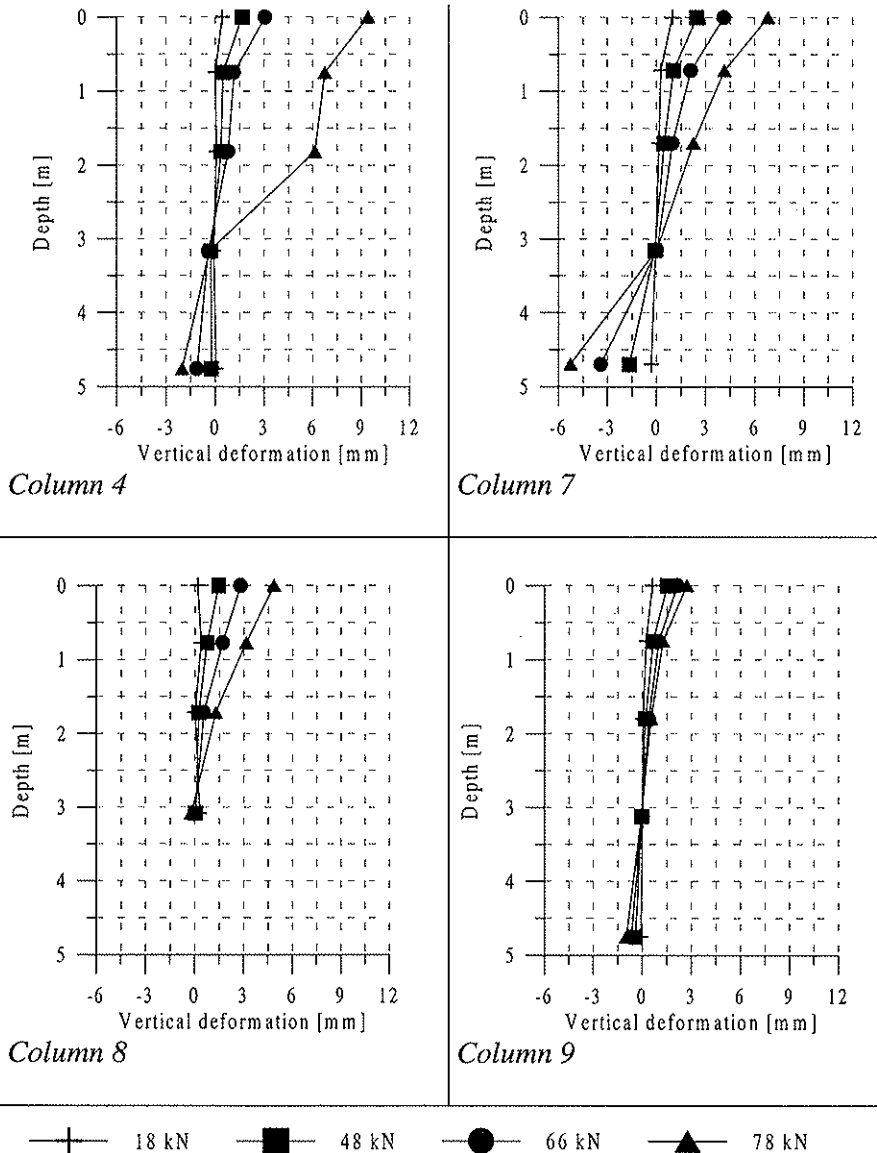


Figure 5.10 Load test results at the Varberg test site.

The column is subjected to a compression load at both ends. The deformation in the column has a maximum positive value at the top of the column, which decreases with depth until it becomes zero at a point below the middle length of the column. Then it changes sign to increase again to a maximum negative value at the bottom of the column. In Figure 5.10, results from columns 4, 7, 8 and 9 are given. Although each load step was measured, only load steps 18 kN, 48 kN, 66 kN and 78 kN are presented. It is important to mention that the values of the deformation for each load step are based on the results observed at the end of the load step with 8 minutes duration.

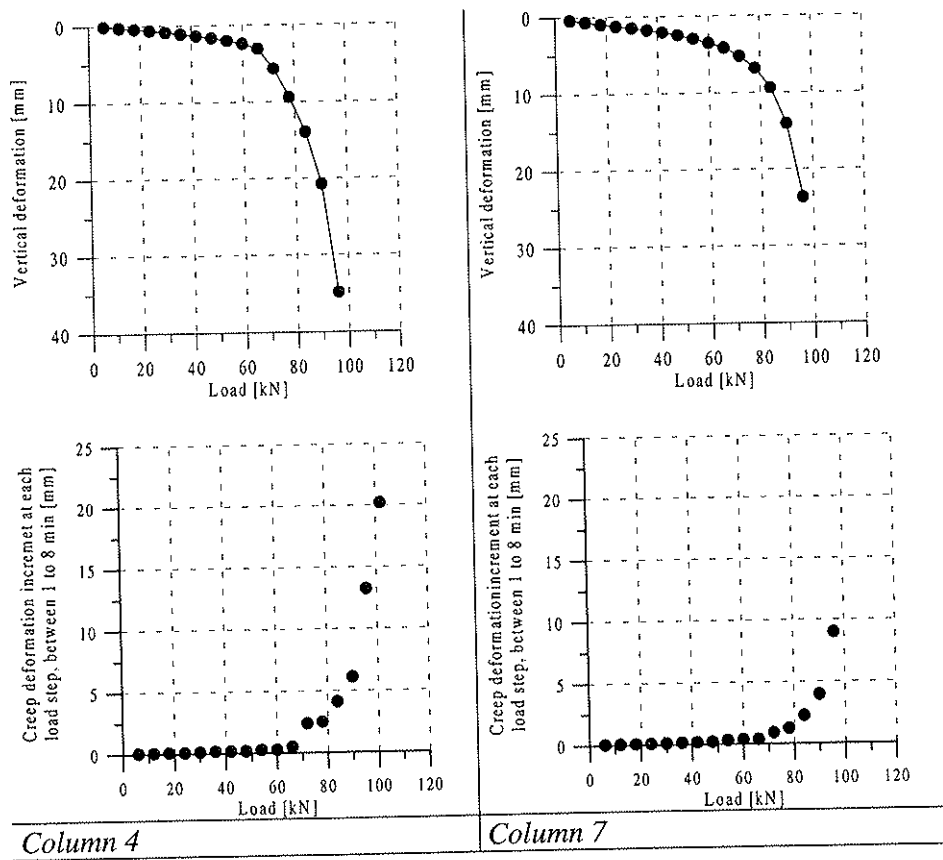


Figure 5.11 Total and creep deformation at the top of columns 4 and 7 as a function of load.

Theoretically, the deformation at the top of the column is larger than the deformation at the bottom, which can be explained by the fact that the horizontal pressure at the bottom of the column is larger than that at the top. In the Varberg test site, there is another factor, which is related to the

increase of the stiffness on the clay with the depth. This can explain why the deformations along the column length change sign at a depth larger than half of the length. Although the bottom plate was pulled up 0.5 m directly after the installation of the column to ensure direct contact with the column material, it seems that the bottom of column 7 was not pulled up enough since the deformations there are still large.

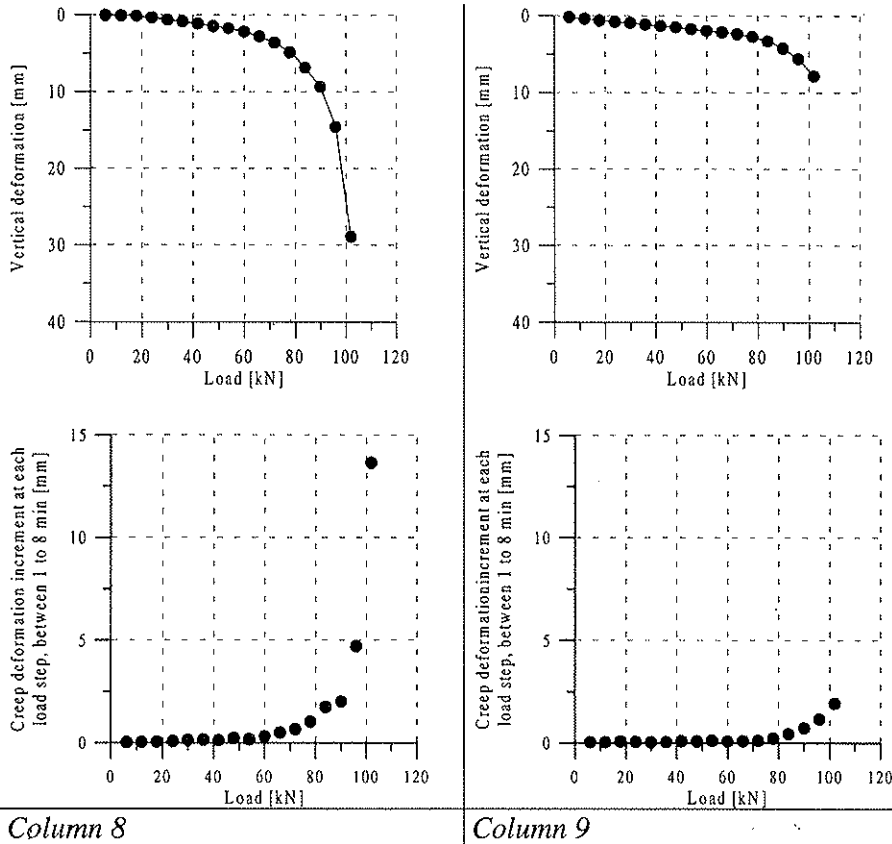


Figure 5.12 Total and creep deformation at the top of columns 8 and 9 as a function of load.

The load test results show that the deformations in column 9 are smaller than the deformations in the other columns shown in Figure 5.10. This can be explained by the fact that column 9 was subjected to a load-unload and reload process. In column 8, it was not possible to place the fourth tell tale to the lowest level and thus no measurement was possible to make at that depth. The first meter of the upper part of the columns had a somewhat different quality, as the clay there originally consisted of dry crust. This is

one of the factors behind the deformations at this part of the columns becoming larger than at the other parts.

The maximum deformation was obtained at the top of the column, and the failure of the column can be defined as local failure occurring at that point. Figure 5.11 and Figure 5.12 show the load-deformation at the top of the lime/cement columns.

The curves in the Figure consist of two parts, an almost straight part, linear with low deformation, followed by a non-linear part with large deformations. In columns 4 and 7, the deformations become non-linear at applied loads of 66 kN. The related deformations at the top of these columns are 3.1 mm and 4.2 mm respectively. As for column 8 and column 9, these loads are 60 kN and 78 kN, and the related deformations at the top of the columns are 2.2 and 2.7 mm, respectively.

The columns were loaded in equal load increments with 8 minutes duration to be able to study the creep deformations in the columns; the results are shown in Figure 5.11 and Figure 5.12. It can be very clearly observed that the creep deformations in the columns increase rapidly directly at the beginning of the non-linear portion of the load-deformation curve, and a creep load capacity can be evaluated.

The creep deformation was studied for different load steps with 7 min time interval (from 1 minute to 8 minutes).

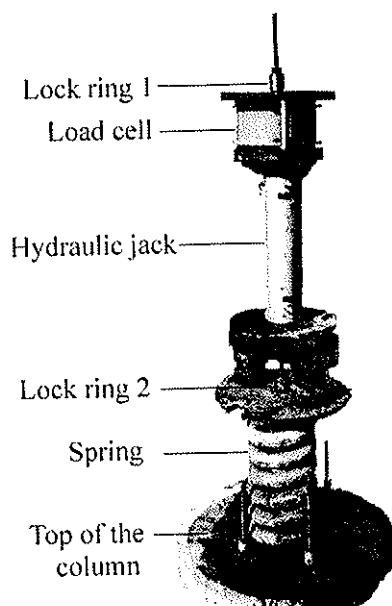


Figure 5.13 Instrumentation used for load test carried out on column 5.

During the load test carried out on column 5, longer time intervals were used in two load steps in order to study the time duration effect on the creep deformation. As for the other columns, the critical load at which the deformation starts to become large was evaluated to be about 60 kN. Two day's time interval was used for the first load step of 30 kN, while 4 day's time interval was selected for the load step of 60 kN. As for the other load steps, the usual 8 minutes time interval was used. The instrumentation of column 5 is shown in Figure 5.13.

It was not possible to use the hydraulic jack to apply a constant load during several days. To solve this problem, a spring with stiffness of about 1.3 kN/mm was placed between the top of the column and the hydraulic jack. Two lock rings were applied, one above the load cell to be used during the usual routine test and the other between the spring and the hydraulic jack to isolate the two parts during the long time interval load test. The load test was first carried out using a 6 kN load step at 8 minutes time interval.

At load step 30 kN, lock ring 2 was locked, and the creep deformations during two days were measured. The applied load decreased from 30 kN to about 28.6 kN, and the total creep deformation during this time interval was only 0.08 mm. Lock ring 2 was unlocked and the load was increased until it reached the predicted failure load of 60 kN. Then the ring was locked again and the creep deformations were measured during four days. During this time the load decreased from 60 to 56.5 kN, and the creep deformation was about 0.31 mm.

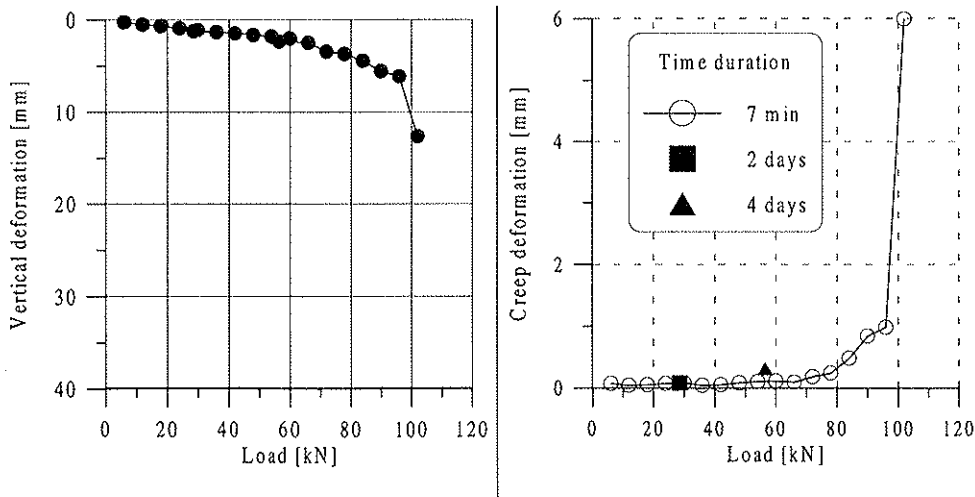


Figure 5.14 Results from load tests carried out on column 5.

The load-deformation curve and the creep deformation at the top of column 5 are presented in Figure 5.14. As is shown in the figure, the creep

deformation increases when the load exceeds 66 kN. At the same time, the total deformations start to increase rapidly.

The 30 kN and 60 kN load increments, where the long-term creep deformations were observed, are within the linear part of the load-deformation curve, which may explain the low creep deformation development with time at these load steps.

Applying the definition of “critical load”, described in Figure 5.8, the critical load for the columns 4, 7, 8 and 9 are about 78 kN, 84 kN 84 kN and 92 kN, respectively.

5.1.6.2 Finite element simulations

The simulations carried out are related to the linear part of the load-deformation curve at the top of the column, which is characterized by small deformations, thus the lime/cement column and the clay are treated as linear elastic materials. Young’s modulus, E , and Poisson’s ratio, ν , are parameters required for the elastic model used for the current problem. Since the water table is located 1 m below the top of the excavated column, the clay below the water table is modeled using undrained analysis.

In the absence of direct measurements of the undrained compression modulus of the clay, an empirical method based on the plastic limit and the undrained shear strength was used. The plastic limit of the clay at the Varberg test site was found equal to about 35%. The following equation is proposed by (Hansbo and Sällfors 1984), to evaluate the elastic modulus of normally consolidated clay.

$$\frac{E_{50}^u}{c_u} = 150 \quad (5.4)$$

E_{50}^u undrained secant modulus at 50 % of the failure load

c_u undrained shear strength of the soil

The undrained shear strength resulting from vane tests varies from about 14 kPa at 2 m depth to about 24 kPa at 6 m depth. According to the above equation, the related undrained modulus of elasticity of the soil is about 2 MPa and 3.5 MPa respectively. The soil parameters used in this model are presented in Table 5.1

Laboratory triaxial tests carried out on large samples of lime/cement columns showed that very low or almost no pore water pressures developed during the tests.

Table 5.1 Material parameters used in the simulation.

Soil type	Material parameters		
	γ [kN/m ³]	E_{ref} [MPa]	ν [-]
Hard crust	17	6	0.3
Clay	16.5	2*	0.495
Column (top)	16.7	To be evaluated	0.3
Column (bottom)	16.7		0.3

* The modulus increase with 0.3 MPa/m.

Furthermore, air bubbles were observed to come from holes made in the column, which shows that small amounts of air trapped by the soil skeleton are present in the column. The lime/cement column is a very stiff material and even degrees of saturation slightly below 100 % will result in the development of very low pore water pressure in the column. This will be discussed in detail in Chapter 6. Therefore, in the proposed numerical model used here, drained analysis is assumed for the lime/cement column, above and below the water table. It is important to mention that preliminary numerical calculations, with drained and undrained material behavior of the lime/cement column, give almost the same results. This can be explained by the fact that the column is surrounded by clay, which in undrained condition acts as a very stiff material, which prevents the column from deforming freely. As was shown in Figure 5.10, the deformations at the top of the column are large and deviate from the remaining part of the column. Two types of column material are assumed. The column material above the water table is assumed to have lower strength than the rest of the column.

The model was implemented using the finite element code, PLAXIS.

Some numerical simulations were carried out assuming that the lime/cement column and the clay behave as elastic, perfectly plastic material obeying a Mohr-Coulomb yield criterion. The last model was to control the plastic state of the two materials at the end of the elastic part of the stress-strain curve.

Beside the elastic material parameters presented in Table 5.1, the additional material parameters needed for this model are: cohesion c' , friction angle, ϕ' , and dilatancy angle, ψ . Effective parameters will be applied for both drained and undrained analysis to define Mohr-Coulomb's yield function. The angle of internal friction ϕ' of the clay was assumed to 30° and the cohesion intercept c' to 2 kPa.

The strength parameters of the lime/cement column used here are based on suggested values presented by Baker et al. (1997) see Table 5.2.

Table 5.2 Stress-strain and strength properties of lime/cement columns, after Baker et al. (1997).

Relative quality	M_{col} [MPa]	c' [kPa]	ϕ' [°]	ν [-]
Low	10	30	35	0.3
Normal	17	50	35	0.3
High	35	100	35	0.3
Very high	175	175	35	0.3

The dilatancy angle, ψ depends on the friction angle and is calculated as

$$\psi \approx \phi - 30^\circ$$

Preliminary simulations were first carried out by selecting the two load steps 48 and 60 kN. The column material was assumed to have the same quality along the whole column length. For each load step, two simulations were conducted with 100 and 300 MPa column stiffness.

The simulation results are plotted together with the field test results for columns 4, 7 and 8, as shown in Figure 5.15. The deformations measured in the field are found between the simulation curves based on column Young modulus, E_{col} , between 100 MPa and 300 MPa.

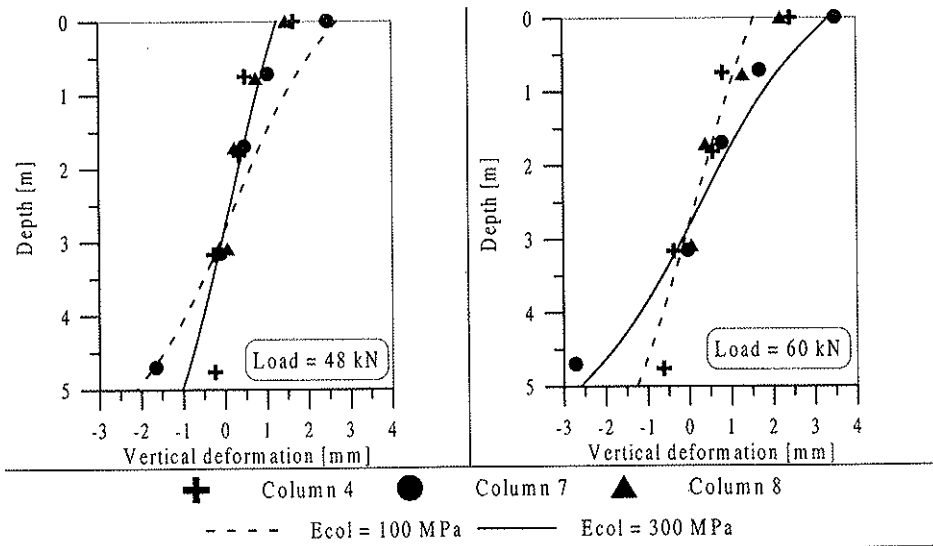


Figure 5.15 Preliminary simulations for columns 4, 7 and 8 at load steps 48 and 60 kN.

However, as mentioned before, the deformations at the bottom of column 7 were rather large, which is caused by the reduced quality of the column material there. Moreover, the simulations show that the upper parts of the column were of poorer quality than the remaining part.

Some of the results of the numerical calculations are presented in Figure 5.16. The results of all the numerical calculations are presented in appendix B.

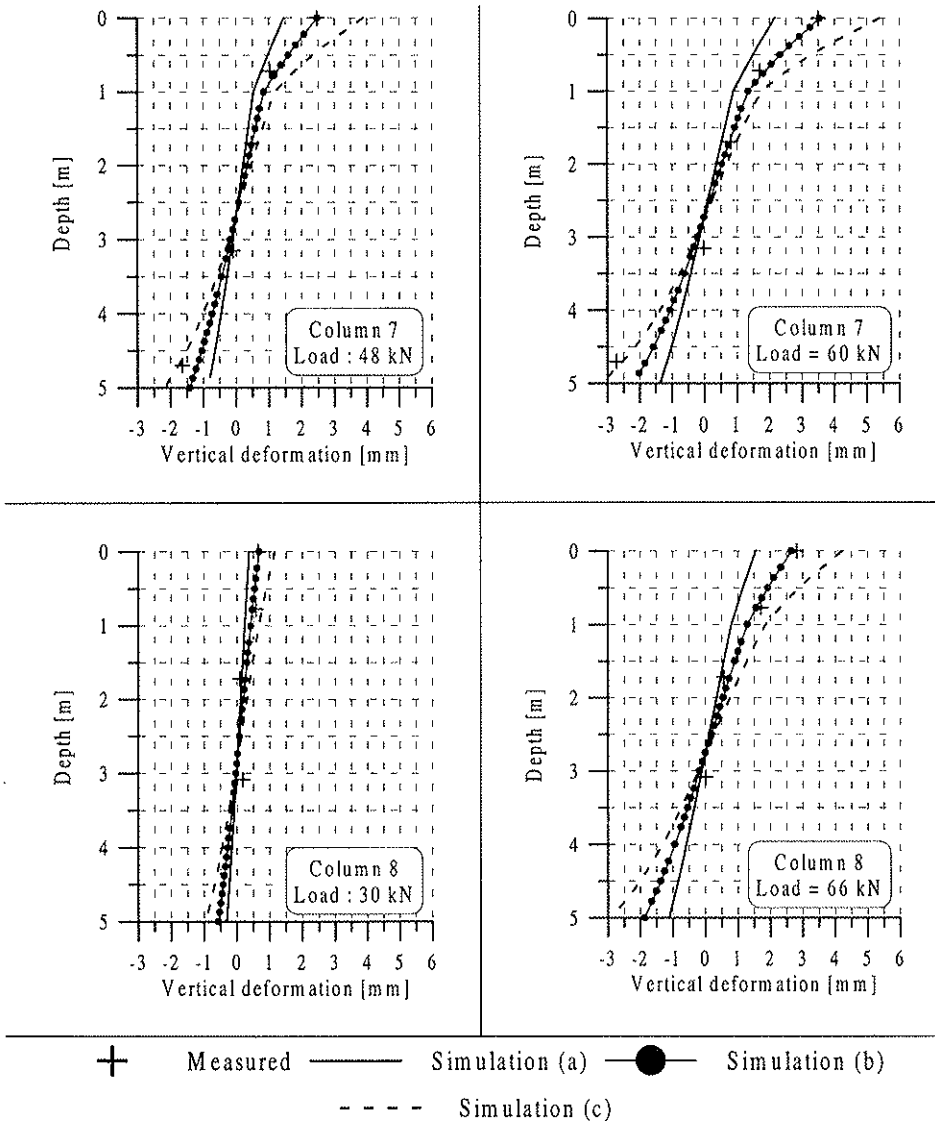


Figure 5.16 Numerical calculation results.

In columns 4, 7 and 8, a local failure was observed to occur at the top of the column. The column secant modulus, E_{50} , was evaluated at the 50 kN load step, which is about 50 % of the failure load. However, more numerical calculations were carried out to evaluate the column modulus at other loads than that related to 50 % of the failure load. As for column 9, no local failure was observed and the secant modulus was calculated at loads of 48 kN and 66 kN.

The measured deformations for a specific load step are presented together with three different curves resulting from numerical calculations. The curve resulting from simulation (b) is the "best fit" curve evaluated from several attempts done by changing the column compression modulus to get the deformations in the column as close as possible to the actually measured deformations, see Figure 5.16. Curves resulting from simulations (a) and (c) are based on curve (b), where the modulus of the columns at the top and the rest of the column was doubled in the case of simulation (a), and decreased by 50 % in the case of simulation (c) to observe the sensitivity of the results.

The values of the lime/cement column modulus obtained from numerical simulation (b) are shown in Table 5.3

Table 5.3 Results of numerical calculations for columns 4, 7 and 8.

Column nr.	Load	Stress	Column Young's modulus	
			The first meter	The rest of the column
	[kN]	[kPa]	[MPa]	[MPa]
4	48	170	120	500
4	54	191	100	500
4	60	212	90	500
4	66	234	80	400
7	36	128	80	200
7	48	170	80	200
7	60	212	70	140
8	30	106	360	360
8	36	128	360	360
8	48	170	200	300
8	66	234	140	200

As indicated by the results shown in the above table, the column Young modulus decreases as the load increases. The reduction in the column stiffness becomes large as the applied load reaches the end of the linear

part of the load-deformation curve. The secant modulus E_{50} of standard size column samples presented in Chapter 6 for both laboratory prepared samples and field mixed samples is much smaller than the secant modulus of the columns evaluated from field load tests at an applied load of about 50 kN.

As was mentioned before, column 9 was subjected to a loading-unloading and reloading processes. Column 9 is observed to have the highest Young modulus in comparison with the other two columns tested, see Table 5.4. The modulus at the top part of the column remained unchanged for the selected applied loads shown in the table while, at the remaining part of the column, a decrease in the column modulus was observed when the applied load was increased.

Table 5.4 Results of numerical calculations for column 9.

Column nr.	Load	Stress	Column Young's modulus	
			The first meter	The rest of the column
	[kN]	[kPa]	[MPa]	[MPa]
9	48	170	120	500
9	66	234	120	400

Other simulations were made to observe how sensitive the results are when the elastic properties of the soil surrounding the column are changed. A slight increase in the calculated column Young modulus was observed, when the Young modulus of the top soil was changed from 6 MPa to 3 MPa, see Table 5.5.

The changes depend mainly on the stiffness of the column. If the column is assumed to be very stiff, the apparent changes in the column modulus caused by a variation of the clay modulus are very limited. In other simulations where an extreme case was studied, Young's modulus of all the surrounding soil was reduced by 50 %, and the column modulus was kept unchanged, after which measured vertical deformations along the column length were compared with the deformations calculated by numerical simulations. In column 4, the differences were small for the applied loads of 48 kN and 66 kN, yet the resulting deformations in 66 kN loading were slightly larger than the deformations calculated with 48 kN applied load. In column 7, the resulting deformations at load 36 kN were limited to stay between the curves resulting from simulation (b) and simulation (c). When the loads increased to 60 kN, the resulting deformations became so large that they almost coincided with the curve resulting from simulation (c).

In column 8, the resulting deformations at 48 kN and 66 kN coincided with curve c. In column 9 the effect was very limited. All the results are presented in appendix B.

Table 5.5 The effect of the reduction of the top soil modulus by 50 % on the column modulus.

Column no.	Load [kN]	Simulations without changes in top soil modulus		Simulations with 50% reduced topsoil modulus	
		Column Young's modulus		Column Young's modulus	
		The first meter [MPa]	The rest of the column [MPa]	The first meter [MPa]	The rest of the column [MPa]
4	48	120	500	140	500
4	66	80	400	130	440
7	36	80	200	100	220
7	60	70	140	100	150
8	48	200	300	220	360
8	66	140	200	160	260

The upper part of the lime/cement column was assumed to have a reduced material quality as a consequence of the nature of the surrounding soil at that depth. Additional limited simulations were carried out to evaluate the column stiffness based on the assumption that the column material is of the same quality along the whole column length.

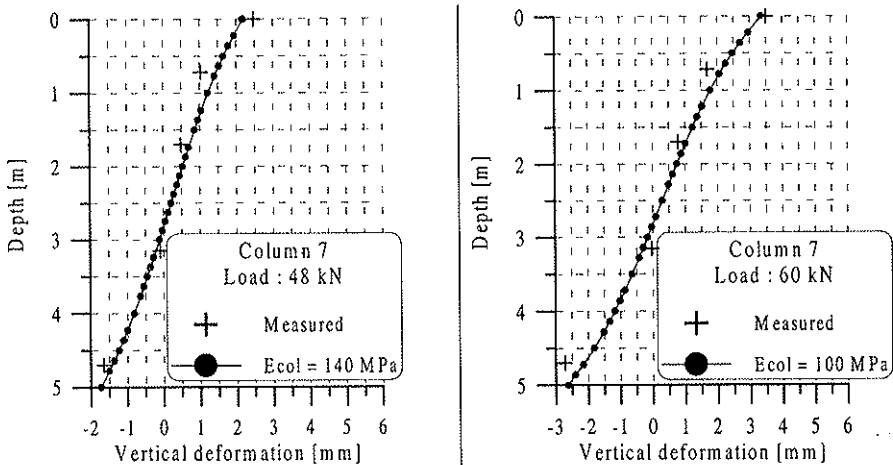


Figure 5.17 Numerical simulations versus measured deformations of columns 7 for constant column material properties along the depth.

This was in fact the case for column 8, since the column modulus was almost the same at the top of the column as for the rest of the column. By using this new assumption, a fair agreement between the measured values and the numerical calculations was observed for column 7. Column 7 was simulated with the applied loads of 48 kN and 60 kN. The evaluated stiffness of the column, E_{col} , was 140 Mpa and 100 Mpa respectively. See Figure 5.17.

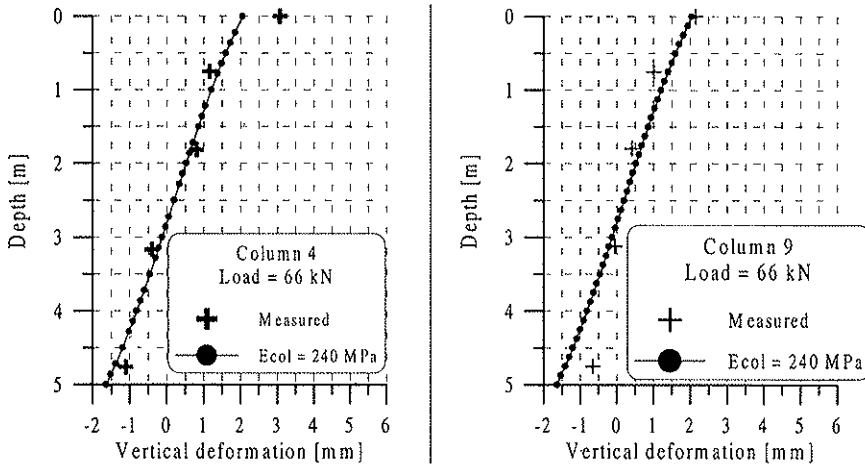


Figure 5.18 Numerical simulations versus measured deformations of columns 4 and 9 for constant column material properties along the depth.

As for columns 4 and 9, many trials were made to fit the measured deformations with numerical results, and relatively poor agreement was achieved. The evaluated Young modulus for columns 4 and 9 at applied load of 66 kN was 240 Mpa.

The results from the plastic simulations shows limited plastic points at the column top and the surrounding soil.

In general, the column modulus evaluated from numerical calculations based on the last assumption is close to the column modulus at the top when two column materials were defined.

Regardless of the assumption made, the important conclusion is that the column modulus evaluated from the load tests at this test site is much larger than the modulus evaluated from laboratory tests carried out on standard size samples. See chapter 6.

5.1.7 The Löftaån test site

The tests were conducted between July and August 1999. Before the tests were carried out, about 0.7 m silty, sandy soil was removed. To get to a better quality of the lime/cement column, another 0.3 m of the clay underlying the silty sand was removed as well. The drilling process performed to make holes for the tell tales caused some damage at the head of the column. The damaged parts were also removed and cement was used to repair the damaged parts and to level the head of the column. During the drilling process, the resisting forces and the drilling velocity were recorded along the length of all the columns. The recorded results are an indirect measurement of the quality of the columns.

Among the 10 columns installed for the load test, a problem appeared during testing of columns *C1* and *D4*. In column *C1* the hydraulic jack tilted, causing damage to the upper part of the column. As for column *D4*, the wire connected to the bottom plate separated making it impossible to conduct a test. During the drilling process, it was decided to continue to drill one of the holes in each of the columns until the bottom plate was reached so that the exact column length could be obtained and the movement of the bottom plate be directly measured. The length of the columns varied between 5.8 m and 6.4 m.

5.1.7.1 Test results

Load tests were conducted on 8 columns. In columns *C2* and *D1*, the tests were terminated at a load step of 140 kN and 124 kN respectively. At these load steps it was not possible to keep the applied load constant due to the large deformation developed at the column top. In these two columns failure of the upper part of the columns was noticed. The total vertical deformations, including the creep deformations directly before failure, were 60 and 48 mm for column *C2* and column *D1*, respectively.

In column *D2*, the wire connected to the bottom plate separated at load step 102 kN when the total vertical deformation at the column top was 25 mm.

As for the remaining 5 columns, the tests were terminated when the applied load reached a value of 170 kN, which is close to the ultimate tensile strength of the wire predicted to be equal to 180 kN. At the end of these tests, the total vertical deformations including the creep deformations at the top of the columns were between 45 and 76 mm.

In columns *C2*, *C5* and *D2*, the vertical deformations were measured at the time when the applied load was reduced to zero. The load step increment in columns *C2*, *C3* and *D3* was 10 kN or 35 kPa for columns with 0.6 m

diameter, while the increment was 11.3 kN or about 40 kPa for the remaining columns.

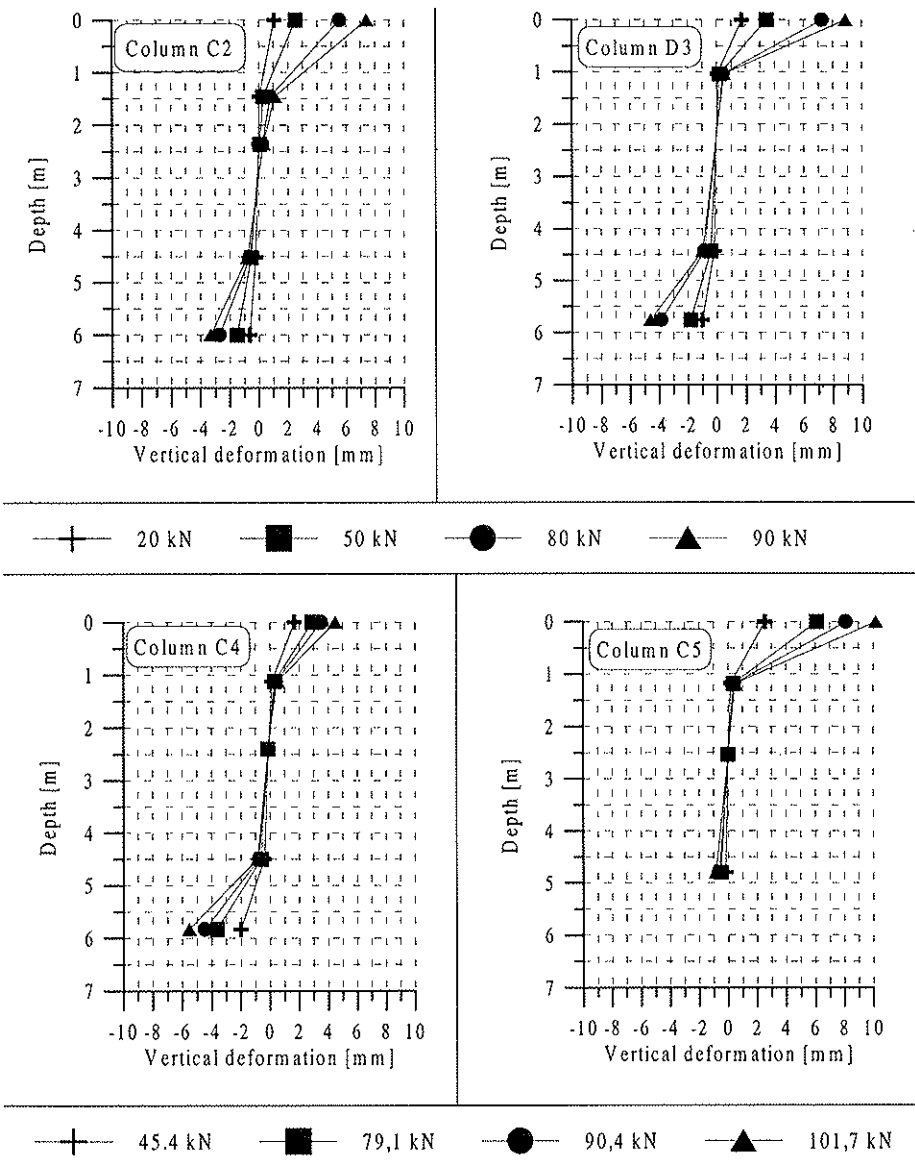


Figure 5.19 Load test results at the Løftaån test site.

The predominant behavior of all the load test results from Løftaån was that the relative deformation of the upper part of the column was larger than for the remaining parts of the column. In columns C4 and D3, large deformations at the bottom of the column were observed as well, which

may be due to insufficient pull-up of the bottom plate directly after the installation of the column. The observations made during the load test provided clear evidence that the lime/cement columns do not consist of fully saturated material. In columns *D1* and *D3*, air bubbles started to come from the columns through the drilled holes when the applied load exceeded 100 kN. At this load level the deformation became larger, and part of the air included in the column started to flow through small cracks, possibly caused by the applied load. In column *C3* air bubbles were seen at 130 kN and more air bubbles started to appear when the applied load reached a value of 160 kN.

As mentioned, the load test on column *D2* was terminated at 102 kN applied load, as the wire connecting the bottom plate separated. However, the load-deformation curve shows that plastic deformations were already reached. Deformation measurements were made when the applied load was reduced to zero, see Figure 5.20.

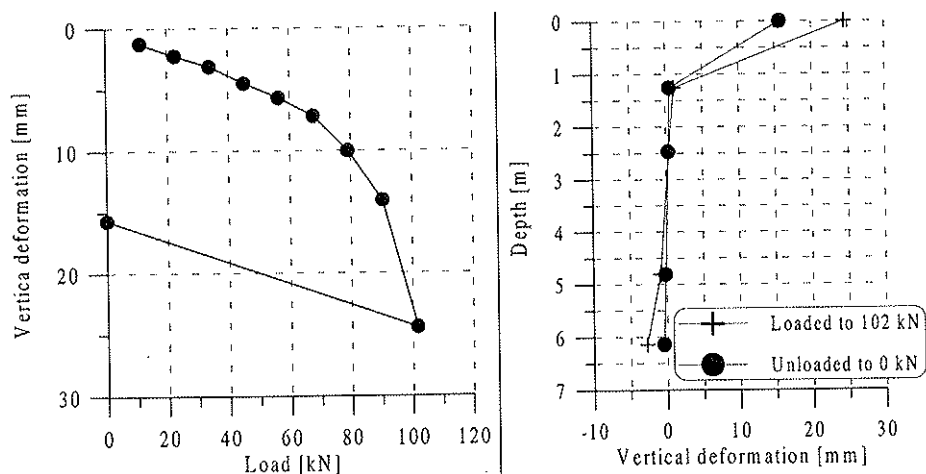
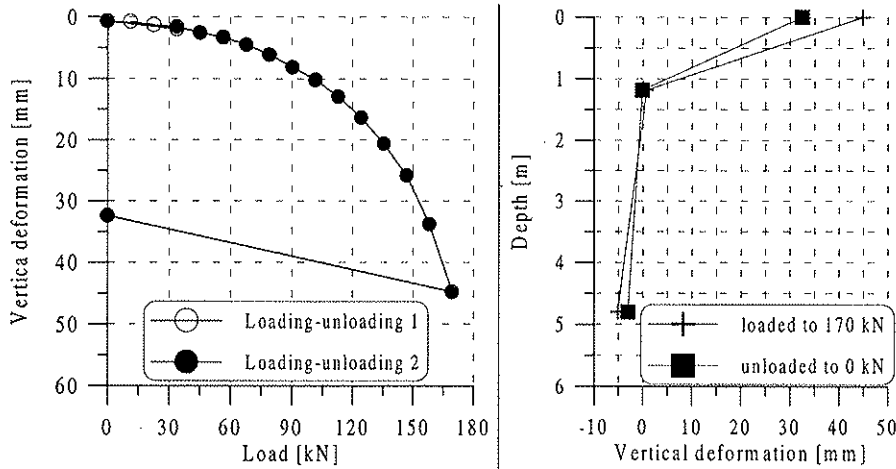


Figure 5.20 Loading and unloading of column *D2*.

At the column head, the plastic deformation after unloading was about 16 mm and very small plastic deformations were observed at the remaining depths of the column.

In the case of column *C5*, the maximum load that the column was subjected to before the unloading was 170 kN, which was much more than in the case of column *D2*. The tell tail at level 6.4 m was missing during the load test and at the last load step the hydraulic jack moved the deformation gauge installed to measure the deformation at 2.53 m depth.

Therefore, no deformation measurements could be made at this depth, see Figure 5.21. The column was first loaded up to about 34 kN and then unloaded to zero. Then the column was directly reloaded to 34 kN as a first load step and increased to 169.5 kN with load steps equal to 11.3 kN. Then the column was again unloaded to zero.



Deformations at the top of column C5

Deformations along the length of column C5

Figure 5.21 Loading and unloading of column C5.

At the first loading-unloading cycle, no plastic deformations were observed and all the deformations were in fact only elastic. At the second cycle, the plastic deformation at the head of the column was about 32 mm. Plastic deformations at the main part of the column were observed and were expected to be large at the bottom of the column.

Column C2 was unloaded before it was again loaded to failure. At failure it was not possible to measure the deformations at the top of the column since the deformation increased very rapidly. The deformation at the top of the column measured after unloading was about 50 mm.

To measure the creep deformation, a time interval of 16 minutes was used between each load step. Columns C2 and D1 were treated first since collapse at the top of the columns was observed, which made it possible to relate the failure load to the load at which creep deformation starts to dominate the total deformation. In Figure 5.22, the creep deformations between 1 and 16 minutes time interval are presented for columns C2 and D1 together with the load-deformation curves. The load-deformation curves show the total, creep and instantaneous deformations at the top of the columns. As at the Varberg test site, the load-deformation curves

consist of two parts; a linear elastic part with low deformation, and a second non-linear part with large deformation.

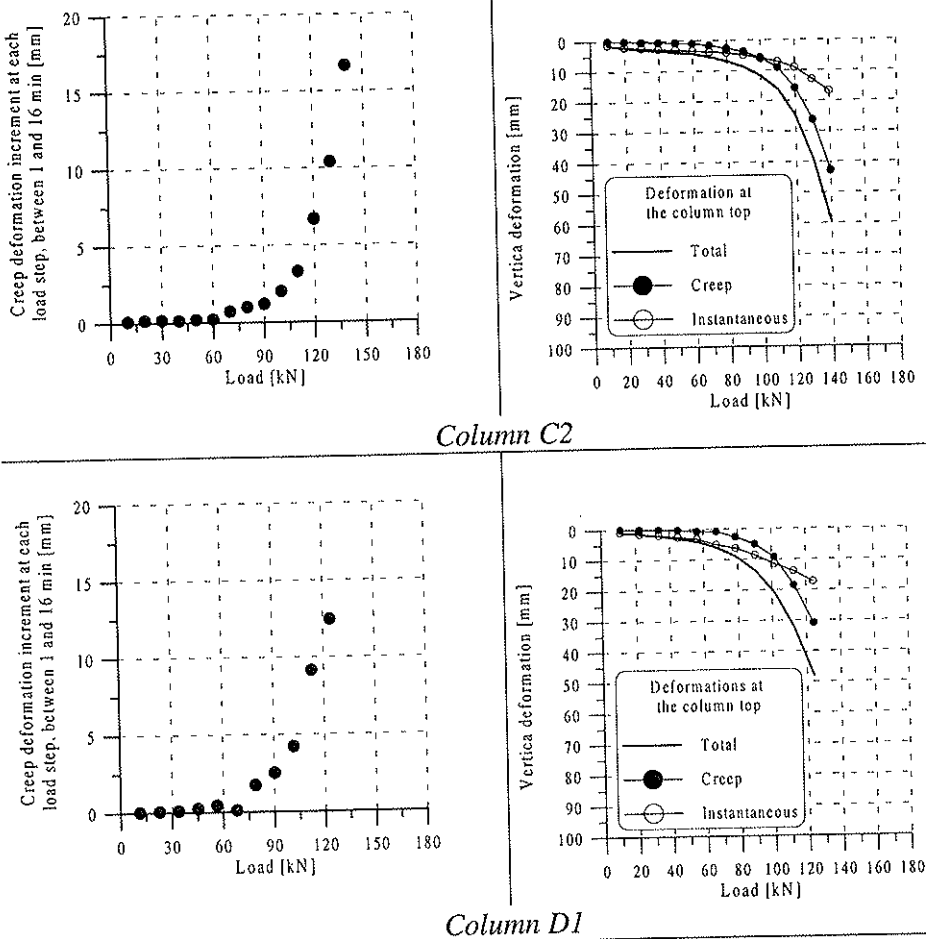


Figure 5.22 Deformations at the top of columns C2 and D1.

In the case of column C2, the creep deformation at the applied load 90 kN was about 3.9 mm which is almost equal to the instantaneous deformation. For the same column, the creep deformation at an applied load of 110 kN was about 9.1 mm, which is double the instantaneous deformation, and at this load the creep deformations dominate the total deformations. As for column D1, the creep deformation was about 2.6 mm at the applied load of 79 kN and the instantaneous deformation was about 6.4 mm. At an applied load of 101 kN, the creep deformation was about 9.3 mm and the instantaneous deformation was about 11.5 mm. At the next load step with

an applied load of 113 kN the creep deformation potentially increased to about 18.5 mm.

By locating the break point on the creep curve, the evaluated creep load was found to be about 110 kN and 102 kN for column *C2* and column *D1*, respectively.

Although there was no sudden failure at the top of column *D3*, the limit between the linear and the non-linear total deformation is very clear. When the applied load reached a value of 100 kN, both the total and the creep deformations started to increase and in the next load step up to 110 kN, the deformations increased very rapidly, see Figure 5.23.

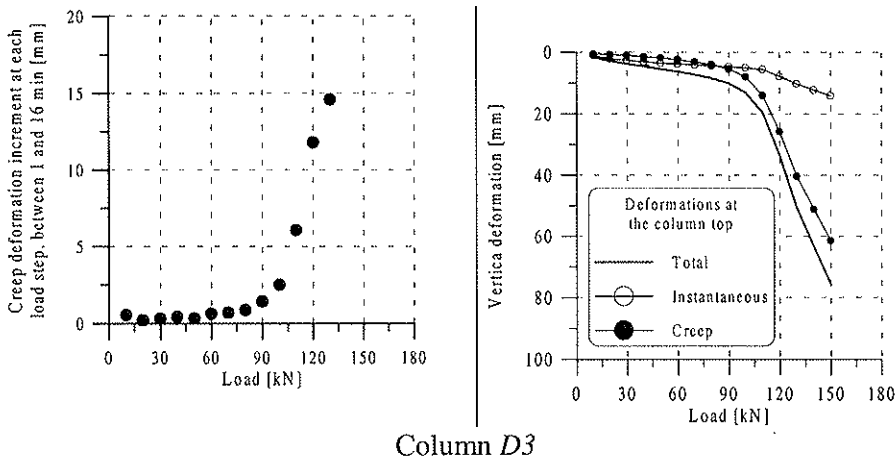


Figure 5.23 Deformations at the top of column *D3*.

The total and the creep deformations at an applied load of 100 kN were about 13 mm and 7.9 mm, respectively.

In columns *C5* and *D5*, a smooth transition was observed from the linear to the non-linear phase. The creep deformations potentially increased as the applied load exceeded a value of 150 kN. In column *C5*, see appendix B, the total and creep deformations between 113 kN and 146 kN separated by 4 load steps increased from 12.9 mm and 5.6 mm to 25.8 mm and 15.2 mm, respectively. By increasing the applied load by one load step, the applied load 158.2 kN caused 33.8 mm total deformation at the column top.

As for column *D5*, the measured total deformation at the top of the column, as the applied load became equal to 148 kN, was 59.4 mm, see Figure 5.24.

As in the case of columns *C5* and *D5*, no collapse was observed at the head of columns *C3* and *C4*. The load test was terminated at an applied load of

170 kN. However, the deformations at the column top started to increase potentially as the applied load exceeded 150 kN, see appendix B.

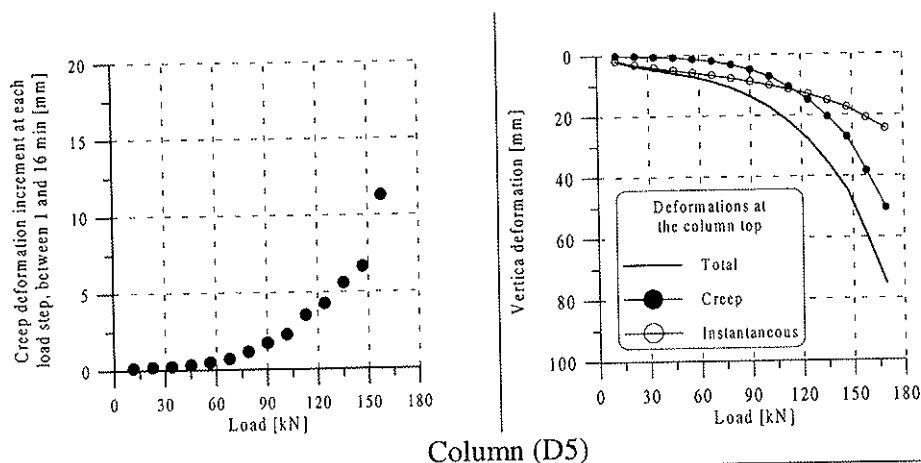


Figure 5.24 Deformations at the top of column D5.

5.1.7.2 The finite element simulations

As at the Varberg test site, the simulations carried out in this section are related to the linear part of the load-deformation curve at the top of the column, where the maximum deformation occurs. The linear elastic model is applied in these simulations.

In the axial symmetrical model used in these simulations, the water table is located at the top of the excavated column and the elastic material parameters applied in this model are presented in Table 5.6.

Undrained triaxial tests were carried out on samples near the Löftaån test site and the undrained modulus of the clay was obtained at three different levels. The length of the columns varied between 5.8 m and 6.4 m.

The exact length of the column was obtained on the basis of holes made in the column down to the bottom plate.

Undrained analysis was assumed for the clay, while, for the reason explained before at the Varberg test site, drained analysis was assumed for the lime/cement column.

In order to control the plastic state of the two materials in some selected simulations at the end of the elastic part of the stress-strain curve, the lime/cement column and the clay was assumed to behave as elastic, perfectly plastic material obeying a Mohr-Coulomb yield criterion.

Table 5.6 Material parameters used in the simulations of the load test results at the LÖftaån test site.

Soil type	depth [m]	Material parameters		
		γ [kN/m ³]	E_{ref} [MPa]	ν [-]
Clay1	0 to 2	15.8	4.3	0.495
Clay 2	2 to 4	15.8	5.4	0.495
Clay 3	4 to 8	15.8	6.6	0.495
Column	0 to L*	15.9	To be evaluated	0.3

* The column length varied between 5.8 m and 6.4 m.

The angle of internal friction ϕ' of the clay is assumed to 30° and the cohesion intercept c' to 2 kPa. The angle of internal friction ϕ' of the lime/cement columns is assumed to 35°, while the cohesion c' is found to be 100 kPa, based on results of triaxial tests carried out on large samples.

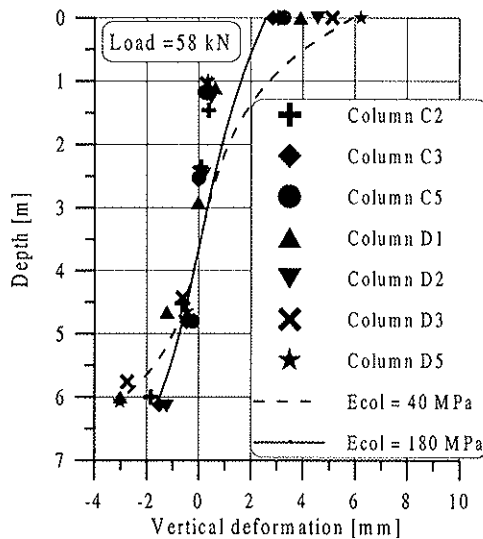
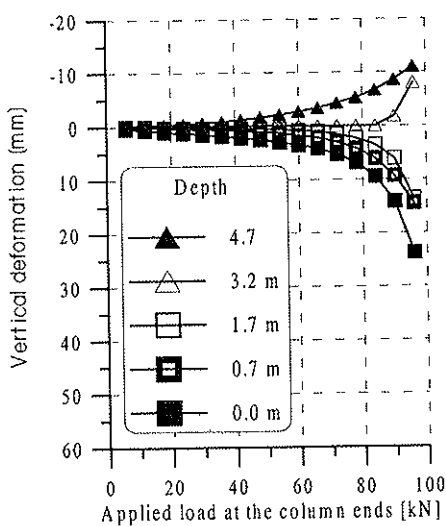


Figure 5.25 Field results of all the tested columns at LÖftaån with 60 kN or 56.5 kN applied load versus numerical results.

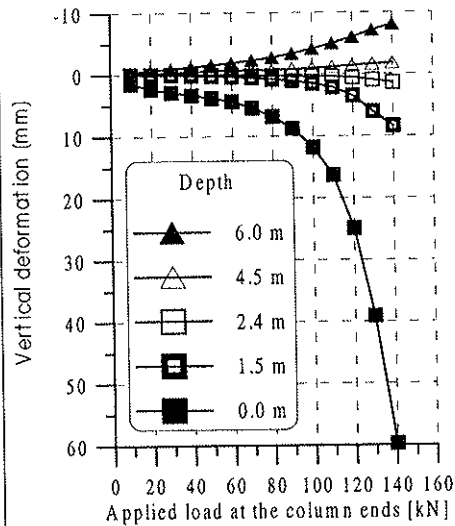
Results of the field tests with applied loads of 60 kN or 56.5 kN, depending on the value of the load increment, were first plotted together with simulation results, see Figure 5.25. The two simulation curves presented in this figure are related to column stiffness of $E_{col} = 40$ MPa and $E_{col} = 180$ MPa, when the applied load was 58 kN.

In the two numerical simulations, the lime/cement column material properties were assumed to be constant with depth. As a first observation from the above figure, the measured vertical deformations at depths between 1 m and 1.5 m are diverging from the curves based on the numerical calculations, especially for columns having an assumed stiffness value of 40 MPa. The extent of this divergence is limited for columns C2, C3, C4 and C5 compared with the rest of the columns. However, there are two possible explanations for the behavior of the measured deformations at that depth. Firstly, the upper part of the columns may have a somewhat different quality, and if so, then the middle part of the column must be used to illustrate the results. It is clear that the slope of the lines connecting the measured vertical deformations at different depths is related directly to the stiffness of the column. The slope of the lines connecting the measured vertical deformations at the middle of the columns is steeper compared to the lines representing the top and the bottom of the columns. In such a case the predicted value of the column stiffness will be high.

Secondly, as mentioned before, the holes were drilled directly before the load tests, while at the Varberg test site the holes were made directly after the installation of the columns by pushing down a corrugated plastic tube to the desired level.



Column 7, the Varberg test site



Column C2, the Löftaån test site

Figure 5.26 Vertical deformations at different levels versus the applied load at the column end from two different test sites.

Figure 5.26 shows measured vertical deformations at different levels caused by loads applied at the top and the bottom of the columns. Column 7 was one of the columns tested at the Varberg test site. The vertical deformations at level 0 m and 0.7 m follow each other smoothly. While in the case of column C2, which was tested at the Löftaån test site, the deformations observed at depth 1.5 m are small and away from the value of the deformation at the column top. As shown in Figure 5.25, the measured vertical deformations of the column at various depths do not increase with increased deformation at the top of the columns.

Clear local failure was observed only in columns C2 and D1 and in these two specific cases the secant modulus, E_{50} , was evaluated at 50 % of the determined failure load. As for the rest of the columns, secant moduli were evaluated at a value of the applied load close to the end of the elastic part of the load-deformation curve.

Figure 5.27 shows results from numerical simulations for columns C2 and D1 as compared with the measured deformations. The rest of the numerical simulations carried out for all the tested columns are presented in appendix B.

For each column, two simulations were conducted. Simulation 1 is based on the assumption that the column material is of the same quality along the column length, while in simulation 2, the upper meter of the column length is assumed to have reduced quality in comparison with the rest of the column.

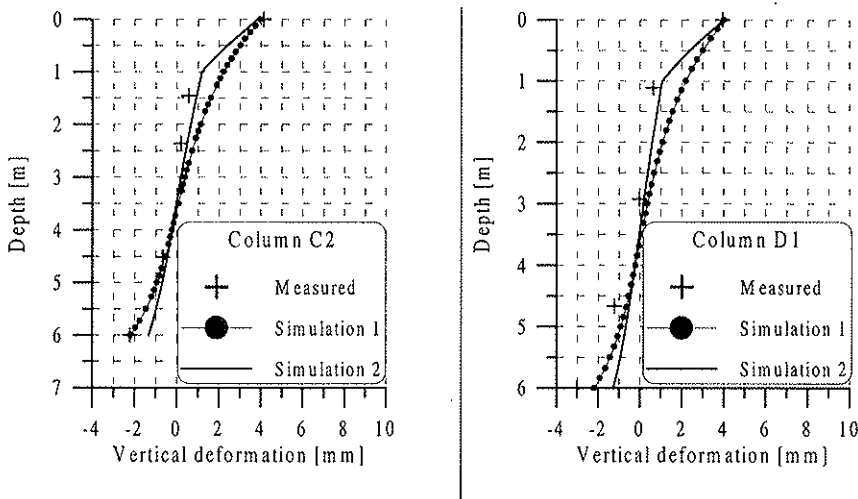


Figure 5.27 Results of the numerical simulations of columns C2 and D1.

The simulation results are presented in Table 5.7. The column Young modulus calculated by simulation 1 varies between 30 MPa and 180 MPa.

In column C3 many calculations were carried out and the results of two of these simulations are presented in the same table to show that the column modulus remained unchanged when the numerical calculations were conducted at loads in the linear part of the load-deformation curve.

The secant modulus E_{50} for column D1 should be calculated at load 62 kN and due to the load increments utilized during the test, this value is located between 57 kN and 68 kN. The load 57 kN is still in the linear part of the load-deformation curve shown in Figure 5.22 while at load 68 kN the deformations start to increase, which may explain the decrease in the column modulus from 80 MPa to 50 MPa, as shown in Table 5.7.

Table 5.7 Results from numerical solutions carried out on all the tested columns at the Löståån test site.

Column	Load	Stress	Column Young's modulus		
			Simulation 1	Simulation 2	
	[kN]	[kPa]	[MPa]	The first meter [MPa]	The rest of the column [MPa]
C2	70	248	90	60	240
C3	80	283	140	80	240
C3	90	318	140	80	240
C4	90	318	180	100	300
C5	68	240	120	80	240
D1	57	205	80	50	240
D1	68	240	50	30	240
D2	68	240	60	30	240
D3	80	283	50	30	240
D5	68	240	30	20	240

The secant moduli calculated numerically in Simulation 1 for columns D1, D2 and D3 are similar to the column moduli evaluated from the triaxial tests carried out on large samples. On the other hand, the secant moduli calculated in Simulation 1 for columns C2 to C5 are much higher than the column moduli evaluated from laboratory tests.

Considering the results of simulation 2, the moduli of the first meter of the columns are still higher than, or equal to, the values evaluated in the laboratory for columns C2 to C5 and D1, while smaller values were obtained for columns D2 to D5. However, Young's moduli of the dominating part of the columns are much higher than the column secant modulus values obtained in the laboratory.

5.2 HYDRAULIC CONDUCTIVITY TESTS

No standard method exists so far for testing and evaluating the hydraulic conductivity of lime/cement column in the field. Pramborg and Albertsson (1992) carried out pressure-permeameter tests on soil stabilized by an admixture of 25 g lime and 35 g cement per kg of natural clay. They determined that the hydraulic conductivity of the treated soil ranged between $5.2 \cdot 10^{-8}$ m/s and $3.5 \cdot 10^{-7}$ m/s, with an average value of $1.4 \cdot 10^{-7}$ m/s. The pressure-permeameter test is usually used to measure soil hydraulic conductivities ranging from $1 \cdot 10^{-5}$ m/s to $1 \cdot 10^{-10}$ m/s. The method was developed in France by Louis Ménard and is quite similar to the well-known pressuremeter test instrument. The method used in this study is called the packer test and is similar to the method used for measurement of hydraulic conductivity in a rock mass.

5.2.1 Test instrumentation

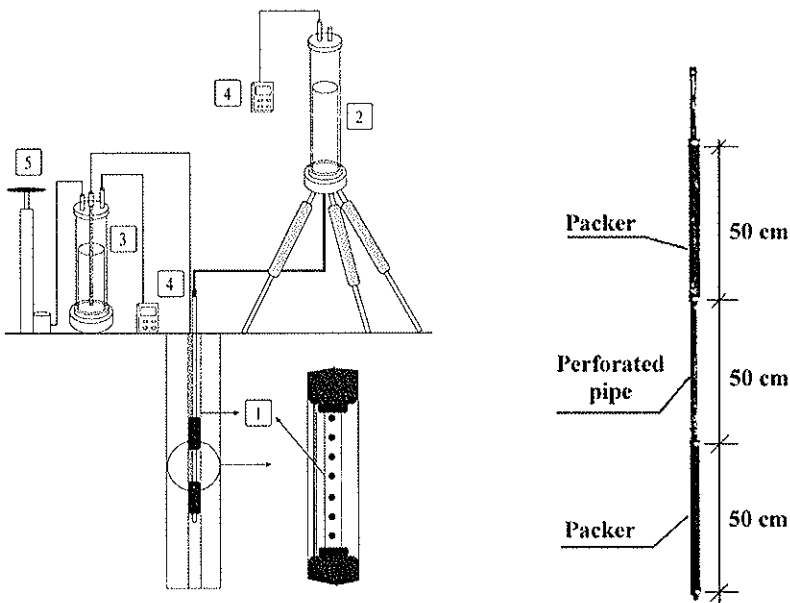


Figure 5.28 In situ hydraulic conductivity test instrument.

The instrument consists of five parts, as illustrated in Figure 5.28. These are probe (1), cylinder (2), cylinder (3), digital pressure gauges (4) and air pump (5). Stiff plastic tubes are used to connect these parts to each other. The probe consists of a single-ended metal standpipe open at the top and

with an inside diameter of about 19 mm. Two inflatable-seals 0.5 m long each, called packers, are used to isolate a 0.50 m segment of an open borehole. In that isolated part, the standpipe is perforated with small holes. The air pump is used to induce pressure in cylinders (3) and (2). The pressure created is measured by using digital pressure gauges. The air pressure in the cylinder (3) is used to force the water to flow into the packers and this in turn will expand the packers against the borehole. The pressure applied must be high enough to create a seal, but at the same time too high pressures must be avoided to prevent expansion and cracking of the lime/cement column. The packers are sufficiently flexible to ensure that a uniform pressure is applied to the wall of the borehole. The inside diameter of cylinder (3) is about 110 mm and it is numbered along the length every 1 mm. By reading the water level in the cylinder, the volume of the water filling the packers can be calculated and controlled. The volume control is very important in case the packers expand against the soft part of the lime/cement column and a further increase in the water volume in the packers may break the expanded packers. A calibration test was performed to evaluate the water volume needed for the packers to expand against a stiff plastic pipe with 60 mm inside diameter. This is actually about the same diameter as the borehole to be drilled in the column center. The results are presented in Figure 5.29.

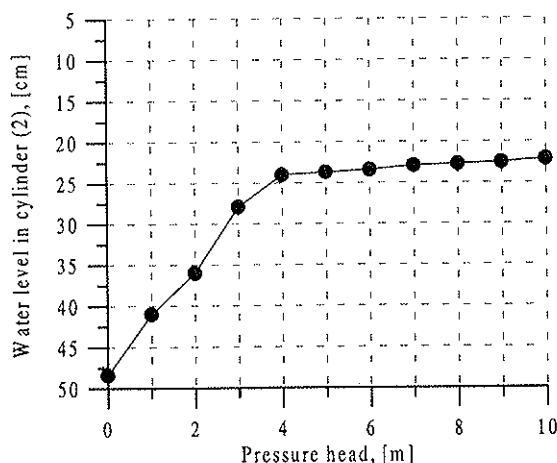


Figure 5.29 Calibration of the packer membranes against a 60 mm diameter plastic pipe.

In Figure 5.29, the change in level in cylinder (3), of the water pumped into the packers, is plotted against the pressure, expressed in meter pressure head used to force the water to flow into the packers. At 4 m

pressure head, the volume of water flowing into the packers started to reduce potentially, and the measured water level in cylinder (3) was about 245 mm corresponding to a volume of about 2330 cm³. The maximum water volume flowing into the packers at the end of the calibration, when the pressure head was 10 m, was about 2500 cm³.

Cylinder (2) with 80 mm inside diameter is placed on a tripod and connected to the standpipe in the probe. The water discharge through the perforated part of the pipe flowing radially in the lime/cement column can be calculated by measuring the change of the water level in the cylinder during a certain interval of time. The water head pressure is measured as the difference between the water level in cylinder (2) and the level of the ground water table. By inducing air pressure at the top of the cylinder, the head pressure can be increased. The air pressure and its change during the test can be measured by using a digital pressure gauge.

5.2.2 Installation and test procedure

The site was prepared before the installation by excavating and exposing the top of the column. As a first step in the installation procedure, a hole was drilled in the center of the lime/cement column along its whole length. The lime/cement column consists of brittle material, and precaution must be taken when selecting the drilling equipment and the drilling method. When a dry rotary drilling was used, it was noticed that the column was badly disturbed. Thus it was not possible to control the volume of water flowing to the packers, which clearly indicated that the borehole diameter was much larger than the target 60 mm hole. Moreover, the drilling process caused cracks in the body of the column around the drilled hole, which made it impossible to perform the hydraulic conductivity test. A wash boring method was used where water is pumped through the drill rod. This method uses rotation drill bit in conjunction with the application of water pressure to advance the hole. The water rises between the borehole wall and the drill rod together with the suspended column particles and overflows at the top of the column. The resulting borehole diameter is about 60 mm. Even when using this method it happened that when the quality of the column at a certain level was not adequate, the borehole became much larger than 60 mm. This was observed at a few levels during the test. During advancing of the borehole, it was possible to record the resistance force and the advancing velocity along the column length. For each column, the levels, at which the test was conducted, were decided on the basis of the force resistance and advancing velocity variation with depth during the drilling operation. It was decided to avoid placing the rubber membrane at levels where the column quality was bad.

With the probe at the decided level, the valve, connecting cylinder (3) in Figure 5.28, was opened and the water flowed to the probe to fill the rubber membranes under a certain pressure, depending on the estimated lime/cement column shear strength. During the time when the rubber membranes were expanding, the water in the borehole, replaced by the volume of the expanding rubber membranes, started to rise in the borehole. Then any air present in the standpipe was pushed out through the perforated part of this pipe, which was isolated by the rubber membranes. No excess pressure can be developed in the isolated part of the pipe. The part of the borehole located under the probe may develop excess water pressure during the expansion of the rubber membranes. However, it was difficult to measure any pressure increase there. When the probe was in position, the standpipe was then connected to cylinder (2). Control was made to remove any possible air bubbles that could have been trapped during the connection. The valve between cylinder (2) and the standpipe was then closed and the instrument was ready for the hydraulic conductivity test.

Before starting the test, both the water level in cylinder (2) and the distance between this level and the ground level at the column top were first measured. The test started when the valve between cylinder (2) and the standpipe was opened. The water discharge at the insulated part of the borehole in the center of the lime/cement column was calculated by measuring the change of the water level in cylinder (2) during a certain time interval. The total head was simply calculated as the elevation from the water level in cylinder (2) to the center of the perforated pipe minus the head pressure caused by the pore water pressure at the center of the perforated pipe.

5.2.3 Traditional methods

Two equations are mainly used to calculate the hydraulic conductivity of the clay based on in situ cylindrical pizometer measurements.

In the case of constant head measurement, the hydraulic conductivity is determined by the following equation:

$$K_{soil} = \frac{1}{F} \cdot \frac{Q}{\Delta H} \quad (5.5)$$

In the falling head case, the equation is given as:

$$K_{soil} = \frac{1}{F} \cdot \frac{A_p}{(t_2 - t_1)} \cdot \ln \left(\frac{H_1}{H_2} \right) \quad (5.6)$$

K_{soil}	hydraulic conductivity of the soil
Q	flow rate
ΔH	constant difference in head
F	shape factor
A_p	area of the standpipe
H_1, H_2	the heads between which the hydraulic conductivity is determined
$t1$	the time when the water level in the standpipe is $H1$
$t2$	the time when the water level in the standpipe is $H2$

Different approaches are used to assign a value of the shape factor to the cylindrical piezometer. Hvorslev (1951) obtained the value of the shape factor as:

$$F = \frac{2 \cdot \pi \cdot l}{\ln \left\{ \frac{l}{d} + \sqrt{1 + \left(\frac{l}{d} \right)^2} \right\}} \quad (5.7)$$

l length of the piezometers
 d diameter of the piezometers

Wilkinson (1968) noted that the value of the shape factor, calculated by Hvorslev's equation, was slightly underestimated and suggested a more accurate value by using the following equation:

$$F = \frac{3 \cdot \pi \cdot l}{\ln \left\{ 1.5 \cdot \frac{l}{d} + \sqrt{1 + \left(1.5 \cdot \frac{l}{d} \right)^2} \right\}} \quad (5.8)$$

5.2.4 Finite element model

In calculating the hydraulic conductivity of the lime/cement column, equation (5.5) or (5.6) can be used. Yet the shape factor presented by Hvorslev and Wilkinson is applicable for piezometers surrounded by infinite soil. This is not the case in the lime/cement problem where two materials with different hydraulic properties surround the probe. Moreover, the probe has another geometry compared to the piezometers. To tackle this problem, a finite element model was used.

Before introducing the model, a review of the theory of groundwater flow will be discussed first. By considering a porous material with a solid matrix and continuous pore space, the storage equation can be written as:

$$-\frac{1}{1+e} \frac{\partial e}{\partial t} = \frac{e}{1+e} \cdot \beta \cdot \frac{\partial u}{\partial t} + \nabla q \quad (5.9)$$

e	void ratio of the medium at time t
β	compressibility of the fluid
u	excess pore pressure at time t
q	specific discharge
∇	gradient

The terms in the above equation state that the compression of the soil is due to the compression of the pore fluid and the amount of water expelled from an element by flow. For steady flow through an incompressible medium the above equation can simply be written as:

$$\nabla q = 0 \quad (5.10)$$

Darcy (1856) expressed the linear relationship between the discharge velocity v and the hydraulic gradient i as:

$$v = \frac{k \cdot \rho_f \cdot g}{\mu} \cdot i \quad (5.11)$$

v	discharge velocity
k	intrinsic hydraulic conductivity
ρ_f	mass density of the fluid
g	acceleration due to gravity
μ	absolute viscosity of the fluid
i	hydraulic gradient

In soil mechanics, the coefficient in Darcy's law is often expressed in term of the hydraulic conductivity K_{soil} .

$$K_{soil} = \frac{k \cdot \rho_f \cdot g}{\mu} \quad (5.12)$$

K_{soil} hydraulic conductivity

The hydraulic velocity in Darcy's law is written as:

$$v = K_{soil} \cdot i \quad (5.13)$$

According to Bernoulli's equation, the hydraulic head is expressed as:

$$H_h = \frac{v^2}{2 \cdot g} + h_p + h_z$$

H_h	hydraulic head
$\frac{v^2}{2 \cdot g}$	velocity head
h_p	pressure head
h_z	elevation head

In seepage problems, the atmospheric pressure is taken as reference pressure and since the velocity head is small (velocity < 1 cm/s, assumed to be zero), the hydraulic head expression will be reduced to be:

$$H_h = h_p + h_z \quad (5.14)$$

In the hydraulic head equation, the pressure head is simply equal to the pore water pressure u divided by the water unit weight γ_w .

The hydraulic gradient is the derivative of the hydraulic head with respect to the drainage path, so the flow velocity in the j direction becomes:

$$v_j = K_j \cdot \frac{dH_h}{dx_j} \quad (5.15)$$

By substitution of equation (5.15) into equation (5.10) the three-dimensional steady state flow becomes:

$$\frac{\partial}{\partial x} (K_x \cdot \frac{\partial H_h}{\partial x}) + \frac{\partial}{\partial y} (K_y \cdot \frac{\partial H_h}{\partial y}) + \frac{\partial}{\partial z} (K_z \cdot \frac{\partial H_h}{\partial z}) = 0 \quad (5.16)$$

Making the assumption that the hydraulic conductivity is constant and that the soil is isotropic with respect to hydraulic conductivity, equation (5.16) is simplified to:

$$\frac{\partial^2 H_h}{\partial x^2} + \frac{\partial^2 H_h}{\partial y^2} + \frac{\partial^2 H_h}{\partial z^2} = 0$$

In the numerical calculations, an axisymmetrical model was used, and the equation related to this model is:

$$\frac{\partial^2 H_h}{\partial r^2} + \frac{1}{r} \cdot \frac{\partial H_h}{\partial r} + \frac{\partial^2 H_h}{\partial z^2} = 0 \quad (5.17)$$

In the preliminary numerical calculations, the finite element program SEEP/W was used. This program is designed for analysis of groundwater

seepage and excess pore-water pressure dissipation problems. Yet, the major calculations were carried out using PLAXIS program. Moreover, in the case when the hydraulic conductivity of the column is much higher than that of the surrounding soil, equation (5.17) was solved using a simple finite difference model implemented in a spreadsheet program. The model is presented in appendix B.

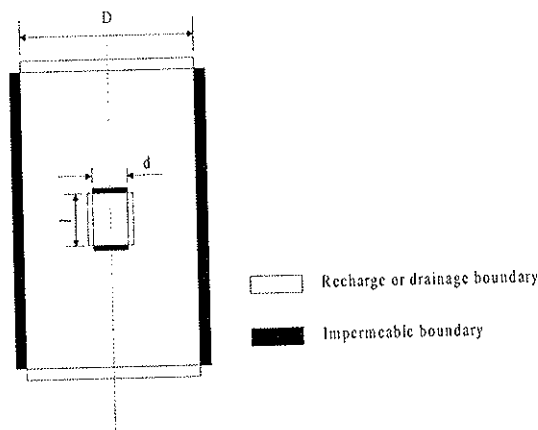


Figure 5.30 Electric analogue model B3 or measurement of shape factor.

The performance and accuracy of the finite element program PLAXIS, were first tested by comparing the calculated results with known analytical solutions and test results.

Brand and Premchitt (1980) constructed an electric analogue model specially used for the shape factor measurements. The model consisted of a cylindrical electrolytic tank, 900 mm in diameter and 500 mm high made of 3 mm thick Perspex. The electrolyte used was water. The model piezometers were located on the axis of the tank and were made of brass.

In a special case, called B3, the boundary conditions selected were close to the case of radial flow in a lime/cement column with a hydraulic conductivity much higher than the hydraulic conductivity of the surrounding clay. This model is shown in Figure 5.30.

The results from the PLAXIS model were very close to the experimental results, as shown in Figure 5.31. It can be noticed that in the same figure the results of the finite element program SEEP are shown.

Previously in this section, two equations were used for calculating the shape factor of hydraulic piezometers surrounded by infinite soil. These equations, presented by Hvorslev and Wilkinson, are numbered in this section as equations (5.7) and (5.8).

Results from numerical calculations carried out using the PLAXIS program are presented in Figure 5.32.

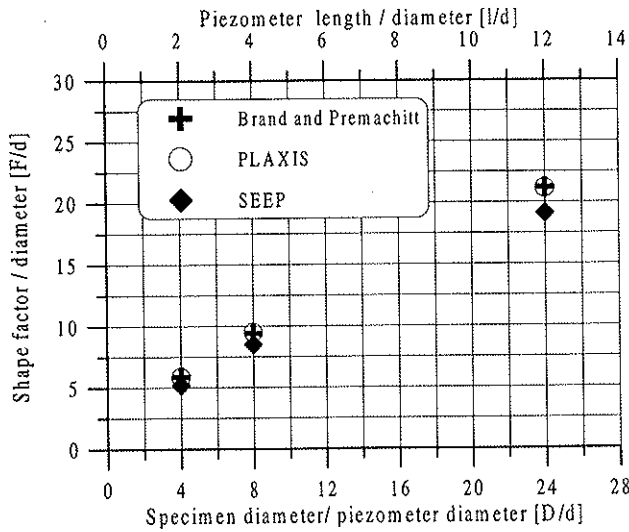


Figure 5.31 PLAXIS and SEEP results compared with measured results.

The figure shows that PLAXIS results were closer to the Wilkinson equation than to the Hvorslev equation, which confirms that the Hvorslev equation underestimates the value of the shape factor.

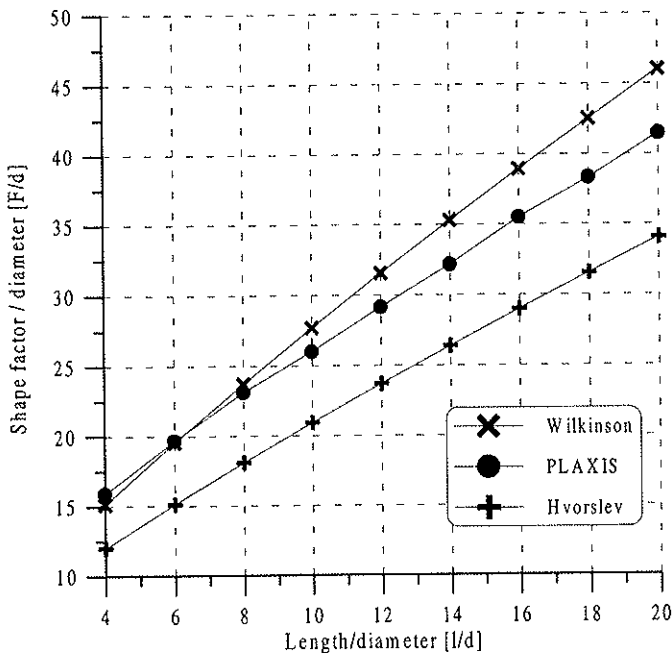


Figure 5.32 Calculated shape factor compared with analytical solutions.

In the above figure, l and d are the length and the diameter of the piezometers, respectively. It should be noted that, in the PLAXIS model, dimensions which were 100 m depth and 200 m diameter were kept constant together with the piezometer diameter, while the length of the piezometers was changed to achieve the required length to diameter ratio. After the fair performance of the PLAXIS program, it was decided to use this program to calculate the shape factor needed to evaluate the hydraulic conductivity of the lime/cement column based on the results from the in situ tests conducted at the Fjärås and Löftaån sites.

The lime/cement column is not a perfect homogenous material, and the properties can vary both over the cross section and along the length. As an assumption and simplification, the column material was assumed to be an isotropic homogeneous material.

An axisymmetric model was established. The suggested model was 4.5 m wide and 9.0 m high. The radii of the lime/cement column and the borehole located at the center of the column were 0.3 m and 0.03 m, respectively. The borehole was drilled all the way along the column length, which was 7.0 m high. The dimensions of the two rubber membranes and the isolated drainage region were 0.03 m radius and 0.50 m high, see Figure 5.33. The basic finite element used in the model was selected to be a 15-noded triangular element.

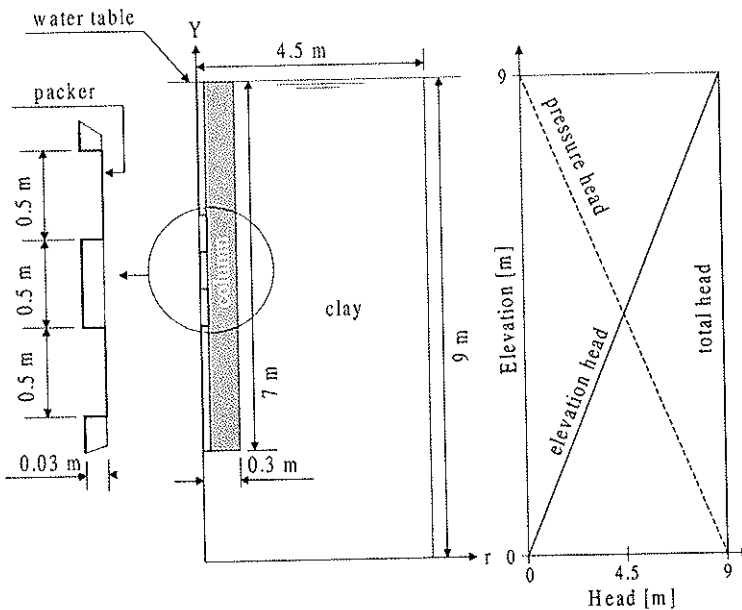


Figure 5.33 Axisymmetric model.

Three types of soil elements were applied in this model; the lime/cement column, the clay soil surrounding the column and the water in the borehole located at the center of the column. The numerical model was aimed to solve a steady state problem. The most needed material property was the hydraulic conductivity of these materials. The rubber membranes were first modeled using non-porous material type. Later on, better results were obtained; when this material type was omitted and the rubber membranes instead were defined as impermeable boundaries, see Figure 5.33.

The water table was defined as a horizontal phreatic line located at the top of the model. As defined previously, the total head is the sum of the pressure head and the elevation head. Figure 5.33 shows that the total head for this model was constant and equal to 9 m, with the exception of a vertical line to the right of the isolated region located between the rubber membranes, where the total head was assumed to be more than 9 m in order to cause the radial flow. All the boundaries located at the line of symmetry to the left of the model were impermeable. The geometry lines representing the rubber membranes were assumed to be impermeable.

The maximum discharge near the flow boundaries was used to calculate the shape factor. Since the model used was an axisymmetric model, the resulting discharge was given per radian and, thus, must be multiplied by $2 \cdot \pi$ to get the discharge as volume per time. The discharge was calculated based on the constant head condition, and the shape factor was calculated using the following equation:

$$F = \frac{Q}{K_{col} \cdot \Delta H} \quad (5.18)$$

The hydraulic conductivity used in the above equation is related to the defined material properties of the lime/cement column.

In the numerical calculations, the hydraulic conductivity of the clay was kept constant while that of the lime/cement column was increased step wise from being equal to that of the clay to a value that was 10000 times larger. This was done in order to observe the effect of the hydraulic conductivity ratio between the lime/cement column and the clay on the calculated shape factor. The results are presented in Figure 5.34.

If the hydraulic conductivity of both the lime/cement column and the clay are equal, then the case becomes almost similar to the flow of piezometers surrounded by infinite soil. As the hydraulic conductivity of the lime/cement column increased relative to the hydraulic conductivity of the clay, the flow across the boundaries between the column and the clay began to reduce and, at a ratio of 50, the boundaries there acted almost as closed flow boundaries.

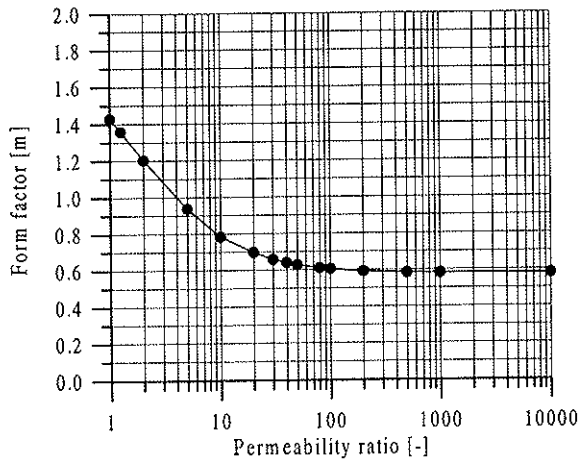


Figure 5.34 The variation of the form factor with different hydraulic conductivity ratios.

When this happens the shape factor will start to decrease from a value of about 1.43 m at a hydraulic conductivity ratio of one to about 0.6 m at a ratio of 50. The decrease is very slow as the ratio exceeds 50, and the value of the shape factor is only about 0.58 m as the ratio increases to 10000.

5.2.5 The Fjärås test site

At this site, hydraulic conductivity tests were conducted on five columns at different depths. Columns 1, 2 and 3 were tested in the summer of 1996. Columns 1 and 2 were single columns while column 3 was part of a column group installed as a wall. In 1997 two more columns, CTH1 and CTH2, were tested. These were single columns. The test instrument described in section 5.2.1 was used in all the columns except for column 2, where a cylinder with a large diameter was used instead of the commonly used cylinder (2). See Figure 5.28. Leakage problems at some levels occurred during the test of columns 1, 2 and 3, which affected the results of the tests. When columns CTH1 and CTH2 were tested, a better routine for the test was used and more reliable results were obtained. The depths at which the tests were carried out are defined as the distance from the head of the column to the center of the perforated pipe.

5.2.5.1 Test results

It was assumed that the flow rate was stabilized at the end of the test, although this is generally not the case in practice.

The most important factor in performing an in situ hydraulic conductivity test is to reach a balance between the applied pressure in the rubber

membranes sealing the borehole and how these membranes act as a perfect seal. Results from laboratory tests carried out on standard size samples may be used as a rough guideline to establish how reliable the field tests are. This must be combined with experience and engineering judgement.

The first column tested at this site was column 2. The test was carried out at three levels, 1.8 m, 4.3 m and 6.4 m. Constant head was applied during the tests and, at level 4.3 m, this was combined with a falling head test. At 1.8 m level, the test was started using a hydraulic head of 5 m, and the pressure in the packers was about 120 kPa. The water in the borehole rose during the test, which indicates that the packers did not act as a seal. The pressure was then increased to about 145 kPa. The average hydraulic conductivity of the lime/cement column evaluated at this level was about $5.0 \cdot 10^{-7}$ m/s see Figure 5.35.

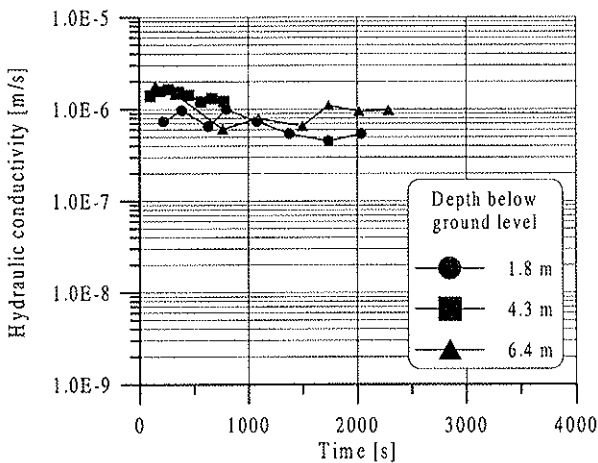


Figure 5.35 In situ hydraulic conductivity test results for column 2.

At 4.3 m depth, the applied hydraulic head was about 3.1 m and the measured hydraulic conductivity after about 13 minutes was $1 \cdot 10^{-6}$ m/s. The test was then terminated and the hydraulic head increased to 6 m. At this time, air bubbles appeared to come from the column and the hydraulic conductivity suddenly increased to become equal to about $2 \cdot 10^{-5}$ m/s (not shown in Figure 5.35). It is very likely that the high pressure in the rubber membranes and the increase of the hydraulic head made it possible to build a microscopical channel in the column structure near the flow region.

The last test on column 2 was carried out at 6.4 m level. The hydraulic head selected was 3.5 m. By mistake the pressure in the rubber membranes was increased up to about 250 kPa. The pressure was then permitted to decrease until it was equal to about 145 kPa. During the first 18 minutes air bubbles started to come from the column, and the hydraulic

conductivity was about $1.5 \cdot 10^{-6}$ m/s. The test was terminated after 38 minutes. The test was restarted again after increasing the hydraulic head to about 6 m. It took only about 5 seconds for about 0.5 liters of water to flow into the lime/cement column. This was clear evidence of the microscopic cracks formed as a result of the combination of high pressure used in the membranes and the rather high hydraulic head.

At this stage the cylinder with a large diameter was replaced with cylinder (2). The next column tested was column 1. Five tests were carried out at 2.5 m, 3.7 m, 4.9 m, 5.6 m and 7.2 m depths. In all these tests the falling head method was applied using hydraulic head between 1.7 m and 2.1 m. At depths 3.6 m, 5.6 m and 7.2 m there was a leakage problem. Efforts were made to reduce this problem by increasing the pressure in the rubber membranes but, as shown in Figure 5.36, the hydraulic conductivity was still relatively high at these levels.

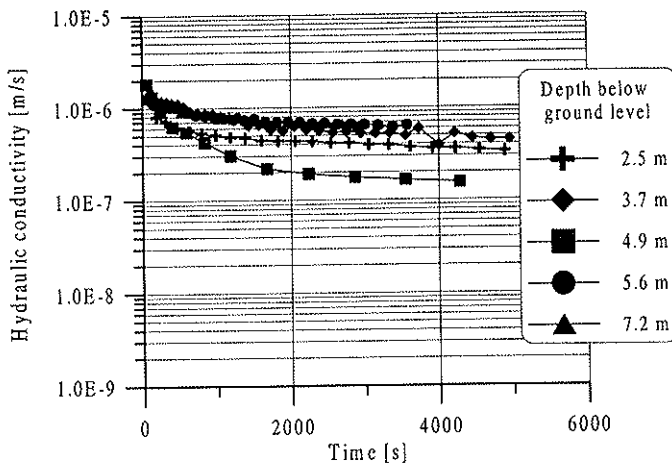


Figure 5.36 In situ hydraulic conductivity test results for column 1.

As was mentioned before, column 3 was part of a wall construction. Tests were conducted at depths 1.8 m, 2.6 m and 4.3 m. At 2.6 m depth, the falling head test was carried out. At the other two depths constant head tests were conducted. Leakage was noticed at 1.8 m depth, as the water level in the hole increased. This explains the rather high value of the hydraulic conductivity obtained at this depth. The hydraulic head used was about 6 m see Figure 5.37.

Test results from 4.3 m depth are not shown in this figure since one of the rubber membranes had burst. The drilling log was then studied to uncover the cause of the failure of this test.

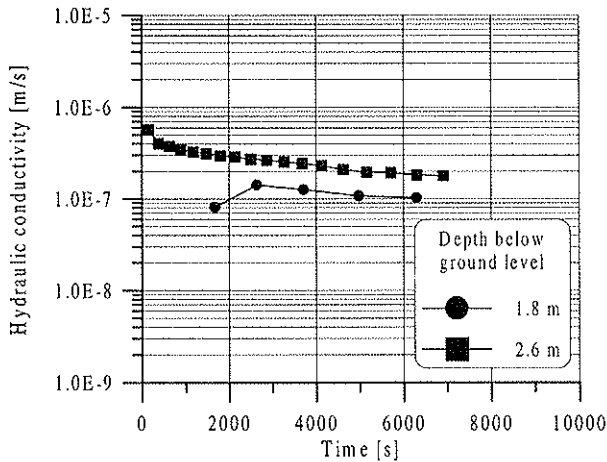


Figure 5.37 In situ hydraulic conductivity test results for column 3.

It was noticed that the column quality was poor at the depth where the membranes were located. Further, under the pressure that the membranes were subjected to, a large increase in the volume of the membranes in that direction occurred, which in turn caused them to burst. In later tests special precaution was taken in order to avoid such problems.

At column CTH1 four tests were conducted and the levels selected were 2.7 m, 5 m, 7.4 m and 9.7 m. The falling head tests were performed and these tests were started with about 2.2 m hydraulic head.

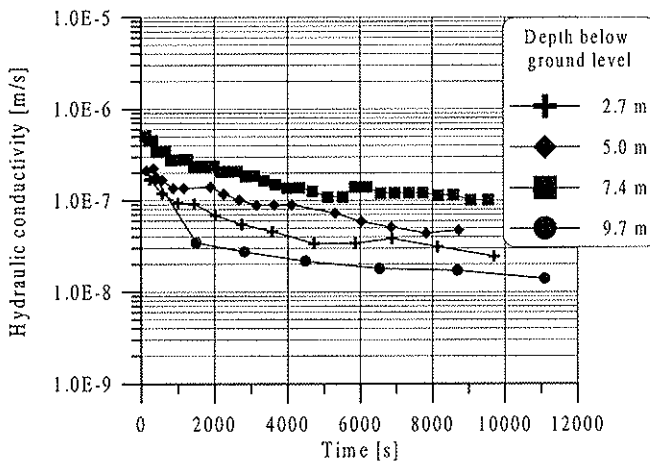


Figure 5.38 In situ hydraulic conductivity test results for column CTH1.

The hydraulic conductivity values were roughly between $1 \cdot 10^{-7}$ m/s to $1 \cdot 10^{-8}$ m/s, with a minimum value at 7.4 m depth. See Figure 5.38.

The last column tested at the Fjärås test site was column *CTH2*. At depths 2.5 m, 4.9 m, 7.3 m, and 9.7 m from the column, head falling head tests were conducted. The tests were started with a hydraulic head of about 2.2 m. The results are presented in Figure 5.39.

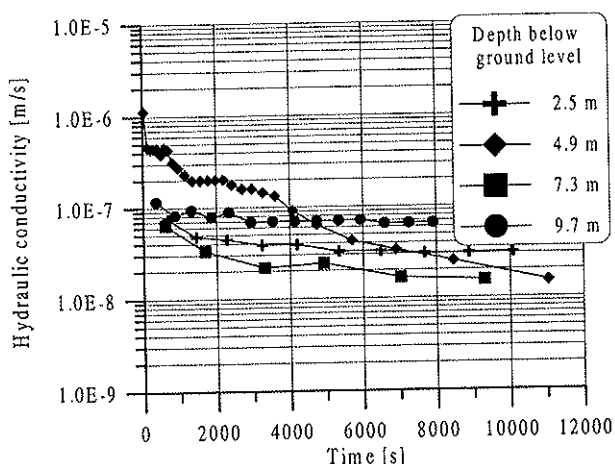


Figure 5.39 In situ hydraulic conductivity test results for column *CTH2*.

Stable hydraulic conductivity values were achieved between $7 \cdot 10^{-8}$ m/s and $1 \cdot 10^{-8}$ m/s at all the depths except at 4.9 m depth, where the conductivity was still reducing and not yet stable.

5.2.6 The Löftaån test site

Ten columns were prepared for test at this site, yet only six columns were tested due to practical difficulties. These six columns were *A1*, *A2*, *A4*, *B1*, *B2*, *B4*.

In situ measurement of the hydraulic conductivity of the clay was carried out at two depths, 2.1 m and 6.1 m below the original ground level. Moreover, the pore water pressure at these two depths was measured, which was necessary when evaluating the total head in the hydraulic conductivity calculation. The tests were carried out during the winter 1999.

5.2.6.1 Test results

The in situ hydraulic conductivity of the clay was measured at two depths using constant-head piezometers. The measured hydraulic conductivity was about $8 \cdot 10^{-10}$ m/s and $7 \cdot 10^{-10}$ m/s at depths 2.1 m and 6.1 m, below the original ground level, respectively, see Figure 5.40.

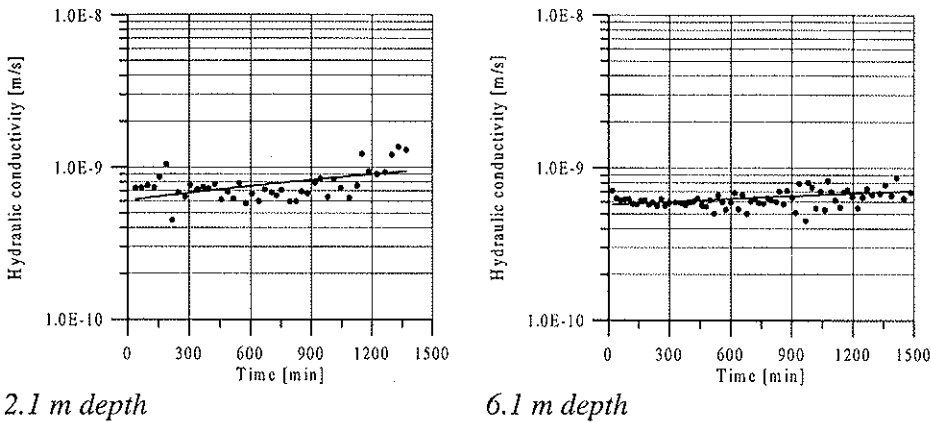


Figure 5.40 The in situ hydraulic conductivity of the clay at two levels.

Column A1 was excavated to a depth of only 0.4 m below the original ground level. Three tests were conducted at 2.4 m, 4.2 m and 5.6 m below the top of the column.

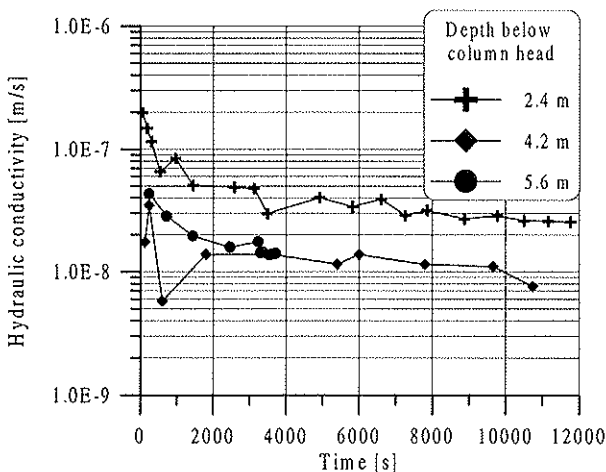


Figure 5.41 In situ hydraulic conductivity test results for column A1.

At depth 2.4 m, the falling head method was used with initial hydraulic head of about 2.1 m. The pressure applied to expand the rubber membranes was about 100 kPa and the amount of water flow to the membranes was about 2.5 liter to be compared with the 2.4 liter used to expand the membranes in a 0.06 m plastic pipe, as shown in section 5.2.1. The measured hydraulic conductivity at this depth was about $3 \cdot 10^{-8}$ m/s or about 40 times the hydraulic conductivity of the clay. At 4.2 m depth the initial hydraulic head was about 1.7 m and the measured hydraulic conductivity was about $1 \cdot 10^{-8}$ m/s. At depth 5.6 m, air pressure was used

in cylinder (2), see Figure 5.28, to increase the initial hydraulic head to about 3.1 m. The change in the pressure in the cylinder with respect to time was measured by a digital pressure gauge. The measured hydraulic conductivity was about $1.5 \cdot 10^{-8}$ m/s. At the same depth, another test was conducted during 36 hours. The hydraulic conductivity was between $1 \cdot 10^{-8}$ m/s and $2 \cdot 10^{-8}$ m/s, see Figure 5.42.

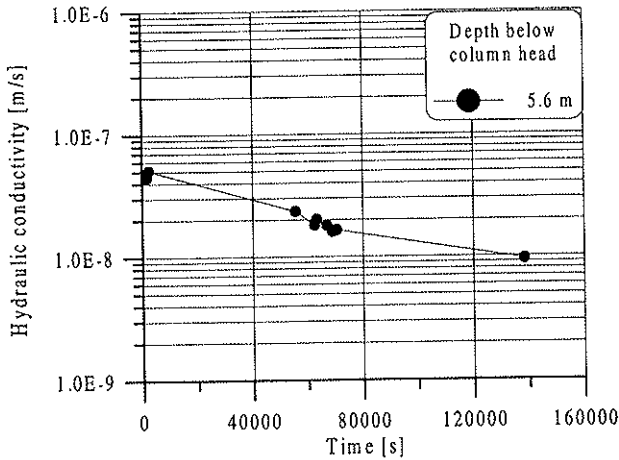


Figure 5.42 In situ hydraulic conductivity test results for column A1 at 5.6 m depth.

Column A2 was tested at three depths, 1.6 m, 3.2 m and 5.2 m. At 1.6 m the hydraulic conductivity was about $7 \cdot 10^{-8}$ m/s. Pressure in the membranes was about 100 kPa while the initial hydraulic head was about 2.0 m, see Figure 5.43.

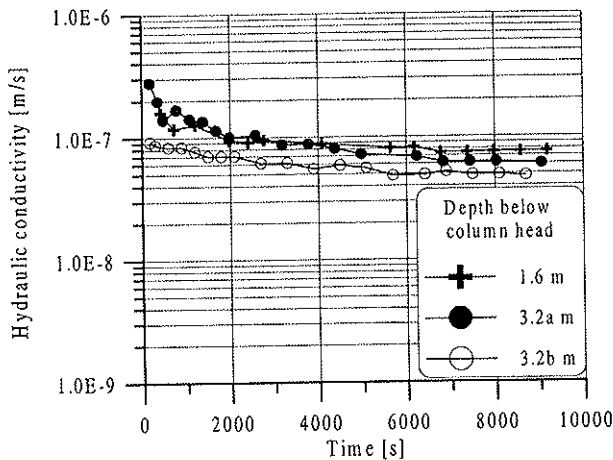


Figure 5.43 In situ hydraulic conductivity test results for column A2.

At 3.2 m depth, three types of tests were conducted. The first two tests, 3.2a and 3.2b, were carried out during about 2.5 hours with a hydraulic head of about 2.0 m. The tests were performed with seven days interval. The hydraulic conductivity varied between $5 \cdot 10^{-8}$ m/s and $6 \cdot 10^{-8}$ m/s. Long-term tests were carried out at 3.2 m depth, as a third test, and another test at 5.2 m depth, as shown in Figure 5.44.

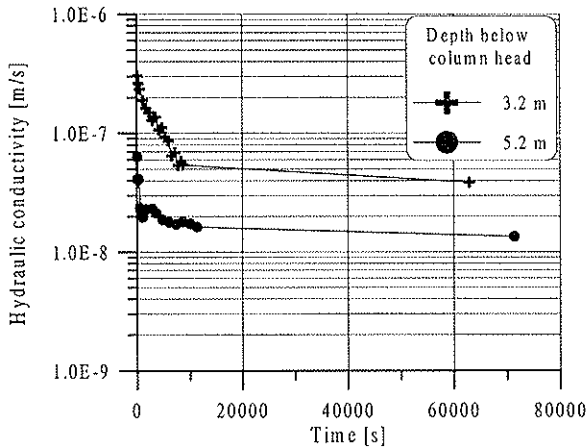


Figure 5.44 In situ hydraulic conductivity test results for column A2 at 3.2 m and 5.2 m depths.

The hydraulic conductivity at 3.2 m depth after 17.5 hours was about $4 \cdot 10^{-8}$ m/s, which was very close to the previous two values at the same depth. At 5.2 m depth, the hydraulic conductivity was about $1.5 \cdot 10^{-8}$ m/s. For column A4, tests were conducted at two depths, 3.2 m and 5.2 m. At these depths, two tests with different initial gradient were carried out. The initial hydraulic head at 3.2 m depth was 2.1 m for the first case and 4.7 m for the second case respectively, and the hydraulic conductivity was found equal to be about $2 \cdot 10^{-8}$ m/s in both tests. In the case of lower initial hydraulic head, the pressure in the packers was increased from 110 kPa to 145 kPa after 7920 seconds, as shown in Figure 5.45.

At 5.2 m depth, two tests with different initial hydraulic head were carried out. The initial heads applied were 1.8 m and 5.0 m respectively. The time duration in the case of lower hydraulic head test was about 30 hours while, in the second case; the test was terminated after 51.4 minutes. The hydraulic conductivity at this depth varied between $2 \cdot 10^{-8}$ m/s and $8 \cdot 10^{-9}$ m/s, see Figure 5.46.

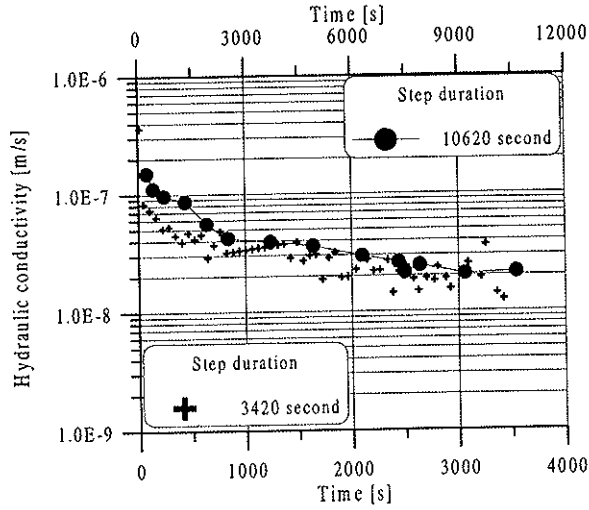


Figure 5.45 In situ hydraulic conductivity test results for column A4 at 3.2 m depth.

Column B1 was tested at two depths, 1.8 m and 3.0 m. At each depth, two tests with different initial hydraulic head were carried out. The applied initial hydraulic heads were 2.3 m and 4.2 m respectively. A rather high hydraulic conductivity was observed at 1.8 m depth in the both cases with a value ranging from $1 \cdot 10^{-7}$ m/s and $8 \cdot 10^{-8}$ m/s.

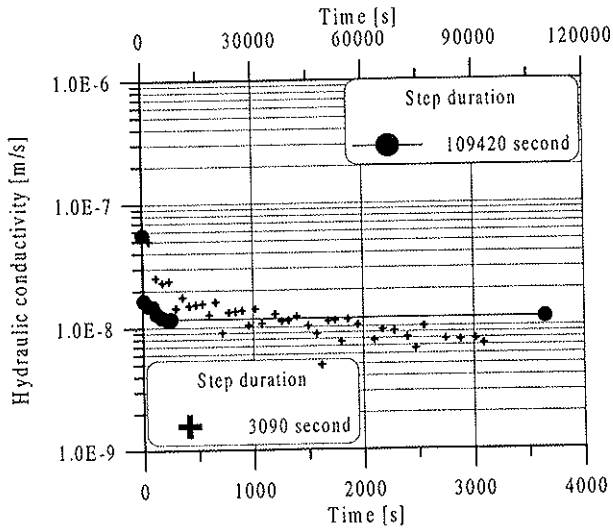


Figure 5.46 In situ hydraulic conductivity test results for column A4 at 5.2 m depth.

During the test with 2.1 m initial hydraulic head, which lasted 14580 seconds, the pressure in the packers was increased twice, first from 100 kPa to 150 kPa after 11640 seconds and then to about 196 kPa after 13380 seconds. No change in the hydraulic conductivity was noticed after these changes, see Figure 5.47.

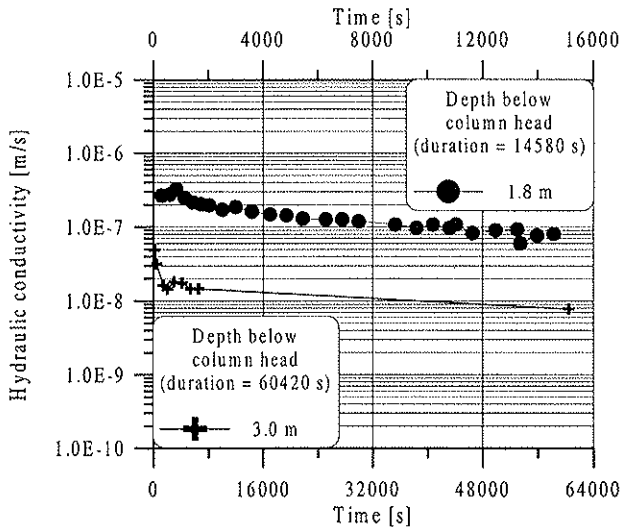


Figure 5.47 In situ falling head hydraulic conductivity test results for column B1 at 1.8 m and 3.0 m depths.

At 3.0 m depth, two different initial hydraulic head were applied, 2.0 m and 5.1 m, respectively. In the case with 2.0 m hydraulic head, the test lasted about 16 hours while in the second case; the test was terminated after 2970 seconds. The hydraulic conductivity at 3.0 m depth varied between a value of about $8 \cdot 10^{-9}$ m/s in the case of lower initial hydraulic head and about $1.5 \cdot 10^{-8}$ m/s in the case of higher initial hydraulic head.

Leakage problems dominated the tests of columns B2 and B4 at smaller depths. Column B2 was tested at three depths. At 1.8 m depth, all the attempts to seal the hole failed, and the test was then moved to the next depth 3.2 m. At the beginning of the test the measured discharge was high and the water was rising in the hole, which was an indication of a leakage problem. The pressure in the packers was increased from 100 kPa to about 198 kPa without clear evidence of progress in the sealing of the borehole. After 10560 seconds the pressure was increased to about 252 kPa and this time the discharge started to decrease. The duration of the test at this depth was about 21 hours and the hydraulic conductivity at the end of the test was about $4 \cdot 10^{-9}$ m/s.

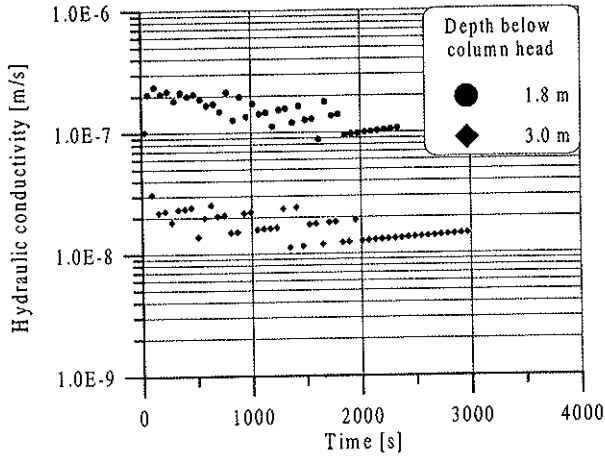


Figure 5.48 In situ constant head hydraulic conductivity test results for column B1 at 1.8 m and 3.0 m depths.

A lower value was expected as the hydraulic conductivity reached a stable value, see Figure 5.49

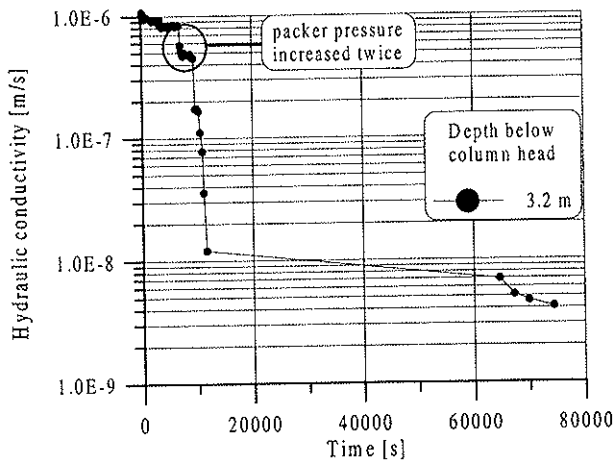


Figure 5.49 In situ hydraulic conductivity test results for column B2 at 3.2 m depth.

At 5.2 m depth the pressure in the packers was 120 kPa at the beginning of the test. As shown in Figure 5.50, the pressure was increased to about 198 kPa after 6780 seconds. At the end of the test, the hydraulic conductivity reached a stable value of about $4 \cdot 10^{-9}$ m/s.

The last column tested was column B4. At 1.5 m depth the discharge was very high, and no recovery was achieved in spite of a pressure increase in

the packers, for about 250 kPa at the end of the tests. Obviously, this part of the column was damaged during the drilling process, and the diameter of the hole at this depth was large since the water flow in the packer was higher than usual. The situation was worst at 3.2 m depth. During the installation of the instrument and when the packers were inflated, no water was seen to rise in the stand-up pipe, which was a clear indication of a real leakage problem at this depth.

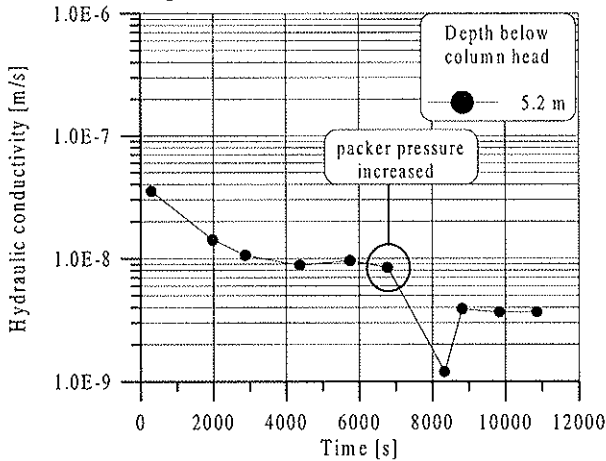


Figure 5.50 In situ hydraulic conductivity test results for column B2 at 5.2 m depth.

When the test was started, the water discharge was so high that it was not possible to measure the time for the flowing water.

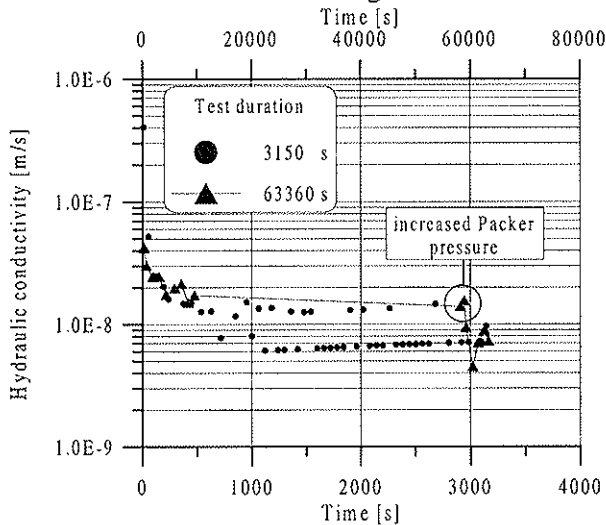


Figure 5.51 In situ hydraulic conductivity test results for column B4 at 5.2 m depth.

The test was continued at the next depth of 5.2 m. At this depth, two tests with different initial hydraulic head were carried out. The initial hydraulic head used at the first case and the second case was about 1.6 m and 4.6 m respectively. During the first test, the pressure in the packers was increased from 110 kPa to about 155 kPa after 59220 seconds. The hydraulic conductivity at 5.2 m depth was about $7 \cdot 10^{-9}$ m/s, see Figure 5.51. The values of the evaluated hydraulic conductivity of the columns tested at the Löftaån test site are shown in the following table.

Table 5.8 The hydraulic conductivity of the lime/cement columns at the Löftaån test site.

Column	Depth [m]	Initial hydraulic head [m]	Hydraulic conductivity [m/s]
A1	2.4	2.1	$2.5 \cdot 10^{-8}$
	4.2	1.7	$1.0 \cdot 10^{-8}$
	5.6	1.5	$2.0 \cdot 10^{-8}$
	5.6	3.0	$1.5 \cdot 10^{-8}$
A2	1.6	2.0	$7.5 \cdot 10^{-8}$
	1.6	4.2	$6.0 \cdot 10^{-8}$
	3.2	2.0	$5.0 \cdot 10^{-8}$
	3.2	3.5	$3.0 \cdot 10^{-8}$
	5.2	1.3	$1.5 \cdot 10^{-8}$
A4	3.2	2.1	$2.0 \cdot 10^{-8}$
	3.2	4.7	$1.5 \cdot 10^{-8}$
	5.2	1.8	$1.0 \cdot 10^{-8}$
	5.2	5.0	$8.0 \cdot 10^{-9}$
B1	1.8	2.2	$8.0 \cdot 10^{-8}$
	1.8	3.7	$1.0 \cdot 10^{-7}$
	3.0	2.1	$8.0 \cdot 10^{-9}$
	3.0	5.1	$1.5 \cdot 10^{-8}$
B2	3.2	1.7	$5.0 \cdot 10^{-9}$
	5.2	1.5	$4.0 \cdot 10^{-9}$
B4	5.2	1.6	$8.0 \cdot 10^{-9}$
	5.2	4.6	$7.0 \cdot 10^{-9}$

6 LABORATORY TESTS

6.1 LABORATORY TESTS ON STANDARD SIZE SAMPLES

6.1.1 Introduction

The unconfined compression test, which is a widely used test for determining the undrained compressive shear strength of soil, is a special case of the triaxial undrained test. In this test, the confined pressure is equal to the atmospheric pressure (i.e., $\sigma_3 = 0$). In common practice the undrained shear strength of the soil c_u is calculated as half the compressive strength by assuming that the internal friction angle ϕ is equal to zero. This may be the case for a fully saturated soil. In fact this is a conservative way of evaluating the shear strength since there are many factors to be considered during the evaluation, for example, the degree of saturation, grain size and fissuring. In the case of the lime/cement columns it is wise to use the compressive strength rather than the shear strength since the material is not fully saturated and the angle of internal friction is not necessarily equal to zero. All the unconfined compression test results in this section are therefore presented in terms of compressive strength. The tests were carried out on samples prepared in the laboratory as well as samples taken from mixed-in-place columns.

Ekström (1994) conducted numerous unconfined compression tests on both field mixed and laboratory prepared samples and suggested that the ratio between the secant modulus E_{50} and the unconfined compressive stress was between 50 and 150. Åhnberg et al. (1995) suggested that, at unconfined compressive strengths between 120 kPa and 300 kPa, the ratio between the secant modulus E_{30} and the unconfined compressive strength was about 90. On the other hand, the ratio of the secant modulus at failure load E_{qu} and the unconfined compressive strength was about 50.

For each unconfined compression test in this study, the unit weight and the water content of the stabilized sample were determined.

Tests on lime/cement columns were carried out to evaluate specific gravity G_s , and the average value obtained was about 2.71.

The degree of saturation of the columns was calculated using equation (6.1).

$$S_r = \frac{\gamma_{col} \cdot G_s \cdot w}{\gamma_w \cdot G_s \cdot (1 + w) - \gamma_{col}} \quad (6.1)$$

S_r degree of saturation

γ_{col}	column unit weight
G_s	column specific gravity
w	moisture content
γ_w	unit weight of water

As the lime/cement column may be of varying quality both over its cross section and along its length, the samples prepared were of the best quality where the mixing process had been adequate. In fact, in few cases, parts of the columns consisted of untreated clay. Selecting small samples may weaken the effect of the column macro structure, especially during hydraulic conductivity tests. During hydraulic conductivity tests, large hydraulic gradients were avoided, and ASTM D 5084 recommendations concerning the maximum hydraulic gradient were followed. The ASTM recommendations are shown in Table 6.1.

Table 6.1 Maximum hydraulic gradient recommended by ASTM D 5084.

Soil hydraulic conductivity [m/s]	Maximum hydraulic gradient [-]
$1 \cdot 10^{-5}$ to $1 \cdot 10^{-6}$	2
$1 \cdot 10^{-6}$ to $1 \cdot 10^{-7}$	5
$1 \cdot 10^{-7}$ to $1 \cdot 10^{-8}$	10
$1 \cdot 10^{-8}$ to $1 \cdot 10^{-9}$	20
Less than $1 \cdot 10^{-9}$	30

6.1.2 The Varberg test site results

6.1.2.1 Classification parameters

The average water content of totally 40 stabilized samples was about 58 % after a storage time of one day and decreased to about 56 % after 56 days. The related degree of saturation according to equation (6.1) was between about 98 % and 96 % respectively. As was mentioned in Chapter 4, the water content of the untreated soil varied between 62 % and 72 %.

6.1.2.2 Unconfined compression tests and evaluation of column stiffness.

Clay samples from depths 1 m to 5 m were stabilized and mixed in the laboratory by using 92 kg/m^3 stabilizing agent. The stabilizing agent consisted of 50 % cement and 50% lime. Unconfined compression tests were carried out on 25 samples after 1, 3, 7, 28 and 56 days of curing. Some of the results, normalized to the maximum compressive strength at 28 days, are shown in Figure 6.1. Very small deviations in the ratio were observed after 1 day to 7 days, while the deviation became large at a curing age of 56 days. The rate of increase in the compressive strength was high at a curing age of 1 to 3 days.

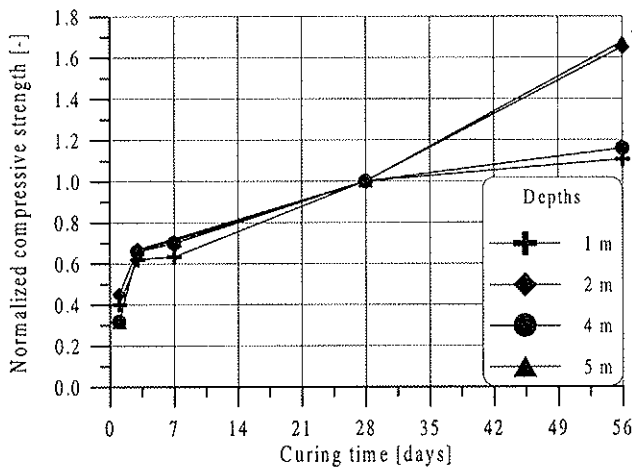


Figure 6.1 The increase with curing time of the normalized maximum unconfined compressive stress of stabilized clay taken from different depths.

Another five tests were carried out on samples taken from mixed-in-place columns. The curing age of the samples tested was 56 days. Generally it

was expected that the unconfined compressive strength of samples taken from mixed-in-place columns was lower than the compressive strength of samples prepared in the laboratory, due to a possible disturbance of the field samples during the coring or trimming of these samples. Still, there are many other factors that cause the difference in the compressive strength, among them the way in which these samples were cured. In this particular case, the compressive strength of field samples was slightly higher compared to the laboratory mixed samples.

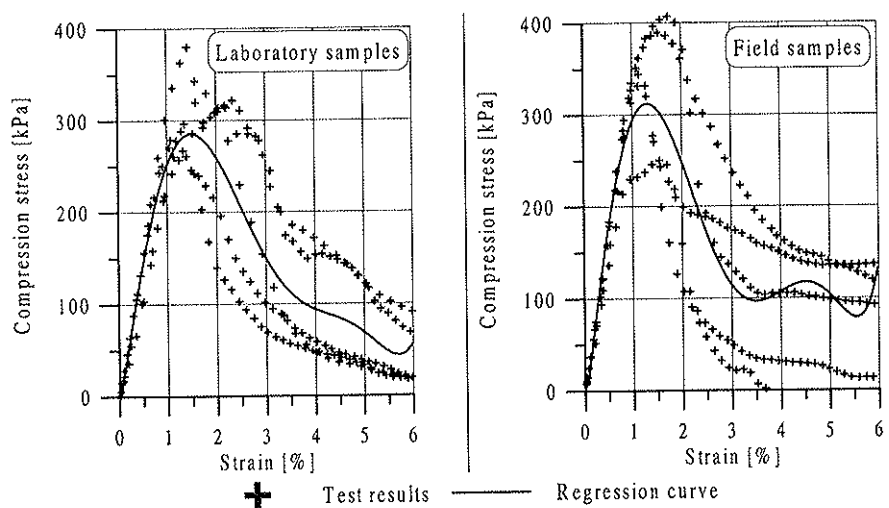


Figure 6.2 Unconfined compression tests on laboratory and field samples of 56 days age.

Young’s modulus of the columns, based on 28 days old laboratory samples, is shown in Table 6.2.

Table 6.2 Young’s modulus of the lime/cement column based on laboratory mixed samples of 28 days old.

Depth m	Unconfined compressive strength [kPa]	Young’s Modulus	
		E_{qu} [MPa]	E_{50} [MPa]
1	284	16.5	23.0
2	201	15.5	14.0
4	241	14.5	19.0
5	217	9.0	20.5

In the same table Young's modulus E_{50} is presented, where E_{50} is the secant modulus of the columns at 50 % of the maximum unconfined compressive strength.

From Table 6.2, the ratio between the secant modulus E_{50} and the unconfined compressive strength is between 70 and 95, while the ratio between E_{qu} and the failure load varies between 40 and 75. In fact this ratio is the reciprocal of the axial strain at failure.

Young's modulus of the lime/cement column can be expected to increase with time. The E_{50} for field samples of 56 days age varied between 30 MPa and 36 MPa with an average of about 32.5 Mpa. The ratio between secant modulus E_{50} and the unconfined compressive strength was between 90 and 140. As shown in Table 6.3, the E_{50} values for laboratory prepared samples were in general lower than the average E_{50} value for field samples.

Table 6.3 Young's modulus of the lime/cement column based on laboratory mixed samples of 56 days age.

Depth m	Unconfined compressive strength		Secant Young's Modulus	
	laboratory [kPa]	field [kPa]	$E_{50, laboratory}$ [MPa]	$E_{50, field}$ [MPa]
1	314	344	30.5	34.0
2	330	407	23.0	33.0
3	261	332	22.0	36.0
4	278	250	30.0	30.0
5	380	390	31.0	34.5

6.1.3 The Fjärås test site results

6.1.3.1 Hydraulic conductivity tests

Only hydraulic conductivity tests were carried out in the laboratory to make a comparison with the results of field hydraulic conductivity tests.

Field-mixed columns from 3 m and 6 m depths were trimmed to samples with 30 mm height and 50 mm diameter. Samples were placed in a triaxial cell and consolidated to the same in situ horizontal pressure. Zero back pressure was used. The direction of the flow was vertical, and the sample was not subjected to any deviator stress. Two test methods were used, the falling head method and a variation of falling head (VFH). In the falling head method, the tests were carried out after adjusting the water level in the burettes in order to be able to start with a certain initial head. A series

of readings were made while the water head was decreasing with time. When evaluating the hydraulic conductivity of the columns, care must be taken to avoid low gradients at which Darcy's law may no longer be applicable. The VFH method was in fact a falling head method with the exception that adjustment were made to have the same initial hydraulic head after each reading. A total of seven samples were tested, and the results of these tests, except for sample *Fj5*, are shown in Table 6.4.

In samples *Fj1* and *Fj4*, the hydraulic conductivity increased as the gradient was increased. Before the VFH test with gradient 5 was carried out on samples *Fj1* and *Fj4*, these samples were subjected to a high gradient. It is very likely that microscopic channels were then created, which may explain the sudden increase of the hydraulic conductivity. Otherwise, experience from the performed tests shows that the gradient usually had little or no effect on the hydraulic conductivity.

Table 6.4 Hydraulic conductivity of 6 field-mixed samples taken at 3 m and 6 m depths.

Sample	Depth m	Hydraulic conductivity		
		Falling head [m/sec]	VFH $i = 2$ [m/sec]	VFH $i = 5$ [m/sec]
<i>Fj1</i>	3	$6.0 \cdot 10^{-9}$	$4.5 \cdot 10^{-9}$	$7.5 \cdot 10^{-8}$
<i>Fj2</i>	3	$2.5 \cdot 10^{-9}$		
<i>Fj3</i>	3	$2.0 \cdot 10^{-8}$	$6.5 \cdot 10^{-9}$	$6.5 \cdot 10^{-9}$
<i>Fj4</i>	3		$3.0 \cdot 10^{-9}$	$9.0 \cdot 10^{-8}$
<i>Fj6</i>	6			$1.5 \cdot 10^{-9}$
<i>Fj7</i>	3			$1.0 \cdot 10^{-9}$
				$1.5 \cdot 10^{-9}$

Disregarding tests with a high gradient, the maximum and the minimum hydraulic conductivity of the lime/cement column are $1.0 \cdot 10^{-8}$ m/s and $1.0 \cdot 10^{-9}$ m/s.

Sample *Fj5*, which is not presented in Table 6.4, was subjected to a high gradient in the first test, and a piping caused the rather high hydraulic conductivity obtained from the series of tests carried out on this sample. In a VFH test and ordinary falling head test, combined with different gradients, the hydraulic conductivity of this sample varied between about $2.0 \cdot 10^{-7}$ m/s and $2.0 \cdot 10^{-6}$ m/s. Details of all tests presented in Table 6.4 are also presented in appendix C.

6.1.4 The Löftaån test site results

6.1.4.1 Classification parameters

As was mentioned in chapter 4, the natural water content, w_n , of the untreated soil was between about 81 % and 87 %, while the density, ρ_{soil} , was between 1.55 t/m³ and 1.58 t/m³. The water content of the treated soil varied depending on the preparation method. A lower water content and thereby a lower degree of saturation was observed in laboratory mixed samples.

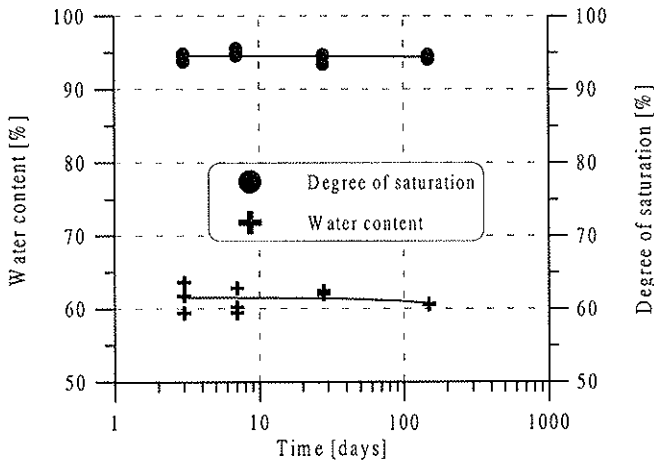


Figure 6.3 Water content and degree of saturation of laboratory mixed samples at different curing ages.

Figure 6.3 shows that the water content of laboratory mixed samples varied between 59.5 % and 63.5 %, while the related degree of saturation varied between 93.5 % and 95.5 %.

The calculated unit weight of these samples was about 15.5 kN/m³. In connection with the large-scale triaxial tests and unconfined compression tests, samples were tested to determine the unit weight and the water content.

Table 6.5 Average value of parameters for field mixed samples.

Sample	Unit weight, γ [kN/m ³]	Water content, w_n , [%]	Degree of Saturation, S_r , [%]
F3	15.3	71.9	98.1
F4	15.3	68.9	96.5
F5	15.5	67.9	97.9

Table 6.5 shows the average values of the classification parameters of field mixed samples. For each column shown in the table, three sets of samples were tested.

6.1.4.2 Unconfined compression tests and evaluation of column stiffness.

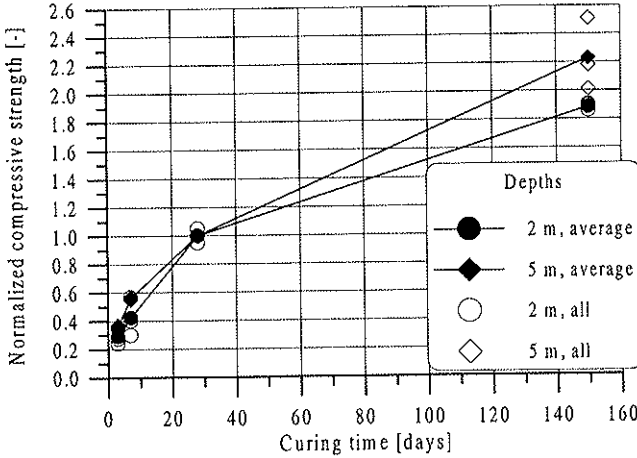


Figure 6.4 The increase with curing time of the normalized maximum unconfined compressive stress of stabilized clay taken from two depths.

The laboratory mixed samples were made by mixing clay obtained from 2 and 5 m depths. A 50/50 per cent lime/cement mixture of about 135 kg/m^3 was used as a stabilizing agent. The increase with time of the normalized maximum unconfined compressive stress is shown in Figure 6.4.

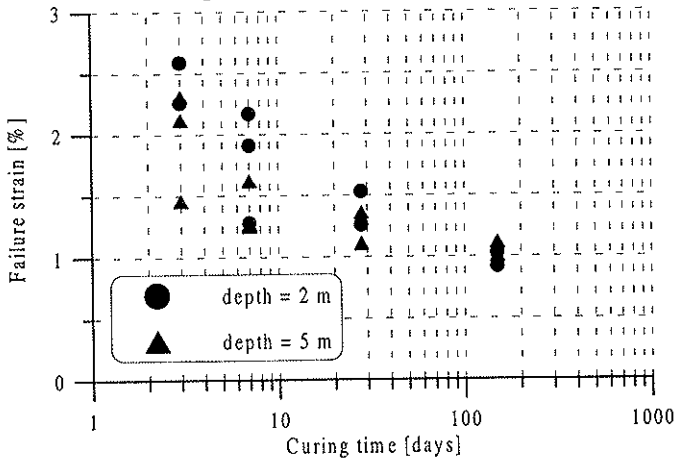


Figure 6.5 The decrease with curing time of the lime/cement column failure strain during unconfined compressive test.

At each depth three samples with the same curing age were tested. The lines presented in the diagram are the average values of the normalized compressive stress at the related depth. A large scatter was observed for the samples located at 5 m depth at a curing age of 150 days.

The failure strain decreased as the curing age increased, see Figure 6.5.

A combination of a decrease of failure strain and an increase of unconfined compressive strength obviously means a marked increase of the column modulus with time. The secant modulus E_{50} for the laboratory prepared samples at curing ages 7, 28 and 150 days is shown in Table 6.6.

Table 6.6 *Young's modulus of the lime/cement column based, laboratory mixed samples of 28 days age.*

Depth m	Young's Modulus 7 days $E_{50,col}$ [MPa]	Young's Modulus 28 days $E_{50,col}$ [MPa]	Young's Modulus 150 days $E_{50,col}$ [MPa]
2a	14.2	48.1	91.2
2b	22.3	51.5	88.4
2c	40.0		
5a	42.0	52.3	111.9
5b	36.0	50.3	98.0
5c	26.0		82.6

Although the soil conditions at the Varberg test site and the Löftaån test site were not the same, a comparison between the column moduli at the age of 28 days shows that, by increasing the stabilizing agent from 92 kg/m³ to 135 kg/m³, the column modulus was increased by about 50 %.

In addition to the laboratory made samples, eight specimens were extracted from columns *F4* and *F3* and trimmed to standard size samples. Unconfined compression tests were then carried out on these samples. The tests were conducted parallel with large-scale triaxial tests carried out on samples taken from the same columns. Samples from column *F4* were tested at the age of 90 days while samples from column *F3* were tested 114 days after the installation of the column. The unconfined compressive strength and the secant modulus, E_{50} , of columns *F4* and *F3* are presented together with results from laboratory prepared samples at the ages of 7, 28 and 150 days in Figure 6.6. An interesting observation in this diagram is that the field samples *F3* and *F4* are located very close to the laboratory samples of 28 days curing age. As already discussed in a previous section in this chapter, this may be related to the mixing process, the disturbance that may be caused by trimming works as well as the curing conditions.

However, it must be kept in mind that the trimmed samples were actually the best part of the lime/cement column specimens.

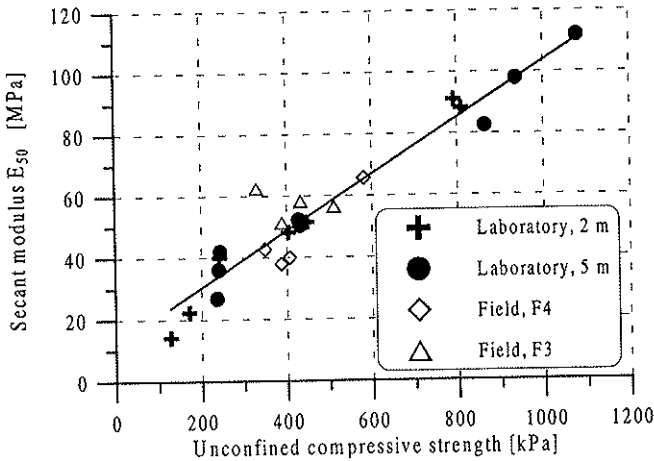


Figure 6.6 The secant modulus E_{50} of the lime/cement column versus the unconfined compressive strength for both laboratory prepared and field mixed samples at different curing ages.

It is important to point out that, in general, the samples used in the unconfined compression tests did not fail in pure shear, as more than one slip surface was sometimes observed during failure.

6.1.4.3 Hydraulic conductivity test

Tests were carried out to obtain the hydraulic conductivity of standard size samples. A series of tests consisting of four samples taken from mixed-in-place columns was carried out. The diameter of the samples was about 50 mm while the length varied between 43 mm and 56 mm. The samples were placed in a triaxial cell and were consolidated to a pressure equal to the in situ horizontal pressure. The determined hydraulic conductivity was between $1 \cdot 10^{-8}$ m/s and $1 \cdot 10^{-9}$ m/s, when a maximum hydraulic gradient according ASTM D5084 of 20 was applied. The initial hydraulic gradient i across the sample was created by a hydraulic head of about 0.1 m, due to the difference in water levels in the burettes, and a pressure head of about 0.9 m caused by the back pressure system. All the samples were tested again with larger hydraulic gradients of about 40 to observe the effect of exceeding the ASTM maximum limit. In this case the back pressure was increased to about 19 kPa. The intention was to conduct a falling head test, but since the back pressure portion of the applied gradient was large, especially when the hydraulic gradient was 40, the tests carried out may be

regarded as constant head tests. The results of these tests are presented in Table 6.7.

Table 6.7 The hydraulic conductivity of samples taken from mixed-in-place columns.

Sample	Dimensions		Hydraulic conductivity	
	Diameter [mm]	Height [mm]	$i = 20$ [m/s]	$i = 40$ [m/s]
F3a	50	50.7	$2 \cdot 10^{-8}$	$2 \cdot 10^{-8}$
F3b	50	52.3	$1 \cdot 10^{-8}$	$1 \cdot 10^{-8}$
				$1 \cdot 10^{-8}$
F4a	50	43.0	$4 \cdot 10^{-9}$	$1 \cdot 10^{-8}$
				$1 \cdot 10^{-8}$
F4b	50	56.0	$2 \cdot 10^{-9}$	$2 \cdot 10^{-9}$
				$2 \cdot 10^{-9}$

As is shown in Table 6.7, the measured hydraulic conductivity of the lime/cement columns varies between $2 \cdot 10^{-8}$ m/s and $2 \cdot 10^{-9}$ m/s. By comparing these results with the hydraulic conductivity of the clay measured in situ, it can be concluded that the lime/cement column is only about 2 to 25 times more permeable than the clay. Moreover, it was shown that the limits of the maximum hydraulic gradient proposed by the ASTM were in the case of the lime/cement column, very conservative. These maximum limits may be intended for compressible soft soils, where an increase of the gradient beyond the limited values may cause consolidation due to seepage pressure and reduction of the measured hydraulic conductivity.

Another test series consisted of four stabilized samples prepared in the laboratory. The falling head method was used in these tests, and for each sample two different initial hydraulic gradients were applied. The diameter of the samples was 50 mm while the height varied between 40 mm and 52 mm. As in the previous test series, the hydraulic gradient consisted of two portions, but at this time two back pressure systems were used connected to the bottom and the top of samples. The first hydraulic gradient was created by two back pressures, 90 kPa and 91.5 kPa, with a pressure difference of 1.5 kPa, while for the second gradient, which was larger than the first one, the back pressures utilized at the two ends were 90 kPa and 96 kPa with a pressure difference of 6 kPa. Obviously, the cell pressure was adjusted so as to have the same effective pressure acting on the sample. The motivation behind the application of the two back pressure systems with high values was to make it easy to get rid of any air bubbles which might obstruct the flow.

The values of the hydraulic gradient applied and the hydraulic conductivity of these samples are shown in Table 6.8.

Table 6.8 The hydraulic conductivity of laboratory prepared samples.

Sample	Hydraulic gradient (i)		Hydraulic conductivity
	Initial [-]	Final [-]	[m/s]
Lab1	6	2.2	$1 \cdot 10^{-8}$
	18	12.0	$1 \cdot 10^{-8}$
Lab2	5	4.4	$8 \cdot 10^{-9}$
	14	12.5	$2 \cdot 10^{-9}$
Lab3	6	1.4	$2 \cdot 10^{-8}$
	18	13.0	$8 \cdot 10^{-9}$
Lab4	5	3.0	$1 \cdot 10^{-8}$
	16	12.5	$5 \cdot 10^{-9}$

The ratio of the hydraulic conductivity of the lime/cement column shown in Table 6.8 to the hydraulic conductivity of the clay is between about 2 and 25. The predominant value of the hydraulic conductivity of the lime/cement column, obtained from laboratory prepared samples, is $1 \cdot 10^{-8}$ m/s. The results from all the hydraulic conductivity tests are presented in appendix C.

6.2 LABORATORY TESTS ON LARGE-SCALE SAMPLES

6.2.1 Triaxial tests

6.2.1.1 *Introduction*

In general, the calculation of the settlement of the lime/cement column treated soil is, among other factors, based on the shear strength of standard size laboratory samples, evaluated from the results of unconfined compression tests. By using empirical formulae, the modulus of elasticity of the lime/cement column is evaluated on the basis of unconfined compression test results. In the previous sections, results from both standard size laboratory mixed and field prepared samples were presented as well as an evaluation of the column modulus. Moreover, in Chapter 5, numerical calculations of the column modulus based on results from in situ load tests were presented. To get better information about the column modulus, large-scale triaxial tests were carried out. Only large samples from the Löftaån test site were extracted and subjected to triaxial testing at the laboratory of the Geotechnical Department of Chalmers University of Technology. At an early stage, and before tests were carried out on the Löftaån samples, two laboratory mixed large samples were tested and the results compared with standard size samples of the same treated material. Since the material of the treated soil used to prepare both large and standard size samples was the same, these two tests were considered as a way to observe the performance of the large triaxial apparatus.

6.2.1.2 *Test instrumentation*

The test equipment which was designed and built within the framework of this project consists of a confining chamber in which the sample is placed and tested, a hydraulic jack connected to a fixed load frame for applying axial force to the samples, a compressed air system to apply regulated pressure, and electronic measurement devices for measuring the applied load, pore pressure, cell pressure and axial deformation. As shown in Figure 6.7, the confining chambers consist of the cell base, cell body, cell top, top cover and the loading piston. All the parts of the cell were manufactured from corrosion resistance material. Three outlet ports exist at the cell bottom. Two of these ports were connected to a pore pressure device as well as to a back pressure system from one side and to the top

and the bottom of the sample from the other side. The third port was used as cell chamber connection and to fill the cell with water and pressurizing the cell.

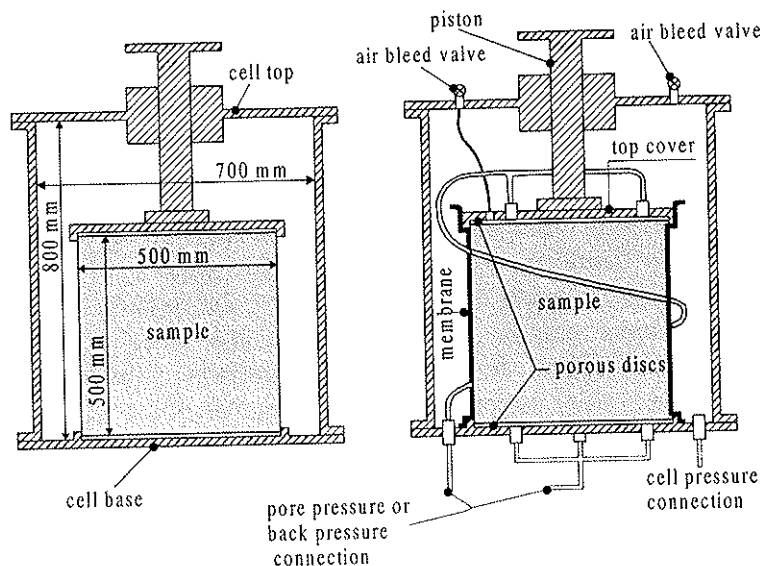


Figure 6.7 Some details of the large-triaxial cell.

The last port was used to empty the water in the cell after finishing the test. The cell bottom was formed to fit a porous disc 500 mm in diameter. The cell body consists of a steel cylinder with 700 mm diameter and 800 mm height. A piston bush, 70 mm in inner diameter, was fitted at the center of the cell top. Another two ports controlled by valves were made at the cell top. One of these ports was used to lead the air away from the cell as it was filled with water, while the other port was used to expel the air from the upper porous disc. The lower end of the piston had a hemispherical shape. The top cap, or the loading cap, was made of about 60 kg steel, and a porous disc was attached to this cap. Two ports were made in the loading cap; one connected the top of the sample to the port made in the cell base and in turn to the pore pressure device and to the back pressure system, and the second port connected the cell top by a small plastic tube for the purpose of de-airing the upper porous disc.

The pressure distribution panel was connected to a constant air pressure system from one side and to three outlet connections to the pressure cylinder system at the other side, see Figure 6.8. The outlet to the cell system was connected to two cylinders different in size. The material of the first cylinder was steel with about 80 mm inside diameter, while the other cylinder was made of transparent hard plastic with about 6 mm inner

diameter. The last small cylinder was used to observe the water level in the steel cylinder. The top and the bottom of the sample were connected to two cylinder systems. Each system consists of a large cylinder with an inner diameter of about 79 mm and a small cylinder with an inner diameter of 12 mm. The two cylinders were made of transparent hard plastic material and connected to each other by tubes supplied with valves. The small diameter cylinder was specially used for hydraulic conductivity tests on samples with low hydraulic conductivity.

The axial load system consists of a hydraulic jack connected to a stiff load frame. A large electrical pump was used to ensure constant applied load during each load increment by continuous circulated feeding of oil to the hydraulic jack. The applied axial load was measured by using an external load cell, and a displacement transducer at the top of the piston was used to measure the axial displacement.

The triaxial apparatus was placed on a thick steel plate that in turn rested on a very stiff steel H section.

6.2.1.3 Calibrations and corrections

To eliminate or reduce the effect of errors during a test, the measuring devices were calibrated before each test was started. Each pressure transducer was calibrated against a reference pressure source and a relation was built between the applied pressure and the electrical output. A calibration line was derived from a set of observed data for each device. A cycle of load/unloading was applied over a full range of the load cell used in the tests. The load cell was calibrated against a test machine, satisfying the demand of the Swedish Standard SS-EN 10 00-2 for class 1. Before a test, the displacement transducer was calibrated against certified slip gauges of accurately known thickness.

The leakage from the pressure system and the cell was controlled periodically, and special attention was paid to the leakage through the piston bush, the valves and through the sample membrane. The time used to control the leakage far exceeded the duration of the actual test.

As mentioned in the previous section, the hydraulic jack was attached to a stiff frame, and the triaxial apparatus was placed on a stiff pedestal. It was necessary to measure the deformation of the system, consisting of the frame and the pedestal. The system was tested by applying a load on a very stiff steel 'specimen', and dial gauges were placed on the pedestal and at the four corners of the frame to measure the deformations. A relationship was then established between the applied load and the supporting system deformation, which was considered during the analysis of the test results. No standard size membrane was available for the triaxial test specimens with a diameter of 500 mm. To reduce the restraining effect of the

membrane enclosing the specimen the extension modulus of different types of rubber membrane material was tested. Among three membrane types, the one used in the triaxial test was a latex rubber 0.5 mm in thickness with an extension stiffness of about 0.45 N/mm.

6.2.1.4 Installation and test procedure

The routine test for the consolidated undrained, *CU*, triaxial test is described in this section

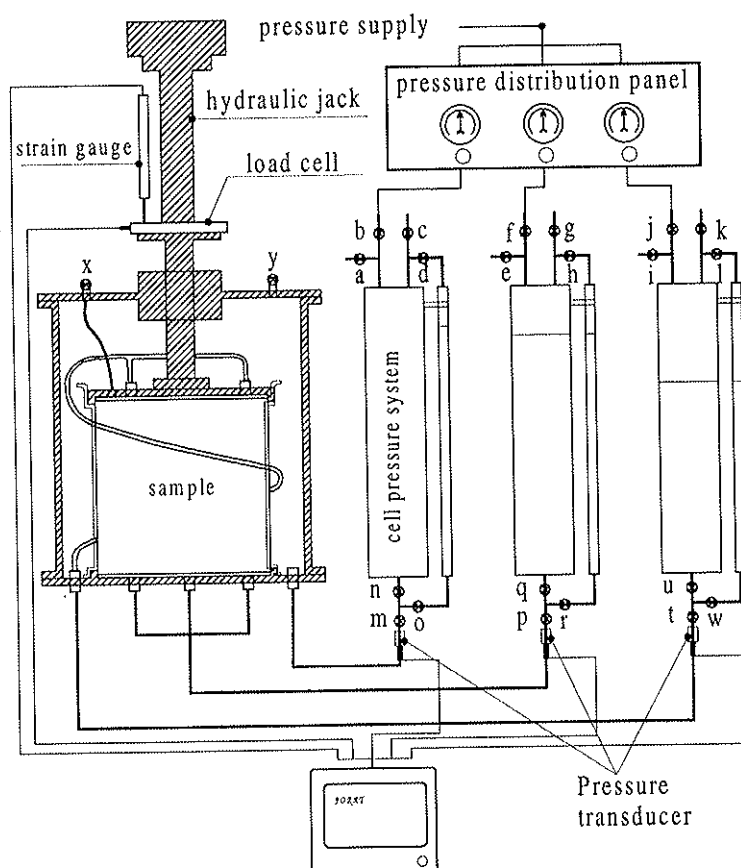


Figure 6.8 Schematic view of the main features of the large-triaxial apparatus.

The test procedure consists of preparing and setting up the sample as well as the test procedure. A steel pipe, 800 mm in diameter, was used as a tool to extract a full-length column in the field. The pipe consisted of two parts, and these two parts were separable along the pipe length. In total three columns were taken up, and 8 large samples were extracted and transported to the laboratory. The manufactured column was 600 mm in

diameter. The samples were trimmed down to 500 mm in diameter and 500 mm height. The trimming was done by hand.

The cylinders connected to the sample were filled with de-aired water. Valve *p* was opened to replace the air in the tube, connecting the cylinder to the cell bottom, by de-aired water. The column samples were flushed with water to compensate for the water lost during the trimming process. The weight of the sample was measured before it was mounted on the cell bottom.

The top cap was placed on the sample, and a plastic tube was used to connect the top cap to the cell bottom. Valve *t* was opened to drive out the air from the newly connected tube and the top porous disc. It was very difficult to de-air the porous disc at the top cover since gravity forces drained the disc, and air replaced the drained water. Finally, the upper porous disc was de-aired using a special technique.

All the drain lines leading to the top and the bottom of the sample were then opened to let the sample get into contact with water as in the field. Isotropic consolidation pressure was then applied by increasing the cell pressure. As was mentioned in the previous section, the weight of the top cap was about 60 kg while the weight of the piston together with the steel plate under the load cell was about 28 kg. The axial stress at the top of the sample was about 3 kPa higher than the radial stress, and at the bottom of the sample the self-weight of the sample resulted in an increase in the axial stress of the sample at that level. In fact, the radial pressure itself was not constant since at the bottom of the sample the pressure of the water column in the cell should be added to the applied pressure. All these factors resulted in a slightly anisotropic stress condition.

After consolidation of the sample, the undrained test was conducted. The axial load was increased in equal load steps and, to imitate the in situ load test, the load was kept constant during a 32-minute time interval. Five electronic channels were connected to the computer to register the applied axial load, the axial deformation, the cell pressure and the pore water pressure at the top and the bottom of the sample.

6.2.1.5 Evaluation of test results and compression modulus

There are many reasons why a soil sample may not be fully saturated during a laboratory test. In the case of the lime/cement columns, the manufacturing of the column is performed using a dry stabilizing agent together with very high air pressure, may be up to 500 kPa. Evidence from field and laboratory tests shows that lime/cement columns are not fully saturated. The fact that gas is a highly compressible material and that the pressure in the water and in the gas is not equal makes the analysis of the partially saturated soil much more complex than for fully saturated soil.

According to Barden (1965), in the case of wet artificially compacted clays with a degree of saturation S_r more than 90%, air in the soil exists in its occluded state and cannot flow as a separate continuous fluid. In the case of a stiff material, like the lime/cement column, the presence of a small amount of air will have a large impact on the pore pressures developing during a triaxial test. The pore pressure parameters A and B are strongly dependent on the degree of saturation. According to Black and Lee (1973), the degree of saturation can be written as:

$$S_{r,i} = \frac{1 - \frac{P_i}{P_i + \Delta u} - C_d \cdot \frac{\Delta \sigma_3}{n_i} \cdot (1 - B)}{1 - \frac{P_i}{P_i + \Delta u} - C_w \cdot B \cdot \Delta \sigma_3} \quad (6.2)$$

$S_{r,i}$	initial degree of saturation
P_i	initial absolute pressure in the pore air corresponding to $S_{r,i}$
Δu	change in pore pressure under undrained condition.
$\Delta \sigma_3$	change in the isotropic cell pressure.
C_w	compressibility of the pore water ($4.8 \cdot 10^{-7} \text{ m}^2/\text{kN}$)
C_d	compressibility of soil skeleton
n_i	initial porosity

Equation (6.2) can be simplified and rewritten in terms of the pore pressure coefficient B

$$B = \frac{\Delta u}{\Delta \sigma_3} = \frac{C_d}{C_d + n_i \cdot S_{r,i} \cdot C_w + n_i \cdot \frac{1 - S_{r,i}}{P}} \quad (6.3)$$

P	absolute pressure in the pore air after application of stress increment.
-----	--

By applying a uniaxial stress, shear stress will be induced in the soil. Using the pore pressure coefficients A and B , the change in pore pressure due to a deviator stress can be calculated by the equation

$$\Delta u_d = A \cdot B \cdot (\Delta \sigma_1 - \Delta \sigma_3) \quad (6.4)$$

To demonstrate the effect of the degree of saturation on the B parameter, Black and Lee (1973) treated four categories of soil. Typical values of the pore pressure coefficient are presented in Table 6.9.

Table 6.9 Variation in B value with increasing degree of saturation for typical soils.

Soil category	Soil compressibility C_d [m ² /kN]	Void ratio e [-]	Pore pressure coefficient B		
			Degree of saturation, S_r		
			100%	99.5%	99.0%
soft	1450	2.0	0.9998	0.992	0.986
medium	14500	0.6	0.9988	0.963	0.930
stiff	145000	0.6	0.9877	0.690	0.510
very stiff	1450000	0.4	0.9130	0.200	0.100

Soft soils - soft normally consolidated clays; Medium soils - compacted silts and clays, and lightly overconsolidated clays; Stiff soils - overconsolidated stiff clays and average sands; Very stiff soils - very dense sands or stiff clays especially at high confining pressure

The B value for fully saturated soft and medium soils is almost equal to unity while the value of B will decrease somewhat for fully saturated stiff and very stiff soils. Partially saturated soil consists of a three-phase system; soil particles, water and gas.

The lime/cement column belongs to the stiff soil category. In section 6.1.4.1, the degree of saturation of small, field mixed samples was around 97 %. With this in mind and by observing the results in Table 6.9, the B coefficient will be very low and, as a consequence, the generated pore pressure is expected to be very low as well.

The lime/cement column is partially saturated, and the shear strength is therefore strongly dependent on the confining pressure and the degree of saturation. It is important to know that the relationship between the shear strength of partially saturated material and the confining pressure is non-linear. The angle of internal friction based on total stress analysis is not a basic property of the lime/cement column material but dependent on the test conditions. The major intention of the triaxial tests conducted was to determine the column modulus, and no attempts were made to evaluate the strength properties of the column. None of the triaxial tests carried out developed a single-plane slip surface and, therefore, only area increasing correction was applied.

In undrained triaxial tests carried out on fully saturated samples, the barrel cross-area correction is based on axial strain since no volume change is allowed. Yet some volume change was observed during the undrained triaxial test conducted on the lime/cement column. In addition to the axial strain, the volumetric strain was used in the calculation of the area modification according to the following equation

$$A_{corr} = \frac{1 - \frac{\Delta V_{col}}{V_{col,o}}}{1 - \epsilon_a} \cdot A_0 \quad (6.5)$$

A_{corr}	corrected area
A_0	initial area of the consolidated specimen
ΔV_{col}	volume change
$V_{col,o}$	volume after consolidation
ϵ_a	axial strain

Radial and axial stresses were calculated at the middle of the specimen. The ratio of the initial height to diameter was equal to one for most of the samples tested. Before discussing the slenderness and end conditions of samples subjected to compression in triaxial testing, practical details will be mentioned. It would be extremely difficult to extract samples from columns taken up in the field with the traditional height to diameter ratio = 2. Besides, with $H/D_i = 1$, it was more practical to trim and mount the samples.

It was the intention that, during a triaxial compression test, the whole sample should be subjected to a uniform axial stress and a uniform displacement field. Tests were carried out to study the influence of the slenderness of the sample and the end conditions on the strength parameters and the mode of failure of the sample. To ensure the development of the Mohr Coulomb failure criterion, the traditional ratio of $H/D_i = 2$ was used. In general, when the ends of the sample are not lubricated, shear stresses will develop at the sample ends and, therefore, the axial stress is no longer a principal stress.

Bishop and Green (1965) found that the angle of internal friction ϕ for a sample with $H/D_i = 2$ and non-lubricated fixed ends was the same as that for well lubricated fixed ends. Furthermore, samples with lubricated ends having $H/D_i = 1$ did not depart very much from the shape of a cylinder up to the strain corresponding to peak strength, while samples with $H/D_i = 2$ did not expand much at the ends of the sample whether lubricated or not. In the last case, the question is whether the use of average cross-sectional sample area to calculate the stress is accurate or not. Rowe and Barden (1964) showed that the angle of internal friction ϕ for samples with $H/D_i = 1$ or 2 with lubricated ends was slightly lower than for samples with $H/D_i = 2$ to 2.7 with non-lubricated ends.

Hartlén (1974) discussed the slenderness and the end condition problems and presented many references regarding this classical problem.

Jacobsen (1967) and Jacobsen (1970) showed that the best results could be obtained if lubricated ends are used and the sample is prepared with $H/D_i = 1$. According to Harremoës et al. (1970), the strength parameters of the sample are underestimated for samples with $H/D_i = 2$. If the sample height to diameter ratio is equal to one and the ends of the sample are well lubricated, all the parts of the sample will undergo the plastic phase. On the other hand, if the ratio is selected to be two at failure, only a small part of the sample in the form of failure surface will undergo the plastic phase while the rest of the sample will remain intact. In an undrained test where the volume of the sample is kept constant, the last case will mean that water can flow to or from the failure zone to the intact parts of the sample. For preloaded material, dilation will occur at the failure zone, where the vacuum will suck up water to the zone, resulting in a reduction in the strength of the material. For samples with $H/D_i = 1$ or 2 with non-lubricated ends, stiff cones will develop at the ends of the sample.

Brown and Gonano (1974) studied the slenderness and end roughness problem in rock mechanics. They observed that, for samples having a range of height to diameter ratio of between 0.5 and 3 with well-lubricated ends, the axial stress-axial strain relationship was the same up to the failure load and that some divergence was noticed after the axial force peak value. On the other hand, for non-lubricated ends, the peak axial stress and strain were slightly higher in samples with an initial height to diameter ratio of 1 compared to a diameter ratio of 2.

Before any triaxial tests on large samples from the Løftaån test site were carried out, two laboratory mixed samples together with a number of standard size samples were prepared for the test. Since the column quality of the large and the standard size samples was about the same, the objective of these tests was only to investigate the performance of the large triaxial apparatus. The two large samples *LC1* and *LC2* had the same failure load of about 540 kPa and the same failure strain of about 0.9 %. The modulus E_{50} for these large samples was between 60 MPa and 70 MPa. The failure load of the small samples was between 560 kPa and 580 kPa, which is slightly larger than the failure load of the large samples. On the other hand, the strain at failure was between 1.5 % and 2.5 %, which far exceeded that of the large samples. In conclusion, the elastic modulus of the small samples was less than that of the large samples, which may be related to the scale factor.

Four large samples from the Løftaån test site were tested during the period between June and July 1999. The dimensions of the samples, curing age and depth from which these samples were taken are shown in Table 6.10. The classification parameters of the samples were already presented in Table 6.5.

Table 6.10 Depth, curing age and dimensions of the trimmed samples.

Sample	Depth [m]	Age [days]	Diameter [mm]	Height [mm]
F2	3.5	98	500	400
F3-a	1.5	114	500	500
F3-b	5.5	108	490	500
F4	1.5	91	500	500

The samples were first consolidated with a cell pressure of between 20 kPa and 30 kPa depending on the depth at which the samples were taken. Undrained compression tests were then carried out. Stepwise axial loading was used and at each step the axial load was increased by 40 kN. When the axial loading had reached the intended value, an equal time interval of 32 minutes between each load step was used to measure the creep deformation of the lime/cement column during the test. Directly before the failure load was reached, both the axial load and the load step duration was reduced by 50% to obtain more data before and after the failure. In this way, the loading rate was kept constant.

The failure load was reached when the hydraulic jack could not keep the axial load constant, except for column *F3*, where no evidence of total collapse was observed.

The predominating behavior of the columns tested was that no or very low pore pressure developed up to a stress level close to the failure load where the samples started to dilate and a negative pore pressure began to develop. In fact, it was not clear whether the pressure in the porous disc or the pore pressure in the samples was measured before the sample started to dilate. Although drained tests were carried out, some volume change was observed during the test since the sample was not fully saturated.

After reaching the failure load the sample was unloaded and the confining pressure was increased from 20 to 100 kPa and then another undrained test was carried out. At the second test a very short time interval of about 5 minutes was used between each load increment.

The main objective of the triaxial tests conducted on large samples was to compare the modulus E_{50} with those evaluated from unconfined compression tests on standard size samples and in situ load tests. The test evaluation will therefore be concentrated on this issue.

In Figure 6.9, the axial stress-strain relationships of consolidated undrained tests on columns *F2*, *F3-a*, *F3-b* and *F4* are presented.

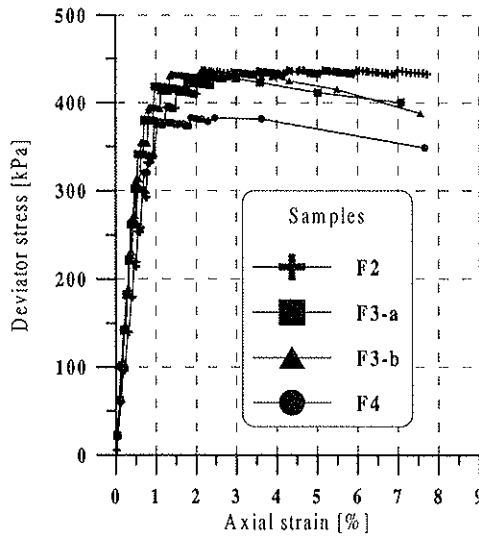


Figure 6.9 Stress-strain relationship of consolidated undrained tests conducted on four different large samples with a confining pressure of between 20 kPa and 30 kPa.

The confining pressure used for samples *F2*, *F3-a* and *F4* was 20 kPa while, for sample *F3-b*, the confining pressure was 30 kPa. The peak deviator stresses observed were almost identical for samples *F2*, *F3-a* and *F3-b* with values of 430 kPa, 420 kPa and 435 kPa respectively. The peak axial stress observed for sample *F4* was 380 kPa.

The influence of the increasing confining pressure on the lime/cement column sample was similar to that of a triaxial test carried out on a rock sample. In general, the axial stress-strain relationship was the same when the confining pressure was increased to 100 kPa in the three samples, with the exception that the peak deviator stress value was increased by the increase of the confining pressure, as shown in Figure 6.10. For clarity, only results achieved at the end of the load increment are presented.

In two samples, *F4* and *F3-a*, the maximum deviator stress values were increased by about 60 kPa after increasing the confining pressure. For soft soil, the stiffness increases by increasing confining pressure, but in the case of the lime/cement column the secant modulus E_{50} decreased with higher confining pressure. As in the case of column *F3-b*, the maximum deviator stress increased by about 35 kPa and the secant modulus E_{50} decreased by only about 5 %. The maximum axial stress and the secant modulus E_{50} of all the tests are presented in Table 6.11.

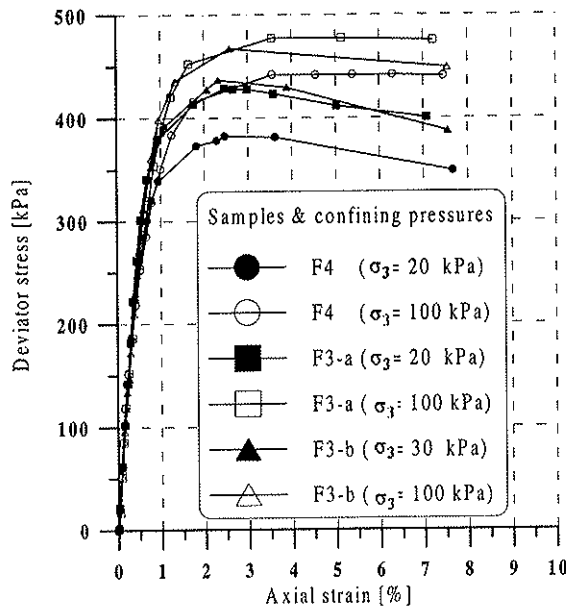


Figure 6.10 Stress-strain relationship for three large samples with different confining pressures.

A comparison between the results of large-scale triaxial tests and unconfined compression tests carried out on standard size samples taken from column *F3* and *F4* with the same curing age, shows that there is quite good agreement with both the maximum deviator stress and the secant modulus E_{50} of these samples. It must be point out that the columns were of good quality and very homogeneous, thus the quality of both the large and the standard size samples was almost identical.

Table 6.11 The secant modulus and the maximum axial stress for all the large-size columns.

Sample	σ_3	Peak deviator stress	Secant Modulus
m	[kPa]	[kPa]	E_{50} [MPa]
F2	20	430	55
F3-a	20	420	62
	100	478	52
F3-b	30	435	57
	100	468	54
F4	20	380	67
	100	440	46

The values of the secant modulus E_{50} for the standard size samples taken from column *F3* vary between 51 MPa and 62 MPa, and the unconfined compressive strength values vary between 330 kPa and 511 kPa. For column *F4*, the values of E_{50} are between 38 MPa and 65 MPa and the values of the unconfined compressive strength are between 349 kPa and 580 kPa.

As mentioned before, the time interval between each load increment was 32 minutes. This was in order to be able to observe the creep strain of the lime/cement column, see Figure 6.11.

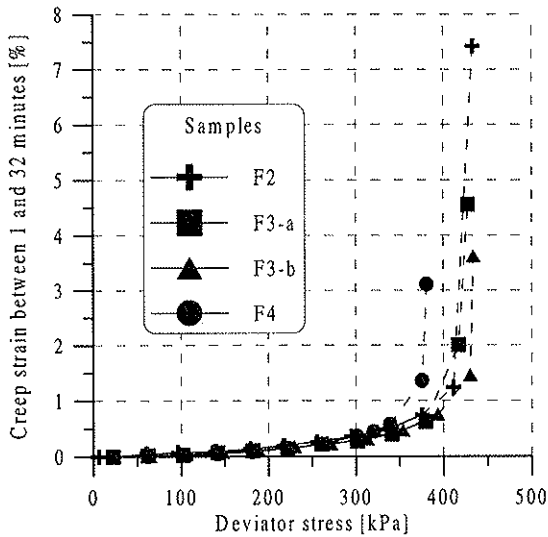


Figure 6.11 Creep strain as a function of deviator stress for all the columns measured during the first triaxial test with 20 or 30 kPa confining pressures.

Creep strains started to increase in all the columns at a deviator stress equal to about 90 % of the failure value. In the creep deformation results measured in the load tests, the value is much lower since in this case only the creep strain in the column material was measured while in the case of the load test, the measurement consisted of both the column and the clay soil materials. Moreover, the lime/cement columns are not a perfect homogeneous material and in the case of in-situ load tests about 6 m length of the column material was subjected to test compared with only 0.5 m length in the triaxial compression test. It is obvious that a certain inhomogeneity could be observed in samples with much larger volume. The broken lines in Figure 6.11 are to show that, at that interval, the creep strains were measured for less than 32 minutes.

The stress paths of the tested columns are almost identical, and therefore only the stress path of column *F3-a* is presented in Figure 6.12.

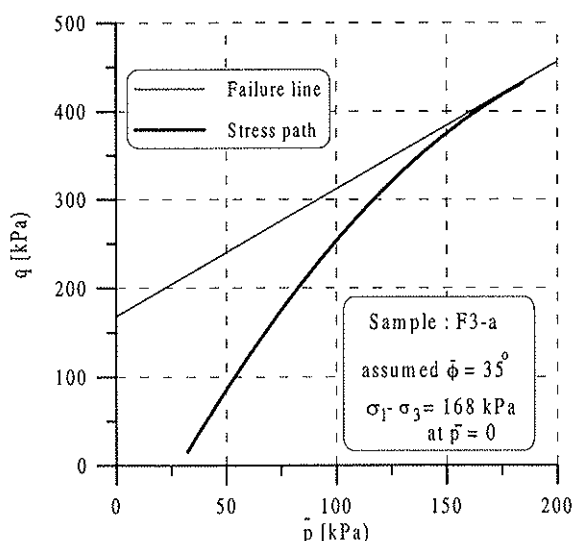


Figure 6.12 Effective stress path of effective stress for triaxial compression test on column *F3-a*.

In Swedish design practice, the effective angle of internal friction ϕ' for lime/cement columns is usually assumed to be 35° and, with this in mind, the calculated deviator stresses for $\bar{p} = 0$ related to this friction angle for the tested columns are almost identical, varying only between 168 kPa to 175 kPa.

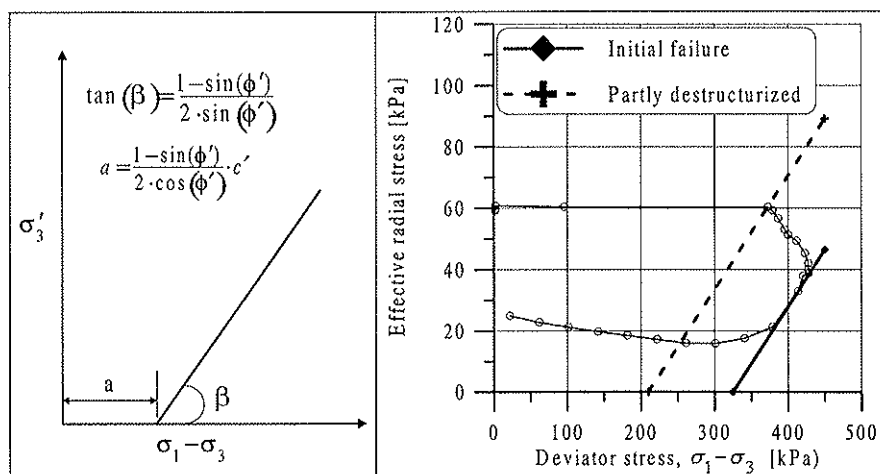


Figure 6.13 Failure stress envelopes plotted in deviator stress space.

According to Steensen-Bach et al. (1996) the traditional technique to evaluate the strength parameters of a structured material, such as the lime/cement column, should not be applied.

A simple soil model to be applied on limestone was suggested, and a deviator stress state method was used to define the stress path, see Figure 6.13. If the assumed value of the effective angle of internal friction ϕ' is applied, then the values of the effective cohesion values c' of the initial failure envelope and for partly destructurized column material are 85 kPa and 55 kPa, respectively. The equations used for these calculations are shown in Figure 6.13.

Finally, to give an idea about the pore pressure and volume strain variation during a triaxial compression test, results from a test carried out on sample F3-a are presented in Figure 6.14.

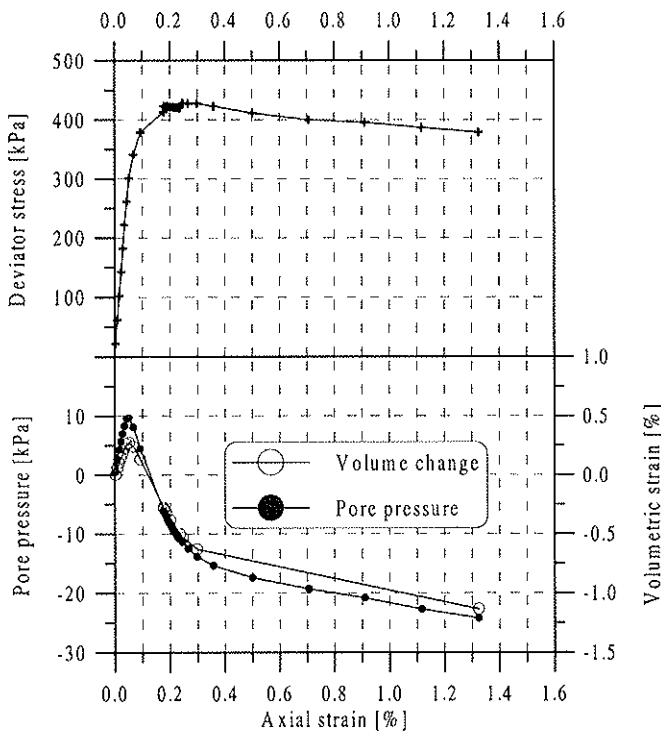


Figure 6.14 Results of triaxial compression test on sample F3-a at 20 kPa confining pressure.

The specimen was consolidated under a confining pressure of 20 kPa. The column specimen acted as overconsolidated material since it started to dilate as the deviatoric stress approached the failure value and a negative pore pressure developed. Again it must be pointed out that it is not clear

whether the positive pore pressure was representative for the sample or for the area close to the porous disc. The sample was not fully saturated, which resulted in some volume change in the sample with a negative value when the specimen started to expand.

6.2.2 Hydraulic conductivity

Hydraulic conductivity tests on large lime/cement column specimens provide an understanding about the hydraulic properties of the material, together with similar standard size samples and in situ hydraulic conductivity tests.

The idea behind this test was to observe the effect of the column material macro-structure on the hydraulic conductivity and to compare the test results with other results obtained from previous tests.

The specimen was extracted from column *F3* and trimmed down to 480 mm in diameter and 400 mm height. The test was carried out using the same large triaxial apparatus as described in the previous section.

The first test was carried out using the falling head test. One back pressure system was used, and a 20 kPa back pressure was connected to the bottom of the specimen, allowing drainage at the top. The values of the gradients used during the test varied between 4 and 5, see Figure 6.15.

The time duration for the test was about 8 days and the measured hydraulic conductivity was around $1 \cdot 10^{-8}$ m/s.

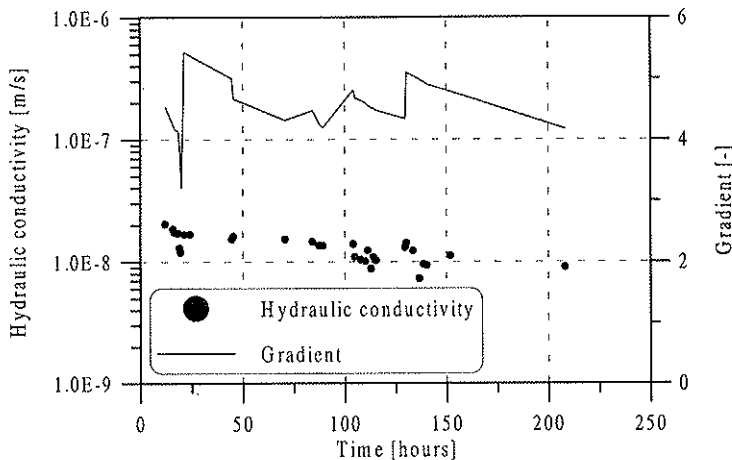


Figure 6.15 Results from the hydraulic conductivity test on specimens taken from column *F3* without application of axial load.

The hydraulic conductivity of a saturated soft soil, measured by the oedometer test, changes under the influence of the applied load. In such a

test the hydraulic conductivity of the soil is reduced with increasing compression stress.

In the next step, the hydraulic conductivity of the lime/cement specimen was determined by subjecting the specimen to axial loading, see Figure 6.16.

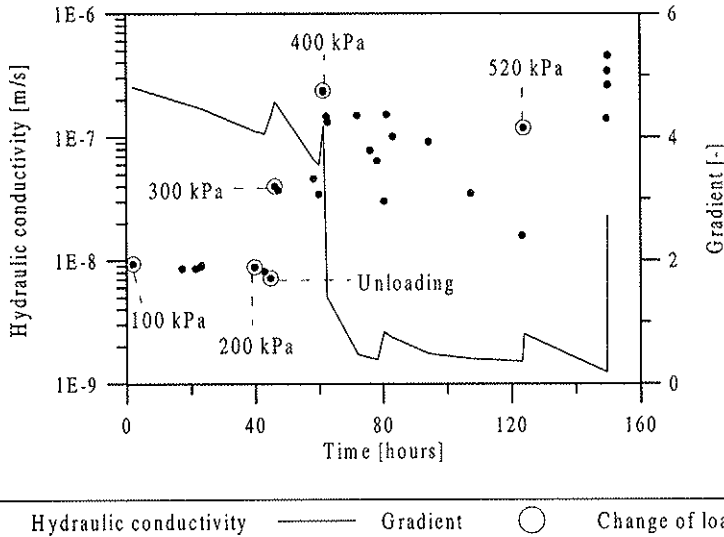


Figure 6.16 Results from hydraulic conductivity tests carried out on specimens taken from column F3 with different axial loading and different gradients.

The test started with a 100 kPa axial load and a gradient of between 4 and 5. The measured hydraulic conductivity was similar to that determined without any axial load with a value of about $1 \cdot 10^{-8}$ m/s. The specimen was loaded to 200 kPa and then unloaded to zero, and the hydraulic gradient remained almost the same. The hydraulic conductivity was increased to about $3 \cdot 10^{-8}$ m/s as the axial load increased to 300 kPa. The change with time of the axial deformations within each load increment was very limited until the loading was increased to 400 kPa, when a sudden increase was observed. This increase was even greater than that observed when the load increased to 520 kPa. It is believed that micro-cracks started to grow, which may explain the sudden increase in the hydraulic conductivity at this stage, reaching a value of about $2 \cdot 10^{-7}$ m/s. It was observed that the hydraulic conductivity became affected by the applied gradient since it decreased when a lower gradient was used. By increasing the axial load to 520 kPa, which was very close to the failure load, the hydraulic conductivity increased again, even with a low gradient, and then it increased rapidly with the increase of the gradient. At the next axial load increment, which is not presented in Figure 6.16, the specimen reached

failure and there was no way of measuring any hydraulic gradient, as the volume of water flow through the sample was large and out of control.

7. CONCLUSIONS

7.1 SETTLEMENT, LOAD DISTRIBUTION AND RATE OF CONSOLIDATION.

Traditionally, a relatively simple method has been used to calculate the long-term and consolidation settlements of lime/cement stabilized soil.

The interaction between the column and the surrounding soil has been treated in this study. This was accomplished by developing an analytical model and 3-dimensional numerical models. The importance of the assumption concerning the stiffnesses and the hydraulic conductivity of the materials is evident

A summary of the conclusions based on the parametric study, is presented below.

- The long-term settlement calculated by using the traditional method expressed by equation (3.7), is about 10 to 25 % lower than that calculated by the proposed analytical method, under the assumption that both the lime/cement column and the surrounding soil act as a linear elastic material. Using E_{col} instead of M_{col} in equation (3.7), the results become closer to that obtained by the analytical solution. Both methods are based on the assumption that the column is extended to firm bottom and thus different results can be expected for floating columns.
- The 3-D linear elastic analysis indicates that the vertical stress in the column increase with depth and reach a maximum value at a few meters below the ground level and thereafter decrease directly, regardless of the column length. The maximum vertical stress in the column will increase with increasing length of the column.
- The maximum vertical stress in the column evaluated from the 3-D analysis is less than that calculated by the traditional method and the difference increases as the column length decreases. Consequently, this mean that the vertical stress in the untreated soil within the stabilized block is larger than that calculated by the traditional method, whereby a larger deformation is expected just like the case explained in the first point. However, since the vertical stress in the column obtained by the traditional method is assumed to be constant

along the whole column length, it may be concluded that the method is still conservative. In the case of columns extending to firm bottom, the vertical stresses in the column calculated by the finite element method is very close to the stresses calculated by the proposed analytical method. However, at higher area ratio, a_s , of about 36 %, the solutions of the traditional and the proposed analytical model are identical and less than that calculated by the 3-D finite element analysis.

- Traditionally, the increase of the vertical stress in the untreated soil below the stabilized block is evaluated by assuming that the whole applied load at the ground surface is transmitted to the bottom of the stabilized block and then distributed using an approximate method called the 2:1 method. The results from the 3-D finite element analysis shows that this method is very conservative and the vertical load increase can be calculated by distributing the applied load from the ground surface using Boussinesq's elastic solution. However the numerical simulations show that there is a limited region with stress concentration directly under the reinforced block. This may be due to numerical problem that can appear at the boundaries between two materials with a high stiffness difference.
- The radial consolidation equation used traditionally used to calculate the degree of consolidation assume that the average applied vertical load is kept constant during the course of consolidation. However, due to the stiffness difference between the two materials, load transfer from the surrounding soil to the lime/cement column will take place and the applied vertical load on the soft soil is therefore no longer constant. The rate of consolidation will be accelerated as the stiffness ratio between the lime/cement column and the surrounding soil increases.

7.2 MECHANICAL PROPERTIES OF THE LIME/CEMENT COLUMNS

The mechanical properties of the lime/cement column stabilized soil is depend on many factors, among them, the properties of the original soil, the amount and type of the stabilizing agent, the mixing method, etc. In the following, some general conclusions based on limited test results are presented.

Comparison is made between test results carried out on laboratory prepared and field mixed samples of standard size and large samples.

Comparison is also made between laboratory and in-situ test results.

- As the curing time increase, the compressive strength of the lime/cement column increases while at the same time the failure strain decreases. As a consequence the column stiffness can be expected to increase with time. No clear evidence was observed that which proved that the increase of the shear strength in the field is faster than that in the laboratory.
- The results of the triaxial compression tests confirmed that the lime/cement column behavior is similar to that of stiff overconsolidated clay. Negative pore pressure due to dilation was observed directly before failure.
- As a lime/cement column is a partially saturated material, in combination with the high stiffness of the material, a very low or no pore pressure developed before the sample started to dilate in a consolidated undrained triaxial compression test. It was also observed during in-situ load tests that air bubbles started to come from the column through the drilled holes, which shoes that a lime/cement column is a partially saturated material.
- Like previous studies, the stiffness of the lime/cement column increased proportionally to the compressive strength. In connection with the Löftaån test site, the secant modulus, E_{50} , is about 100 times the unconfined compressive strength of both laboratory prepared and field mixed lime/cement samples.
- The secant Young modulus, E_{50} , evaluated from in-situ tests at the Varberg test site is much higher than that evaluated from unconfined compression tests for both laboratory prepared and field mixed

samples. At the top of the column where the confining pressure is low, the ratio of the secant modulus, E_{50} , to the failure load, for column 4, 7 and 8 was between 240 and 300.

- Different values of column secant modulus were obtained from in-situ load tests carried out at the LÖftaån test site depending on the assumptions made during the numerical analysis. If the column quality at the top was assumed to be lower than the rest of the column then, the stiffness obtained was higher and in some columns lower than that evaluated from triaxial tests conducted on large samples. As for the rest of the column, much higher column stiffness was obtained. On the other hand, if the column was assumed to be of the same quality over the whole length, then the secant modulus obtained from numerical simulations was equal or in most of the cases larger than that obtained from triaxial tests conducted on large column samples. The ratio of the secant modulus to the failure load for column C2 and D1, where local failure at the top of the column was observed, was about 120 and 180 for the first and second simulation assumptions, respectively.
- The secant Young modulus, E_{50} , evaluated from triaxial tests carried out on large lime/cement samples was slightly higher than that evaluated from unconfined compression tests performed on field mixed standard size samples. With the increase of the confining pressure, no significant increase in the column stiffness was observed in all the triaxial tests carried out on large samples.
- Short-term creep strain measured in all the columns during the triaxial compression tests became significant at about 90 % of the failure load. During the in-situ load tests, the creep deformations became high at about 80 % of the failure load. In the triaxial compression test, only the creep strain in the column material was measured while in the case of the load test, the measurement consisted of both the column and the clay soil materials moreover, the lime/cement columns are not a perfect homogeneous material and in the case of in-situ load tests about 6 m length of the column material was subjected to test compared with only 0.5 m length in the triaxial compression test. It is obvious that a certain inhomogeneity could be observed in samples with much larger volume. This may explain the difference in creep load resulting from the two tests.

7.3 HYDRAULIC CONDUCTIVITY OF THE LIME/CEMENT COLUMNS

As in the case of mechanical properties, the hydraulic properties are dependent on the type of the soil, stabilizing agent and the mixing procedure. Also here the conclusions made are of a general character.

- Low hydraulic conductivity was measured and compared with values usually assumed in the calculation of rate of settlement. Neglecting the high hydraulic conductivity due to leakage problems in the in-situ tests at the Varberg test site, the hydraulic conductivity of the lime/cement columns varies between about 10 and 100 times that of the original soil with an average value of about 50. At the same test site, the values of the hydraulic conductivity of the lime/cement standard size field-mixed samples vary between 1 and 90 times that of the original soil with an average value of about 20. In the case of the Löftaån test site, the values of the hydraulic conductivity of the lime/cement columns vary between 10 and 100 times that of the clay with an average value of 30. The values of hydraulic conductivity obtained from laboratory tests carried out on field-mixed and laboratory prepared lime/cement samples are similar and vary between 3 and 25 times that of the clay with an average value of about 10.
- Better control of leakage problem and test preparation in the laboratory compared with that in the field can be among the reasons of why the hydraulic conductivity evaluated in laboratory tests is lower than that evaluated from in-situ tests.
- One hydraulic conductivity test on a large lime/cement sample was conducted and the value of the measured hydraulic conductivity when no deviator stress was applied on the sample was about the same as that of standard size samples. An increase in the hydraulic conductivity was observed with the increase of the deviator stress applied on the large sample.

7.4 FUTURE RESEARCH

The numerical model presented in chapter 3 for calculating the consolidation settlement in lime/cement-stabilized clay assumed linear elastic material, and no load distribution was considered within the stabilized block. Furthermore, only columns to firm bottom were treated. A new model needs to be developed to cover the issues mentioned above.

In-situ tests with trial embankment are needed to follow up the settlements as well as pore pressure development in both treated and untreated soil. The test results can then be compared with the results of the models presented in this study.

The effect of the degree of saturation of the lime/cement column on the mechanical parameter of the material is in need for further studies. Triaxial compression tests presented in most of the papers were carried out by applying a combination of a high back pressure and a high confining pressure which is in fact is among the methods used to saturate soil materials. Triaxial tests need to be carried out on large and standard size lime/cement samples subjected to conditions similar to those existing in the field. Furthermore, more in-situ load tests need to be carried out with the possibility of measuring pore pressure development in the lime/cement column.

REFERENCES

- Alamgir, M., Miura, N. and Madhav, M. R. (1993). "Analysis of granular column reinforced ground: I Estimation of interaction shear stresses" *Reports of the Faculty of Science and Engineering, Saga University* Vol. 22, No. 1, pp. 111-118.
- Alamgir, M., Miura, N. and Madhav, M. R. (1994). "Analysis of granular column reinforced ground-II : Stress transfer from granular column to soil" *Reports of the Faculty of Science and Engineering, Saga University* Vol. 23, No. 1, pp. 81-94.
- Alamgir, M., Miura, N., Poorooshasb, H. B. and Madhav, M. R. (1996). "Deformation analysis of soft ground reinforced by columnar inclusions" *Computers and Geotechnics* Vol. 18, No. 4, pp. 267-290.
- Baker, S. (1999). "Numerical analysis of load distribution between lime/cement columns and surrounding soil using finite element method". *Proceedings Dry Mix Methods for Deep Soil Stabilization*, Stockholm, pp. 215-220.
- Baker, S. (1999). "Three dimensional consolidation settlement of stabilized soil using lime/cement columns". *Proceedings Dry Mix Methods for Deep Soil Stabilization*, Stockholm, pp. 207-213.
- Baker, S., Liedberg, N. S. D. and Sällfors, G. (1997). "Deformation properties of lime cement stabilised soil in the working state". *Proceedings 14th International Conference on Soil Mechanics and Foundation Engineering*, Hamburg, pp. 1667-1672.
- Balasubramaniam, A. S. and Buensuceso, B. R. (1989). "On the overconsolidated behaviour of lime treated soft clay". *Proceedings 12th International Conference on Soil Mechanics and Foundation Engineering*, Rio de Janeiro, pp. 1335-1338.
- Barden, L. (1965). "Consolidation of compacted and unsaturated clay" *Géotechnique* Vol. 15, No. 3, pp. 267-286.
- Barron, J. R. (1948). "Consolidation of fine-grained soils by drain wells" *ASCE*, Vol. 113, pp. 718-754.
- Bengtsson, P. E. and Holm, G. (1984). "Kalkpelare som drän (Lime column as a drain)". *Proceedings 9th Nordic Geotechnical Conference, NGM*, Linköping, pp. 391-398.
- Biot, M. A. (1941). "General theory of three-dimensional consolidation" *Journal of applied physics* Vol. 12, No. 2, pp. 155-164.
- Bishop, A. W. and Green, G. E. (1965). "The influence of end restraint on the compression strength of a cohesionless soil" *Géotechnique* Vol. 15, No. 3, pp. 243-266.

- Black, D. K. and Lee, K. L. (1973). "Saturation laboratory samples by back pressure" *ASCE* Vol. 99, No. SM1, pp. 75-93.
- Brady, B. H. G. and Brown, E. T. (1985). "Rock Mechanics", George Allen & Unwin Ltd, London, pp. 527.
- Brand, E. W. and Premchitt, J. (1980). "Shape factors of cylindrical piezometers" *Géotechnique* Vol. 30, No. 4, pp. 369-384.
- Bromhead, E. N. (1996). "Interpretation of constant head in situ permeability tests in soil zones" *Géotechnique* Vol. 46, No. 1, pp.133-143
- Broms, B. B. (1984). "Stabilization of soil with lime columns. Design Handbook", 3rd Edition, Lime Column AB, 51.
- Broms, B. B. (1993). Lime stabilization. "Ground Improvement", Moseley, M. P., Maryland, Blackie Academic & Professional, pp. 65-99
- Broms, B. B. (1999). "Keynote lecture: Design of lime, lime/cement and cement columns". *Proceedings Dry Mix Method for Deep Soil Stabilization*, Stockholm, pp. 125-153.
- Broms, B. B. and Boman, P. (1979). "Stabilisation of soil with lime columns" *Ground engineering* Vol. 12, No. 4, pp. 23-32.
- Brown, E. T. and Gonano, L. P. (1974). "Improved compression test technique for soft rock" *Journal of the Geotechnical Engineering Division, ASCE* Vol. 100, No. GT2, pp. 196-199.
- Carlsten, P. and Ekström, J. (1995). "Lime and lime/cement columns, guide at design, installation and control", Swedish geotechnical society, Report 4:95, Linköping, pp. 103.
- Darcy, H. (1856). *Les fontaines publiques de la ville de Dijon*. Paris.
- Edstam, T. (1996). "Erfarenhetsbank för kc-pelare.", Swedish Deep Stabilization, Report No. 1, Linköping, pp. 154.
- Ekström, J. (1994). "Kontroll av kalkcementpelare-slutrapport med redovisning av fältförsök i Ljungskile.", Report B 1994:3, Göteborg.
- Goughnour, R. R. (1983). "Settlement of vertically loaded stone columns in soft ground". *Proceeding 8th European Conference on Soil Mechanics and Foundation Engineering*, Helsinki, pp. 235-240.
- Hansbo, S. (1960). "Consolidation of clay, with special reference to influence of vertical sand drains", Swedish Geotechnical Institute, Report No. 18, Stockholm, pp. 160.
- Hansbo, S. (1981). "Consolidation of fine-grained soils by prefabricated drains.". *Proceedings 10th International Conference on Soil Mechanics and Foundation Engineering*, Stockholm, pp. 12-22.

- Hansbo, S. (1994). "Foundation Engineering", Elsevier Science B.V., Amsterdam, pp. 519.
- Hansbo, S. and Sällfors, G. (1984). Jordmekanik (soil mechanic). "Handboken Bygg: Geoteknik", LiberFörlag, Stockholm, pp. 103-137
- Harremoës, P., Jacobsen, M. H. and Ovesen, K. (1970). "Laerebog i geoteknik. Polyteknisk Forlag. Köpenhamn".
- Hartlén, J. (1974). "Skånska moränlerors hållfasthets- och bärighetsegenskaper", Thesis Ph. D., Geotechnical Department, Chalmers University of Technology, Göteborg.
- Head, K. (1998). "Manual of soil laboratory testing, 3: Effective stress tests", 2nd edition, John Wiley & Sons, Chichester, pp. 428.
- Head, K. H. (1994). "Manual of soil laboratory testing, 2: Permeability, shear strength and compressibility tests", 2nd edition, John Wiley & sons, Inc., New York, pp. 440.
- Hibbitt, K. S. I. (1997). "ABAQUS/ Standard, Theory Manual, User's Manual Volume I, II, III, Post Manual", Ver. 5.7, Rhode Island.
- Hvorslev, M. J. (1951). Time-lag and soil permeability in ground-water observations. Waterways experiments station, US corps of engrs, Vicksburg, Mississippi, Bulletin No. 36.
- Jacobsen, M. H. (1967). "The undrained shear strength of a preconsolidated boulder clay". *Geotechnical conference*, Oslo, pp. 119-122.
- Jacobsen, M. H. (1970). Strength and deformation properties of preconsolidated moraine clays. (Danmarks geotekniska institute) Bull. No. 27, pp. 21-35.
- Kivelö, M. (1994). "Odränerade provbelastningar av kalkcementpelare i fält", Royal Institute of Technology, Report 3002, Stockholm, pp. 62.
- Lahtinen, P. O. and Vepsäläinen, P. E. (1983). "Dimensioning deep-stabilization using the finite element method". *Proceedings 8th European Conference on Soil Mechanics and Foundation Engineering*, Helsinki, pp. 933-936.
- Liedberg, N. S. D., Baker, S., Smekal, A. and Ekström, J. (1996). "Samverkan mellan kalkcementpelare och lera (Interaction of lime/cement columns and clay)", Chalmers University of Technology, Report B1996:1, Göteborg, pp. 107.
- Lo, D. O. K. (1991). "Soil improvment by vertical drains", Thesis Doctoral, Department of Civil Engineering, University of Illinois, Urbana.
- Geo-slope International Ltd., (1994). "Computer program Seep/W for finite element seepage analysis", User's Guide, Ver. 3, Calgary.

- Mattes, N. S. and Poulos, H. G. (1969). "Settlement of single compressible pile" *soils and foundations division, ASCE* Vol. 95, No. SM1, pp. 189-207.
- Mckinley, J. D. (1998). "Coupled consolidation of a solid, infinite cylinder using a Terzaghi formulation" *Computers and Geotechnics* Vol. 23, No. 3, pp. 193-204.
- Nakano, H. and Ito, T. (1983). "Mechanism of Ko-consolidation and its deformation characteristics". *Proceedings 8th European conference on Soil Mechanics and Foundation Engineering*, Helsinki, pp. 389-392.
- Poorooshasb, H. B., Alamgir, M. and Miura, N. (1996,a). "Application of an integro-differential equation to the analysis of geotechnical problems" *Structural Engineering and Mechanics* Vol. 4, No. 3, 227-342.
- Poorooshasb, H. B. and Meyerhof, G. G. (1996). "Consolidation settlement of rafts supported by stone columns" *Geotechnical engineering* Vol. 27, No. 2, pp. 83-92.
- Poorooshasb, H. B. and Meyerhof, G. G. (1997). "Analysis of behaviour of stone column and lime column" *Computers and Geotechnics* Vol. 20, No. 1, pp. 47-70.
- Poorooshasb, H. B., Miura, N. and Alamgir, M. (1996,b). "Refinement of a numerical technique for solution of geotechnical problems". *Proceedings 3rd Asian-Pacific Conference on Computational Mechanics*, Seoul, pp. 2145-2150.
- Poulos, H. G. and Davis, E. H. (1974). "Elastic solution for soil and rock mechanics", John Eiley & Sons, Inc., New York, pp. 411.
- Pramborg, B. and Albertsson, B. (1992). "Udersökning av kalk/cementpelare (Investigation of lime/cement columns)". *Proceedings 11th Nordic Geotechnical Conference, NGM*, Alborg, pp. 149-156.
- Rowe, P. W. and Barden, L. (1964). "Importance of free ends in triaxial testing" *Journal of Soil Mechanics and Foundations Division, ASCE*, Vol. 90, No. SM1, pp. 1-27.
- Steensen-Bach, J. O., Bengtsson, P. E. and Rocgbeck, Y. (1996). "Large scale triaxial tests on samples from lime-cement columns". *Proceedings 12th Nordic Geotechnical Conference, NGM*, Reykjavík, pp. 135-146.
- Tang, X. W. and Onitsuka, K. (1998). "Consolidation of ground with partially penetrated vertical drains" *Geotechnical Engineering* Vol. 29, No. 2, pp. 209-231.

- Terashi, M. and Tanaka, H. (1983). "Settlement analysis for deep mixing method". *Proceedings 8th European Conference on Soil Mechanics and Foundation Engineering*, Helsinki, pp. 955-960.
- Ugural, A. C. and Fenster, S. F. (1995). "Advanced strength and applied elasticity", Prentice-Hall Inc., New Jersey, pp. 570.
- Wallays, M., Delapierre, J. and Poel, J. v. d. (1983). "Load transfer mechanism in soil reinforced by stone or sand columns". *Proceedings 8th European Conference on Soil Mechanics and Foundation Engineering*, Helsinki, pp. 313-317.
- Vermmer, P. A. and Brinkgreve, R. B. J. (1998). "PLAXIS, Finite Element code for Soil and Rock Analyses", Ver. 7.0, Balkema (manual to computer code), Rotterdam.
- Wilkinson, W. B. (1968). "Constant head in situ permeability tests in clay strata" *Géotechnique* Vol. 18, No. 2, pp. 172-194.
- Yoshikuni, H. and Nakanodo, H. (1974). "Consolidation of soils by vertical drain wells with finite permeability" *Soils and foundation* Vol. 14, No. 2, pp. 35-46.
- Yoshikuni, H. and Nakanodo, H. (1975). "Consolidation of a clay cylinder with external radial drainage" *Soils and foundation* Vol. 15, No. 1, pp. 35-46.
- Åhnberg, H. (1996). "Stress Dependent Parameters of cement stabilised soils". *Proceedings 2nd International Conference On Ground Improvement Geosystem*, IS-Tokyo, pp. 387-392.
- Åhnberg, H., Johansson, S.-E., Retelius, A., Ljungkrantz, C., Holmqvist, L. and Holm, G. (1995). "Cement och kalk för djupstabilisering av jord. En kemisk-fysisk studie av stabiliseringseffekter. (Stabilising of soil using cement and lime. A study of soil improvements effects)", Swedish Geotechnical Institute, Report 48, Linköping, pp. 213.

References

A ANALYTICAL ELASTIC MODEL OF VERTICALLY LOADED LIME/CEMENT STABILIZED SOIL

In this unit cell model, the treated soil is modeled as a solid cylinder while the untreated soil is considered as a thick cylinder surrounding the column.

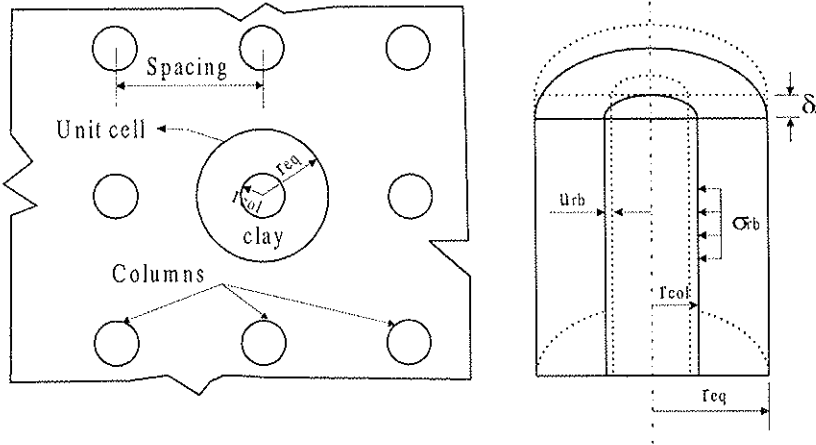


Figure A-1 The lime/cement column stabilized system and the unit cell model.

From Figure A-1, the radius of the unit cell system, r_{eq} , is equal to about 0.564 times the column spacing for the square column pattern. The untreated soil is considered as a thick cylinder since the thickness of this cylinder, $r_{eq} - r_{col}$, is more than 10 % of the column radius, r_{col} , which is the condition for classifying the treated soil as a thick cylinder, Ugural, A.C. and Fenster, S.F. (1995). Thus, the stress variation with radius can no longer be disregarded.

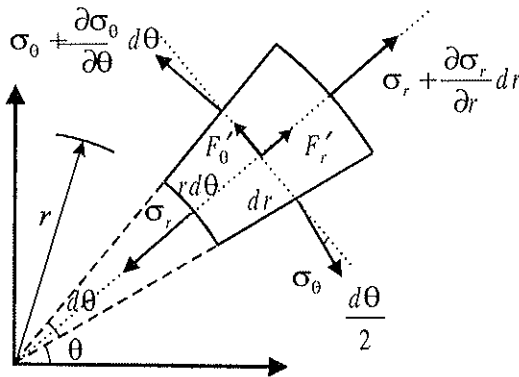


Figure A-2 Stress element in polar coordinates.

A.1 GENERAL

The polar equation of equilibrium in Figure A-2 is

$$\frac{d\sigma_r}{dr} + \frac{\sigma_r - \sigma_\theta}{r} + F_r = 0 \quad (\text{A.1})$$

F_r radial force per unit volume

When $F_r = 0$, the above equation can be written as

$$\frac{d\sigma_r}{dr} + \frac{\sigma_r - \sigma_\theta}{r} = 0 \quad (\text{A.2})$$

Assuming that plane sections remain plane, then the longitudinal strain is constant Ugural, A.C. and Fenster, S.F. (1995), or

$$\sigma_r + \sigma_\theta = A = \text{constant} \quad (\text{A.3})$$

The above equation can be rewritten as

$$\sigma_\theta = A - \sigma_r \quad (\text{A.4})$$

Substituting equation (A.3) into equation (A.2) one obtains

$$\frac{d\sigma_r}{dr} + \frac{2 \cdot \sigma_r}{r} = \frac{A}{r} \quad (\text{A.5})$$

The solution of the differential equation (A.5) is

$$\sigma_r = \frac{B}{r^2} + \frac{A}{2} \quad (\text{A.6})$$

B is an integration constant.

Substituting equation (A.6) into equation (A.4) to define σ_θ in terms of the constants (A) and (B), gives

$$\sigma_\theta = -\frac{B}{r^2} + \frac{A}{2} \quad (\text{A.7})$$

A.2 UNTREATED SOIL

Using the geotechnical sign convention, where the negative sign is used for tension and the positive sign for compression, then

$$\varepsilon_{rsoil} = -\frac{dw_{rsoil}}{dr} \quad (A.8)$$

$$\varepsilon_{\theta soil} = -\frac{w_{rsoil}}{r} \quad (A.9)$$

w_{rsoil} radial deformation of the untreated soil

Using Hook's law the vertical stress in the untreated soil can be written as

$$\sigma_{zsoil} = 2 \cdot G_{soil} \cdot \varepsilon_{zsoil} + \lambda_{soil} \cdot (\varepsilon_{zsoil} + \varepsilon_{rsoil} + \varepsilon_{\theta soil}) \quad (A.10)$$

$$\sigma_{zsoil} + \sigma_{rsoil} + \sigma_{\theta soil} = \frac{E_{soil}}{1 - 2 \cdot \nu_{soil}} \cdot (\varepsilon_{zsoil} + \varepsilon_{rsoil} + \varepsilon_{\theta soil}) \quad (A.11)$$

$$G_{soil} = \frac{E_{soil}}{2 \cdot (1 + \nu_{soil})}$$

$$\lambda_{soil} = \frac{\nu_{soil} \cdot E_{soil}}{(1 + \nu_{soil}) \cdot (1 - 2 \cdot \nu_{soil})}$$

E_{soil} Young's modulus of the untreated soil

ν_{soil} Poisson's ratio of the untreated soil

Substituting equations (A.3), (A.8), (A.9) and (A.10) into equation (A.11) we get

$$\frac{dw_{rsoil}}{dr} + \frac{w_{rsoil}}{r} = 2 \cdot \varepsilon_{zsoil} \cdot \nu_{soil} - \frac{\nu_{soil}}{\lambda_{soil}} \cdot A \quad (A.12)$$

The solution of the differential equation (A.12) is:

$$u_{rsoil} = \varepsilon_{zsoil} \cdot \nu_{soil} \cdot r - \frac{\nu_{soil}}{2 \cdot \lambda_{soil}} \cdot r \cdot A + \frac{C}{r} \quad (A.13)$$

C integration constant

By the following derivation it will be possible to relate the new integration constant (C) to the constant (B) presented in equations (A.6) and (A.7).

$$\sigma_{rsoil} - \sigma_{\theta soil} = 2 \cdot G_{soil} \cdot (\varepsilon_{rsoil} - \varepsilon_{\theta soil}) = 2 \cdot G_{soil} \cdot \left(\frac{w_{rsoil}}{r} - \frac{dw_{rsoil}}{dr} \right)$$

Since $\sigma_{rsoil} - \sigma_{\theta soil} = \frac{2 \cdot B}{r^2}$ then

$$\frac{B}{r^2} = G_{soil} \cdot \left(\frac{w_{rsoil}}{r} - \frac{dw_{rsoil}}{dr} \right) \quad (A.14)$$

Now, by using equation (A.13), the following equations can be written

$$\frac{dw_{rsoil}}{dr} = \varepsilon_{zsoil} \cdot v_{soil} - \frac{v_{soil}}{2 \cdot \lambda_{soil}} \cdot A - \frac{C}{r^2}$$

$$\frac{u_{rsoil}}{r} = \varepsilon_{zsoil} \cdot v_{soil} - \frac{v_{soil}}{2 \cdot \lambda_{soil}} \cdot A + \frac{C}{r^2}$$

Substituting the above two equations into equation (A.14) we get

$$C = \frac{B}{2 \cdot G_{soil}}$$

Equation (A.13) can now be written as:

$$w_{rsoil} = \varepsilon_{zsoil} \cdot v_{soil} \cdot r - \frac{v_{soil}}{2 \cdot \lambda_{soil}} \cdot r \cdot A + \frac{B}{2 \cdot G_{soil} \cdot r} \quad (A.15)$$

Since $\varepsilon_{\theta soil} = -\frac{w_{rsoil}}{r}$ then

$$\varepsilon_{\theta soil} = \frac{v_{soil}}{2 \cdot \lambda_{soil}} \cdot A - \frac{B}{2 \cdot G_{soil} \cdot r^2} - \varepsilon_{zsoil} \cdot v_{soil} \quad (A.16)$$

The constants A and B are to be determined based on consideration of the conditions pertaining to the inner and outer surfaces.

At $r = r_{eq}$ $\varepsilon_{\theta soil} = 0$

$$B = \frac{G_{soil} \cdot v_{soil}}{\lambda_{soil}} \cdot r_{eq}^2 \cdot A - 2 \cdot G_{soil} \cdot v_{soil} \cdot r_{eq}^2 \cdot \varepsilon_{zsoil} \quad (A.17)$$

At $r = r_{col}$ $\varepsilon_{\theta soil} = \varepsilon_{bou}$

$$B = r_{col}^2 \cdot G_{soil} \left(\frac{v_{soil}}{\lambda_{soil}} \cdot A - 2 \cdot v_{soil} \cdot \varepsilon_{zsoil} - 2 \cdot \varepsilon_{bou} \right) \quad (A.18)$$

Solving equations (A.17) and (A.18) for constants (A) and (B) we obtain

$$A = -\frac{2 \cdot a_s}{1 - a_s} \cdot \frac{\lambda_{soil}}{v_{soil}} \cdot \varepsilon_{bou} + 2 \cdot \lambda_{soil} \cdot \varepsilon_{zsoil} \quad (A.19)$$

$$B = -\frac{r_{col}^2}{1 - a_s} \cdot 2 \cdot G_{soil} \cdot \varepsilon_{bou} \quad (A.20)$$

Where

a_s ratio of the area of the treated soil to the area of the unit cell

σ_{zsoil} can be written in term of ε_{bou} and ε_{zsoil} as

$$\sigma_{zsoil} = M_{soil} \cdot \varepsilon_{zsoil} - 2 \cdot \frac{a_s}{1 - a_s} \cdot \lambda_{soil} \cdot \varepsilon_{bou} \quad (A.21)$$

A.3 TREATED SOIL

The treated soil is considered as a solid cylinder, and the radial and the tangential stresses are equal and constant at any distance from the column center. The tangential strain at the boundary was previously defined as ε_{bou} , and this symbol will be used in the treated soil equations.

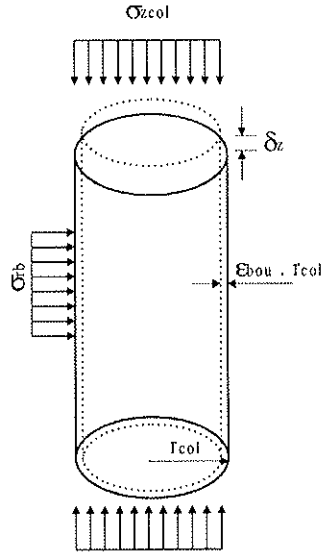


Figure A-3 Stresses acting on the treated soil.

The vertical and the radial stresses in the treated soil will be derived as

$$\sigma_{zcol} = M_{col} \cdot \varepsilon_{zcol} + 2 \cdot \lambda_{col} \cdot \varepsilon_{bou} \quad (A.22)$$

The radial or tangential stress at the boundary between the treated and untreated soil will be denoted as σ_{rb} .

$$\sigma_{rb} = \lambda_{col} \cdot \varepsilon_{zcol} + 2 \cdot (G_{col} + \lambda_{col}) \cdot \varepsilon_{bou} \quad (A.23)$$

A.4 COMPOSED

Using equation (A.6), the radial stress at the same boundary can be written as

$$\sigma_{rb} = -\frac{2}{1-a_s} \cdot G_{soil} \cdot \varepsilon_{bou} - \frac{a_s}{1-a_s} \cdot \frac{\lambda_{soil}}{v_{soil}} \cdot \varepsilon_{bou} + \lambda_{soil} \cdot \varepsilon_{zsoil} \quad (A.24)$$

As was assumed before, the plane section remains plane during the course of settlement. This means that the vertical strains in both treated and untreated soil are equal. With this in mind, equations (A.23) and (A.24) can be solved for ε_{bou} and ε_z .

$$\varepsilon_{bou} = F_{z0} \cdot \varepsilon_z \quad (A.25)$$

$$F_{z0} = -\frac{\lambda_{col} - \lambda_{soil}}{2 \cdot (\lambda_{col} + G_{col}) + \frac{1}{1-a_s} \cdot \left(2 \cdot G_{soil} + \frac{a_s \cdot \lambda_{soil}}{v_{soil}} \right)} \quad (1.26)$$

Finally, the force equilibrium in the vertical direction requires that:

$$\sigma_v = a_s \cdot \sigma_{zcol} + (1-a_s) \cdot \sigma_{zsoil} \quad (A.27)$$

σ_v vertical applied stress

The two equations (A.21) and (A.22) can be rewritten in another form as:

$$\sigma_{zcol} = (M_{col} + 2 \cdot \lambda_{col} \cdot F_{z0}) \cdot \varepsilon_z \quad (A.28)$$

$$\sigma_{zsoil} = \left(M_{soil} - 2 \cdot \frac{a_s}{1-a_s} \cdot \lambda_{soil} \cdot F_{z0} \right) \cdot \varepsilon_z \quad (A.29)$$

The last two equations together with equation (A.27) will make it possible to evaluate the vertical strain as:

$$\varepsilon_z = \frac{\sigma_v}{a_s \cdot \sigma_{zcol} + (1-a_s) \cdot \sigma_{zsoil}} \quad (A.30)$$

Or, in terms of the elastic deformation and geometrical parameters of the treated and untreated soil, the equation becomes

$$\varepsilon_z = \frac{\sigma_v}{a_s \cdot (M_{col} + 2 \cdot \lambda_{col} \cdot F_{z0}) + (1-a_s) \cdot (M_{soil} - 2 \cdot \frac{a_s}{1-a_s} \cdot \lambda_{soil} \cdot F_{z0})}$$

B FILED TESTS

B.1 LOAD TEST

B.1.1 The Varberg test site

B.1.1.1 Numerical calculations

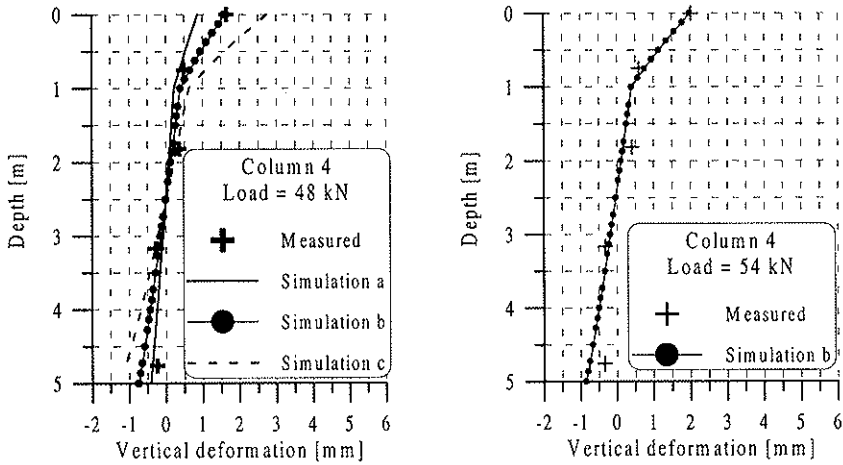


Figure B.1 Results from numerical simulations on column 4 at 48 kN and 54 kN applied load.

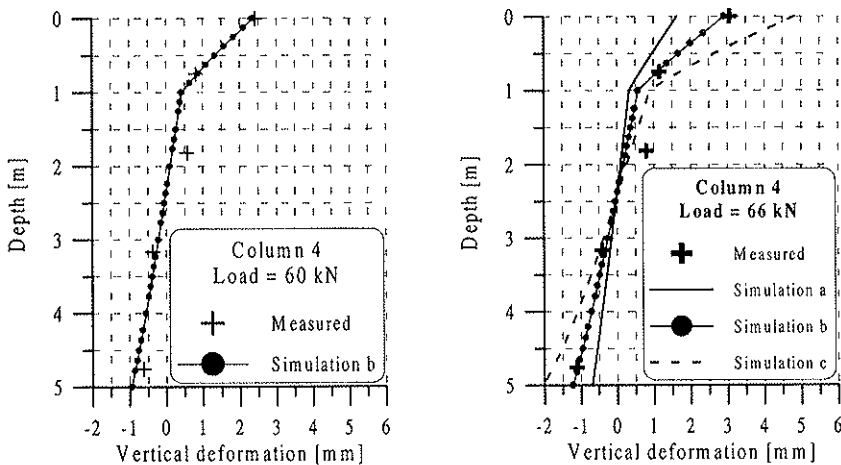


Figure B.2 Results from numerical simulations on column 4 at 60 kN and 66 kN applied load.

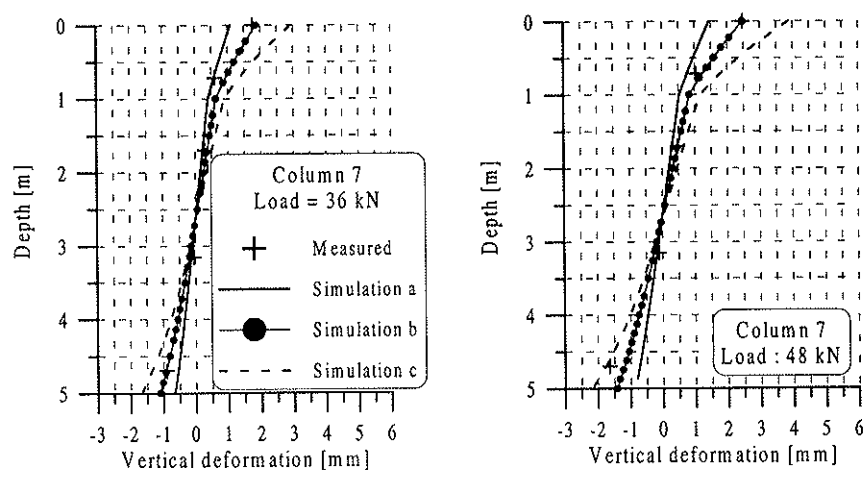


Figure B.3 Results from numerical simulations on column 7 at 36 kN and 48 kN applied load.

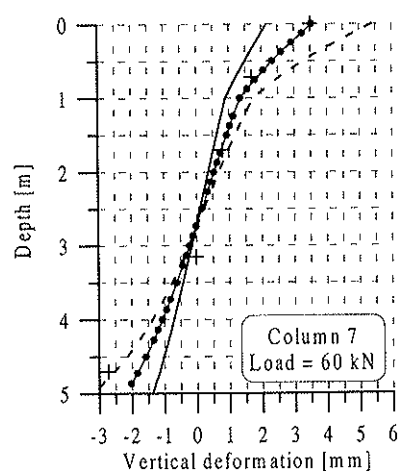


Figure B.4 Results from numerical simulations on column 7 at 60 kN applied load.

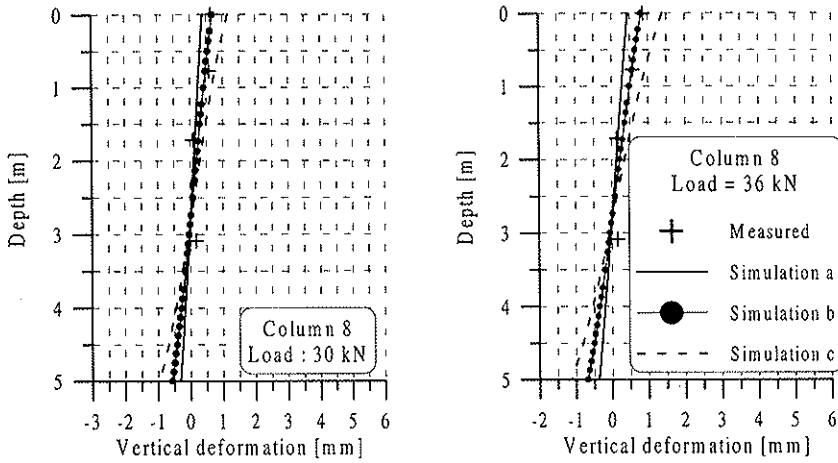


Figure B.5 Results from numerical simulations on column 8 at 30 kN and 36 kN applied load.

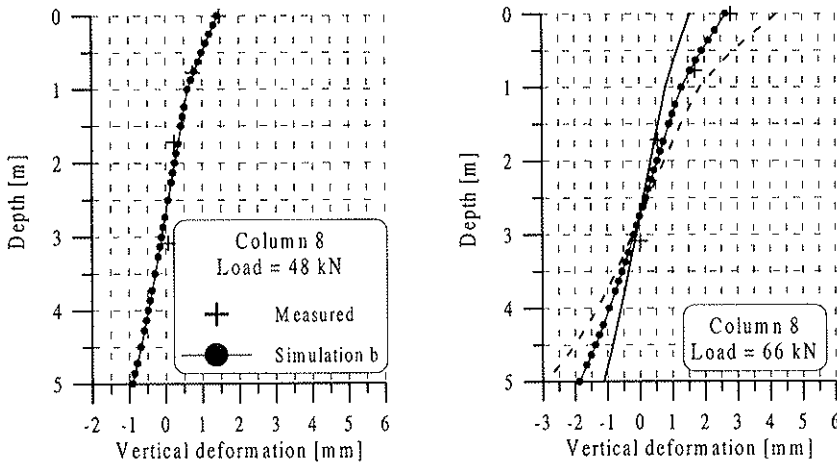


Figure B.6 Results from numerical simulations on column 8 at 48 kN and 66 kN applied load.

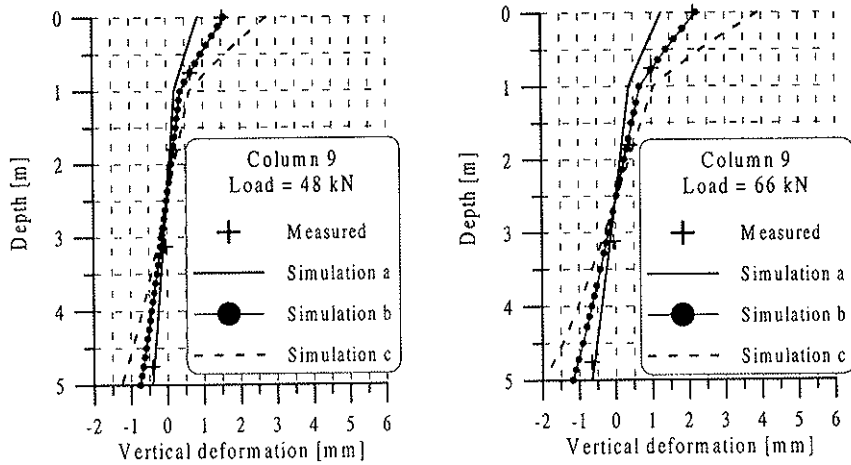


Figure B.7 Results from numerical simulations on column 9 at 48 kN and 66 kN applied load.

B.1.2 The LÖftaån test site

B.1.2.1 Test results

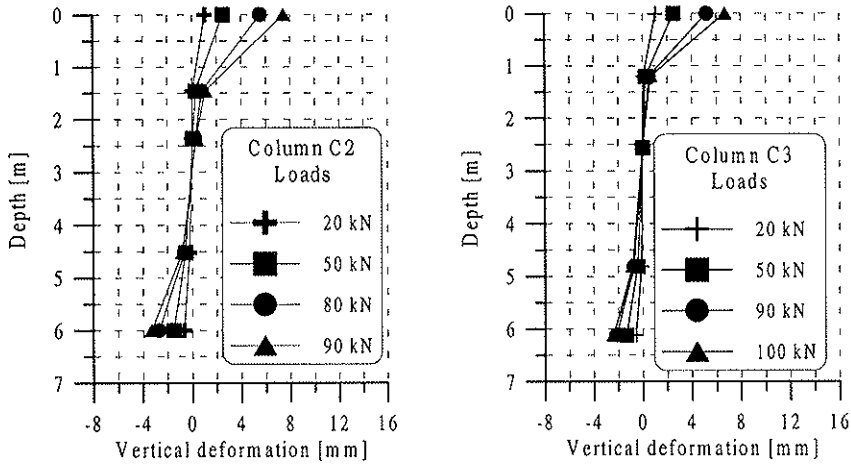


Figure B.8 Some selected load test results at the LÖftaån test site for columns C2 and C3.

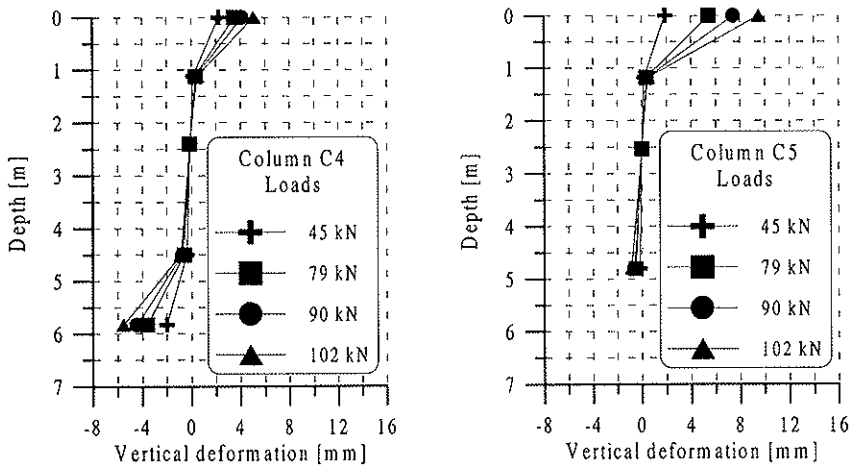


Figure B.9 Some selected load test results at the LÖftaån test site for columns C4 and C5.

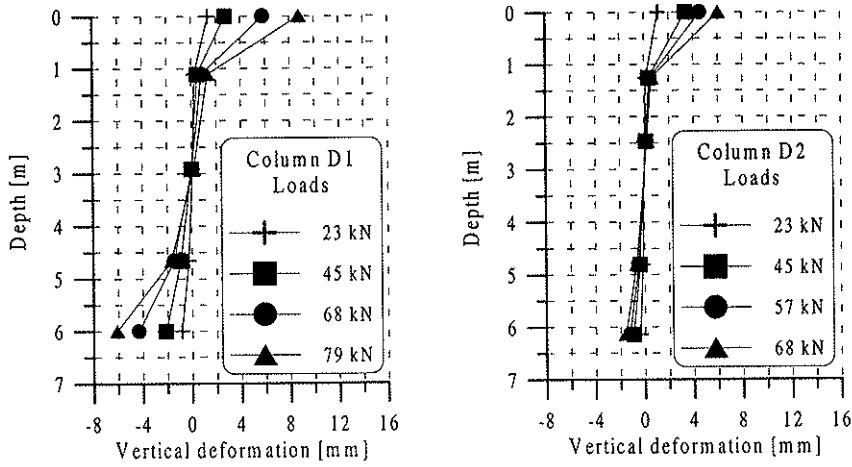


Figure B.10 Some selected load test results at the LÖftaån test site for columns D1 and D2.

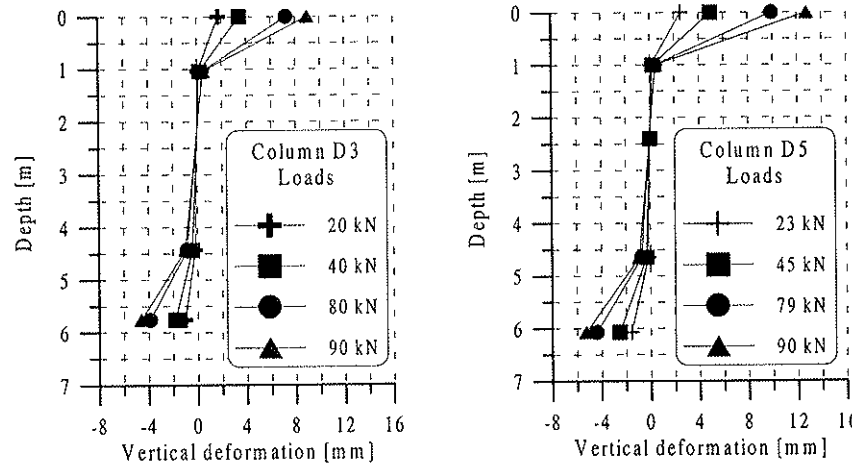
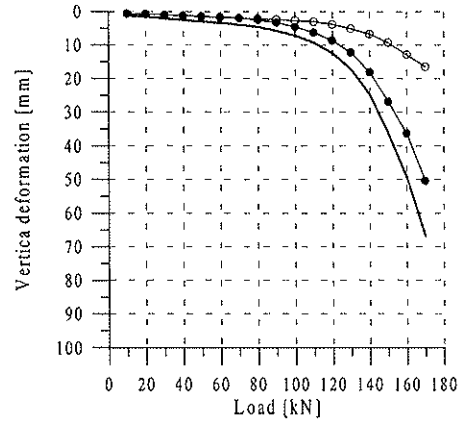
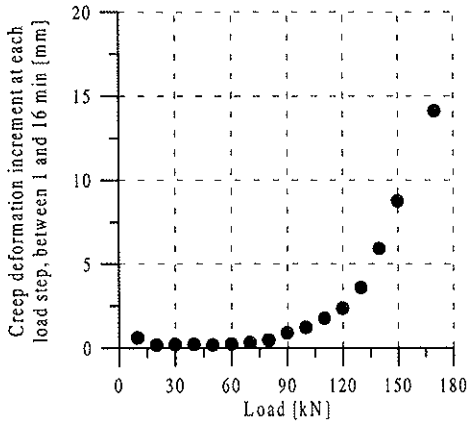
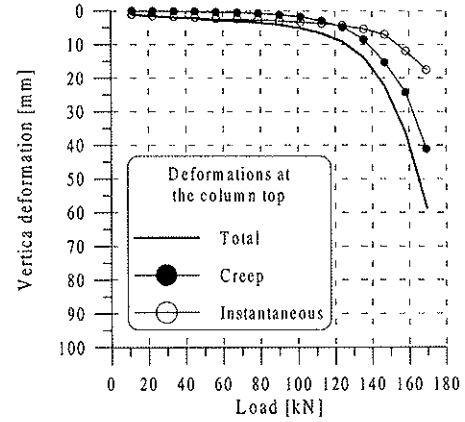
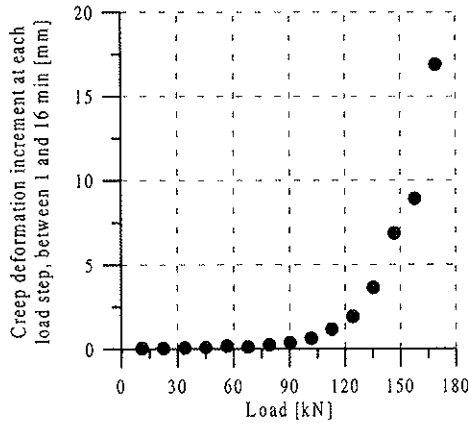


Figure B.11 Some selected load test results at the LÖftaån test site for columns D3 and D5.

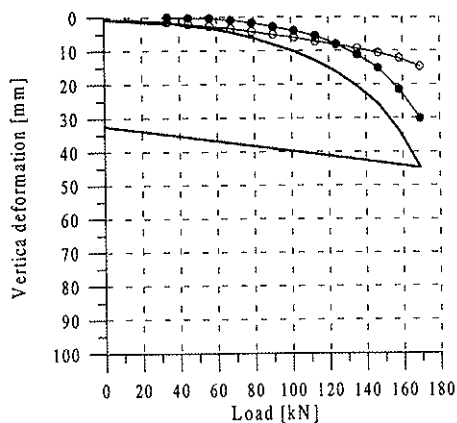
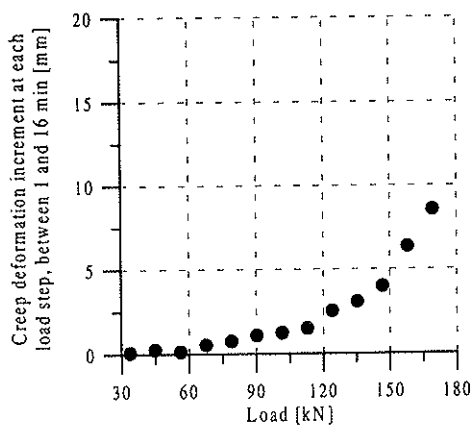


Column C3

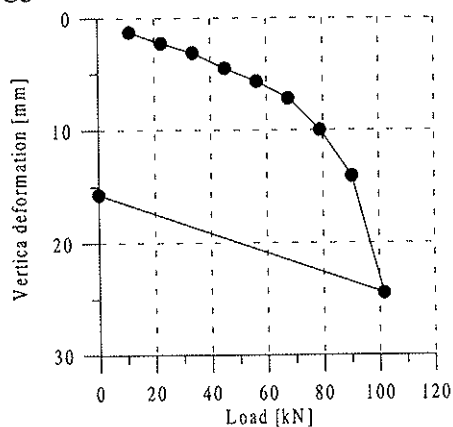
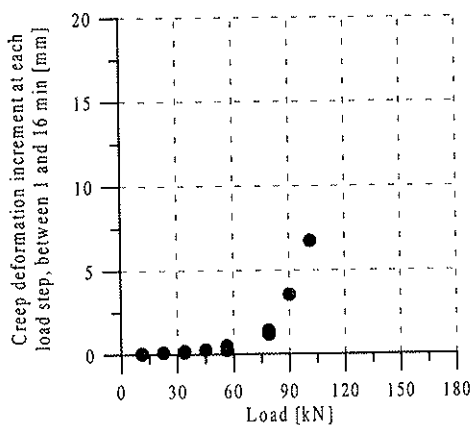


Column C4

Figure B.12 Deformation at the top of columns C3 and C4.



Column C5



Column D2

Figure B.13 Deformation at the top of columns C5 and D2.

B.1.2.2 Numerical results

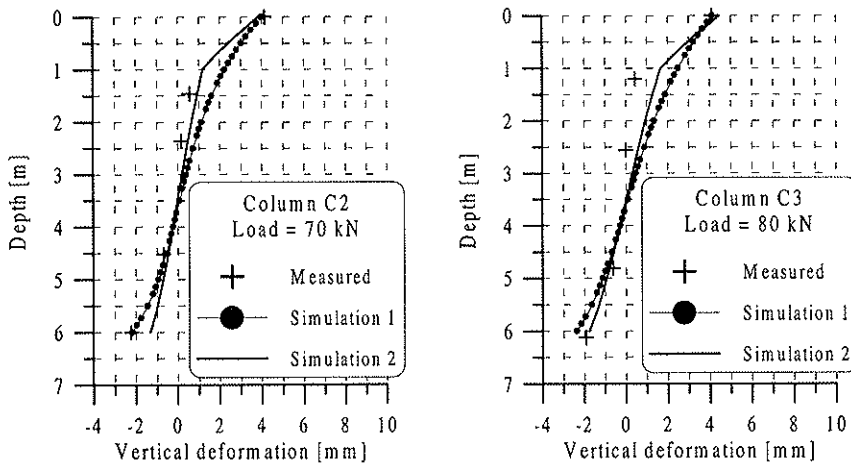


Figure B.14 Results from numerical simulations on columns C2 and C3 at the Löftaån test site.

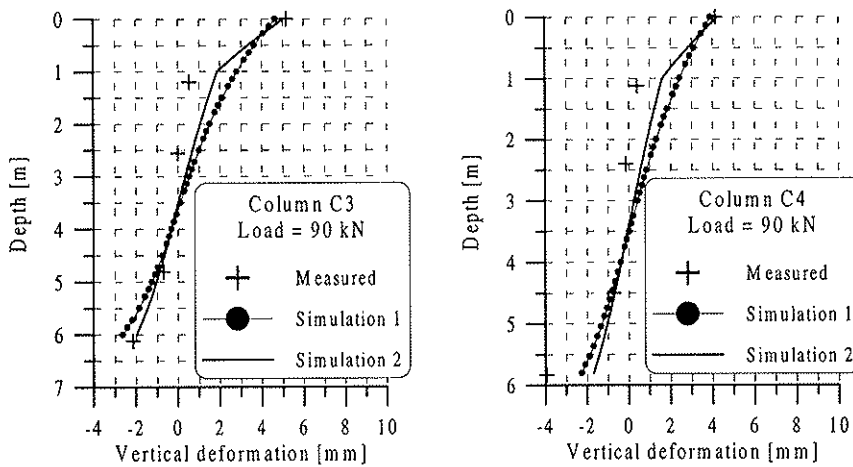


Figure B.15 Results from numerical simulations on columns C3 and C4 at the Löftaån test site.

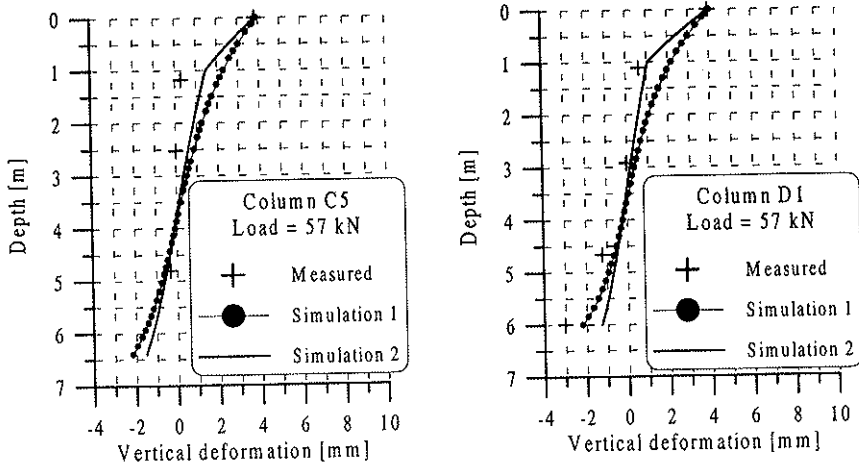


Figure B.16 Results from numerical simulations on columns C5 and D1 at the L fta n test site.

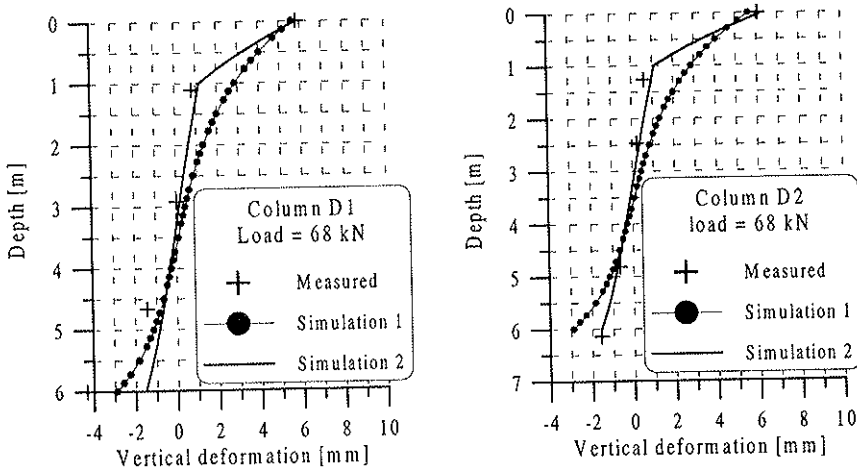


Figure B.17 Results from numerical simulations on columns D1 and D2 at the L fta n test site.

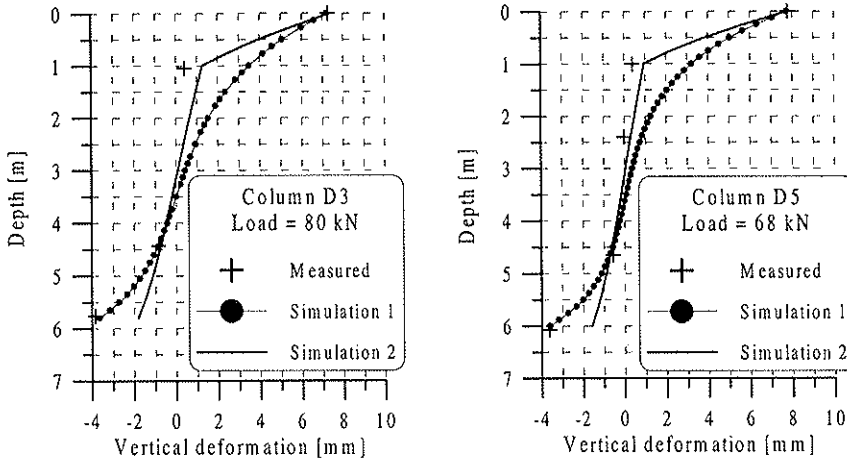


Figure B.18 Results from numerical simulations on columns D3 and D5 at the Löftaån test site.

B.2 HYDRAULIC CONDUCTIVITY TEST

B.2.1 Finite difference solution for the three-dimensional steady state flow

The solution presented here is only applicable when the permeability of the lime/cement column is much higher than that of the original soil so that no flow will occur from the column to the surrounding soil.

Equation (B.1) is the general form for steady state flow.

$$\frac{\partial}{\partial x} \left(K_x \cdot \frac{\partial h}{\partial x} \right) + \frac{\partial}{\partial y} \left(K_y \cdot \frac{\partial h}{\partial y} \right) + \frac{\partial}{\partial z} \left(K_z \cdot \frac{\partial h}{\partial z} \right) = 0 \quad (\text{B.1})$$

If the hydraulic conductivity in the three directions is equal, then equation (B.1) can be written as

$$\frac{\partial^2 h}{\partial x^2} + \frac{\partial^2 h}{\partial y^2} + \frac{\partial^2 h}{\partial z^2} = 0 \quad (\text{B.2})$$

For polar coordinate system the above equation becomes

$$\left(\frac{\partial^2 h}{\partial r^2} + \frac{1}{r} \cdot \frac{\partial h}{\partial r} \right) + \frac{\partial^2 h}{\partial z^2} = 0 \quad (\text{B.2})$$

Using Taylor expansion, the terms in the above equation can be expressed in finite difference form as

$$\frac{\partial^2 h}{\partial r^2} = \frac{h_{i,j+1} - 2 \cdot h_{i,j} + h_{i,j-1}}{\Delta r^2} \quad (\text{B.3})$$

$$\frac{\partial h}{\partial r} = \frac{h_{i,j+1} - h_{i,j-1}}{2\Delta r} \quad (\text{B.4})$$

$$\frac{\partial^2 h}{\partial z^2} = \frac{h_{i+1,j} - 2 \cdot h_{i,j} + h_{i-1,j}}{\Delta z^2} \quad (\text{B.5})$$

where

Δr Distance increment in the r-direction
 Δz Distance increment in the z-direction

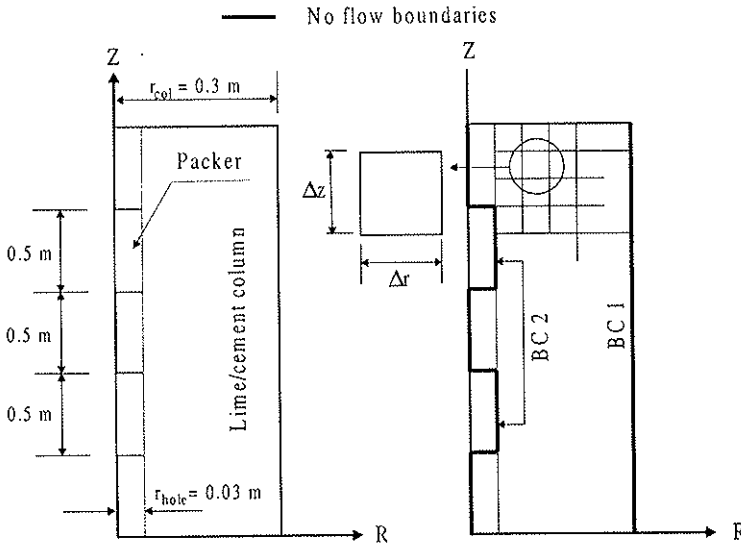


Figure B.19 Geometry and boundary conditions of the model.

Substituting equations (B.3), (B.4) and (B.5) into equation (B.2) the finite different solution of $h_{i,j}$ is written as

$$h_{i,j} = \frac{(\Delta r^2 \cdot \Delta z^2)}{2 \cdot (\Delta r^2 + \Delta z^2)} \cdot \left[\frac{h_{i,j+1} + h_{i,j-1}}{\Delta r^2} + \frac{1}{r_{i,j}} \cdot \frac{h_{i,j+1} - h_{i,j-1}}{2 \cdot \Delta r} + \frac{h_{i+1,j} + h_{i-1,j}}{\Delta z^2} \right] \quad (\text{B.6})$$

The above equation together with the following boundary conditions can be solved in a spreadsheet program

BC1

$$\frac{\partial h}{\partial r} = 0 \Rightarrow h_{i,j+1} = h_{i,j-1}$$

Substituting the above condition in equation (B.6) we get

$$h_{i,j} = \frac{(\Delta r^2 \cdot \Delta z^2)}{2 \cdot (\Delta r^2 + \Delta z^2)} \cdot \left[\frac{2 \cdot h_{i,j-1}}{\Delta r^2} + \frac{h_{i+1,j} + h_{i-1,j}}{\Delta z^2} \right]$$

BC2

$$\frac{\partial h}{\partial r} = 0 \Rightarrow h_{i,j-1} = h_{i,j+1}$$

Substituting the new condition in equation (B.6) we get

$$h_{i,j} = \frac{(\Delta r^2 \cdot \Delta z^2)}{2 \cdot (\Delta r^2 + \Delta z^2)} \cdot \left[\frac{2 \cdot h_{i,j+1}}{\Delta r^2} + \frac{h_{i+1,j} + h_{i-1,j}}{\Delta z^2} \right]$$

C LABORATORY TESTS

C.1 LABORATORY TESTS ON STANDARD SIZE SAMPLES

C.1.1 The Fjärås test site results

C.1.1.1 Hydraulic conductivity test

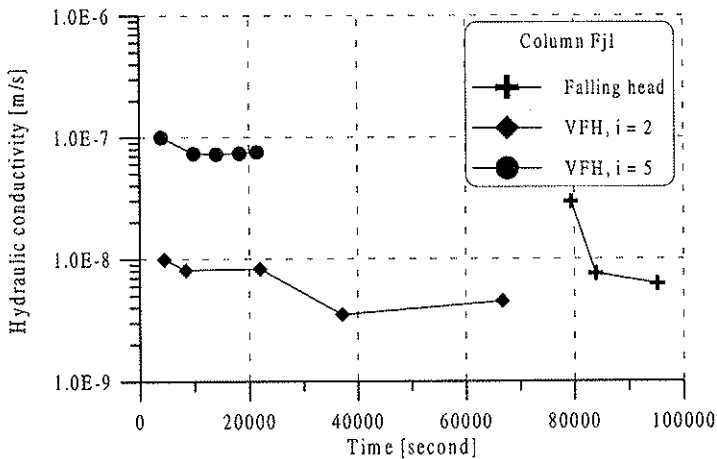


Figure C.1 Laboratory hydraulic conductivity test results for sample Fj1.

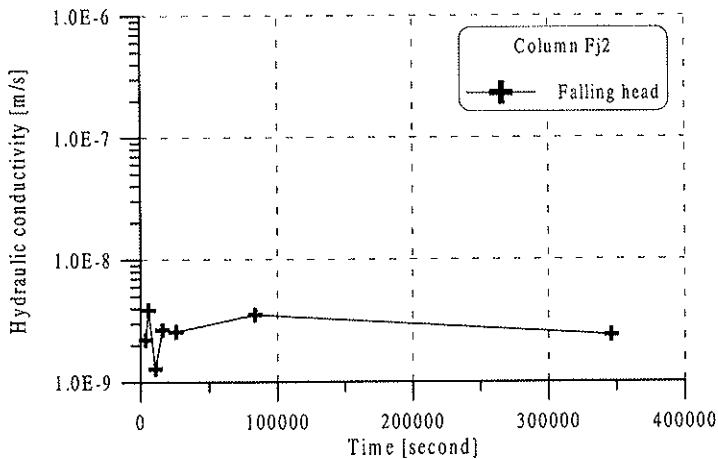


Figure C.2 Laboratory hydraulic conductivity test result for sample Fj2.

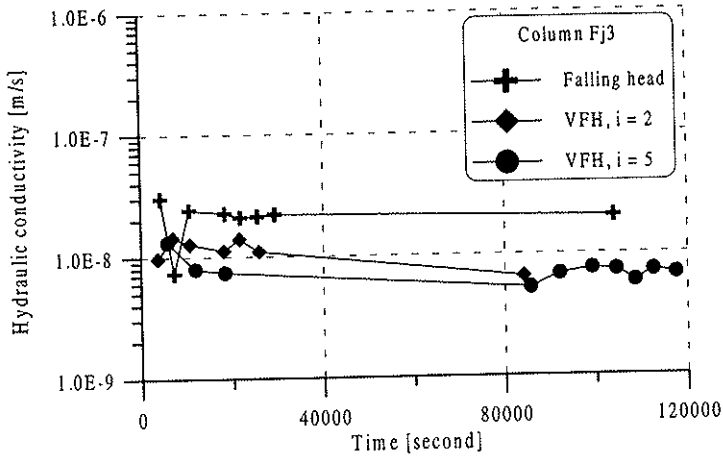


Figure C.3 Laboratory hydraulic conductivity test results for sample Fj3.

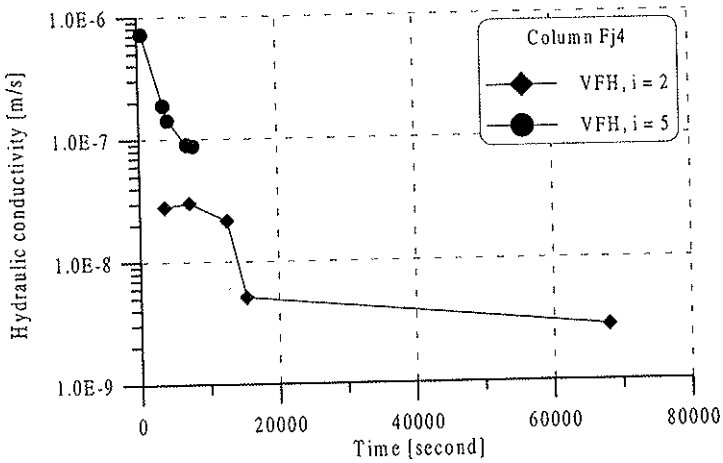


Figure C.4 Laboratory hydraulic conductivity test results for sample Fj4.

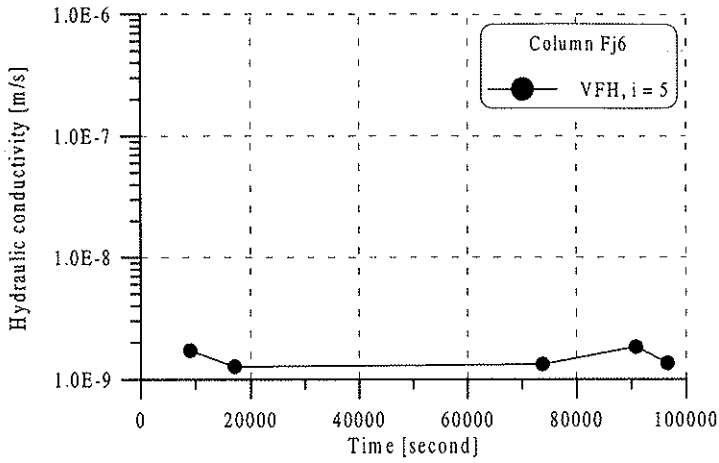


Figure C.5 Laboratory hydraulic conductivity test result for sample Fj6.

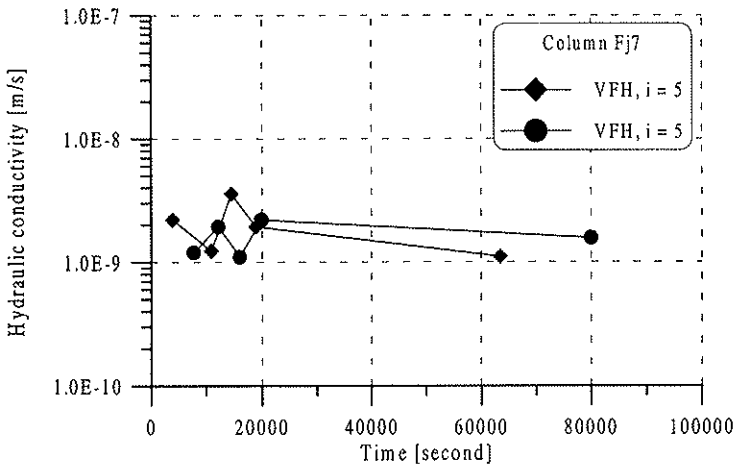


Figure C.6 Laboratory hydraulic conductivity test results for sample Fj7.

C.1.1.2 The Löstaan test site results

C.1.1.3 Hydraulic conductivity test

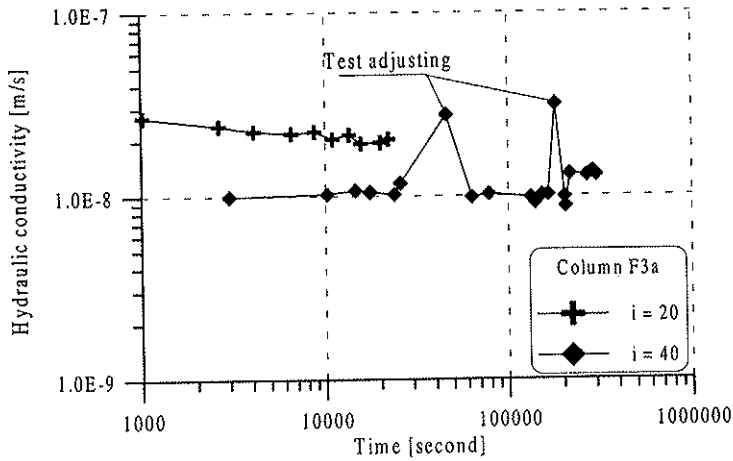


Figure C.7 Laboratory hydraulic conductivity test results for sample F3a, taken from mixed-in-place columns.

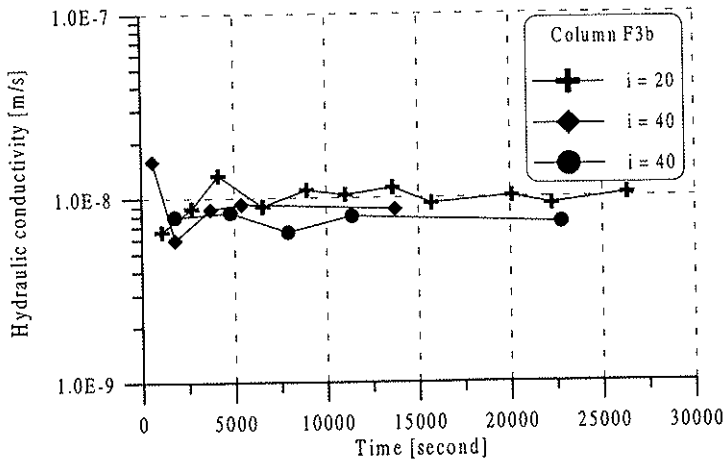


Figure C.8 Laboratory hydraulic conductivity test results for sample F3b, taken from mixed-in-place columns.

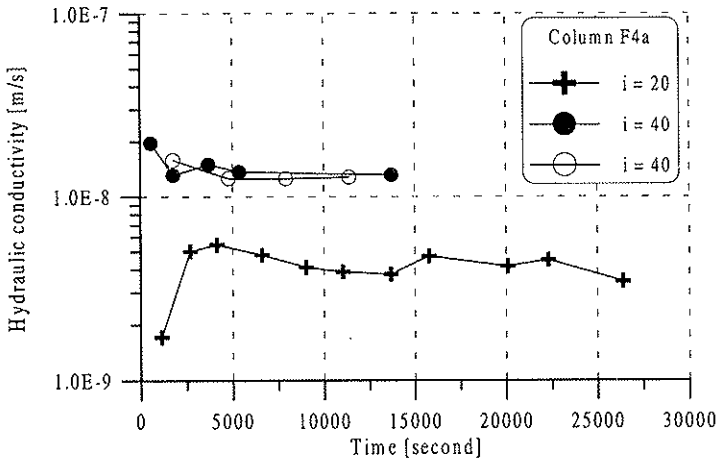


Figure C.9 Laboratory hydraulic conductivity test results for sample F4a, taken from mixed-in-place columns.

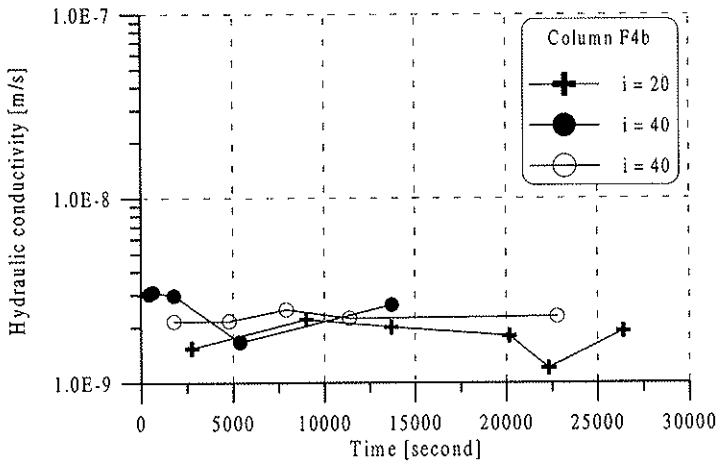


Figure C.10 Laboratory hydraulic conductivity test results for sample F4b, taken from mixed-in-place columns.

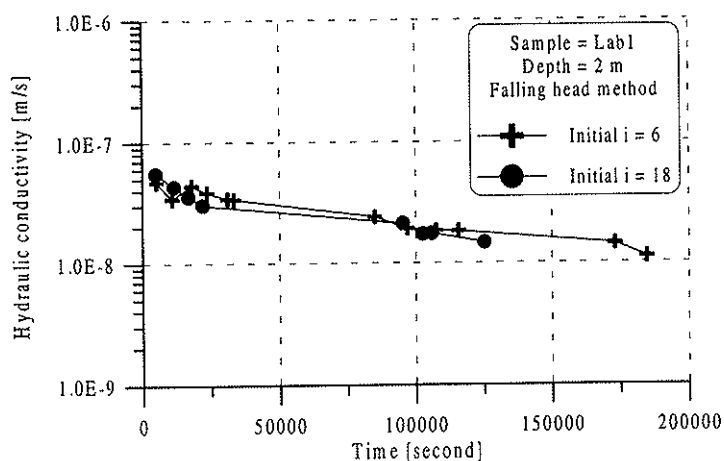


Figure C.11 Hydraulic conductivity test results for laboratory prepared sample, Lab1.

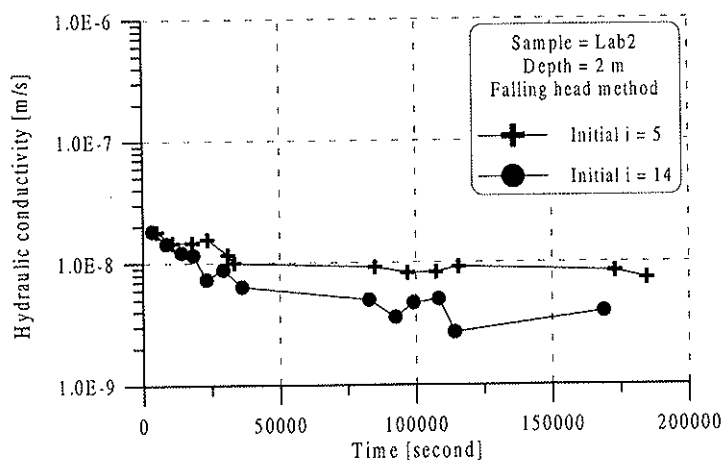


Figure C.12 Hydraulic conductivity test results for laboratory prepared sample, Lab2.

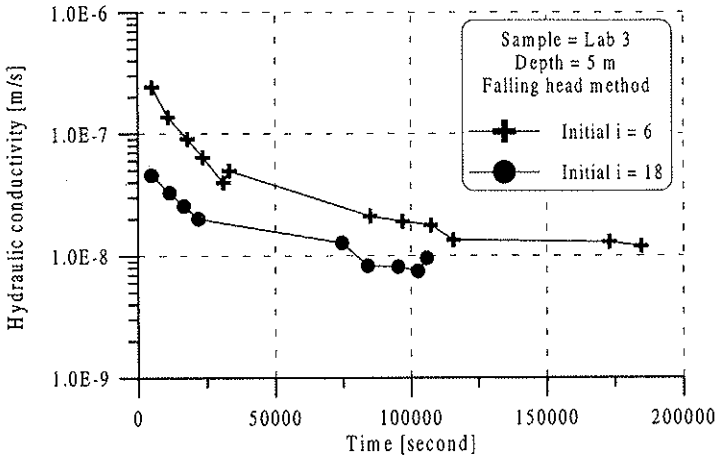


Figure C.13 Hydraulic conductivity test results for laboratory prepared sample, Lab3.

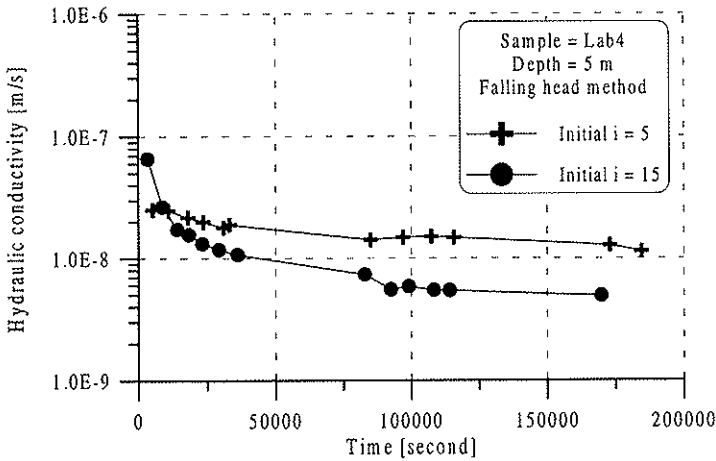


Figure C.14 Hydraulic conductivity test results for laboratory prepared sample, Lab4.

Publikationer utgivna av Svensk Djupstabilisering

Arbetsrapport

1. **Arlandabanan, Norra Böjen.** 1998
Sättningar hos järnvägsbank på kc-pelare.
Ulf Stjerngren, Jacobson & Widmark
2. **KC-förstärkning för schakt inom spont, Filipstad Brygge, Oslo.** 1998
Phung Doc Long, Stabilator AB & Håkan Bredenberg, Stabilator AB
3. **Inblandningsmekanismer vid djupstabilisering med kalk-,** 1998
kalk/cementpelare och cementpelare
Stefan Larsson, Tyréns
4. **Undersökning av KC-pelare med avseende på dess "homogenitet".** 1998
Roland Tränk, SGI
5. **Bestämning av egenskaper i cellstabiliserad torv.** 1998
Nenad Jelusic, Vägverket Region Mitt, Torbjörn Edstam, SGI
& Yvonne Rogbeck, SGI
6. **Rörelser och porttryck vid kalkpelarinstallation.** 1998
Redovisning av mätresultat.
Åke Johansson, SGI
7. **Masstabilisering av väg 590, Askersund.** 1998
Yvonne Rogbeck, SGI
8. **KC-pelarförstärkning av instabil slänt. E4, delen Nyland - Ullånger,** 1998
Västernorrlands län. Åtgärder och mätningar.
Leiv Viberg, SGI, Bertil Eriksson, Vägverket Produktion Mitt
& Stefan Johansson, Vägverket Produktion Mitt
9. **Grunnforsterkning med kalksementpælar.** 1999
Stein Christensen, Arnstein Watn, Steinar Nordal, Arnfinn Emdal,
Torbjørn Lund & Thomas Kristiansen
10. **Dimensioneringsvägledning för djupstabilisering.** 1999
Översättning av Finska Vägverkets klarlägganden 18/1997.
ISSN 0788-3722, ISBN 951-726-344-9
11. **Historik och svenska erfarenheter av kalkstabilisering** 1999
av vägterrasser
Stefan Gustafsson, Scandiaconsult
12. **Undersökning i fält av stabiliseringseffekt i organisk jord och lera** 2000
Tobias Hansson, Hercules Grundläggning AB, Yvonne Rogbeck, SGI,
& Leif Säfström, Vägverket Region Mälardalen
13. **Utvärdering av verksamheten inom Svensk Djupstabilisering** 2000
Vetenskaplig uppläggning. Måluppfyllelse av FoU-plan

- | | | |
|-----|---|------|
| 14. | Stabilisering av torv i laboratoriemiljö
– utveckling av referensmetod
Fredrik Larsson & Stefan Mårtensson, LTU | 2000 |
| 15. | Djupstabilisering med kalk-cementpelare – Provfält
Lars O Johansson, SGI | 2000 |
| 16. | Laboratorieunblandning för stabilisering av lera – Referensmetod
Torbjörn Edstam, SGI | 2000 |
| 17. | Kalkcementpelarförstärkning för bro – Funktionsuppföljning
Västkustbanan, delen Sätinge – Lekarekulle.
Bro över väg N359U (km 35/603)
Marius Tremblay | 2000 |

Rapport

- | | | |
|----|---|------|
| 1. | Erfarenhetsbank för kalk-cementpelare.
Torbjörn Edstam | 1997 |
| 2. | Kalktypens inverkan på stabiliseringsresultatet. En förstudie.
Helen Åhnberg & Håkan Pihl | 1997 |
| 3. | Stabilisering av organisk jord med
cement- och puzzolanreaktioner
Karin Axelsson, Sven-Erik Johansson & Ronny Andersson | 2000 |
| 4. | Provbänk på kalk/cementpelarförstärkt gyttja och
sulfidhaltig lera i Norrala
Rolf Larsson | 1999 |
| 5. | Masstabilisering
Nenad Jelusic | 2000 |
| 6. | Blandningsmekanismer och blandningsprocesser
– med tillämpning på pelarstabilisering
Stefan Larsson | 2000 |

DISTRIBUTION:

Svensk Djupstabilisering

c/o SGI, 581 93 Linköping

Tel: 013- 20 18 42. **Fax:** 013-20-19 14. **E-post:** birgitta.sahlin@swedgeo.se



Svensk Djupstabilisering

c/o SGI, 581 93 Linköping
Tel: 013-20 18 61, Fax: 013- 20 19 14.
Internet: www.swedgeo.se/sd